ARS JOURNAL
RUSSIAN SUPPLEMENT

Igor Jurkevich, Editor

Published Under National Science Foundation Grant-in-Aid

Stability of a Cylindrical Shell Under Twisting, External Pressure and Compression

O. I. TEREBUSHKO

A SUFFICIENTLY extensive literature already exists covering questions of shell stability. In recent years, a great deal of attention has been paid to works in which the post-critical state of shells has been studied. These studies show that for certain types of loads (for example, compression of cylindrical shells along the generatrix), post-critical equilibrium states are possible for external loads which are several times smaller than the critical ones. This explains why the loss of shell stability usually occurs abruptly for loads considerably smaller than the critical ones.

Research devoted to stability and the post-critical state of cylindrical shells, loaded by compression, pressure or twisting, and also by some combination of these loads, was made by Kh. M. Mushtari, A. S. Vol'mir, S. V. Aleksandrovskii, L. R. Ispravnikov, F. S. Isanbayeva, V. L. Agamirov, L. Donnell, T. Karman, Tsu-Tao Loo, I. Kempner, W. Nash and other authors.

Until now, no sufficiently detailed study has been made of the stability (in a linear or nonlinear formulation) of cylindrical shells, loaded with one of the types of loads—compression, twisting or transverse pressure. In some works [for example (1, 2, 4 and 6)[1]], stability was considered with the simultaneous action of compression and transverse pressure. There has been an absolutely insufficient exploration of the stability of cylindrical shells, loaded under other combinations of force factors—by compression and twisting, by twisting and transverse pressure, by compression, transverse pressure and twisting.

The aim of this work is to study the post-critical state of cylindrical shells, loaded by twisting, compression and external pressure and to determine the upper and lower values of the critical combination of loads, causing stability losses.

Basic Notation

h, l = thickness and length of cylindrical shell

r = radius of mean surface

E, ν = modulus of elasticity and Poisson number

m = number of spiral waves along periphery with loss of stability from twisting

κ = tangent of angle formed by direction of spiral wave with cylinder generatrix

n = number of longitudinal half-waves along circumference with stability loss from compression or transverse pressure

L_ϑ = length of half-wave in transverse section of shell, $L_\vartheta = \pi r/n$

L_x = length of half-wave toward generatrix

i = number of half-waves along length of shell, $i = l/L_x$

q = intensity of external pressure, uniformly distributed along surface

s = median value of tangential stresses under twisting

$$s = \frac{M_{cr}}{2\pi r^2 h}$$

p = median value of compression stresses

$$p = \frac{P}{2\pi r h}$$

$q^* = \dfrac{ql^4}{Eh^4}$ = dimensionless external pressure parameter

$p^* = \dfrac{pl^2}{Eh^2}$ = dimensionless compression stress parameter

$s^* = \dfrac{s}{E} \times \dfrac{l^2}{h^2}$ = dimensionless tangential stress parameter

$H = \dfrac{l^2}{rh}$ = dimensionless parameter, characterizing geometric dimensions of shells

u, v, w = displacements of points of shell median surface in direction of axes x, y, z oriented in relation to shell, as indicated in Fig. 1

$D = \dfrac{Eh^3}{12(1-\nu^2)}$ = cylindrical rigidity

Section 1 Formulation of the Problem. Assumptions

Let us consider the round cylindrical shell, loaded by compression stress P and torque M_{cr}, uniformly distributed along the end section, and also the transverse external pressure q, uniformly distributed along the shell surface (Fig. 1). The shell can lose stability both as a result of one of the force factors and under the influence of a combination of these factors. Our aim is to determine the upper and lower values of critical load combinations, i.e., to obtain a functional relationship which will make it possible, using assigned values of two forms of loads, to calculate the value of a third causing stability loss.

We understand as upper values of critical combinations those values of simultaneously acting loads (P, M_{cr} and q) which cause a "low" stability loss. Upper critical load combinations can be obtained as a result of solving stability problems in a linear formulation.

As lower values of critical combinations we will use the least values of simultaneously acting loads P, M_{cr} and q which can maintain in equilibrium the elastic cylindrical shell which has lost stability. The lower critical load combinations can be determined as a result of the investigation of the post-critical equilibrium states of shells, i.e., as a result of solving shell stability in a nonlinear formulation.

In solving the problem the following assumptions were made:

1 The shell material is completely elastic and obeys Hooke's law.

2 The h/r ratio of the shell is small; the shell slopes.

3 The hypothesis of direct normals is considered applicable.

4 The considered shell has sufficient length ($l \gg 4.9\sqrt{rh}$); therefore, the influence of the edge effect can be ignored (8).

Translated from "Design of Three-Dimensional Structures," vol. 5, 1959, pp. 502-522. Translated by Primary Sources, New York.

[1] Numbers in parentheses indicate References at end of paper.

5 Displacements u and v of points of the median surface are small as compared with thicknesses h of shell, and deflections w are of the order of one thickness.

Section 2 Boundary Conditions. Basic Relationships. Method of Solution

Let us allot the following properties to shell supports:

1 They do not prevent the shell from rotating in plane xz; in addition, buckling at shell edges equals zero

$$\frac{\partial^2 w}{\partial x^2} + \nu \frac{\partial^2 w}{\partial y^2} = 0 \qquad \text{when} \qquad x = 0, x = l$$

2 Shell edges can freely slide along the supports along the axis x, i.e., the supports do not create any thrust stresses when the shell is bending.

3 The supports do not obstruct the uniform axisymmetrical deformation of shells under the action of transverse pressure q

$$w = f_0 \qquad \text{when} \qquad x = 0, x = l$$

Relative deformations and changes in the curvature of the median surface are expressed in terms of displacements by the following approximate equations

$$\epsilon_{x0} = \frac{\partial u}{\partial x} + \frac{1}{2}\left(\frac{\partial w}{\partial x}\right)^2$$

$$\epsilon_{y0} = \frac{\partial v}{\partial y} - \frac{w}{r} + \frac{1}{2}\left(\frac{\partial w}{\partial y}\right)^2$$

$$\gamma_{xy} = \frac{\partial u}{\partial y} + \frac{\partial v}{\partial x} + \frac{\partial w}{\partial x} \times \frac{\partial w}{\partial y}$$

$$\kappa_x = -\frac{\partial^2 w}{\partial x^2}$$

$$\kappa_y = -\frac{\partial^2 w}{\partial y^2}$$

$$\kappa_{xy} = -\frac{\partial^2 w}{\partial x \partial y}$$

The relationships between the internal stresses and deformations have the form

$$\sigma_{x0} = \frac{E}{1-\nu^2}(\epsilon_{x0} + \nu\epsilon_{y0}) \qquad M_x = D(\kappa_x + \nu\kappa_y)$$

$$\sigma_{y0} = \frac{E}{1-\nu^2}(\epsilon_{y0} + \nu\epsilon_{x0}) \qquad M_y = D(\kappa_y + \nu\kappa_x)$$

$$\tau_{xy} = \frac{E}{2(1+\nu)} \times \gamma_{xy} \qquad M_{xy} = D(1-\nu)\kappa_{xy}$$

The equilibrium state of the cylindrical shell element is described by the following system of nonlinear differential equations

$$D\nabla^2\nabla^2 w = q + h\left[\frac{\partial^2 \varphi}{\partial y^2} \times \frac{\partial^2 w}{\partial x^2} + \frac{\partial^2 \varphi}{\partial x^2} \times \left(\frac{\partial^2 w}{\partial y^2} + \frac{1}{r}\right) - 2\frac{\partial^2 \varphi}{\partial x \partial y} \times \frac{\partial^2 w}{\partial x \partial y}\right] \qquad [1]$$

$$\frac{1}{E}\nabla^2\nabla^2\varphi = \left(\frac{\partial^2 w}{\partial x \partial y}\right)^2 - \frac{\partial^2 w}{\partial x^2}\left(\frac{1}{r} + \frac{\partial^2 w}{\partial y^2}\right) \qquad [2]$$

Systems [1–2] can be solved by variational methods, for example by the Bubnov-Galerkin or Ritz method. The Ritz method presents the least rigid conditions in selecting the approximate deflection function—satisfying only the geometric boundary conditions, while the Bubnov-Galerkin method (in its standard form) has to satisfy both the geometric and static boundary conditions. For that reason we worked with the Ritz method.

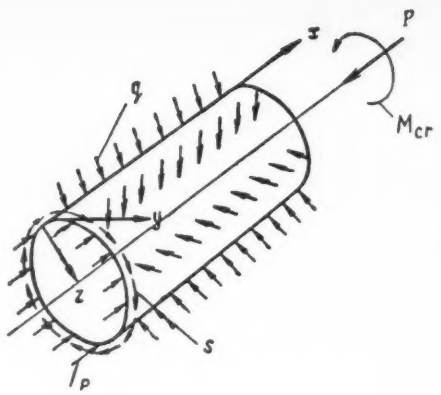

Fig. 1

As the deflection function w, we use the following expression

$$w = f_0 + f_1 \sin\frac{\pi x}{l} \sin m\left(\theta + \kappa\frac{x}{r}\right) + f_2 \sin \alpha x \sin n\theta + f_3 \sin^2\frac{\pi x}{l} \qquad [3]$$

where

$$\alpha = \frac{i\pi}{l} \qquad \theta = \frac{y}{r}$$

The first term characterizes the uniform axisymmetrical deformation where there is a uniform transverse compression of the shell; the second, the emergence of spiral waves, arising when the shell is twisted. The third term reflects the emergence of waves, running along the shell and along the circumference with alternate bulging; the last term, the axisymmetrical, but nonuniform, deformation along the shell length, with the deflection directed toward the center.

Introducing quantities defined by

$$\lambda_1 = \frac{m\kappa}{r} + \frac{\pi}{l} \qquad \lambda_2 = \frac{m\kappa}{r} - \frac{\pi}{l}$$

we obtain the following expression for w

$$w = f_0 + (f_1/2)[(\sin m\theta \sin \lambda_1 x - \cos m\theta \cos \lambda_1 x) - (\sin m\theta \sin \lambda_2 x - \cos m\theta \cos \lambda_2 x)] + f_2 \sin \alpha x \sin n\theta + f_3 \sin^2(\pi x/l) \qquad [4]$$

Section 3 Derivation of Basic Nonlinear Equations

There are four unknown parameters in the deflection expression [4]—f_0, f_1, f_2 and f_3 which we find from the minimum energy conditions of the system

$$\frac{\partial Z}{\partial f_0} = 0 \qquad \frac{\partial Z}{\partial f_1} = 0 \qquad \frac{\partial Z}{\partial f_2} = 0 \qquad \frac{\partial Z}{\partial f_3} = 0 \qquad [5]$$

In addition, we employ the condition that the shell be closed. From this the periodicity requirements of function $\partial v/\partial y$ follow.

The following is the course of the solution to the problem. Derivatives $\partial^2 w/\partial x^2$, $\partial^2 w/\partial y^2$, $\partial^2 w/\partial x \partial y$ are determined first by consecutive differentiation of the deflection function [4]. Then, integrating Equation [2], we find the function of stresses φ. Further, we compute the energy of the system

$$Z = U_c + U_{bend} - A \qquad [6]$$

where U_c is the energy of the shell median surface, computed according to the formula

$$U_c = \frac{hr}{2E} \times \int_0^l \int_0^{2\pi} \left[\left(\frac{\partial^2 \varphi}{\partial x^2} \right)^2 + \left(\frac{\partial^2 \varphi}{r^2 \partial \theta^2} \right)^2 - 2\nu \frac{\partial^2 \varphi}{\partial x^2} \times \frac{\partial^2 \varphi}{r^2 \partial \theta^2} + 2(1+\nu) \left(\frac{\partial^2 \varphi}{\nu x \times r \partial \theta} \right)^2 \right] d\theta dx \qquad [7]$$

U_{bend} is the bending energy of the shell, determined by expression

$$U_{bend} = \frac{Dr}{2} \int_0^l \int_0^{2\pi} \left[\left(\frac{\partial^2 w}{\partial x^2} \right)^2 + \left(\frac{\partial^2 w}{r^2 \partial \theta^2} \right)^2 + 2\nu \frac{\partial^2 w}{\partial x^2} \times \frac{\partial^2 w}{r^2 \partial \theta^2} + 2(1-\nu) \left(\frac{\partial^2 w}{\partial x r \partial \theta} \right)^2 \right] d\theta dx \qquad [8]$$

A is the total work of all external forces, calculated according to expression

$$A = \frac{1}{2} hpr \int_0^l \int_0^{2\pi} \left(\frac{\partial w}{\partial x} \right)^2 dx d\theta + sh \int_0^l \int_0^{2\pi} \frac{\partial w}{\partial x} \times \frac{\partial w}{\partial \theta} dx d\theta + qr \int_0^l \int_0^{2\pi} w dx d\theta + 2\pi rhlp \frac{p - \nu \sigma_{y0}}{E} + 4\pi rhl \frac{s^2(1+\nu)}{E} \qquad [9]$$

We obtain the relationship between f_0 and f_1, f_2 and f_3 from the periodicity conditions of function $\partial v/\partial y$. For $\partial v/\partial y$ we have the expression

$$\frac{\partial v}{\partial y} = \epsilon_{y0} - \frac{1}{2} \left(\frac{\partial w}{\partial y} \right)^2 + \frac{w}{r} \qquad [10]$$

where

$$\epsilon_{y0} = \frac{1}{E} \left(\frac{\partial^2 \varphi}{\partial x^2} - \nu \frac{\partial^2 \varphi}{\partial y^2} \right)$$

Since $\partial v/\partial y$ is a periodic function, then the sum of the periodic terms, entering in Equation [10], should have equalled zero. From this condition, we obtain

$$f_0 = \frac{1}{8} f_1^2 \frac{m^2}{r} + \frac{1}{8} f_2^2 \frac{n^2}{r} - \frac{1}{2} f_3 + \frac{\sigma_{y0}}{E} r - \nu \frac{p}{E} r \qquad [11]$$

The expression for determining σ_{y0} can be obtained from condition $\partial Z/\partial f_0 = 0$. Transforming, we find the well-known expression for σ_{y0}

$$\sigma_{y0} = q(r/h) \qquad [12]$$

If the expression for energy Z is represented in the dimensionless form $\bar{Z} = [Z/(\frac{1}{2}Ehr\pi l)] \times (l^4/h^4)$ and the following definitions introduced

$$\beta = \frac{ml}{\pi r} \qquad \gamma = \frac{nl}{\pi r} \qquad \zeta_1 = \frac{f_1}{h} \qquad \zeta_2 = \frac{f_2}{h} \qquad \zeta_3 = \frac{f_3}{h}$$

$$p^* = \frac{p}{E} \times \frac{l^2}{h^2} \qquad s^* = \frac{s}{E} \times \frac{l^2}{h^2} \qquad q^* = \frac{q}{E} \times \frac{l^4}{h^4} \qquad H = \frac{l^2}{rh}$$

and taking $(m\kappa/r) = (2\pi/l)$, leading to equalities $\lambda_1 = 3(\pi/l)$ and $\lambda_2 = (\pi/l)$, then following transformation, from minimum energy conditions $\bar{Z}$ we obtain the following system of nonlinear algebraic equations, establishing the relationship of parameters ζ_1, ζ_2, ζ_3 to the loads acting on the shell

$$L_1 \zeta_1^2 + L_2 \zeta_2^2 + L_3 \zeta_3^2 - L_4 \zeta_3 + L_5 - 5p^* - (\beta_2/H) q^* - 4\beta s^* = 0 \qquad [13]$$

$$L_6 \zeta_2^2 + L_2 \zeta_1^2 + L_7 \zeta_3^2 - L_{10} \zeta_3 + L_8 - i^2 p^* - (\gamma^2/H) q^* - 0 \qquad [14]$$

$$L_3 \zeta_1^2 \zeta_3 + L_7 \zeta_2^2 \zeta_3 - \tfrac{1}{2} L_4 \zeta_1^2 - \tfrac{1}{2} L_{10} \zeta_2^2 + L_9 \zeta_3 - 2p^* \zeta_3 = 0 \qquad [15]$$

In the system of Equations [13–15], the coefficients of L have the following values

$$L_1 = \frac{\pi^2}{16} \beta^4 \left[1 + \frac{1}{(4+\beta^2)^2} \right] \qquad [16]$$

$$L_2 = \frac{\pi^2}{32} \left\{ \frac{(3\gamma - i\beta)^4}{[(\beta+\gamma)^2 + (i+3)^2]^2} + \frac{(3\gamma - i\beta)^4}{[(\beta-\gamma)^2 + (i-3)^2]^2} + \frac{(3\gamma + i\beta)^4}{[(\beta+\gamma)^2 + (i-3)^2]^2} + \frac{(3\gamma + i\beta)^4}{[(\beta-\gamma)^2 + (i+3)^2]^2} + \frac{(\gamma - i\beta)^4}{[(\beta+\gamma)^2 + (i+1)^2]^2} + \frac{(\gamma - i\beta)^4}{[(\beta-\gamma)^2 + (i-1)^2]^2} + \frac{(\gamma + i\beta)^4}{[(\beta+\gamma)^2 + (i-1)^2]^2} + \frac{(\gamma + i\beta)^4}{[(\beta-\gamma)^2 + (i+1)^2]^2} + \frac{2(\gamma+\beta)^2 (3\gamma-\beta)^2}{[(\gamma-\beta)^2+4]^2} + \frac{2(\gamma-\beta)^2 (3\gamma+\beta)^2}{[(\gamma+\beta)^2+4]^2} + 2\beta^2\gamma^2 \right\} \qquad [17]$$

$$L_3 = \frac{\pi^2}{2} \beta^4 \left[\frac{1}{(25+\beta^2)^2} + \frac{1}{(9+\beta^2)^2} + \frac{2}{(1+\beta^2)^2} \right] \qquad [18]$$

$$L_4 = \beta^2 H \left[\frac{1}{4} + \frac{9}{(9+\beta^2)^2} + \frac{1}{(1+\beta^2)^2} \right] \qquad [19]$$

$$L_5 = \frac{H^2}{2\pi^2} \left[\frac{81}{(9+\beta^2)^2} + \frac{1}{(1+\beta^2)^2} \right] + \frac{\pi^2}{24(1-\nu^2)} [(9+\beta^2)^2 + (1+\beta^2)^2] \qquad [20]$$

$$L_6 = (\pi^2/16)(i^4 + \gamma^4) \qquad [21]$$

$$L_7 = \pi^2 \gamma^4 \left\{ \frac{1}{[(2+i)^2+\gamma^2]^2} + \frac{1}{[(2-i)^2+\gamma^2]^2} \right\} \qquad [22]$$

$$L_8 = \frac{H^2}{\pi^2} \times \frac{i^4}{(i^2+\gamma^2)^2} + \frac{\pi^2}{12(1-\nu^2)} (i^2+\gamma^2)^2 \qquad [23]$$

$$L_9 = \frac{H^2}{2\pi^2} + \frac{2\pi^2}{3(1-\nu^2)} \qquad [24]$$

$$L_{10} = 2\gamma^2 H\left[\frac{1}{8} + \frac{1}{(1+\gamma^2)^2}\right] \qquad [25]$$

The separated terms are nonzero, if $i = 1$.

The assumption that $(m\kappa/r) \cong (2\pi/l)$ is in agreement with the computations and experiments of L. Donnell (10) for thin-walled and not too short shells, for which $H = (l^2/rh) \geq 100$. This assumption considerably simplifies the expression for U_ε.

Section 4 Solution of the Linear Problem

Letting $\zeta_1 = \zeta_2 = \zeta_3 = 0$, in the system of Equations [13–14], we obtain the following two independent equations

$$\frac{H^2}{2\pi^2}\left[\frac{81}{(9+\beta^2)^2} + \frac{1}{(1+\beta^2)^2}\right] + \frac{\pi^2}{24(1-\nu^2)} \times$$

$$[(9+\beta^2)^2 + (1+\beta^2)^2] - 5p^* - \frac{\beta^2}{H} q^* - 4\beta s^* = 0 \qquad [26]$$

$$\frac{H^2}{\pi^2} \times \frac{i^4}{(i^2+\gamma^2)^2} + \frac{\pi^2}{12(1-\nu^2)}(i^2+\gamma^2) - i^2 p^* -$$

$$\frac{\gamma^2}{H} q^* = 0 \qquad [27]$$

Equation [26] establishes the relationship between load parameters p^*, q^* and s^* in the supposition that the form of wave formation at the moment of stability loss for the shell corresponds to the second term of Equation [3]

$$w = f_1 \sin\frac{\pi x}{l} \sin m\left(\theta + \kappa\frac{x}{r}\right)$$

Equation [27] establishes the relationship between parameters p^* and q^* on the assumption that at the moment of stability loss the form of wave formation corresponds to the third term of Equation [3]

$$w = f_2 \sin \alpha x \sin n\theta$$

Assuming that $q = 0$, it is easy to obtain from Equation [27] the known expression for the upper critical compression stress of the cylindrical shell. Supposing the waves to be square ($L_x = L_\theta$ and, consequently $i = \gamma$), we obtain

$$p^* = \frac{H^2}{\pi^2 4i^2} + \frac{\pi^2 i^2}{3(1-\nu^2)} \qquad [28]$$

Further, determining i from condition $(\partial p^*/\partial i) = 0$ and substituting in Equation [28], we obtain $p_B^* = H/\sqrt{3(1-\nu^2)}$, and for $\nu = 0.3$

$$p_B^* = 0.6H \qquad [29]$$

or in a dimensional form

$$p_B = 0.6E(h/r) \qquad [30]$$

With the loss of stability from external pressure alone, longitudinal waves are formed with half-wave lengths of $L_x = l$. In addition $i = 1$

$$q^* = \frac{H^3}{\pi^2\gamma^2(1+\gamma^2)^2} + \frac{\pi^2 H}{12(1-\nu^2)\gamma^2}(1+\gamma^2)^2 \qquad [31]$$

The value of γ in function H can be obtained from condition $\partial q^*/\partial\gamma = 0$, which leads to equation

$$\xi^5 - 2\xi^4 - \frac{H^2 12(1-\nu^2)}{\pi^4}(3\xi - 2) = 0 \qquad [32]$$

where the value $(1+\gamma)$ was designated through ξ.

Having determined γ in relation to H, from Equation [32], and having substituted in Equation [31], we obtain the corresponding value q_B^*.

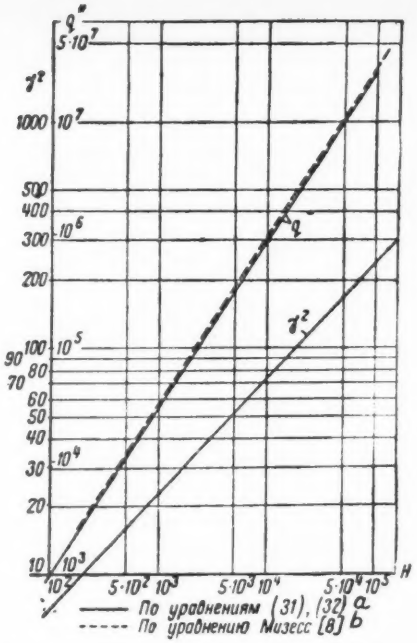

Fig. 2 Translations: [a]According to Equations [31 and 32]; [b]according to Mizes Equation [8]

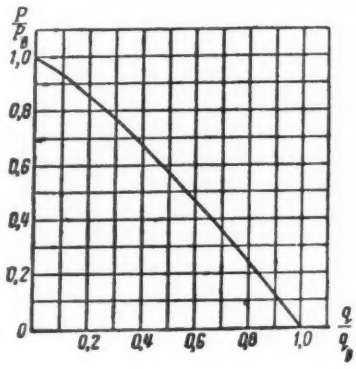

Fig. 3

In Fig. 2, the relationship is shown of γ^2 and q_B^* to H, obtained from Equations [31 and 32]. The same figure gives the relationship of q_B^* to H according to the Mizes equation (8). The graphical relationship found by us is well approximated by the following expression

$$q_B^* = K_{q_B} H^{3/2} \qquad [33]$$

or in the dimensional form

$$q_B = K_{q_B} E\left(\frac{h}{r}\right)^{5/2}\frac{r}{l} \qquad [34]$$

where K_{q_B} is a coefficient, changing from 0.92 when $H = 10^5$, to 1 when $H = 200$.

Let us consider the cases of the simultaneously acting p^* and q^*. It follows from Equation [27] that with assigned values of i and γ a linear relationship is established between p^* and q^*. However, if i and γ are selected in such a way that the least values of p^* and q^* are obtained, then the linearity is destroyed. The curve, corresponding to the least values of

the combination of p^* and q^*, caused by the loss in stability, is inclined toward the straight line family in Equation [27].

As calculations made by us show, if there is a simultaneous action of transverse pressure q and compression p, with an assigned p, the least values of q are obtained when $i = 1$.

The value γ, corresponding to the minimum q^*, with an assigned p^*, we obtain from the condition $\partial q^*/\partial\gamma = 0$, where $q^* = f(H, \gamma, p^*)$ is determined by Equation [27].

A graph is presented in Fig. 3 showing the relationship of q/q_B to p/p_B plotted according to Equation [27]. In the computations, the value γ was determined from the condition $\partial q^*/\partial\gamma = 0$. The graphic relationship of q/q_B to p/p_B is well approximated by the equation of the form

$$\frac{p}{p_B} + \left(\frac{q}{q_B}\right)^{5/4} = 1 \qquad [35]$$

In Equation [35], p_B and q_B are determined by formulas [30 and 34].

Let us conduct an investigation of Equation [26], establishing the relationship of p^*, q^*, s^* to the geometric parameter H of the shell in the hypothesis that with stability loss, spiral waves are formed. We will assume that $s^* \pm 0$ and that p^* and q^* can be both equal and not equal to zero.

Let us first consider the case of pure twisting. Substituting

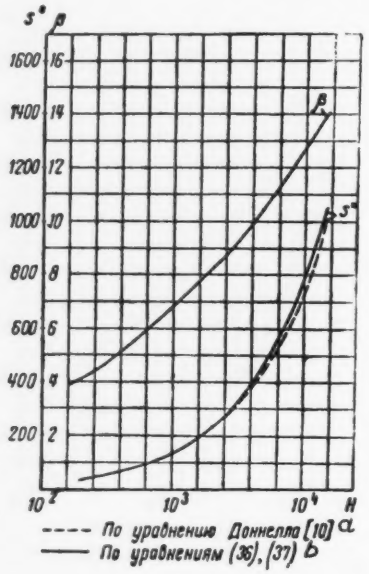

Fig. 4 Translations: [a]According to Donnell Equation [10]; [b]according to Equations [36 and 37]

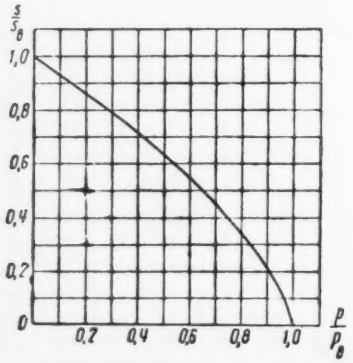

Fig. 5

$p^* = q^* = 0$ in Equation [26], we obtain

$$\frac{H^2}{2\pi^2}\left[\frac{81}{(9+\beta^2)^2} + \frac{1}{(1+\beta^2)^2}\right] + \frac{\pi^2}{24(1-\nu^2)}\left[(9+\beta^2)^2 + (1+\beta^2)^2\right] = 4\beta s^* \qquad [36]$$

We find the equation for determining β in relation to H, from the condition $\partial s^*/\partial\beta = 0$

$$(H^2/\pi^2)\left[81(1+\beta^2)^3(9+5\beta^2)^3 + (9+\beta^2)^3(1+5\beta^2)\right] - \frac{\pi^2}{12(1-\nu^2)}(9+\beta^2)^3(1+\beta^2)^3\left[(9+\beta^2)(3\beta^2-9) + (1+\beta^2)(3\beta^2-1)\right] = 0 \qquad [37]$$

Presented in Fig. 4 are curves $\beta = f_1(H)$ and $s_B^* = f_2(H)$, plotted according to Equations [36 and 37]. There too, a graph is shown of the relationship of s^* to H, plotted according to the Donnell formula.

Calculations according to the approximate Equations [36 and 37] are in good accord with the results of the Donnell solution (10). The graphic relationship of s_B^* to H, found by us, can be approximated by the expression

$$s_B^* = 0.775H^{3/4} \qquad [38]$$

or in the dimensional form

$$s_B = 0.775E\left(\frac{h}{r}\right)^{5/4}\left(\frac{r}{l}\right)^{1/2} \qquad [39]$$

Formula [39] coincides with the expression for determining critical shear stress, when twisting cylindrical shells, obtained by Donnell (10) and Kh. M. Mushtari (7). However, the numerical coefficient when $\nu = 0.3$ equals 0.746 in the Donnell formula and -0.765 in the formula of Kh. M. Mushtari.

Under the simultaneous action of torque and compression, Equation [26] acquires the form

$$\frac{H^2}{2\pi^2}\left[\frac{81}{(9+\beta^2)^2} + \frac{1}{(1+\beta^2)^2}\right] + \frac{\pi^2}{24(1-\nu^2)}\left[(9+\beta^2)^2 + (1+\beta^2)^2\right] = 5p^* + 4\beta s^* \qquad [40]$$

The upper values of the critical combination of load parameters p^* and s^* can be found, with the substitution in Equation [40] of value β, from the conditions of a minimum s^*, with an assigned value of p^*.

After transformations, from condition $\partial s^*/\partial\beta = 0$, we obtain

$$AH^2 + BH + C = 0 \qquad [41]$$

where

$$A = \frac{\beta^2}{\pi^2}\left[\frac{81}{(9+\beta^2)^3} + \frac{1}{(1+\beta^2)^3}\right] + \frac{1}{4\pi^2}\left[\frac{81}{(9+\beta^2)^2} + \frac{1}{(1+\beta^2)^2}\right]$$

$$B = -1.5(p^*/p_B^*)$$

$$C = \frac{\pi^2}{48(1-\nu^2)}\left[(9+\beta^2)^2 + (1+\beta^2)^2\right] - \frac{\pi^2\beta^2}{12(1-\nu^2)}\left[(9+\beta^2) + (1+\beta^2)\right]$$

A graph is presented in Fig. 5 showing the relationship of s/s_B to p/p_B. This graphic relationship is approximated by an expression of the form

$$\frac{p}{p_B} + \left(\frac{s}{s_B}\right)^{3/2} = 1 \qquad [42]$$

Under the simultaneous action of the twisting moment and transverse pressure, Equation [26] takes on the form

$$\frac{H^2}{2\pi^2}\left[\frac{81}{(9+\beta^2)^2}+\frac{1}{(1+\beta^2)^2}\right]+$$
$$\frac{\pi^2}{24(1-\nu^2)}\left[(9+\beta^2)^2+(1+\beta^2)^2\right]=4\beta s^*+\frac{\beta^2}{H}q^* \quad [43]$$

The relationship between β and H, to which the minimum value of s^* correspond with an assigned q^*/q_B^* ratio, can be obtained from condition $\partial s^*/\partial\beta = 0$ of minimum s^*. This condition provides

$$A'H^2 + B'H^{1/2} + C' = 0 \quad [44]$$

where

$$A' = A \qquad B' = \tfrac{1}{4}\beta^2(q^*/q_B^*) \qquad C' = C$$

A graphic relationship was plotted from Equations [43 and 44] (Fig. 6), approximated by the expression

$$\left(\frac{s}{s_B}\right)^{3/2}+\left(\frac{q}{q_B}\right)^{5/4}=1 \quad [45]$$

Curves of Figs. 4, 5 and 6, approximated by Equations [35, 42 and 45], are the upper boundaries of stability regions in corresponding coordinates. The points, lying above these boundaries, correspond to load combinations, causing a loss in shell stability.

The intersection of the surface bounding the region of stability from above (in variables p/p_B, q/q_B, s/s_B) with the corresponding coordinate planes gives the curves in Figs. 4, 5 and 6. Taking Equations [35, 42 and 45] into consideration, the equation for the surface, bounding the stability region from above, is represented in the form

$$\frac{p}{p_B}+\left(\frac{q}{q_B}\right)^{5/4}+\left(\frac{s}{s_B}\right)^{3/2}=1 \quad [46]$$

If the load values p, q, s, acting on a shell, substituted in Equation [46], lead to the inequality

$$\frac{p}{p_B}+\left(\frac{q}{q_B}\right)^{5/4}+\left(\frac{s}{s_B}\right)^{3/2}>1$$

then the given load combination p, q, s, causes stability loss in the shell.

Values p_B, q_B, s_B in Equation [46] are determined according to the equations in [30, 34 and 39].

Section 5 Solution of the Nonlinear Problem

a Determination of p_H^*

In order to obtain the relationship of p_H^* to the geometric parameter of shell H, use is made of Equations [14 and 15], setting $\zeta_1 = 0$ and $q^* = 0$ in them. We obtain

$$L_6\zeta_2^2 + L_7\zeta_3^2 - L_{10}\zeta_3 + L_8 - i^2p^* = 0 \quad [47]$$

$$L_7\zeta_2^2\zeta_3 - \tfrac{1}{2}L_{10}\zeta_2^2 + L_9\zeta_3 - 2p^*\zeta_3 = 0 \quad [48]$$

Values of coefficients $L_6 - L_{10}$ are determined by expressions [21–25].

Studying the influence of the number of half-waves along the x-axis of the shell, it is possible to reach the conclusion that i has a very small influence on the critical compression stress. Therefore, when calculating p_H^*, and henceforth, we will assume that $i = 1$. Solving system [47–48] relative to p^*, we obtain

$$p^* = \frac{a_0 - a_1\zeta_3 + a_2\zeta_3^2 - a_3\zeta_3^3}{\tfrac{1}{2}L_{10} + a_4\zeta_3} \quad [49]$$

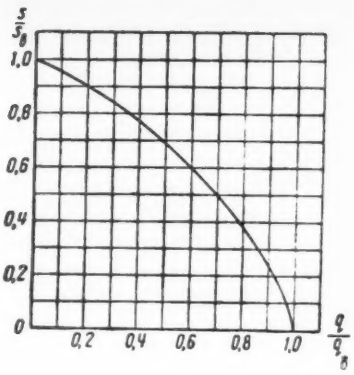

Fig. 6

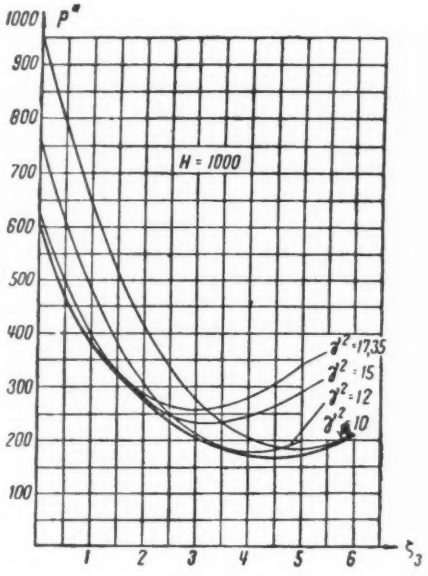

Fig. 7

where

$a_0 = \frac{1}{2}L_8L_{10}$
$a_1 = \frac{1}{2}L_{10}^2 + L_7L_8 - L_6L_9$
$a_2 = \frac{3}{2}L_7L_{10}$
$a_3 = L_7^2$
$a_4 = 2L_6 - L_7$

The values ζ_2 and ζ_3 are connected by the relationship

$$\zeta_2^2 = \frac{(L_9 - 2p^*)\zeta_3}{\tfrac{1}{2}L_{10} - L_7\zeta_3} \quad [50]$$

In Fig. 7, the relationship is shown of p^* to ζ_3 for different values of γ^2 when $H = 1000$. As is evident from these graphs, the value of parameter $\gamma^2 = nl/\pi E$ has a strong influence on both p_B^* and p_H^*. The reduction of γ^2 takes place in accordance with the growth of deflection deformation, i.e., the waves broaden toward the circumference (L_θ/L_x ratio increases). The influence of γ on p_H^* is greater for shells of small and medium length ($H = 200 - 1000$). As calculations made by us have shown, p_H^* is not a linear function of H

$$p_H^* = K_{pH}H \quad [51]$$

Coefficient K_{pH} in Equation [51] depends on H.

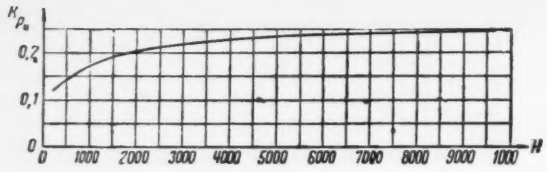

Fig. 8

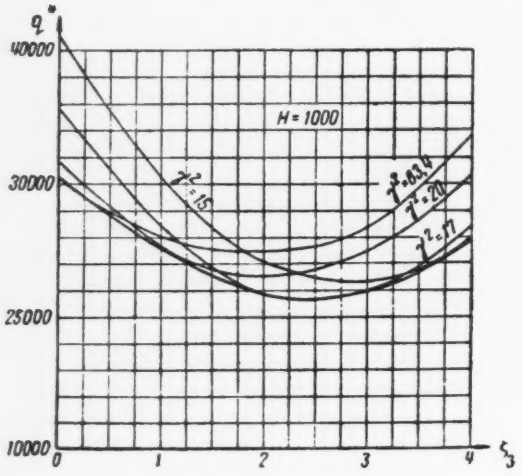

Fig. 9

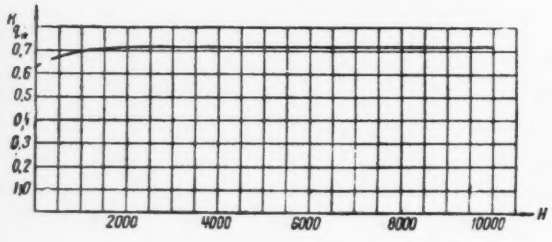

Fig. 10

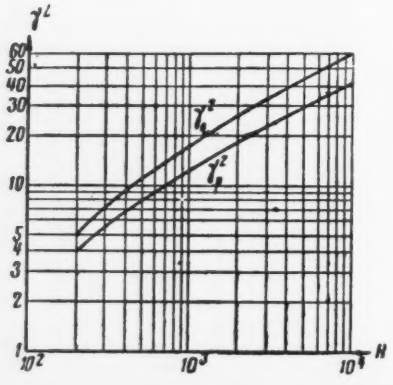

Fig. 11

As is evident from the graph in Fig. 8, K_{pH} changes from 0.12, when $H = 200$ to 0.24, when $H = 10{,}000$. However, H has a marked influence on the value of K_{pH} only within a range of values $H = 200 - 2000$. With further increases in H the value of coefficient K_{pH} is stabilized, approaching the value of 0.24–0.25.

The expression for the lower critical stress in the dimensional form has the form

$$p_H = K_{pH}(Eh/r) \qquad [52]$$

where K_{pH} is determined from the graph in Fig. 8.

b Determination of q_H^*

Assuming $\zeta_1 = p^* = 0$, in the system of equations [14–15], we obtain a system of equations, establishing the relationship of q^* to deflection, from which it is possible to define q_H^*

$$L_6\zeta_2^2 + L_7\zeta_3^2 - L_{10}\zeta_3 + L_8 - (\gamma^2/H)q^* = 0 \qquad [53]$$

$$L_7\zeta_2^2\zeta_3 - \tfrac{1}{2}L_{10}\zeta_2^2 + L_9\zeta_3 = 0 \qquad [54]$$

From systems [53–54], we obtain

$$\zeta_2^2 = \frac{L_9\zeta_3}{\frac{1}{2}L_{10} - L_7\zeta_3} \qquad [55]$$

$$q^* = \frac{H}{\gamma^2}\left[\frac{L_6L_9\zeta_3}{\frac{1}{2}L_{10} - L_7\zeta_3} + L_7\zeta_3^2 - L_{10}\zeta_3 + L_8\right] \qquad [56]$$

In Fig. 9, graphs of $q^* = f(\zeta_3)$ are presented which were plotted from Equation [56] for different values of γ^2, when $H = 1000$. The lower value of the critical pressure parameter q_H^* can be calculated from the formula

$$q_H^* = K_{qH}H^{3/2} \qquad [57]$$

For q_H the formula has the form

$$q_H = K_{qH}E\left(\frac{h}{r}\right)^{5/2}\frac{r}{l} \qquad [58]$$

where coefficient K_{qH}, as is evident from the graph in Fig. 10, changes from 0.624, when $H = 200$ to 0.716, when $H = 10{,}000$. Within the range of values for H the median integrated value of K_{qH} equals 0.69.

A graph is pictured in Fig. 11 showing the relationship of parameter γ^2, corresponding to the lower values of loads p_H and q_H, to the geometric parameter of shell H.

c Determination of s_H^*

We determine the magnitude of the lower critical shear stress from the system of Equations [13 and 15], assuming that $\zeta_2 = p^* = q^* = 0$. In addition, Equations [13 and 15] take on the form

$$L_1\zeta_1^2 + L_3\zeta_3^2 - L_4\zeta_3 + L_5 - 4\beta s^* = 0 \qquad [59]$$

$$L_3\zeta_1^2\zeta_3 - \tfrac{1}{2}L_4\zeta_1^2 + L_9\zeta_3 = 0 \qquad [60]$$

From systems [59 and 60], we obtain

$$\zeta_1^2 = \frac{L_9\zeta_3}{\frac{1}{2}L_4 - L_3\zeta_3} \qquad [61]$$

$$s^* = \frac{1}{4\beta}\left[\frac{L_1L_9\zeta_3}{\frac{1}{2}L_4 - L_3\zeta_3} + L_3\zeta_3^2 - L_4\zeta_3 + L_5\right] \qquad [62]$$

In Fig. 12 graphs are presented of the relationships of s^* to ζ_3, plotted according to Equation [62] for $H = 1000$ and of several values for parameter β.

As is evident from these graphs, after the loss of stability by the shell due to twisting, no changes occur in the size of parameter β. This indicates that after the loss of stability by the shell no changes occur in the number of spiral waves m as a function of the deflection deformation.

The lower value of the critical shear stress parameter s_H^* can be calculated according to formula

$$s_H^* = K_{sH} H^{3/4} \qquad [63]$$

For s_H, the formula has the form

$$s_H = K_{sH} E \left(\frac{h}{r}\right)^{5/4} \left(\frac{r}{l}\right)^{1/2} \qquad [64]$$

Coefficient K_{sH} depends very little on H and its value, as calculations have shown, can be accepted as equal to 0.65.

We present the following combined formulas for computing the critical loads of compression, external pressure and twisting

$$p = K_p E \frac{h}{r} \qquad q = K_q E \frac{(h/r)^{5/2}}{(l/r)} \qquad s = K_s E \frac{(h/r)^{5/4}}{(l/r)^{1/2}}$$

It is evident from the presented formulas that the magnitude of the shell's relative thickness h/r exerts the greatest influence on the value of the critical load. The critical compression load is linearly dependent on h/r (there is no rigorous linearity for the lower critical stress), whereas the critical external pressure q and the critical twisting stress s are dependent to a greater extent.

The relative length of the shell l/r also influences the size of the critical loads. The relative length of shells has a slight influence on the size of p; with a reduction of l/r the lower critical compression stress p_H is reduced somewhat. As is evident from the presented formulas, shell length exerts a very large influence on critical pressure and on critical twisting stress. Increases in the relative lengths of shells l/r lead to reductions of q and s.

d Determination of $(p, q)_H$

We find the expression for the determination of lower critical combination of compression stress p and the external pressure q from the system of Equations [14–15], assuming that $\zeta_1 = 0$

$$L_6\zeta_2^2 + L_7\zeta_3^2 - L_{10}\zeta_3 + L_8 - p^* - (\gamma^2/H)q^* = 0 \qquad [65]$$

$$L_7\zeta_2^2\zeta_3 - \tfrac{1}{2}L_{10}\zeta_2^2 + L_9\zeta_3 - 2p^*\zeta_3 = 0 \qquad [66]$$

Transforming the system of Equations [65–66], we obtain the following expression

$$\frac{\gamma^2}{H} q^* = \frac{\tfrac{1}{2}L_8L_{10} - [\tfrac{1}{2}L_{10} + (2L_6 - L_7)\zeta_3]p^* - (\tfrac{1}{2}L_{10}^2 + L_7L_8 - L_6L_9)\zeta_3 + \tfrac{3}{2}L_7L_{10}\zeta_3^2 - L_7\zeta_3^3}{\tfrac{1}{2}L_{10} - L_7\zeta_3} \qquad [67]$$

Equation [67] establishes the relationship between the combination of external loads p^* and q^* and the deflection parameter of the shell ζ_3. For ζ_3, which converts the left-hand side of Equation [67] to the minimum, we obtain the lower critical value of parameter q^*, for an assigned p^*.

Taking into consideration that curve $q^* = f(\zeta_3)$ has an extremely flat minimum, and that therefore an error of several percent in defining ζ_3 leads to an error of less than one per cent in defining q^*, and also that $L_7/\frac{1}{2}L_{10}$ is a very small quantity, especially with large values of H, it is possible to determine the magnitude of ζ_3, corresponding to q_H^*, according to the following approximate formula

$$\zeta_3 \cong \frac{\tfrac{1}{2}L_{10} + L_7L_8 - L_6L_9 + (2L_6 - L_7)p^*}{3L_7L_{10}} \qquad [68]$$

Substituting the value ζ_3, found in Equation [68], in [67] we obtain q_H^*. Coefficients $L_6 - L_{10}$ are calculated according to formulas [21–25]. In order to compute the coefficients $L_6 - L_{10}$ and q_H^* one must know the size of $\gamma^2 = nl/\pi r$, for which q^* has a minimum. In the foregoing, we determined the values of γ_p^2 and γ_p^2 as a function of the parameter H, corresponding to the lower critical loads q_H^* and p_H^* when loading shells with one kind of stress (curves γ_q^2 and γ_p^2 in Fig. 11). Thus, for example, when $H = 1000$, $\gamma_p^2 = 12$ and $\gamma_q^2 = 17$. With the simultaneous action of two forms of loads p and q, the parameter γ_{pq}^2 should evidently have a value between γ_p^2 and γ_q^2

$$\gamma_p^2 < \gamma_{pq}^2 < \gamma_q^2$$

Let us suppose that γ_{pq}^2 changes within a given range according to the linear law

$$\gamma_{pq}^2 = \gamma_q^2 - (\gamma_q^2 - \gamma_p^2)(p/p_H) \qquad [69]$$

As calculations made by us have shown, the relationship of p/p_H to q/q_H is very close to linear.

As is evident from Equation [67], deviations from the linear relationship occur because of the influence of p/p_H on γ_{pq}^2 (and consequently on L_6–L_{10}) and on ζ_3. However, the total influence of p/p_H on all coefficients is such that deviations from the linear relationship are slight. In practical computations for the equation of the lower limit of stability, in cases of simultaneously acting p and q, it is possible to take the equation of the straight line

$$\frac{p}{p_H} + \frac{q}{q_H} = 1 \qquad [70]$$

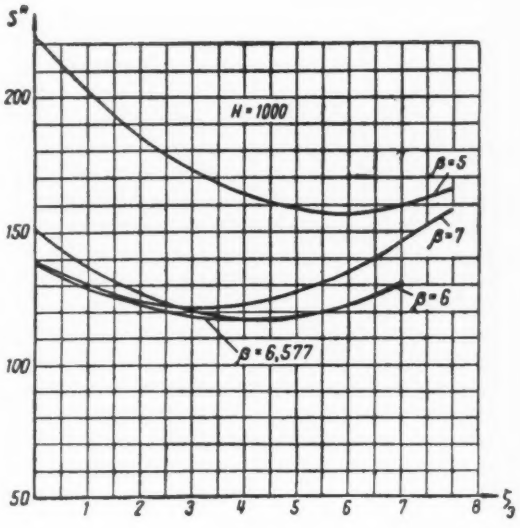

Fig. 12

e Determination of $(s,q)_H$ and $(s,p)_H$

Assuming $\zeta_2 = 0$, from equation systems [13 and 15], we obtain

$$L_1\zeta_1^2 + L_2\zeta_3^2 - L_4\zeta_3 + L_5 - 5p^* - (\beta^2 q^*/H) - 4\beta s^* = 0 \qquad [71]$$

$$L_3\zeta_1^2\zeta_3 - \tfrac{1}{2}L_4\zeta_1^2 + L_9\zeta_3 - 2p^*\zeta_3 = 0 \qquad [72]$$

Considering p^* and q^* as assigned and solving this system

of equations for s^*, we obtain

$$s^* = \frac{1}{4\beta(\frac{1}{2}L_4 - L_3\zeta_3)}\left\{\frac{1}{2}L_4L_8 - \left[\frac{5}{2}L_4 + (2L_1 - 5L_3)\zeta_3\right]p^* - \frac{\beta^2}{H}\left(\frac{1}{2}L_4 - L_3\zeta_3\right)q^* - \left(\frac{1}{2}L_4^2 + L_3L_4 - L_1L_9\right)\zeta_3 + \frac{3}{2}L_3L_4\zeta_3^2 - L_3^2\zeta_3^2\right. \quad [73]$$

Considering that $(L_3/\frac{1}{2}L_4)$ is a small quantity, it is possible to find an approximate value of ζ_3 which makes s^* a minimum, according to the following formula

$$\zeta_3 \leqq \frac{\frac{1}{2}L_4^2 + L_3L_5 - L_1L_9 + (2L_1 - 5L_3)p^* - (\beta^2q^*/H)L_3}{3L_3L_4} \quad [74]$$

Calculations conducted by us, using Equations [72 and 73], for shells with different values of parameter H showed that an approximate linear relationship exists for loads, defining the lower values of critical combinations, i.e., the following equations obtain

$$\frac{p}{p_H} + \frac{s}{s_H} = 1 \quad [75]$$

$$\frac{q}{q_H} + \frac{s}{s_H} = 1 \quad [76]$$

Where three forms of loads act simultaneously, p, q and s, the stability region is bounded from below by the surface, which in variables p/p_H, q/q_H, s/s_H is described by equation

$$\frac{p}{p_H} + \frac{q}{q_H} + \frac{s}{s_H} = 1 \quad [77]$$

Equation [77] is the equation of a plane. The values p_H, q_H and s_H are determined by formulas [52, 58 and 64].

Thus, we obtained the two equations [46 and 77] which restrict the region of values of p, q and s, causing a stability loss from above [46] and from below [77]. If p_0, q_0 and s_0 denote values of loads, causing a loss of stability for shells under experiment, then the following inequalities should occur

$$\frac{p_0}{p_H} + \frac{q_0}{q_H} + \frac{s_0}{s_H} > 1$$

$$\frac{p_0}{p_B} + \left(\frac{q_0}{q_B}\right)^{5/4} + \left(\frac{s_0}{s_B}\right)^{3/2} < 1 \quad [79]$$

A comparison with experiments, conducted by L. R. Ispravnikov (5), V. L. Agamirov (1) and the author, confirmed the correctness of inequalities [78 and 79].

If, for the critical design loads, we take the lower critical values, then the ratio $p_0/p_H = m_p$ can be defined as the coefficient of the stability margin for the shell under compression; $q_0/q_H = m_q$ is the coefficient of stability margin for shells, loaded by external pressure; $(p_0/p_H) + (s_0/s_H) = m_{ps}$ is the coefficient of stability margin for shells, loaded by a combination of compression and twisting, etc.

As has been shown by comparing calculations with experiments, the coefficients of stability margin fall within the following ranges

$$1.1 < m_p < 3$$
$$1.15 < m_q < 1.7$$
$$1.07 < m_s < 1.15$$
$$1.48 < m_{pq} < 3.2$$
$$1.55 < m_{ps} < 2.7$$
$$1.3 < m_{qs} < 1.8$$

Conclusions

1 Under certain forms of loading (compression), equilibrium states are possible for cylindrical shells, when the stresses are several times smaller than the upper critical states, defined by the linear theory of shells. Experiments show that existing stresses, under which stability loss occurs, lie between the upper and lower values of critical stresses. For some forms of loading (twisting) the difference between the upper and lower critical stresses is small ($s_H = 0.84s_B$).

2 In all cases, calculation of shell stability using the lower values of critical loads is fully reliable:

a When compressing shells

$$p_H = K_{pH}E(h/r)$$

where, on the basis of theoretical calculations and experiments, it is possible to take $K_{pH} \approx 0.18$

b When loading shells with transverse pressure

$$q_H = \frac{K_{qH}E\,(h/r)^{5/2}}{l/r}$$

where $K_{qH} \approx 0.69$

c When twisting shells

$$s_H = \frac{K_{sH}E(h/r)^{5/4}}{(l/r)^{1/2}}$$

where $K_{sH} = 0.65$.

3 In those cases where a combination of loads act on the shell, the loss of shell stability also occurs when the values of loads, entering into the combination and lying between the upper and lower critical combination values, are determined by the expressions

$$\frac{p}{p_B} + \left(\frac{q}{q_B}\right)^{5/4} + \left(\frac{s}{s_B}\right)^{3/2} = 1 \qquad \frac{p}{p_H} + \frac{q}{q_H} + \frac{s}{s_H} = 1$$

The result of our calculations of the stability of cylindrical shells according to formulas, determining the lower critical values of load combinations, is sufficiently reliable.

References

1 Agamirov, V. L., "Stability of Closed Cylindrical Shells With the Combined Action of Axial Compression and External Pressure," Dissertation of the N. Ye. Zhukov VVIA (Air Force Engineering Academy), 1955.

2 Aleksandrovskii, S. V., "On the Stability of Cylindrical Shells With Large Deflections," Collection, "Computations on Lateral Structures," issue III, Stroiizdat (State Publishing House for Literature on Construction and Architecture), 1955.

3 Vol'mir, A. S., "Flexible Plates and Shells," Gostekhteoretizdat (State Publishing House of Theoretical and Technical Literature), 1956.

4 Isanbayeva, F. S., "Determination of Lower Critical Loads for Cylindrical Shells Under Thorough Compression," *Reps. of Kazan Branch of Acad. Sci. USSR, Phys.-Math. and Tech. Sci. Series*, no. 7, 1955.

5 Ispravnikov, L. R., "Experimental Study of the Stability of Cylindrical Shells Under Axial Compression, Twisting and Transverse Pressure," Proc. of N. Ye. Zhukov VVIA, issue 535, 1955.

6 Mushtari, Kh. M. and Sachenkov, A. V., "On the Stability of Cylindrical and Conical Circular Shells With the Simultaneous Action of Axial Compression and Normal External Pressure," Prikladnaya Matematika i Mekhanika (J. Appl. Math. and Mech.), issue 6, 1954, pp. 667–674.

7 Mushtari, Kh. M., and Galimov, K. Z., "Nonlinear Theory of Elastic Shells," Tatknigoizdat (Tatar Publishing House), 1957.

8 Timoshenko, S. P., "Stability of Elastic Systems," E Gostekhteoretizdat, 1955.

9 "Designer Manual for Calculating the Durability of Gas Turbine Engines," issue 5, Izd. Obor. Prom. (State Publishing House of the Defense Industry).

10 Donnell L. H., "Stability of Thin-Walled Tubes Under Torsion," NACA Rep., no. 479, 1934.

11 Sturm, R. G., "Stability of Thin Cylindrical Shells in Torsion," Proc. Amer. Soc. Civ. Engng., vol. 73, no. 4.

12 Loo, Tsu-Tao, "Effects of Large Deflections and Imperfections on the Elastic Buckling of Cylinders Under Torsion and Axial Compression," Proc. of Second U. S. Natl. Congress of Appl. Mech., New York, 1954.

13 Nash, W. A., "Buckling of Initially Imperfect Cylindrical Shells Subjected to Torsion," J. Appl. Mech., March 1957, vol. 24, no. 1.

Interpolation Averaged Variants of the Canonical Problem of Celestial Mechanics

N. D. Moiseyev

Introduction

THE PRESENT article is an extension and a generalization of our previous paper "On Interpolation Averaged Variants of the Restricted Three-Body Problem."[1]

The generalization consists, in the first place, in considering any problem in celestial mechanics that allows us to write the differential equations in canonical form, whereas in the previous article we dealt only with the restricted circular three-body problem.

In the second place, the generalization consists in including linear interpolation averaging, based on the use of interpolation elements which can be formed not only from the angular Keplerian phase coordinates M, ω, Ω from which were formed the "interpolation anomalies" in the paper cited, but also from the other Keplerian phase coordinates, for example, from the quantities $\sqrt{a}$, $\sqrt{p}$, $\sqrt{p}\cos i$, or from quantities analogous to them.

1 Twice Averaged Variant of the Canonical Problem

Let the differential equations of the canonical problem of celestial mechanics in question be

$$\frac{d\xi_1}{dt} = \frac{\partial H}{\partial \eta_1} \qquad \frac{d\xi_2}{dt} = \frac{\partial H}{\partial \eta_2} \qquad \frac{d\xi_3}{dt} = \frac{\partial H}{\partial \eta_3}$$

$$\frac{d\eta_1}{dt} = -\frac{\partial H}{\partial \xi_1} \qquad \frac{d\eta_2}{dt} = -\frac{\partial H}{\partial \xi_2} \qquad \frac{d\eta_3}{dt} = -\frac{\partial H}{\partial \xi_3} \qquad [1]$$

where the characteristic function

$$H = H(\xi_1, \xi_2, \xi_3, \eta_1, \eta_2, \eta_3, t) \qquad [2]$$

may or may not explicitly contain the time t. In the latter case Equations [1] will permit a first integral of the form

$$H(\xi, \xi_2, \xi_3, \eta_1, \eta_2, \eta_3) = \text{const} \qquad [3]$$

We shall stipulate that the canonical variables or elements

$$(\xi_1, \xi_2, \xi_3, \eta_1, \eta_2, \eta_3) \qquad [4]$$

be divided into two groups; the first is

$$(\xi_1, \xi_2, \xi_3) \qquad [5]$$

and the second is

$$(\eta_1, \eta_2, \eta_3) \qquad [6]$$

With the aid of an interpolation treatment, based on the use of the method of least squares and the methods of linear correlation theory, we shall form the following "interpolation element"

$$\alpha_1 = a_1^{(1)}\xi_1 + a_2^{(1)}\xi_2 + a_3^{(1)}\xi_3 \qquad [7]$$

from elements of the first group [5].[2] In the interval of time embraced by the interpolation treatment

$$t_0 \leqslant t \leqslant t_1 \qquad [8]$$

let the variation intervals of the elements of the first group [5] be respectively

$$\xi_{10} \leqslant \xi_1 \leqslant \xi_{11}$$

$$\xi_{20} \leqslant \xi_2 \leqslant \xi_{21}$$

$$\xi_{30} \leqslant \xi_3 \leqslant \xi_{31} \qquad [9]$$

Assuming that

$$a_1^{(1)} \neq 0 \qquad [10]$$

we determine the quantity ξ_1 from Equation [7]

$$\xi_1 = \frac{1}{a_1^{(1)}}\alpha_1 - \frac{a_2^{(1)}}{a_1^{(1)}}\xi_2 - \frac{a_3^{(1)}}{a_1^{(1)}}\xi_3 \qquad [11]$$

and substitute in the characteristic function [2]. This gives

$$H = H[\xi_1(\alpha_1, \xi_2, \xi_3), \xi_2, \xi_3, \eta_1, \eta_2, \eta_3, t] \qquad [12]$$

We shall form the twice averaged expression for the characteristic function H [12] with respect to the variables ξ_2 and ξ_3 over the intervals [9] of their possible values with the aid of the expression

$$[H] = \frac{1}{(\xi_{21} - \xi_{20})} \times \frac{1}{(\xi_{31} - \xi_{30})} \int_{\xi_2=\xi_{20}}^{\xi_{21}} \int_{\xi_3=\xi_{30}}^{\xi_{31}} H d\xi_2 d\xi_3 \qquad [13]$$

In the process of integration the quantities ξ_2 and ξ_3 are considered mutually independent variables, whereas the quantities

$$\alpha_1, \eta_1, \eta_2, \eta_3, t \qquad [14]$$

are considered constant.

The twice averaged characteristic function $[H]$ [13] will be an explicit function of the variables [14]

$$[H] = [H](\alpha_1, \eta_1, \eta_2, \eta_3, t) \qquad [15]$$

while we may consider that it will also depend on the variables [5], of which α_1, determined as an intermediate variable from Equation [7], may be considered an explicit function. Accepting this condition, we shall get the twice averaged characteristic function $[H]$ in the following form

$$[H] = [H][\alpha_1(\xi_1, \xi_2, \xi_3), \eta_1, \eta_2, \eta_3, t] \qquad [16]$$

Translated from *Contributions of the State Astronomical Institute of P. K. Sternberg*, vol. 24, 1954, pp. 3–9. Translated by Research Information Service, New York.

[1] *Vestnik MGU* (Bull. of Moscow University), no. 2, 1950, p. 29.

[2] In a certain sense Equation [7] may also be called an "empirical integral."

We shall agree to apply the term "twice interpolation averaged variant" of a given problem [1] to that problem, the differential equations of which are obtained from Equations [1] by replacing their true characteristic function H [2] with its twice interpolation averaged form $[H]$ [13 or 16].

Accordingly, these differential equations will be

$$\frac{d\xi_1}{dt} = \frac{\partial[H]}{\partial\eta_1} \qquad \frac{d\xi_2}{dt} = \frac{\partial[H]}{\partial\eta_2} \qquad \frac{d\xi_3}{dt} = \frac{\partial[H]}{\partial\eta_3}$$

$$\frac{d\eta_1}{dt} = -\frac{\partial[H]}{\partial\xi_1} \qquad \frac{d\eta_2}{dt} = -\frac{\partial[H]}{\partial\xi_2} \qquad \frac{d\eta_3}{dt} = -\frac{\partial[H]}{\partial\xi_3} \qquad [17]$$

Bearing in mind Equations [16 and 7], we can rewrite Equations [17] in the following form

$$\frac{d\xi_1}{dt} = \frac{\partial[H]}{\partial\eta_1} \qquad \frac{d\xi_2}{dt} = \frac{\partial[H]}{\partial\eta_2} \qquad \frac{d\xi_3}{dt} = \frac{\partial[H]}{\partial\eta_3}$$

$$\frac{d\eta_1}{dt} = -\frac{\partial[H]}{\partial\alpha_1}a_1^{(1)} \qquad \frac{d\eta_2}{dt} = -\frac{\partial[H]}{\partial\alpha_1}a_2^{(1)}$$

$$\frac{d\eta_3}{dt} = -\frac{\partial[H]}{\partial\alpha_1}a_3^{(1)} \qquad [18]$$

Here we can eliminate the quantity $(\partial[H])/(\partial\alpha_1)$ from the three equations of the second group. This leads to the following three equations in total differentials

$$\begin{vmatrix} d\eta_1 & d\eta_2 \\ a_1^{(1)} & a_2^{(1)} \end{vmatrix} = 0 \qquad \begin{vmatrix} d\eta_2 & d\eta_3 \\ a_2^{(1)} & a_3^{(1)} \end{vmatrix} = 0 \qquad \begin{vmatrix} d\eta_3 & d\eta_1 \\ a_3^{(1)} & a_1^{(1)} \end{vmatrix} = 0 \qquad [19]$$

Integrating these equations, we obtain the following three first integrals of the system of Equations [17]

$$\begin{vmatrix} \eta_1 & \eta_2 \\ a_1^{(1)} & a_2^{(1)} \end{vmatrix} = A_3 \qquad \begin{vmatrix} \eta_2 & \eta_3 \\ a_2^{(1)} & a_3^{(1)} \end{vmatrix} = A_1$$

$$\begin{vmatrix} \eta_3 & \eta_1 \\ a_3^{(1)} & a_1^{(1)} \end{vmatrix} = A_2 \qquad [20]$$

Of these three integrals only two are independent. The relationship between the constants

$$A_1, A_2, A_3 \qquad [21]$$

is given by the equation

$$A_1a_1^{(1)} + A_2a_2^{(1)} + A_3a_3^{(1)} = 0 \qquad [22]$$

which may be considered as describing the condition of perpendicularity of a vector $\mathbf{A}$ with the components [21] to a vector $\mathbf{a}^{(1)}$ with the components

$$a_1^{(1)}, a_2^{(1)}, a_3^{(1)} \qquad [23]$$

The geometrical form in the space of variables [6], corresponding to Equations [20] for our three first integrals of Equations [18] of the twice interpolation averaged problem, will be a straight line, for which the vector $\mathbf{a}^{(1)}$ with the components [23] will be the direction vector.

The geometrical form in the space of variables [5], corresponding to Equation [7], given the constancy of the interpolation element α_1, will be a plane, for which the vector $\mathbf{a}^{(1)}$ with the components [23] will be a normal vector.

Thus, on combining the three-dimensional coordinate system [5] with the three-dimensional coordinate system [6], the integral line [20] proves perpendicular to the plane [7] corresponding to a constant value of the interpolation element α_1.

Arbitrariness in the choice of the constants [21], only two of which are independent, makes possible the arbitrary displacement of the integral line [20] without changing its direction.

Finally, by virtue of the perpendicularity condition [22], the vector $\mathbf{A}$ with the components [21] proves parallel to the plane [7] corresponding to a constant value of the interpolation element α_1. Utilizing our freedom to choose the starting point of this vector, we may consider it located in the plane [7] of constant value of α_1.

To conclude this section, it can be pointed out that, should the characteristic function H [2] be independent of time, when in the unaveraged problem there exists the integral [3], an integral of the same form

$$[H][\alpha_1(\xi_1, \xi_2, \xi_3), \eta_1, \eta_2, \eta_3] = \text{const} \qquad [24]$$

will exist in the twice interpolation averaged variant of the problem also.

In this case knowledge of the three integrals, i.e., the integral [24] and the two independent integrals out of the three new linear integrals [20], enables us to proceed to the complete solution of Equations [17] of the twice interpolation averaged problem with the aid of quadratures.

2 Once Averaged Variant of the Canonical Problem

With the aid of an interpolation treatment, based on the method of least squares and the methods of linear correlation theory, we shall form the following two "interpolation elements"

$$\alpha_1 = a_1^{(1)}\xi_1 + a_2^{(1)}\xi_2 + a_3^{(1)}\xi_3$$

$$\alpha_2 = a_1^{(2)}\xi_1 + a_2^{(2)}\xi_2 + a_3^{(2)}\xi_3 \qquad [25]$$

from elements of the first group [5].[3] As before, the time interval and the intervals of variation of the elements of the first group will correspond to Equations [8 and 9].

Assuming that

$$\mathfrak{a}_{12} = \begin{vmatrix} a_1^{(1)} & a_2^{(1)} \\ a_1^{(2)} & a_2^{(2)} \end{vmatrix} \neq 0 \qquad [26]$$

from Equations [25] we determine the quantities ξ_1 and ξ_2

$$\xi_1 = \frac{1}{\mathfrak{a}_{12}}\begin{vmatrix} \alpha_1 & a_2^{(1)} \\ \alpha_2 & a_2^{(2)} \end{vmatrix} - \frac{\mathfrak{a}_{32}}{\mathfrak{a}_{12}}\xi_3$$

$$\xi_2 = \frac{1}{\mathfrak{a}_{12}}\begin{vmatrix} a_1^{(1)} & \alpha_1 \\ a_1^{(2)} & \alpha_2 \end{vmatrix} - \frac{\mathfrak{a}_{13}}{\mathfrak{a}_{12}}\xi_3 \qquad [27]$$

where

$$-\mathfrak{a}_{23} = \mathfrak{a}_{32} = \begin{vmatrix} a_3^{(1)} & a_2^{(1)} \\ a_3^{(2)} & a_2^{(2)} \end{vmatrix} \qquad \mathfrak{a}_{13} = \begin{vmatrix} a_1^{(1)} & a_3^{(1)} \\ a_1^{(2)} & a_3^{(2)} \end{vmatrix} \qquad [26a]$$

and substitute these expressions in the characteristic function H [2].

This gives

$$H = H[\xi_1(\alpha_1, \alpha_2, \xi_3), \xi_2(\alpha_1, \alpha_2, \xi_3), \xi_3, \eta_1, \eta_2, \eta_3, t] \qquad [28]$$

We shall form a once averaged expression for the characteristic function H [28] with respect to the variable ξ_3 over the interval [9] of its possible values with the aid of the relationship

$$[H] = \frac{1}{(\xi_{31} - \xi_{30})}\int_{\xi_3=\xi_{30}}^{\xi_{31}} H d\xi_3 \qquad [29]$$

In the process of integration the quantities

$$\alpha_1, \alpha_2, \eta_1, \eta_2, \eta_3, t \qquad [30]$$

are considered constant.

This "interpolation averaged" characteristic function $[H]$

[3] In a sense Equations [25] may also be called "empirical integrals."

[29] will be a function of the variables [30]

$$[H] = [H](\alpha_1, \alpha_2, \eta_1, \eta_2, \eta_3, t) \qquad [31]$$

Considering the "interpolation elements" α_1 and α_2 as intermediate variables, defined by Equations [25], we shall get this interpolation averaged characteristic function [29] in the following form

$$[H] = [H][\alpha_1(\xi_1, \xi_2, \xi_3), \alpha_2(\xi_1, \xi_2, \xi_3), \eta_1, \eta_2, \eta_3, t] \qquad [32]$$

We shall agree to apply the term "once interpolation averaged variant" of the given problem [1] to the problem, the differential equations of which are obtained from Equations [1] by replacing the characteristic function H [2] with its once interpolation averaged form [29 or 32].

Accordingly, these differential equations will be

$$\frac{d\xi_1}{dt} = \frac{\partial[H]}{\partial\eta_1} \qquad \frac{d\xi_2}{dt} = \frac{\partial[H]}{\partial\eta_2} \qquad \frac{d\xi_3}{dt} = \frac{\partial[H]}{\partial\eta_3}$$

$$\frac{d\eta_1}{dt} = -\frac{\partial[H]}{\partial\xi_1} \qquad \frac{d\eta_2}{dt} = -\frac{\partial[H]}{\partial\xi_2} \qquad \frac{d\eta_3}{dt} = -\frac{\partial[H]}{\partial\xi_3} \qquad [33]$$

or, on taking into account Equations [32 and 25]

$$\frac{d\xi_1}{dt} = \frac{\partial[H]}{\partial\eta_1} \qquad \frac{d\xi_2}{dt} = \frac{\partial[H]}{\partial\eta_2} \qquad \frac{d\xi_3}{dt} = \frac{\partial[H]}{\partial\eta_3}$$

$$\frac{\partial\eta_1}{dt} = -\frac{\partial[H]}{\partial\alpha_1}a_1^{(1)} - \frac{\partial[H]}{\partial\alpha_2}a_1^{(2)}$$

$$\frac{d\eta}{dt} = -\frac{\partial[H]}{\partial\alpha_1}a_2^{(1)} - \frac{\partial[H]}{\partial\alpha_2}a_2^{(2)}$$

$$\frac{d\eta_3}{dt} = -\frac{\partial[H]}{\partial\alpha_1}a_3^{(1)} - \frac{\partial[H]}{\partial\alpha_2}a_3^{(2)} \qquad [34]$$

Eliminating from the last three equations the two quantities $(\partial[H])/(\partial\alpha_1)$ and $(\partial[H])/(\partial\alpha_2)$ gives us the following equation in total differentials

$$\begin{vmatrix} d\eta_1 & d\eta_2 & d\eta_3 \\ a_1^{(1)} & a_2^{(1)} & a_3^{(1)} \\ a_1^{(2)} & a_2^{(2)} & a_3^{(2)} \end{vmatrix} = 0 \qquad [35]$$

Integrating, we find the following linear first integral of the system of differential equations of the once interpolation averaged problem [34]

$$\begin{vmatrix} \eta_1 & \eta_2 & \eta_3 \\ a_1^{(1)} & a_2^{(1)} & a_3^{(1)} \\ a_1^{(2)} & a_2^{(2)} & a_3^{(2)} \end{vmatrix} = \mathfrak{A} \qquad [36]$$

where $\mathfrak{A}$ is an arbitrary constant. This integral can be rewritten in the form

$$\mathfrak{a}_{23}\eta_1 + \mathfrak{a}_{31}\eta_2 + \mathfrak{a}_{12}\eta_3 = \mathfrak{A} \qquad [37]$$

with the foremention values of the constants

$$\mathfrak{a}_{23} \quad \mathfrak{a}_{31} \quad \mathfrak{a}_{12} \qquad [38]$$

The geometrical force in the space of the variables [5], corresponding to Equations [25 or 27], given the constancy of the interpolation elements α_1 and α_2, is a straight line, the direction vector of which $\vec{\mathfrak{a}}$ has as its components the quantities [38].

The geometrical form in the space of the variables [6], corresponding to Equation [36 or 37], describing the linear integral with arbitrary constant $\mathfrak{A}$, is a plane, the normal vector of which is the same vector $\vec{\mathfrak{a}}$ with the components [38].

On combining coordinate system [5] with coordinate system [6], the "interpolation line" [25 or 27] proves perpendicular to the "integral plane" [36 or 37].

Varying the arbitrary constant $\mathfrak{A}$ of the integral [36 or 37] involves the displacement of the "integral plane" without its ceasing to be perpendicular to the "interpolation line."

To conclude this section, it may be pointed out that the "interpolation line" [25], instead of being determined from the two equations [25], may be determined from a combination of three equations, equivalent to this pair and having the form

$$\begin{vmatrix} \xi_1 & \xi_2 \\ \mathfrak{a}_{23} & \mathfrak{a}_{31} \end{vmatrix} = \mathfrak{a}_3 \qquad \begin{vmatrix} \xi_2 & \xi_3 \\ \mathfrak{a}_{31} & \mathfrak{a}_{12} \end{vmatrix} = \mathfrak{a}_1 \qquad \begin{vmatrix} \xi_3 & \xi_1 \\ \mathfrak{a}_{12} & \mathfrak{a}_{23} \end{vmatrix} = \mathfrak{a}_2 \qquad [39]$$

where the following notation is employed

$$\mathfrak{a}_1 = \begin{vmatrix} a_1^{(1)} & \alpha_1 \\ a_1^{(2)} & \alpha_2 \end{vmatrix} \qquad \mathfrak{a}_2 = \begin{vmatrix} a_2^{(1)} & \alpha_1 \\ a_2^{(2)} & \alpha_2 \end{vmatrix} \qquad \mathfrak{a}_3 = \begin{vmatrix} a_3^{(1)} & \alpha_1 \\ a_3^{(2)} & \alpha_2 \end{vmatrix} \qquad [40]$$

3 General Formulation of the Results

Considering the contents of the foregoing two sections and remembering that we can exchange the roles of the first and second groups of canonical variables without affecting the results obtained in the foregoing, we may formulate the following two general theorems relating to the connection between the method of linear interpolation averaging and the integrals of the canonical interpolation averaged problem obtained by such averaging.

Theorem 1. The double linear interpolation averaging of the characteristic function along a certain interpolation plane in the space of the first (second) group of canonical variables necessitates the existence of two integrals, linear in relation to the canonical variables of the second (first) group, corresponding to a two-parameter family of mutually parallel integral lines in the space of this second (first) group of variables, these integral lines being conditionally orthogonal to the interpolation plane employed.

Theorem 2. The single linear interpolation averaging of the characteristic function along a certain interpolation line in the space of the second (first) group of canonical variables necessitates the existence of a single integral, linear in relation to the canonical variables of the first (second) group, corresponding to a one-parameter family of mutually parallel integral planes in the space of this first (second) group of variables, these integral planes being conditionally orthogonal to the interpolation line employed.

Footnote: The expression "conditional orthogonality" as used here has the sense of orthogonality for a conditional combination of the coordinate system corresponding to the first group of canonical variables with the coordinate system corresponding to the second group of these variables.

In conclusion, note that all of the foregoing are related to a canonical system of the sixth order. It is obvious that analogous results may be obtained in the same way for a canonical system of any order. There is no need to discuss the details here.

Complete Averaging of Canonical Problem of Celestial Mechanics With Several Intermediate Elements

N. D. MOISEYEV

Introduction

THE PRESENT article is one part of our series of papers devoted to the examination of simplified variants of celestial mechanics problems, obtained with the aid of averaging. This article is most closely related to the group of papers concerning the so-called "interpolation averaging" variants of celestial mechanics problems.

1 Complete Averaging of Canonical Problem With Several Intermediate Elements

Let there be given a canonical problem with a system of equations with motion in the following form

$$\frac{d\xi_k}{dt} = \frac{\partial H}{\partial \eta_k} \qquad \frac{d\eta_k}{dt} = -\frac{\partial H}{\partial \xi_k} \qquad k = 1, 2, \ldots n \quad [1]$$

where

$$H = H(\xi_1 \ldots \xi_n, \eta_1 \ldots \eta_n, t) \quad [2]$$

In some particular cases, the time t may not enter into the characteristic function [2].

Let there be specified, furthermore, a definite number m of function ζ_l of the canonical variables (or canonical elements) of the given problem

$$\zeta_l = \zeta_l(\xi_1 \ldots \xi_n, \eta_1 \ldots \eta_n) \qquad l = 1, 2, \ldots m \quad [3]$$

We shall henceforth call these quantities ζ_l "intermediate elements."

We break up the complete system of $2n$ canonical elements of the problem

$$\xi_1, \xi_2 \ldots \xi_n, \eta_1, \eta_2 \ldots \eta_n \quad [4]$$

into two groups. One of these, including certain m of the canonical elements

$$\xi_1, \xi_2 \ldots \xi_{m'} \; \eta_1, \eta_2 \ldots \eta_{m''} \qquad m' + m'' = m \quad [5]$$

we shall call the "main group." The second group, consisting of $2n - m$ remaining canonical elements

$$\xi_{m'+1} \ldots \zeta_n \; \eta_{m''+1} \ldots \eta_n \quad [6]$$

we shall call the "supplementary group."

Let us solve Equation [3] with respect to the "main" canonical elements. This yields

$$\xi_{k'} = \xi_{k'}(\zeta_1 \ldots \zeta_m, \xi_{m'+1} \ldots \xi_n, \eta_{m''+1} \ldots \eta_n) \qquad k' = 1, 2, \ldots m'$$
$$\eta_{k''} = \eta_{k''}(\zeta_1 \ldots \zeta_m, \xi_{m'+1} \ldots \xi_n, \eta_{m''+1} \ldots \eta_n) \qquad k'' = 1, 2, \ldots m'' \quad [7]$$

We eliminate with the aid of these formulas the "main" canonical elements from the characteristic function [2]. The results of such an elimination will be denoted by symbol

$$H^* = H^*(\zeta_1 \ldots \zeta_m, \xi_{m'+1} \ldots \xi_n, \eta_{m''+1} \ldots \eta_n, t) \quad [8]$$

This transformed characteristic function H^* is averaged over all the "supplementary" canonical elements [6] in a certain specified region of their values

$$\underline{\xi}_{k'} \leqslant \xi_{k'} \leqslant \bar{\xi}_{k'} \qquad k' = m' + 1 \ldots n$$
$$\underline{\eta}_{k''} \leqslant \eta_{k''} \leqslant \bar{\eta}_{k''} \qquad k'' = m'' + 1 \ldots n \quad [9]$$

This averaging is performed with the aid of the formula

$$\bar{H} = \frac{1}{\prod_{k'=m'+1}^{n} (\bar{\xi}_{k'} - \underline{\xi}_{k'}) \prod_{k''=m''+1}^{n} (\bar{\eta}_{k''} - \underline{\eta}_{k''})} \int_{\xi_{m'+1}=\underline{\xi}_{m'+1}}^{\bar{\xi}_{m'+1}} \cdots \int_{\eta_n=\underline{\eta}_n}^{\bar{\eta}_n} H^* d\xi_{m'+1} \ldots d\eta_n \quad [10]$$

subject to the following three conditions:

1 The intermediate elements [3] are considered constant during the process of integration.

2 The quantity t is considered constant during the process of integration.

3 The "supplementary" canonical variables [6], over which the averaging is performed, are treated in the process of integration as variables that are independent of each other.

This averaging of the characteristic function will be called complete averaging with m intermediate elements [3].

The "completely averaged" characteristic function $\bar{H}$ thus obtained will depend only on the m intermediate elements [3] and on the time t

$$\bar{H} = \bar{H}(\zeta_1 \ldots \zeta_m, t) \quad [11]$$

Considering now the intermediate elements [3] as indeed the intermediate variables, the completely averaged characteristic function $\bar{H}$ will henceforth be considered as depending on all canonical elements [4] through the intermediate elements [3]

$$\bar{H} = \bar{H}[\zeta_1(\xi_1 \ldots \xi_n, \eta_1 \ldots \eta_n) \ldots \zeta_m(\xi_1 \ldots \eta_n, t), t] \quad [12]$$

We now set up a system of canonical differential equations, obtained from system [1] by substituting for the true characteristic function H the result $\bar{H}$ obtained by complete averag-

Translated from *Contributions of the State Astronomical Institute of P. K. Sternberg*, vol. 24, 1954, pp. 10–16. Translated by J. George Adashko.

ing. We have

$$\frac{d\xi_k}{dt} = \frac{\partial \tilde{H}}{\partial \eta_k} \qquad \frac{d\eta_k}{dt} = -\frac{d\tilde{H}}{\partial \xi_k} \qquad k = 1, 2, \ldots n \quad [13]$$

The problem presented by this system of equations [13] will be called the simplified version of the given problem [1], obtained by complete averaging with m intermediate elements [3].

In expanded form, Equations [13] can be written as follows

$$\frac{d\xi_k}{dt} = \sum_{l=1}^{m} \frac{\partial \tilde{H}}{\partial \zeta_l} \frac{\partial \zeta_l}{\partial \eta_k} \qquad \frac{d\eta_k}{dt} = -\sum_{l=1}^{m} \frac{\partial \tilde{H}}{\partial \zeta_l} \frac{\partial \zeta_l}{\partial \xi_k}$$
$$k = 1, 2, \ldots n$$
$$\ldots\ldots\ldots\ldots\ldots\ldots\ldots\ldots\ldots\ldots\ldots\ldots\ldots\ldots\ldots\ldots [14]$$

2 Certain Particular Types of Intermediate Elements and of Their Characteristic Function

An analysis of certain particular forms of the intermediate elements is of certain interest. Worthy of attention among these particular forms is primarily the case of linear intermediate elements, when Equation [3] has the following particular form

$$\zeta_l = \sum_{k=1}^{n} (r_{lk}\xi_k + s_{lk}\eta_k) \qquad l = 1, 2, \ldots m \quad [15]$$

where

$$r_{lk} \qquad s_{lk} \quad [16]$$

are specified numbers.

For these linear intermediate elements, the system of equations of the completely averaged problem [14] assumes the following simple form

$$\frac{d\xi_k}{dt} = \sum_{l=1}^{m} \frac{\partial \tilde{H}}{\partial \zeta_l} s_{lk} \qquad \frac{d\eta_k}{dt} = -\sum_{l=1}^{m} \frac{\partial \tilde{H}}{\partial \zeta_l} r_{lk} \qquad k =$$
$$1, 2, \ldots n$$
$$\ldots\ldots\ldots\ldots\ldots\ldots\ldots\ldots\ldots\ldots\ldots\ldots\ldots\ldots\ldots\ldots [17]$$

Another of the more common particular forms of intermediate elements worthy of attention is

$$\zeta_l = \sum_{k=1}^{n} [f_{lk}(\xi_k) + g_{lk}(\eta_k)] \qquad l = 1, 2, \ldots m \quad [18]$$

where

$$f_{lk}(\xi_k) \qquad g_{lk}(\eta_k) \quad [19]$$

are specified functions of the indicated arguments, which may be, for example, algebraic polynomials, etc.

As to the dependence of the completely averaged characteristic function $\tilde{H}$ on the intermediate elements [3], the following particular cases are worthy of interest.

a In the first of these special elements the function $\tilde{H}$ is determined by the formula

$$\tilde{H} = \tilde{H}(\tilde{\tilde{H}}, t) \quad [20]$$

where the auxiliary function $\tilde{\tilde{H}}$ is independent of the time t

$$\tilde{\tilde{H}} = \tilde{\tilde{H}}(\zeta_1 \ldots \zeta_m) \quad [21]$$

b The second interesting special case is one in which $\tilde{H}$ is determined by the formula

$$\tilde{H} = \sum_{l=1}^{m} \tilde{H}_l \quad [22]$$

and each of the partial functions $\tilde{H}$ depends only on one intermediate element that corresponds to it in number, and possibly on t

$$\tilde{H}_l = \tilde{H}_l(\zeta_l, t) \quad [23]$$

Even simpler modifications of cases "a" and "b" respectively are the following cases:

a′ in which

$$\tilde{H} = \tilde{H}(\zeta_1 \ldots \zeta_m) \quad [24]$$

b′ in which

$$\tilde{H} = \sum_{l=1}^{m} \tilde{H}_l(\zeta_l) \quad [25]$$

3 Differential Equations for Intermediate Elements and Their Integration in Particular Cases

Calculating the total derivatives with respect to time of the intermediate elements [3] with the aid of the differential Equations [14] of the completely averaged problems, the following system of differential equations is obtained for the intermediate elements

$$\frac{d\zeta_l}{dt} = \sum_{k=1}^{n} \sum_{\lambda=1}^{m} \frac{\partial \tilde{H}}{\partial \zeta_\lambda} \left[\frac{\partial \zeta_l}{\partial \xi_k} \frac{\partial \zeta_\lambda}{\partial \eta_k} - \frac{\partial \zeta_l}{\partial \eta_k} \frac{\partial \zeta_\lambda}{\partial \xi_k} \right]$$
$$l = 1, \ldots m \quad [26]$$

We consider several particular cases, in which integrals of Equations [26] can be obtained.

In the first particular case there is only one intermediate element, one with $m = 1$. Then the system [26] yields for this single intermediate element ζ_1 the equation

$$(d\zeta_1/dt) = 0 \quad [27]$$

This yields the integral

$$\zeta_1(\xi_1 \ldots \xi_n, \eta_1 \ldots \eta_n) = \zeta_{10} = \text{const} \quad [28]$$

In the particular case when the completely averaged characteristic function $\tilde{H}$ is independent of the time t, i.e., case [24], this integral [28] is equivalent to the energy integral applicable to that case

$$\tilde{H}(\zeta_1) = \text{const} \quad [29]$$

We now consider the case of an arbitrary number of intermediate elements, and assume that the completely averaged characteristic function is represented by an equation of the form [20]. Now the equation for the auxiliary function $\tilde{\tilde{H}}$ becomes

$$\frac{d\tilde{\tilde{H}}}{dt} = \frac{\partial \tilde{H}}{\partial \tilde{\tilde{H}}} \sum_{k=1}^{n} \sum_{l=1}^{m} \sum_{\lambda=1}^{m} \frac{\partial \tilde{\tilde{H}}}{\partial \zeta_l} \frac{\partial \tilde{\tilde{H}}}{\partial \zeta_\lambda} \left[\frac{\partial \zeta_l}{\partial \xi_k} \frac{\partial \zeta_\lambda}{\partial \eta_k} - \frac{\partial \zeta_l}{\partial \eta_k} \frac{\partial \zeta_\lambda}{\partial \xi_k} \right] = 0 \quad [30]$$

leading to the integral

$$\tilde{\tilde{H}}(\zeta_1 \ldots \zeta_m) = \text{const} \quad [31]$$

If the completely averaged characteristic function is independent of the time, i.e., case [24], this integral [31] coincides with the energy integral for the completely averaged problem.

We now consider the particular case of linear intermediate elements [15]. The differential equations [26] for the intermediate elements then assume the form

$$\frac{d\zeta_l}{dt} = \sum_{\lambda=1}^{m} R_{l\lambda} \frac{\partial H}{\partial \zeta_\lambda} \qquad l = 1, 2, \ldots m \quad [32]$$

where

$$R_{l\lambda} = \sum_{k=1}^{n} (r_{lk}s_{\lambda k} - s_{lk}r_{\lambda k}) \qquad [33]$$

are numerical constants.

Equations [32] are linear in the intermediate elements if the completely averaged characteristic function $\bar{H}$ is a quadratic form in the intermediate elements themselves.

4 Integration of the Differential Equations for Canonical Elements in Certain Particular Cases

The system of differential equations [14] for the canonical elements of the completely averaged problem can be completely or partially integrated in final form in some particular cases.

Such a case, for example, is that of complete averaging with a single intermediate element, if this intermediate element itself is a linear function of the canonical variables. Specifically, $m = 1$ and when Equation [15] applies, Equations [14] become

$$\frac{d\xi_k}{dt} = \frac{\partial \bar{H}(\zeta_1, t)}{\partial \zeta_1} s_{1k} \qquad \frac{d\eta_k}{dt} = -\frac{\partial \bar{H}(\zeta_1, t)}{\partial \zeta_1} r_{1k}$$

$$k = 1, 2, \ldots n$$

.....[34]

Given the integral [28], the right halves of these equations become known functions of the time, so that the integration of the system can be readily brought to a conclusion.

In the somewhat more complicated case when $m = 1$ and the intermediate element is defined by Equation [18], the system [14] becomes

$$\frac{d\xi_k}{dt} = \frac{\partial \bar{H}(\zeta_1, t)}{\partial \zeta_1} g_{1k}'(\eta_k) \qquad \frac{d\eta_k}{dt} = -\frac{\partial \bar{H}(\zeta_1, t)}{\partial \zeta_1} f_{1k}'(\xi_k)$$

$$k = 1, 2, \ldots n$$

.....[35]

This leads to the following system of n total differential equations

$$f_{1k}'(\xi_k)d\xi_k + g_{1k}'(\eta_k)d\eta_k = 0 \qquad k = 1, 2, \ldots n \qquad (36]$$

which yield the following aggregate of n first integrals of the problem

$$f_1(\xi_k) + g_{1k}(\eta_k) = C_k \qquad k = 1, 2, \ldots n \qquad [37]$$

This permits integration of Equation [35] in quadratures.

We now turn to the case when the number of intermediate elements is greater than one. Assuming these elements to be linear and defined by Equation [15], the system of differential equations for the canonical elements will have in this case the form [17]. If the number of intermediate elements m is less than $2n$, total number of canonical variables, elimination of the m quantities

$$\frac{\partial \bar{H}}{\partial \zeta_1}, \frac{\partial \bar{H}}{\partial \zeta_2}, \ldots \frac{\partial \bar{H}}{\partial \zeta_m} \qquad [38]$$

leads to $(2n - m)$ independent homogeneous equations, with constant coefficients, in the time derivatives of the canonical elements. Integration of these equations yields the following aggregate of $(2n - m)$ first integrals of the problem. These intervals are linear in the canonical elements

$$\begin{vmatrix} \xi_1 & -s_{11} \ldots & -s_{m1} \\ \ldots & \ldots & \ldots \\ \xi_{m'} & -s_{1m'} \ldots & -s_{mm'} \\ \eta_1 & r_{11} \ldots & r_{m1} \\ \ldots & \ldots & \ldots \\ \eta_{m''} & r_{1m''} \ldots & r_{mm''} \\ \xi_{k'} & -s_{1k'} \ldots & -s_{mk'} \end{vmatrix} = C_{k'}$$

$$k' = m' + 1, \ldots n \qquad [39']$$

$$\begin{vmatrix} \xi_1 & -s_{11} \ldots & -s_{m1} \\ \ldots & \ldots & \ldots \\ \xi_{m'} & -s_{1m} \ldots & -s_{mm'} \\ \eta_1 & r_{11} \ldots & r_{m1} \\ \ldots & \ldots & \ldots \\ \eta_{m''} & r_{1m''} \ldots & r_{mm''} \\ \eta_{k''} & r_{1k''} \ldots & r_{mk''} \end{vmatrix} = C_{k''}$$

$$k'' = m'' + 1, \ldots n \qquad [39'']$$

with $m' + m'' = m$.

The same integrals can be rewritten in the form

$$\sum_{q=1}^{m'} R_{q1}(k')\xi_q + \sum_{q=m'+1}^{m} R_{q1}(k')\eta_q + R_{m+1,1}(k')\xi_{k'} = C_{k'}$$

$$k' = m' + 1 \ldots n$$

.....[40]

and

$$\sum_{q=1}^{m'} S_{q1}(k'')\xi_q + \sum_{q=m'+1}^{m} S_{q1}(k'')\eta_q + S_{m+1,1}(k'')\eta_{k''} = C_{k''}$$

$$k'' = m'' + 1 \ldots n$$

.....[40'']

where

$$R_{q1}(k') \qquad S_{q1}(k'') \qquad [41]$$

are numerical constants, while $C_{k'}$ and $C_{k''}$ are arbitrary constants.

Knowledge of these $(2n - m)$ integrals reduces the order of the system of equations for the canonical elements from $2n$ to m. If the characteristic function is found to be independent of the time after complete averaging, the system of equations for the canonical elements can be integrated in quadratures whenever the number $(2n - m)$ of integrals [40] is not less than n, i.e., whenever $m \leq n$.

Reviewer's Comment

In this paper the author continues the application of his "averaging" procedures to the disturbing function. The basic procedures involved are the same ones as described in the preceding paper (p. 387). It seems that in the present paper these averaging procedures are applied to the fullest possible extent, in particular to the canonic form of the differential equations of motion, and to the related characteristic function.

Again it appears that the results are of interest for actual application to such problems where a simplified and approximate derivation of certain characteristic features of the orbital motion is desired. The principles involved are simple, and the main contents consist (when compared with the earlier publications by the same author on the averaging procedures in celestial mechanics) in the repeated application of the same principles to different forms of the differential equations and of the disturbing function, rather than in new approaches as such.

—Eugene K. Rabe
Dept. of Astronomy
University of Cincinnati

Averaged Variants of a Semirestricted Planar Problem of Three Bodies[1]

N. D. MOISEYEV

THE PURPOSE of this work is the exposition of those fundamental simplified variants of an unrestricted problem of three bodies which are obtained from it by certain averaging.

The ways of averaging an unrestricted disturbing function which we are considering, are analogous to those considered and systematized in our previous articles devoted to averaged variants of a restricted problem of three-body masses. Therefore, the contents and structure of the present work are analogous to those of the articles mentioned. The full analogy is disturbed only by the specific difference between an unrestricted and a restricted problem. In the first place, the distinction between the circular and elliptical variants is no longer essential, as it was in the restricted problem. Further, the formal distinction between the internal and external variants of averaged schemes is not necessary. However, considerations in the selection of an averaging variant, which results in a great degree of correspondence between the averaged and unaveraged schemes, remain in force.

Before proceeding further with averaged variants of the unrestricted problem, we shall begin with the consideration of the same question for a simpler semirestricted problem of three-body masses. The semirestricted problem is obtained from the original unrestricted problem by eliminating the so-called indirect term from the disturbing function. It is equivalent to the following: The sun P_0 moves under the gravitational attraction of planets P_1 and P_2, but is considered motionless relative to the barycentric reference system. This implies that the sun has no acceleration relative to the absolute reference system.

The second simplification which we introduce in the formulation of a semirestricted problem of three bodies consists in the following. In the true unrestricted problem, basic parts of the disturbing function describing heliocentric motion of planets P_1, P_2 contain masses $m_0 + m_1$, and $m_0 + m_2$. However, in the simplified variant the mass of the stationary sun P_0 which replaced the true sun is taken equal to m_0 in both disturbing functions.

Despite these two simplifications a semirestricted problem of three bodies does not seem to be lacking in interest and practical value in problems of celestial mechanics.

When the present work was discussed at the meeting of the faculty of celestial mechanics of the Moscow State University, it was noted that such a problem can be of interest as an intermediate approximate scheme for satellite problems such as "sun-Earth-moon" (G. N. Duboshin's remark), and for the problem of a double star in the gravitational field of the center of Galaxy (B. M. Shchegolev's remark).

For the problem of motion of an asteroid or a comet influenced by the sun's attraction, the semirestricted problem seems to be of smaller value than the genuine restricted problem of three bodies. (This fact was noted by Duboshin and Shchegolev.)

The significance of a semirestricted problem for the theory of motion of two large mutually gravitating planets attracted by the sun is not obvious, although it is greater than that of a restricted problem of three bodies.

1 Fundamental Equations of the Semirestricted Planar Problem of Three Bodies

By the semirestricted problem of three bodies we mean the problem of motion of two mutually attracting bodies P_1 and P_2 in the gravitational field of one motionless attracting center P_0.

If the masses of the bodies P_0, P_1 and P_2 are designated respectively by m_0, m_1 and m_2, and the nonattracted body P_0 is placed in the origin of coordinates (x, y), then, for the planar problem, we have the following differential equations of motion

$$\begin{aligned} m_1\ddot{x}_1 &= -k^2\frac{m_1m_0}{r_1^3}x_1 - k^2\frac{m_1m_2}{r_{12}^3}(x_1 - x_2) \\ m_1\ddot{y}_1 &= -k^2\frac{m_1m_0}{r_1^3}y_1 - k^2\frac{m_1m_2}{r_{12}^3}(y_1 - y_2) \end{aligned} \quad \ldots\ldots [1.1]$$

$$\begin{aligned} m_2\ddot{x}_2 &= -k^2\frac{m_2m_0}{r_2^3}x_2 - k^2\frac{m_1m_2}{r_{12}^3}(x_2 - x_1) \\ m_2\ddot{y}_2 &= -k^2\frac{m_2m_0}{r_2^3}y_2 - k^2\frac{m_1m_2}{r_{12}^3}(y_2 - y_1) \end{aligned} \quad \ldots\ldots [1.2]$$

where (x_1, y_1) and (x_2, y_2) are the coordinates of the moving bodies P_1 and P_2 respectively; r_1 and r_2, their distances from the attracting body P_0

$$\begin{aligned} r_1 &= \sqrt{x_1^2 + y_1^2} \\ r_2 &= \sqrt{x_2^2 + y_2^2} \end{aligned} \quad \ldots\ldots [2]$$

and

$$r_{12} = r_1^2 + r_2^2 - 2r_1r_2\cos\vartheta \qquad [3]$$

is the relative distance between bodies P_1 and P_2, where

$$\vartheta = l_2 - l_1 \qquad [4]$$

is either the difference of longitudes l_2 and l_1 of the bodies P_2 and P_1, or the angle between directions from body P_0 to P_1 and P_2.

The system of equations [1] can be rewritten as follows

$$\begin{aligned} m_1\ddot{x}_1 &= -k^2\frac{m_1m_0}{r_1^3}x_1 + m_1\frac{\partial W_1}{\partial x_1} \\ m_1\ddot{y}_1 &= -k^2\frac{m_1m_0}{r_1^3}y_1 + m_1\frac{\partial W_1}{\partial y_1} \end{aligned} \quad \ldots\ldots [5.1]$$

$$\begin{aligned} m_2\ddot{x}_2 &= -k^2\frac{m_2m_0}{r_2^3}x_2 + m_2\frac{\partial W_2}{\partial x_2} \\ m_2\ddot{y}_2 &= -k^2\frac{m_2m_0}{r_2^3}y_2 + m_2\frac{\partial W_2}{\partial y_2} \end{aligned} \quad \ldots\ldots [5.2]$$

Translated from *Contributions of the State Astronomical Institute of P. K. Sternberg*, vol. 21, 1952, pp. 3–18. Translated by Alexander G. Godlevsky.

[1] This paper is Part 1 of "Some Fundamental Simplified Schemes of Celestial Mechanics Obtained by Averaging an Unrestricted Problem of Three Bodies," by the author.

where

$$W_1 = k^2 m_2 \times (1/r_{12}) \qquad [6.1]$$

$$W_2 = k^2 m_1 \times (1/r_{12}) \qquad [6.2]$$

$$W_2 = (m_1/m_2) W_1 \qquad [6.3]$$

are the disturbing functions for the first and second bodies P_1 and P_2.

The elimination of terms with disturbing functions in Equations [5] leads to differential equations of undisturbed motion which will be Keplerian for each of the bodies P_1 and P_2 around the motionless attracting center P_0. If we introduce in the usual manner the osculating Keplerian elements—semimajor axis a, parameter p, longitude of perihelion ω, and Keplerian variable M = mean anomaly—we obtain for the motion in the Keplerian phase space

$$K_4\begin{pmatrix} a_1, & p_1, & M_1, & \omega_1 \\ a_2, & p_2, & M_2, & \omega_2 \end{pmatrix} \qquad [7]$$

the following differential equations

$$\frac{da_1}{dt} = \frac{2\sqrt{a_1}}{k\sqrt{m_0}} \frac{\partial W_1}{\partial M_1}$$

$$\frac{dp_1}{dt} = \frac{2\sqrt{p_1}}{k\sqrt{m_0}} \frac{\partial W_1}{\partial \omega_1}$$

$$\frac{dM_1}{dt} = \frac{k\sqrt{m_0}}{a_1^{3/2}} - \frac{2\sqrt{a_1}}{p\sqrt{m_0}} \frac{\partial W_1}{\partial a_1}$$

$$\frac{d\omega_1}{dt} = -\frac{2\sqrt{p_1}}{k\sqrt{m_0}} \frac{\partial W_1}{\partial p_1}$$

..... [8.1]

$$\frac{da_2}{dt} = \frac{2\sqrt{a_2}}{k\sqrt{m_0}} \frac{\partial W_2}{\partial M_2}$$

$$\frac{dp_2}{dt} = \frac{2\sqrt{p_2}}{k\sqrt{m_0}} \frac{\partial W_2}{\partial \omega_2}$$

$$\frac{dM_2}{dt} = \frac{k\sqrt{m_0}}{a_2^{3/2}} - \frac{2\sqrt{a_2}}{k\sqrt{m_0}} \frac{\partial W_2}{\partial a_2}$$

$$\frac{d\omega_2}{dt} = -\frac{2\sqrt{p_2}}{k\sqrt{m_0}} \frac{\partial W_2}{\partial p_2}$$

..... [8.2]

This system of equations, of the eighth order, and systems [5 and 1], possesses two integrals: The integral of areas and the integral of energy. In rectangular coordinates, i.e., for the system [1], these integrals are obtained in the usual manner and have the following form

$$m_1(x_1\dot{y}_1 - y_1\dot{x}_1) + m_2(x_2\dot{y}_2 - y_2\dot{x}_2) = P \qquad [9]$$

and

$$\frac{1}{2} m_1(\dot{x}_1^2 + \dot{y}_1^2) + \frac{1}{2} m_2(\dot{x}_2^2 + \dot{y}_2^2) = k^2 \times \left(\frac{m_1 m_0}{r_1} + \frac{m_2 m_0}{r_2} + \frac{m_1 m_2}{r_{12}}\right) + H \qquad [10]$$

respectively, where P and H are arbitrary constants.

For the derivation of the same integrals in Keplerian phase coordinates [7], we note first that the disturbing functions W_1 and W_2 depend on the longitudes of the perihelia ω_1 and ω_2 only through the angle ϑ which, according to the formula

$$\vartheta = (v_2 - v_1) + (\omega_2 - \omega_1) = (v_2 - v_1) + \omega \qquad [11]$$

contains only the difference of longitudes $\omega = (\omega_2 - \omega_1)$, but not the longitudes themselves.

Therefore, the following holds

$$m_1 \frac{\partial W_1}{\partial \omega_1} = -m_2 \frac{\partial W_2}{\partial \omega_2} \qquad [12]$$

Introducing in Equation [12] the expression for $(\partial W_1/\partial \omega_1)$ and $(\partial W_2/\partial \omega_2)$ from the second equations of the subsystems [8.1 and 8.2], we obtain an equation in total differentials

$$\frac{m_1 k\sqrt{m_0}}{2\sqrt{p_1}}\, dp_1 + \frac{m_2 k\sqrt{m_0}}{2\sqrt{p_2}}\, dp_2 = 0 \qquad [13]$$

which, after integration, gives us the integral of areas

$$k m_1\sqrt{m_0}\sqrt{p_1} + k m_2\sqrt{m_0}\sqrt{p_2} = p' \qquad [14.1]$$

or

$$m_1\sqrt{p_1} + m_2\sqrt{p_2} = P \qquad [14.2]$$

To obtain the energy integral in Keplerian phase coordinates [7], we form the total time derivative of the disturbing functions W_1 and W_2 using differential equations [8]. Thus, we have

$$\frac{\partial W_1}{dt} = \frac{\partial W_1}{\partial a_1}\frac{da_1}{dt} + \frac{\partial W_1}{\partial p_1}\frac{dp_1}{dt} + \frac{\partial W_1}{\partial M_1}\frac{dM_1}{dt} + \frac{\partial W_1}{\partial \omega_1}\frac{\omega_1}{dt} + \frac{\partial W_1}{\partial a_2}\frac{da_2}{dt} + \frac{\partial W_1}{\partial p_2}\frac{dp_2}{dt} + \frac{\partial W_1}{\partial M_2}\frac{dM_2}{dt} + \frac{\partial W_1}{\partial \omega_2}\frac{d\omega_2}{dt} =$$

$$\frac{\partial W_1}{\partial M_1}\frac{k\sqrt{m_0}}{a_1^{3/2}} + \frac{\partial W_1}{\partial M_2}\frac{k\sqrt{m_0}}{a_2^{3/2}} + \left(\frac{\partial W_1}{\partial a_2}\frac{\partial W_2}{\partial M_2} - \frac{\partial W_1}{\partial M_2}\frac{\partial W_2}{\partial a_2}\right)\frac{2\sqrt{a_2}}{k\sqrt{m_0}} + \left(\frac{\partial W_1}{\partial p_2}\frac{\partial W_2}{\partial \omega_2} - \frac{\partial W_1}{\partial \omega_2}\frac{\partial W_2}{\partial p_2}\right)\frac{2\sqrt{p_2}}{k\sqrt{m_0}} \qquad [15]$$

Further, making use of relation [6.3] between the disturbing functions W_1 and W_2, we obtain

$$\frac{dW_1}{dt} = \frac{\partial W_1}{\partial M_1}\frac{k\sqrt{m_0}}{a_1^{3/2}} + \frac{m_2}{m_1}\frac{\partial W_2}{\partial M_2}\frac{k\sqrt{m_0}}{a_2^{3/2}} \qquad [16]$$

Employing now the partial derivatives of disturbing functions with respect to mean anomalies from the first equations of the subsystems [8.1 and 8.2], we obtain an equation in total derivatives

$$\frac{dW_1}{dt} = \frac{k^2 m_0}{2a_1^2}\frac{da_1}{dt} + \frac{m_2}{m_1}\frac{k^2 m_0}{2a_2^2}\frac{da_2}{dt} \qquad [17]$$

Integrating this equation we obtain the desired energy integral in either of the two following forms

$$\frac{k^2 m_0}{2a_1} + \frac{m_2}{m_1}\frac{k^2 m_0}{2a_2} + W_1 = H'$$

or

$$\frac{k^2 m_0 m_1}{2a_1} + \frac{k^2 m_0 m_2}{2a_2} + m_1 W_1 = H \qquad [18.1]$$

By the application of formula [6.3] the same integral can be expressed also as follows

$$\frac{k^2 m_0 m_1}{2a_1} + \frac{k^2 m_0 m_2}{2a_2} + m_2 W_2 = H \qquad [18.2]$$

This could have been obtained by a direct calculation which starts with the formation of the total time derivative of the disturbing function W_2. In the formulas [18], H designates the constant of integration.

In addition to this, the following can be noted. From the integral of areas [14.2] we have

$$\sqrt{p_1} = \frac{P}{m_1} - \frac{m_2}{m_1}\sqrt{p_2} \qquad [14.3]$$

Consequently, variables p_1 and p_2 entering the disturbing function W_1 of our problem are not independent. It can be assumed that of these two parameters only p_2 is independent. The dependence of W_1 on p_2 occurs in two ways: p_2 enters the disturbing function directly as well as through p_1 determined by Equation [14.3]. Consequently we replace p_1 in the disturbing function W_1 by the expression [14.3]. We denote this result by $(W_1)_p$.

Then, the total partial derivative of the function $(W_1)_p$, with respect to p_2, will be expressed through partial derivatives of W_1 with respect to parameters p_1 and p_2 as follows

$$\frac{\partial(W_1)_p}{\partial p_2} = \frac{\partial W_1}{\partial p_2} + \frac{\partial W_1}{\partial p_1}\frac{dp_1}{dp_2} = \frac{m_2}{m_1}\frac{\partial W_2}{\partial p_2} + \frac{\partial W_1}{\partial p_1}\left(-\frac{m_2}{m_1}\frac{\sqrt{p_1}}{\sqrt{p_2}}\right) \qquad [19]$$

Introducing in [19] the expressions for partial derivatives $\partial W_1/\partial p_1$ and $\partial W_2/\partial p_2$ from the last equation of the subsystems [8.1 and 8.2], we obtain

$$\frac{\partial(W_1)_p}{\partial p_2} = -\frac{m_2}{m_1} \times \frac{k\sqrt{m_0}}{2\sqrt{p_2}}\frac{d\omega_2}{dt} + \frac{m_2}{m_1}\frac{k\sqrt{m_0}}{2\sqrt{p_1}} \times \frac{\sqrt{p_1}}{\sqrt{p_2}}\frac{d\omega_1}{dt}$$

or

$$\frac{d\omega}{dt} = -\frac{2\sqrt{p_2}}{k\sqrt{m_0}}\frac{\partial(W_2)_p}{\partial p_2} \qquad [20]$$

$$\omega = \omega_2 - \omega_1$$

Equation [20] can be considered as one of the equations of the system [8]. It can also be assumed that the last equations of subsystems [8.1 and 8.2] have been separated from system [8]. These separated equations are to be integrated following the integration of the remaining equations which form a system of the seventh order.

The two integrals written in the foregoing—those of areas [14] and of energy [18]—can be used to lower the order of the required system by 2. Thus, the order of the system subject to integration would finally be equal to 5.

No other integrals of the system are being directly considered.

2 Doubly Averaged Semirestricted Problem of Three Bodies

The doubly averaged semirestricted problem of three bodies is obtained from the problem considered in the previous paragraph by replacing, in the differential equations of motion, the disturbing functions W_1 and W_2 by their double averages with respect to the mean anomalies M_1 and M_2. These averages are defined by

$$[W_1] = \frac{1}{4\pi^2}\int_{M_1=0}^{2\pi}\int_{M_2=0}^{2\pi} W_1 dM_1 dM_2 \qquad [21.1]$$

$$[W_2] = \frac{1}{4\pi^2}\int_{M_1=0}^{2\pi}\int_{M_2=0}^{2\pi} W_2 dM_1 dM_2 \qquad [21.2]$$

where M_1 and M_2, during integration, are considered mutually independent. The coordinates of the bodies P_1 and P_2 are expressed through the corresponding Keplerian phase coordinates a, p, ω and M according to the formulas of undisturbed motion. The elements a, p and ω are considered constant in the process of averaging.

After such double averaging, we obtain disturbing functions which depend only on the semiaxes a, the parameters p and the longitudes of perihelia ω

$$[W_1] = [W_1](a_1, a_2, p_1, p_2, \omega_2 - \omega_1) \qquad [22.1]$$

$$[W_2] = (m_1/m_2)[W_1] \qquad [22.2]$$

Because the doubly averaged disturbing functions are not dependent on mean anomalies, the equations of motion give at once two additional integrals. This is in addition to the integrals of areas and energy found previously. Thus

$$a_1 = \text{const} \qquad [23.1]$$

and

$$a_2 = \text{const} \qquad [23.2]$$

The equations for mean anomalies separate from the system and will be integrated after the integration of remaining equations. Also the integral of areas permits us to separate the equation for the parameter p_1.

Thus it remains to integrate a system of two equations

$$\frac{dp_2}{dt} = \frac{2\sqrt{p_2}}{k\sqrt{m_0}}\frac{\partial([W_2])_p}{\partial\omega}$$

$$\frac{d\omega}{dt} = -\frac{2\sqrt{p_2}}{k\sqrt{m_0}}\frac{\partial([W_2])_p}{\partial p_2} \qquad [24]$$

which will possess the energy integral in the form

$$[W_1] = \text{const} \qquad [25.1]$$

or

$$[W_2] = \text{const} \qquad [25.2]$$

Clearly the integration is reduced to quadratures. Subsequently the separated equations are integrated.

Thus, the doubly averaged (or Gaussian) semirestricted problem of three bodies in a plane is completely solved in quadratures.

3 Singly Averaged Semirestricted Problem of Three Bodies

The singly averaged semirestricted problem of three bodies results from the problem considered in the first paragraph. The transformation is effected by replacing W_1 and W_2 in differential equations [8] by their singly averaged values, with respect to the mean anomaly M_1. These averages are defined by the following formulas

$$[W_1] = \frac{1}{2\pi}\int_{M_1=0}^{2\pi} W_1 dM_1 \qquad [26.1]$$

$$[W_2] = \frac{1}{2\pi}\int_{M_1=0}^{2\pi} W_2 dM_1 \qquad [26.2]$$

where the coordinates of the bodies P_1 and P_2 are assumed expressed through the corresponding Keplerian phase coordinates a, p, M and ω by the formulas of undisturbed motion. In the process of integration only the mean anomaly M_1 is considered variable. All other Keplerian phase coordinates [7] are taken to be constant.

In the restricted case such a singly averaged problem had two variants: The internal and the external ones, corresponding to the cases when the body P_1, whose motion is being studied, has an osculating Keplerian orbit inside or outside a similar orbit for the body P_2, whose motion is considered as given. For the unrestricted and semirestricted problems formally there would be no difference between the external and internal variants of the problem because of the equivalence of the bodies P_1 and P_2. However, if one takes under consideration the requirement of close correspondence between the averaged and the unaveraged schemes, it will appear that the singly averaged semirestricted (and the unrestricted) problem

of three bodies will satisfy this demand in case, when the orbit of the bodies P_1, with respect to whose anomaly the averaging is done, has a smaller semimajor axis a_1 than the orbit of the body P_2. We will consider this case a basic one.

The averaged disturbing functions [26], obtained as a result of averaging, will satisfy the formula [22.2] and will depend only on arguments

$$(a_1, p_1, a_2, p_2, M_2, \omega) \qquad [27]$$

Consequently, the differential equations of the problem obtained from Equations [8] by replacing disturbing functions by their averaged values [26] will have the integral

$$a_1 = \text{const} \qquad [28]$$

in addition to the integral of areas [14] and integral of energy. The energy integral has the following forms

$$(k^2 m_0 m_2/2a_2) + m_1[W_1] = \text{const} \qquad [29.1]$$

or

$$(k^2 m_0 m_2/2a_2) + m_2[W_2] = \text{const} \qquad [29.2]$$

Considering the fact that the integrals [28 and 14] were used for substituting the constant value a_1 and for expressing p_1 through p_2 and the constant of areas, and ignoring equations separated from the basic system, we obtain the following system of differential equations

$$\frac{da_2}{dt} = \frac{2\sqrt{a_2}}{k\sqrt{m_0}} \frac{\partial[W_2]}{\partial M_2}$$

$$\frac{dp_2}{dt} = \frac{2\sqrt{p_2}}{k\sqrt{m_0}} \frac{\partial[W_2]}{\partial \omega}$$

$$\frac{dM_2}{dt} = \frac{k\sqrt{m_0}}{a_2^{3/2}} - \frac{2\sqrt{a_2}}{k\sqrt{m_0}} \frac{\partial[W_2]}{\partial a_2}$$

$$\frac{d\omega}{dt} = -\frac{2\sqrt{p_2}}{k\sqrt{m_0}} \frac{\partial[W_2]}{\partial p_2} \qquad [30]$$

which is to be integrated. It is of the fourth order, but admits one integral, namely the integral of energy [29] which has not yet been used.

Thus, the situation with the integration of the system [30] is in a certain sense analogous to the case of the unaveraged restricted circular planar problem of three bodies.

Taking advantage of the fact that the independent variable t does not explicitly enter the disturbing function, one can easily eliminate the time t and use another independent variable, for example, the mean anomaly M_2. Instead of system [30], this will lead to a system of the third order with 1 integral of energy [29]. Employing this integral, the order of the system can be lowered by 1. However, this will not contribute to the simplification of the equations.

After integrating this system, the remaining equations can be solved by quadratures.

4 Improved Singly Averaged Semirestricted Problem of Three Bodies

Following N. F. Rein's idea already used in our previous articles on averaged variants of a restricted problem of three bodies, it is possible to construct refined averaged variants for a semirestricted problem as well. These variants are based on the idea of excluding from averaging the "circular component" of motion and extending the averaging over its "eccentric component" only. This approach is particularly suitable in cases when the eccentricity of the corresponding point remains small.

Thus, the averaged values of disturbing function are computed according to the following formulas

$$[W_1] = \frac{1}{2\pi} \int_{M_1=0}^{2\pi} W_1 dM_1 \qquad [31.1]$$

and

$$[W_2] = \frac{1}{2\pi} \int_{M_1=0}^{2\pi} W_2 dM_1 \qquad [31.2]$$

where the following assumptions are made:

1 The coordinates of the points P_1 and P_2 are expressed by Keplerian phase coordinates [7] by the formulas of undisturbed motion.

2 The difference of longitudes of the points P_1 and P_2 is represented by the formula

$$\vartheta = v_2 - \mu_1 - (v_1 - M_1) \qquad [32]$$

where

$$\mu_1 = M_1 - \omega \qquad [33]$$

In the process of integration with respect to M_1, the values of Keplerian phase coordinates [7], with the exception of the mean anomaly M_1, are considered constant. The quantity μ_1, determined by [33], is also taken constant. As to the M_1, it is considered variable only in the expression for the radius vector r_1 and in the equation of center $v_1 - M_1$, entering into formula [32].

As a result of such averaging "in Rein's sense," we obtain averaged values of disturbing functions which depend only on the arguments

$$(a_1, p_1, a_2, p_2, M_2, \mu_1) \qquad [34]$$

These averaged disturbing functions will depend on the averaged mean anomaly M_1 and the difference of longitudes of perihelia only through μ_1.

Therefore, the following formula will hold

$$\frac{\partial[W_1]}{\partial \mu_1} = \frac{\partial[W_1]}{\partial M_1} = -\frac{\partial[W_1]}{\partial \omega} = \frac{\partial[W_1]}{\partial \omega_1} \qquad [35]$$

In addition, Equation [22.2] will apply connecting the averaged values of both disturbing functions.

A corresponding system of differential equations of the disturbed motion, obtained from the Equations [8] by the replacement of disturbing functions by their averaged values [31], will, as before, possess the integrals of areas [14] and of energy [18].

The combination of the first and the second equations of the subsystem [8.1] results in one more integral. Namely, by virtue of Equation [35] these two equations lead to the following equation in total derivatives

$$\frac{da_1}{\sqrt{a_1}} = \frac{dp_1}{\sqrt{p_1}}$$

Integrating, we obtain the following Rein integral

$$\sqrt{a_1} = \sqrt{p_1} + \text{const} \qquad [36]$$

Now, let us form a differential equation for the quantity μ_1, determined by Equation [33]. Using this formula as well as the averaged (in the sense mentioned in the foregoing) equations of the subsystems [8.1 and 8.2], we can write the following

$$\frac{d\mu_1}{dt} = \frac{dM_1}{dt} + \frac{d\omega_1}{dt} - \frac{d\omega_2}{dt} = \frac{k\sqrt{m_0}}{(\sqrt{a_1})^3} - \frac{1}{k\sqrt{m_0}} \frac{\partial[W_1]}{\partial\sqrt{a_1}} - \frac{1}{k\sqrt{m_0}} \frac{\partial[W_1]}{\partial\sqrt{p_1}} + \frac{1}{k\sqrt{m_0}} \frac{\partial[W_2]}{\partial\sqrt{p_2}} =$$

$$\frac{k\sqrt{m_0}}{(\sqrt{a_1})^3} + \frac{1}{k\sqrt{m_0}} \frac{\partial[W_1]}{\partial\sqrt{a_1}} - \frac{1}{k\sqrt{m_0}} \frac{\partial[W_1]}{\partial\sqrt{p_1}} + \frac{1}{k\sqrt{m_0}} \times \frac{m_1}{m_2} \frac{\partial[W_1]}{\partial\sqrt{p_2}} \qquad [37]$$

Assuming that p_2 is expressed through p_1 by means of the integral of areas [14], and that p_1 is expressed through a_1 by means of the Rein integral [36], and agreeing that the symbol of partial derivative with respect to a_1 denotes the complete partial derivative with respect to this argument, we rewrite [37] as follows

$$\frac{d\mu_1}{dt} = \frac{k\sqrt{m_0}}{(\sqrt{a_1})^3} - \frac{1}{k\sqrt{m_0}} \frac{\partial[W_1]}{\partial\sqrt{a_1}} \qquad [38]$$

Making use of Rein and area integrals for expressing a_1 through p_1 and p_1 through p_2, the equation will take the following form

$$\frac{d\mu_1}{dt} = f(a_2, p_2, M_2, \mu_1) \qquad [39]$$

Thus we may assume that the system of equations to be integrated is the following set of four equations of the first order

$$\frac{da_2}{dt} = \frac{2\sqrt{a_2}}{k\sqrt{m_0}} \frac{\partial[W_2]}{\partial M_2}$$

$$\frac{dp_2}{dt} = -\frac{2\sqrt{p_2}}{k\sqrt{m_0}} \frac{\partial[W_2]}{\partial\mu_1}$$

$$\frac{dM_2}{dt} = \frac{k\sqrt{m_0}}{a_2^{3/2}} - \frac{2\sqrt{a_2}}{k\sqrt{m_0}} \frac{\partial[W_2]}{\partial a_2}$$

$$\frac{d\mu_1}{dt} = f(a_2, p_2, M_2, \mu_1)$$

. . . . . [40]

In the system considered, there remains one unused energy integral of the form [29.2].

After the integration of the system [40] the solution of the problem is completed by quadratures.

Thus, the improved singly averaged variant of the semirestricted planar problem of three bodies appears—as far as the order of the system of equations subject to integration is concerned—to be analogous to the restricted circular planar problem of three bodies.

5 Improved Doubly Averaged Semirestricted Problem of Three Bodies

When the osculating eccentricity remains small not only for the body P_1, but for the second body P_2 as well, it seems appropriate to consider the doubly averaged improved variant.

This variant will be obtained if the disturbing function W_1 and W_2 are replaced by their doubly averaged values computed according to the following formulas

$$[W_1] = \frac{1}{4\pi^2} \int_{M_1=0}^{2\pi} \int_{M_2=0}^{2\pi} W_1 dM_1 dM_2 \qquad [41.1]$$

$$[W_2] = \frac{1}{4\pi^2} \int_{M_1=0}^{2\pi} \int_{M_2=0}^{2\pi} W_2 dM_1 dM_2 \qquad [41.2]$$

The integration is carried out with the following assumptions:

1 The coordinates of the bodies P_1 and P_2 are expressed in terms of Keplerian phase coordinates [7] by the formulas of undisturbed motion.

2 The difference of longitudes of the bodies P_1 and P_2 is given by

$$\vartheta = \mu_{12} + (v_2 - M_2) - (v_1 - M_1) \qquad [42]$$

where

$$\mu_{12} = M_2 - M_1 + \omega \qquad [43]$$

3 In the process of integration with respect to M_1 and M_2, the values of Keplerian phase coordinates are considered constant except M_1 and M_2. The value μ_{12} determined by Equation [43] is likewise considered constant. The quantities M_1 and M_2 are considered variable only in the expressions for corresponding radii vectors r_1 and r_2 and in the equations of the center $(v_1 - M_1)$ and $(v_2 - M_2)$, which enter Equation [42]. In the process of integration, the values M_1 and M_2 are considered mutually independent. As a result of such double averaging—"the averaging in Gauss-Rein sense"—one obtains averaged values of the disturbing functions which depend only on arguments

$$(a_1, a_2, p_1, p_2, \mu_{12})$$

These functions will depend on the mean anomalies M_1 and M_2 and on longitudes of the perihelia ω_1 and ω_2 only through the corresponding differences entering μ_{12}.

Therefore, in addition to Equation [22.2], we have the following formulas

$$\frac{\partial[W_1]}{\partial\mu_{12}} = -\frac{\partial[W_1]}{\partial M_1} = \frac{\partial[W_1]}{\partial M_2} = -\frac{\partial[W_1]}{\partial\omega_1} = \frac{\partial W_1]}{\partial\omega_2} = \frac{\partial[W_1]}{\partial\omega} \qquad [44]$$

The corresponding system of differential equations of the disturbed motion is obtained from Equations [8] by replacing the disturbing functions by their averaged values [41]. The resulting system has the integrals of areas and energy which are identical with [14 and 18]

The combination of the first two equations of the subsystem [8.1] described in the previous paragraph, gives Rein integral

$$\sqrt{a_1} = \sqrt{p_1} + \text{const} \qquad [45]$$

An analogous combination of the first two equations of the subsystem [8.2] gives the second Rein integral

$$\sqrt{a_2} = \sqrt{p_2} + \text{const} \qquad [46]$$

Using these two Rein integrals and the integral of areas we can reduce the problem to a system of two differential equations of the first order—each relative to the two desired functions. As the first of these we can take, for example, the parameter p_2, and as the second, the value μ_{12} [43]. For this system, which has the following form

$$(dp_2/dt) = f_1(p_2, \mu_{12})$$

$$(d\mu_{12}/dt) = f_2(p_2, \mu_{12})$$

. . . . . [47]

one integral will be known

$$f_3(p_2, \mu_{12}) = \text{const} \qquad [48]$$

This integral is nothing else than the integral of energy written in terms of the Rein integral and the integral of areas.

Using the integral [48] we can integrate the system [47]. Following this the solution of the whole problem is reduced to quadratures.

Thus, the doubly averaged improved semirestricted planar problem of three bodies of Gauss-Rein is solved completely by reduction to quadratures.

5 Delaunay-Hill Singly Averaged Semirestricted Problem of Three Bodies

Let k_1 and k_2 be two positive integers. Let the "Anomaly of Delaunay" associated with a pair of numbers (k_1, k_2) be the quantity defined by the formula

$$D = k_1 M_2 - k_1 M_1 \qquad [49]$$

This formula can be utilized to express the mean anomaly M_1 in terms of the Delaunay anomaly D and the mean

anomaly M_1

$$M_2 = \frac{1}{k_2} D + \frac{k_1}{k_2} M_1 \qquad [50]$$

Now the mean values of the disturbing functions in a Delaunay-Hill singly averaged semirestricted planar problem of three bodies are determined by

$$[W_1] = \frac{1}{2\pi k_2} \int_{M_1=0}^{2\pi k_2} W_1 dM_1 \qquad [51.1]$$

$$[W_2] = \frac{1}{2\pi k_2} \int_{M_1=0}^{2\pi k_2} W_2 dM_1 \qquad [51.2]$$

To integrate, the following conditions are assumed:

1 The coordinates of the bodies P_1 and P_2 are expressed by the Keplerian phase coordinates [7] according to the formulas of undisturbed motion.

2 Following this, the mean anomaly M_2 is expressed in terms of the mean anomaly M_1 and the Delaunay anomaly by Equation [50].

3 In the process of integration only the mean anomaly M_1 is considered variable. All the elements of the osculating orbits a_1, a_2, p_1, p_2, ω_1, ω_2, as well as the Delaunay anomaly D, are considered constant in this integration.

This averaging yields the averaged values of disturbing functions which depend solely on the following arguments

$$(a_1, a_2, p_1, p_2, D, \omega) \qquad [52]$$

The dependence on the anomalies M_1 and M_2 occurs through the Delaunay anomaly D [49].

Consequently, in addition to Equation [22.2] we have the following formula

$$\frac{\partial[W_1]}{\partial D} = \frac{1}{k_2} \frac{\partial[W_1]}{\partial M_2} = -\frac{1}{k_1} \frac{\partial[W_1]}{\partial M_1} \qquad [53]$$

The differential equations of motion for the Delaunay-Hill problem in the Keplerian phase space will be obtained from Equations [8] by replacing the disturbing functions by their averaged values [51].

These equations will, as before, have the integrals of areas and energy as given by [14 and 18].

In addition, it will be possible to obtain one more integral connecting the values of semimajor axes a_1 and a_2. This integral can be called the integral of semi-axes. We note that the first equations of the subsystems [8.1 and 8.2] can, by the use of Equation [53], be transcribed in the following form

$$\frac{da_1}{dt} = -\frac{2\sqrt{a_2}}{k\sqrt{m_0}} k_1 \times \frac{\partial[W_1]}{\partial D} \qquad [54.1]$$

$$\frac{da_2}{dt} = +\frac{2\sqrt{a_2}}{k\sqrt{m_0}} k_2 \times \frac{m_1}{m_2} \frac{\partial[W_1]}{\partial D} \qquad [54.2]$$

Combining these we obtain an equation in total derivatives

$$\frac{m_1}{k_1} \frac{da_1}{2\sqrt{a_1}} + \frac{m_2}{k_2} \frac{da_2}{2\sqrt{a_2}} = 0 \qquad [54.3]$$

the integration of which will give us the "integral of semi-axes" mentioned in the foregoing

$$\frac{m_1}{k_1} \sqrt{a_1} + \frac{m_2}{k_2} \sqrt{a_2} = \text{const} \qquad [55]$$

Employing the integrals of areas and semi-axes, the a_1 and p_1 in the disturbing function can be expressed in terms of a_2 and p_2, respectively. Assuming that the substitution has been carried out and that the symbols $(\partial/\partial a_2)$ and $(\partial/\partial p_2)$ represent the complete partial derivatives with respect to the corresponding arguments a_2 and p_2, we have the following system of four differential equations

$$\frac{da_2}{dt} = +\frac{2\sqrt{a_2}\, k_2}{k\sqrt{m_0}} \frac{\partial[W_2]}{\partial D}$$

$$\frac{dp_2}{dt} = \frac{2\sqrt{p_2}}{k\sqrt{m_0}} \frac{\partial[W_2]}{\partial \omega}$$

$$\frac{dD}{dt} = k\sqrt{m_0}\left(\frac{k_2}{a_2^{3/2}} - \frac{k_1}{a_1^{3/2}}\right) - \frac{k_2 \times 2\sqrt{a_2}}{k\sqrt{m_0}} \frac{\partial[W_2]}{\partial a_2}$$

$$\frac{d\omega}{dt} = -\frac{2\sqrt{p_2}}{k\sqrt{m_0}} \frac{\partial[W_2]}{\partial p_2}$$

. . . . . [56]

The derivation of the last equation, namely the equation for the difference of longitudes of the perihelia ω, was given at the end of Section 1, where it was designed as Equation [20].

The equation for the Delaunay anomaly D is deduced as follows. Differentiation of Equation [49] gives

$$\frac{dD}{dt} = k_2 \frac{dM_2}{dt} - k_1 \frac{dM_1}{dt}$$

Introduction of the expressions for (dM_2/dt) and (dM_1/dt) from the third equations of the subsystems [8.1 and 8.2] yields

$$\frac{dD}{dt} = k\sqrt{m_0}\left(\frac{k_2}{a_2^{3/2}} - \frac{k_1}{a_1^{3/2}}\right) - \frac{1}{k\sqrt{m_0}} \times \left(k_2 \frac{\partial[W_2]}{\partial\sqrt{a_2}} - \frac{m_2}{m_1} k_1 \frac{\partial[W_2]}{\partial\sqrt{a_1}}\right) \qquad [57]$$

Using the integral of semi-axes [55] and assuming that the symbol $\partial/\partial a_2$ designates the complete partial derivative with respect to a_2, we obtain the equation for dD/dt of [56]. In this equation the value a_1, appearing in the first parenthesis on the right, is assumed to be expressed through a_2 by the integral of semi-axes [55].

The disturbing function $[W_2]$ in system [56] depends only on arguments

$$(a_2, p_2, D, \omega) \qquad [58]$$

Consequently, it has the following integral

$$\frac{k^2 m_0 m_1}{2a_1(a_2)} + \frac{k^2 m_0 m_2}{2a_2} + m_2[W_2] = \text{const} \qquad [59]$$

where a_1 is assumed to be expressed through a_2 by Equation [55]. The integral [59] is but a modification of the integral of energy [18] corresponding to the considered Delaunay-Hill problem.

The direct derivation of the integral [59] from the system [56] can proceed as follows. We have

$$\frac{d[W_2]}{dt} = \frac{\partial[W_2]}{\partial a_2}\frac{da_2}{dt} + \frac{\partial[W_2]}{\partial p_2}\frac{dp_2}{dt} + \frac{\partial[W_2]}{dD}\frac{dD}{dt} + \frac{\partial[W_2]}{\partial \omega} \times \frac{d\omega}{dt} = k\sqrt{m_0}\left(\frac{k_2}{a_2^{3/2}} - \frac{k_1}{a_1^{3/2}}\right)\frac{\partial[W_2]}{\partial D}$$

Hence, using the first equation of system [56] and the equation [54.3] we obtain

$$\frac{d[W_2]}{dt} = k^2 m_0 \left(\frac{1}{2a_2^2} - \frac{k_1}{k_2 a_1^{3/2} \times 2\sqrt{a_2}}\right)\frac{da_2}{dt} = k^2 m_0 \left[\frac{1}{2a_2^2}\frac{da_2}{dt} + \frac{m_1}{m_2} \times \frac{1}{2a_1^2}\frac{da_1}{dt}\right]$$

Integrating this equation we obtain the integral [59].

Integral [59] appears to be the only known integral of the fourth-order system [56].

Conclusion

In conclusion we note that a similar analysis is applicable to other variants of the planar semirestricted problem of three bodies.

Among these, of particular interest is the variant which could be called interpolation averaged. It is based on the fact that in the averaging process a certain linear combination of angular variables of the disturbing function remains invariant. In an earlier paper on the averaged variants of the restricted three-body problem this combination was defined as the interpolation anomaly.

The interpolation averaged variants appear to be important not only in the restricted problem of three bodies, but in the semirestricted and unrestricted problems as well.

Reviewer's Comment

While the so-called restricted problem of three bodies considers the motion of one body of infinitesimally small mass relative to two finite masses moving about their common center of mass in circular orbits, the author's "semirestricted problem" deals with the orbits of two finite masses of the same order (two planets) relative to one much more massive central body (sun). In such a system the author neglects the gravitational action of the two smaller masses on the large central mass. By means of the integral of areas the orbital parameter p_1 of the one planetary mass m_1 can be eliminated. Subsequently the author applies his method of "averaging," as developed in his earlier papers and essentially based on Gauss' comparable treatment of the secular perturbations, to eliminate certain periodic terms from the disturbing function. This leads to certain integrals of the now simplified differential equations of motion. Of particular interest is the elimination of certain periodic terms, depending on the mean anomalies M_1 and M_2 of the two moving masses in the form of angular arguments $D = k_2M_2 - k_1M_1$, similar to the elimination method employed by Delaunay in his treatment of the lunar theory. The author calls this "averaging according to Delaunay-Hill."

All the analytical operations involved are rather elementary, but the results are of interest with regard to orbital problems where a first-order approximation to the orbital motion in the case as specified and simplified by the author is desired. The presentation is very clear with regard to concepts and conclusions.

—Eugene Rabe
Dept. of Astronomy
University of Cincinnati

Cosmic Rays and Outer Space[1]

S. N. VERNOV[2]

THE CREATION of artificial satellites and space rockets has made it possible, for the first time, to conduct direct investigations of outer space. Less than three years have elapsed since the launching of the first artificial Earth satellite. But already we are able to draw certain conclusions from the various experiments that have been undertaken in outer space, and to give an account of phenomena the very existence of which had not previously been suspected, phenomena for whose discovery we are indebted solely to the flights of the artificial satellites.

The density of matter in outer space is very low. At the same time, there exist there different types of radiation. Going on in outer space are continuous processes of the transition of energy from one form to another. The kinetic energy of matter is transformed into the energy of a magnetic field, and vice versa. The energy of magnetic fields is spent in accelerating atomic nuclei and in creating cosmic rays.

As a result of these processes energy is distributed more or less evenly among the various forms. The energy density of cosmic rays attains approximately the energy density of the magnetic field. The latter is approximately equal to the energy density of the motion of matter, and so on.

The even distribution of energy among these forms is a fundamental property of outer space. This is why we shall not be able to gain an understanding of the structure of the universe without investigating the different kinds of radiation that prevail within it.

The investigation of cosmic rays has long been at the center of attention of contemporary scientists. The experiments of D. V. Skobel'tsin (member of Acad. Sci. USSR) have demonstrated that this type of radiation consists of particles possessing high energies. The investigation of cosmic rays, therefore, permits solution of two fundamental problems: 1 Ascertainment of the properties of the medium in which the rays originate (i.e., the properties of cosmic space itself), and 2 the utilization of cosmic rays for bombardment of atomic nuclei.

Translated from *Izvestiia Akademii Nauk SSSR* (News of Acad. Sci. USSR), vol. 30, no. 8, 1960, pp. 10–26. Translated by Robert Addis.

[1] This is an expanded version of the transcribed shorthand record of a talk given by the author at the General Meeting of the Academy of Sciences of the USSR, June 10, 1960.

[2] Corresponding Member of the Academy of Sciences of the USSR.

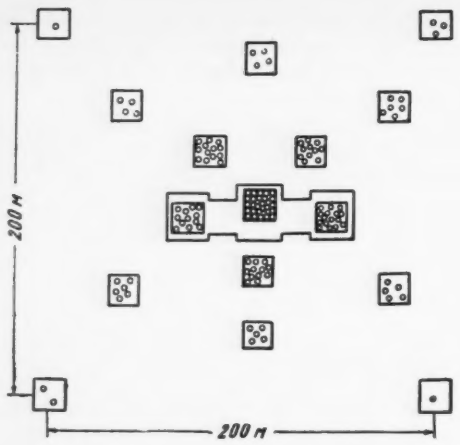

Fig. 1 Diagram of apparatus for studying super-energetic particles. Apparatus belongs to Institute of Nuclear Physics of Moscow State University

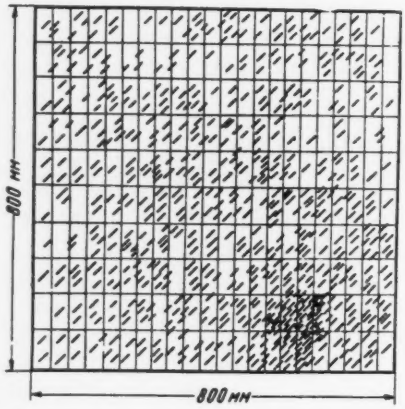

Fig. 2 Depiction of particle distribution inside diffusion chamber

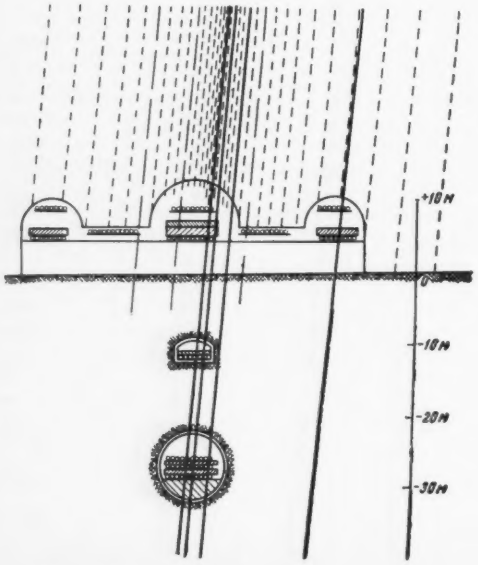

Fig. 3 Schematic cross section of Moscow State University's apparatus for studying super-energetic particles

My talk today will be devoted to the first of these problems. It seems to me, though, that I ought not fail to mention, if only briefly, those experiments that are demonstrating the presence among cosmic rays of particles possessing energies as high as 10^{18} ev. I should not fail, either, to specify those types of data that present-day physicists can obtain solely by means of studying cosmic rays.

First of all, I should like to tell you something of the kind of apparatus that we use to investigate super-energetic particles. Such particles are extremely rare. For this reason, if our apparatus is to record the presence of any appreciable number of them, its dimensions must be quite large. It consists of numerous separate detectors set out at intervals of several hundred meters from one another. These detectors all work together, as a unit, recording the arrival time of the particles to within millionths of a second. The plunging of a super-energetic cosmic ray particle into Earth's atmosphere can be detected owing to the fact that, as a result of various interactions of the particle and its offspring with atomic nuclei, intense fluxes of particles are created. By the time that such a flux has reached the surface of Earth, it consists of many millions of particles. These physical phenomena are called "wide atmospheric showers."

Fig. 1 is a diagram of the apparatus belonging to the Moscow State University. It was designed by me in collaboration with G. B. Khristiansen and G. T. Zatsepin. At the center is the building housing the cosmic-ray laboratory. Situated around the building are a number of mobile laboratories, linked to the building by means of high frequency cable. Part of the equipment is installed in an underground laboratory. In all, the apparatus includes 5000 counters and 150 ionization chambers, which operate simultaneously. Whenever a wide atmospheric shower shows up in the vicinity, a special control system dispatches a command through the high frequency cable to all the counters and ionization chambers, and to an array of cameras. The function of the cameras is to record the readings of all the instruments

Fig. 1 shows the picture that was seen when a cosmic ray particle having an energy of 10^{15} ev plunged into Earth's atmosphere. The energy of that particle exceeded by more than 10,000 times the maximum energy attained by means of modern accelerators. Since the particle hit approximately the center of our apparatus, the density of particles in the shower caused by it decreased with increasing distance from the apparatus center. The number of particles recorded is represented in the figure by the little circles. The density of the latter at the different points shows very clearly the decrease in the density of particles with increasing distance from the center of the shower. Knowing the number of particles actually recorded, we are able to determine the total number of them contained in the shower (in this case it was approximately one million). Placed at the center of the apparatus was a diffusion chamber, which enabled us to photograph all the particles that passed through.

The distribution of particles inside the diffusion chamber is depicted in Fig. 2. Each of the short black lines there represents one particle. The center of the shower is easily discerned.

With these photographs here I wish to show you how, with complete reliability, we determine the number of particles in an atmospheric shower. With this same apparatus we are able, at the same time, to measure the energy of the particles. Multiplying the number of particles by the average energy required to form each of them, we arrive at the energy of the primary particle. Thus, the existence among cosmic rays of particles possessing ultra high energies is not just a hypothesis of physicists; it is an indisputably established fact.

Supported by these data, we may use cosmic rays to investigate the properties and components of the atomic nucleus.

Fig. 3 shows how investigations of this type are carried out at the Cosmic Ray Laboratory of the Moscow State

University. We see there the laboratory building, resting on the ground surface, and two laboratories underground. The nearly vertical broken lines represent electrons belonging to a wide atmospheric shower. Their number is seen to increase with decreasing distance from the shower center. They are rapidly absorbed by relatively shallow thicknesses of Earth and do not penetrate to the underground laboratories.

A large role in the development of an atmospheric shower is played by the so-called nuclear reactive particles (protons, neutrons, etc.), which have a capacity for violent interaction with atomic nuclei. Because of this they quickly dissipate their energy and can penetrate the ground to a depth of no more than several meters (see Fig. 3, the broken lines having the longest segments).

There are particles in an atmospheric shower, however, that do possess great penetrating power. These are represented in Fig. 3 by the solid lines. They are the so-called nuclear passive particles—in this case, μ mesons. Many of them are able to penetrate through a thickness of Earth of some 30 m, and do hit our underground laboratories.

What has been determined as a result of these measurements?

We shall mention, first of all, the narrow beams of particles that pass through great thicknesses of matter. Though our investigations are not yet concluded, there can be no doubt that these phenomena attest to the existence of new processes involving ultra high energies. It seems to us that this is the road that will lead us to the answer to that fundamental question facing modern physics, the question as to the structure of the elementary particles.

Already we have succeeded in obtaining a certain amount of data on the nature of the processes occurring at ultra high energies. It has been experimentally established, for example, that practically every time a super-energetic particle collides with an atomic nucleus a violent interaction occurs. We have thereby discovered yet another marked difference between the properties of the atomic nucleus and those of the atom itself. In addition, as experiment has shown, upon collision with an atomic nucleus a primary particle loses only a portion of its energy.

Investigation of the super-energetic particles among cosmic rays is of great importance, also, because of its relevance to the study of those regions of the universe that are remote from us. We may now assume that the super-energetic particles originate outside our galaxy. Their energy is so great that they pass right through its magnetic fields. If there should exist particles having energies of 10^{20} ev, for them our galaxy would be completely transparent. Thus, with the aid of cosmic rays we are able, so to speak, to obtain unique "x-ray" pictures of outer space.

Let us now consider those regions of space in the immediate vicinity of Earth.

As I stated at the outset, a fundamental property of the universe consists in the fact that there can exist within it radiation whose energy density is commensurable with the energy density of a magnetic field. In the vicinity of Earth there is an extremely powerful magnetic field. For this reason the radiation intensity near Earth ought to be very high.

That this indeed is the case, has been learned through the flights of the artificial satellites. Investigation has revealed that Earth is girded by two belts of radiation, an inner and an outer belt. The radiation levels within those belts are very high. In this connection, of course, the question arises as to the possible harmful effects of that radiation on future space travelers. This factor will have to be taken into account in the designing of manned space vehicles.

Investigation of the different types of radiation in outer space began with the flight of Sputnik II. With the launching of Sputnik III and of the first three Soviet space rockets, larger scale experiments were undertaken. Apparatus to be installed in a satellite vehicle must meet certain requirements. It must be able to withstand great acceleration and vibration, and must perform reliably under conditions of changing temperature and pressure. Most important of all is that its weight and electric power consumption be minimal. This latter requirement virtually precludes the use of radio tubes in the complex scientific instruments. Using semiconductors, however, makes it possible to construct an apparatus capable of carrying out a wide variety of measurements.

To determine the number of electrically charged particles we have used gas discharge counters. To analyze the content of the different types of radiation we have used scintillation counters.

The studies have been made by me in collaboration with A. Ye. Chudakov, Yu. I. Logachev, P. V. Vakulov, Ye. V. Gorchakov and A. G. Nikolayev.

Fig. 4a is a schematic block diagram of one of our scintillation counters. A photomultiplier records the flashes of light that occur in a sodium iodide crystal. The quantities of light in the flashes are proportional to the amounts of energy released inside the crystal when the different types of radiation pass through it. Thus, by recording the flashes of different magnitude we are able to measure simultaneously the respective amounts of the different types of radiation, i.e., the number of quanta of x-rays, gamma rays, and the number of high energy particles able to penetrate the crystal. The figure shows the circuits for thresholds I, II and III. There is a circuit at the top that permits measurement of the total effect of all the radiations.

The number of instruments of the types depicted in Figs. 4a and 4b employed on the space flights was very great indeed. During the flight of Sputnik II it was discovered that at latitudes above 60 deg an anomalous increase occurred in the radiation level. A particularly marked increase was observed on Nov. 7, 1957. Fig. 5 shows the results of the measurements that were made. The broken line depicts the average change in the radiation level recorded by Sputnik II as it flew on other occasions through those same latitudes. From the figure it is evident that both instruments in the satellite vehicle registered an increase of more than 50 per cent in the radiation intensity. The level of cosmic radiation at that time was constant. It is obvious, therefore, that the observed phenomenon indicated the presence of low energy particles.

A highly sensitive scintillation counter was installed in Sputnik III to record the presence of any x-rays. By utilizing the fact that, when the hull or outer casing of a satellite vehicle is bombarded by electrons, x-rays are produced, we were able to detect with this instrument even relatively weak electron currents.

A sample of the recordings made by a scintillation counter aboard Sputnik III is shown in Fig. 6. The broken line indicates the number of cases in which the amount of energy released in the scintillation counter's sodium iodide crystal exceeded 35 kev. We observe that when the satellite vehicle was in the higher geomagnetic latitudes the instruments registered a sharp rise in the radiation level. This means that within a certain range of latitudes some new radiation is encountered. The zone or region in which this new radiation exists constitutes Earth's outer radiation belt.

Comparative evaluation of the different data contained in Fig. 6 permits us to draw certain conclusions concerning the nature of the particles in the outer belt. The solid lines in the figure denote the total ionization caused by radiation of all types. The observed fluctuations are attributed to the rotation of the satellite vehicle. A large increase in the number of flashes that is not accompanied by a correspondingly large increase in the total ionization means that the light flashes in the crystal are a little too small. Our calculations show that the amount of energy released inside the crystal averages less than 100 kev. Thus, when the satellite vehicle entered the outer radiation belt, the scintillation counter showed the presence of x-rays produced by bombard-

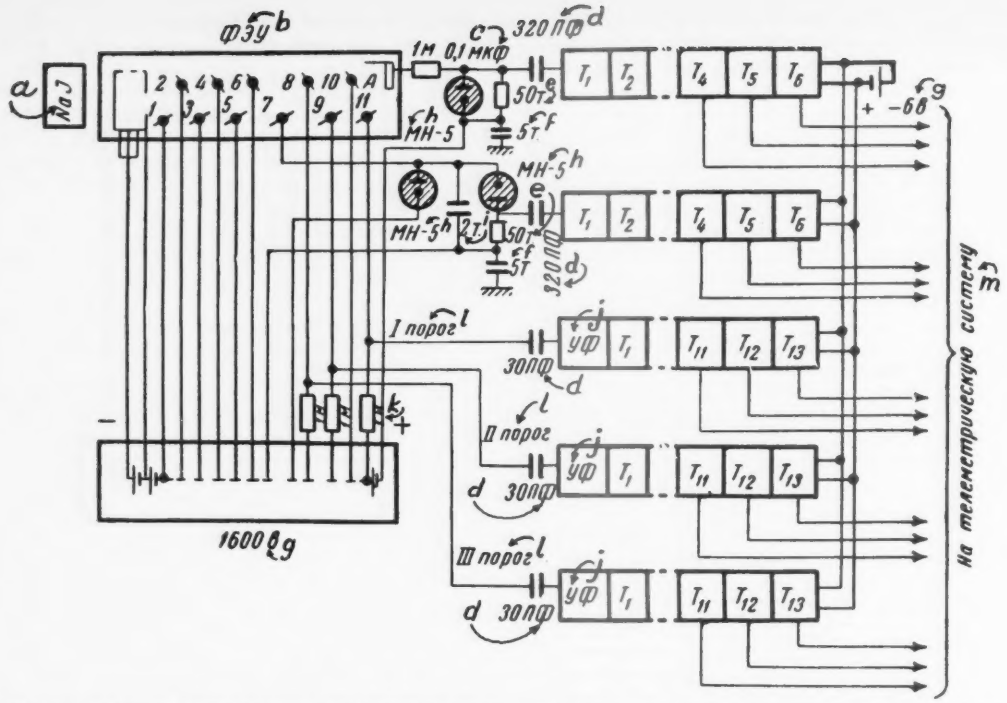

Fig. 4a Schematic block diagram of scintillation counter. The instrument permits measurement of the number of pulses with three different energy thresholds, also of the amount of ionization, by recording the average current of the anode and of the seventh dynode. Translations: a—sodium iodide; b—photomultiplier; c—μf; d—$\mu\mu$f; e—50 kilohms; f—5000 $\mu\mu$f; g—designates volts; h—tube designation; i—2000 $\mu\mu$f; j—photocurrent amplifier; k—1 megohm; l—threshold; m—to telemetering system

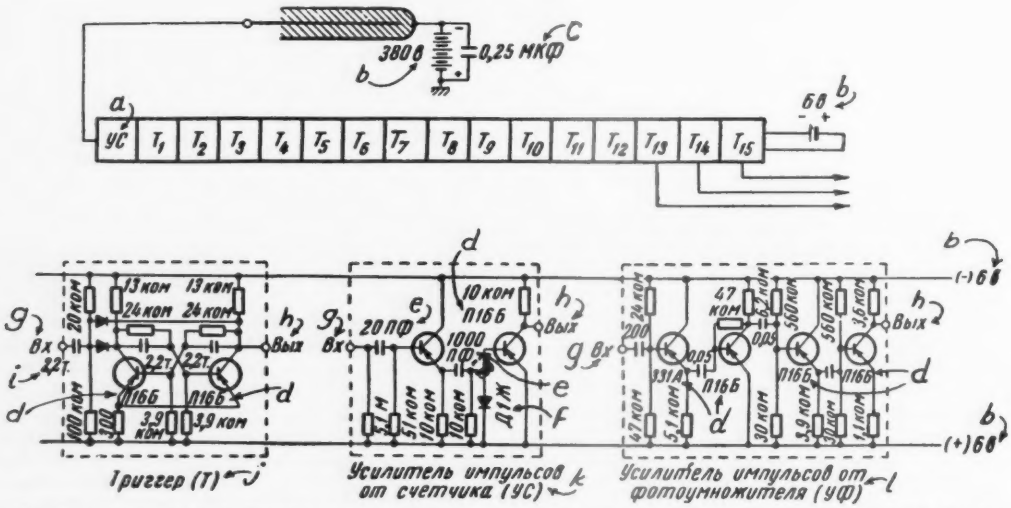

Fig. 4b Schematic block diagram of gas discharge counter, and schematic diagrams of typical electronic blocks. Translations: T, trigger; KOM, kilohms; M, megohms. a—counter-pulse amplifier; b—designates volts; c—μf; d—designation of transistor; e—$\mu\mu$f; f—designation of diode; g—input; h—output; i—2200 $\mu\mu$f; j—trigger(T); k—counter-pulse amplifier; l—photomultiplier-pulse amplifier

ment of the vehicle hull by relatively low energy electrons. We conclude, therefore, that in the outer radiation belt electrons are present.

Analysis of the data provided by Sputnik III has made it possible to determine the configuration of the outer radiation belt in the vicinity of Earth's surface.

Fig. 7 is a schematic diagram of a large portion of the Northern Hemisphere. The little star marks the position of the geomagnetic pole. The solid black dots mark the boundary of the outer radiation belt at a height above Earth's surface of 270 km; the white circles mark its boundary at an altitude of 600 km.

Analysis of our results has shown that the boundaries of the outer radiation belt coincide with the isochasms, i.e., with those imaginary lines connecting places on Earth's surface at which there is the same mean frequency of auroras. The radio signals from Sputnik III recorded in Antarctica indicate that in the vicinity of the geomagnetic pole there is

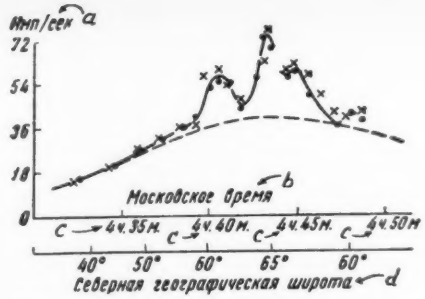

Fig. 5 Sample recording of increased radiation intensity in higher latitudes, made Nov. 7, 1957, aboard Sputnik II. Broken line depicts the average change in radiation intensity encountered here by Sputnik II on other occasions. Translations: a—pulses per second; b—Moscow time; c—denotes hr and min; d—north latitude

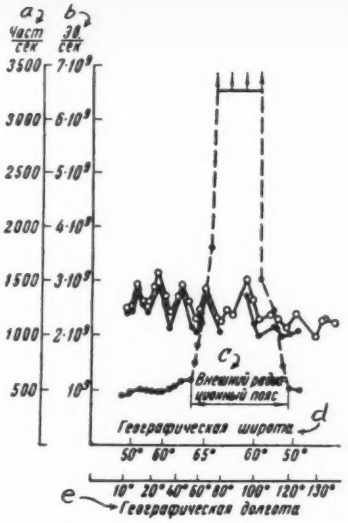

Fig. 6 Typical recording of scintillation counter readings in higher latitudes of Northern Hemisphere. Translations: a—particles per sec; b—ev per sec; c—outer radiation belt; d—latitude; e—longitude

no additional radiation present. On the basis of our experiments we can state that, near Earth's surface, the outer radiation belt is found within the range of geomagnetic latitudes from 55 to 70 deg. This permits the further conclusion that the belt extends for some 60,000 km and is bounded from within and without by the magnetic lines of force that intersect Earth's surface at geomagnetic latitudes of 55 and 70 deg, respectively. To explain this, let us examine the motion within Earth's magnetic field of the particles comprising the outer radiation belt. The strength of Earth's magnetic field is such that only particles possessing energies substantially in excess of 10^{10} ev are able to reach any point on Earth's surface, by undergoing a slight deflection within the magnetic field. As indicated in the foregoing, th electrons in the outer radiation belt have an energy much lower than this, an energy such that they move along the magnetic field's lines of force, in trajectories that wrap themselves spiralwise around those lines of force. If, in the process, the particles strike a region where the magnetic field becomes stronger, their movement along the lines of force first slows down, then is reversed. In other words, the particles will be reflected from, or bounced off, a region in which the magnetic field is strong enough.

In Fig. 8 a particle trajectory is projected into a meridian plane. Following a path that wraps itself spiralwise around the line of force, the particle is reflected, bounced back, at the indicated points in the higher latitudes. In this way it travels back and forth, back and forth, between the Northern and Southern Hemispheres. In addition, because of the inhomogeneity of Earth's magnetic field, it simultaneously revolves around Earth.

The motion of the particles being of this nature, we ought to observe a sharp rise in the radiation level inside the radiation belts as distance from Earth increases along the magnetic lines of force. During the flight of Sputnik III we had an opportunity to study radiation levels at different distances from Earth's surface. We made a comparative evaluation of data obtained at altitudes of 270 and 600 km (in the Northern Hemisphere) and 1800 km (in the Southern Hemisphere). As the altitude increased from 270 to 600 km, a significant increase in radiation intensity along the line of force was observed. As the altitude increased from 400 to 1800 km, the radiation intensity increased 40 times. This means that the flow of electrons along the lines of force is a two-way flow. Indeed, if the particles did not flow alternately both ways, back and forth, along the lines of force, but moved along them one way only, the radiation level would hardly rise at all with increasing distance from Earth.

Thus, as a result of our investigations we have succeeded in demonstrating that the radiation level actually does rise

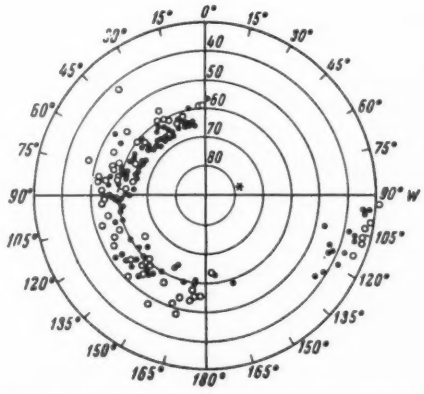

Fig. 7 During period May 15–June 18, 1958, Sputnik III, proceeding from the lower latitudes of the Northern Hemisphere, entered Earth's outer radiation belt at the points indicated by the black dots and emerged from it at the points indicated by the white circles. The white circles denote a higher flight altitude

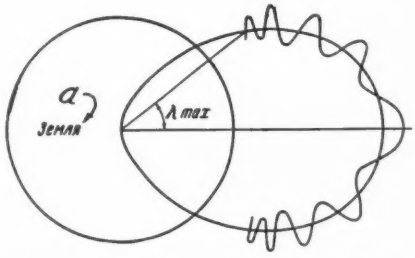

Fig. 8 Schematic representation of projection onto meridional plane of motion of a radiation belt particle in Earth's magnetic field. λ = latitude. Translation: a—Earth

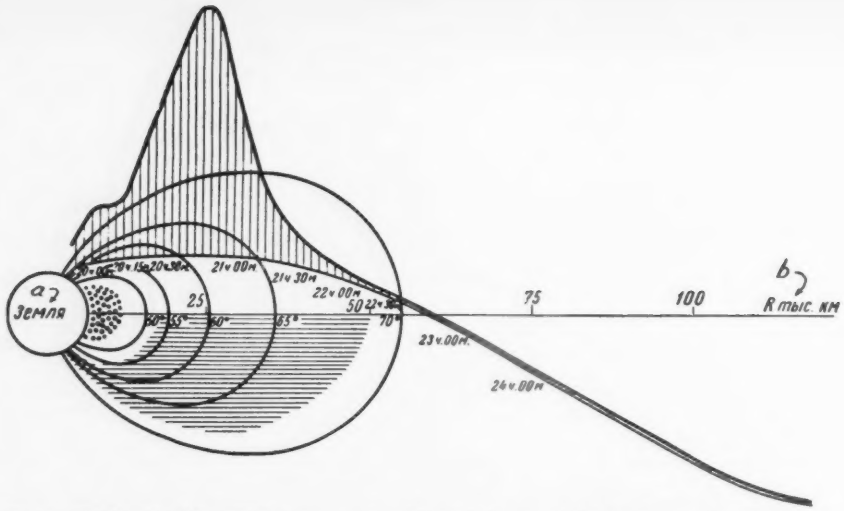

Fig. 9 Flight path of first Soviet space rocket described in terms of the geomagnetic coordinates. At intervals along the flight path the flight time is given (in Moscow time). Indicated also, by the vertical lines, are the radiation levels encountered along the flight path at the respective points at which the lines intersect it. Radiation level was determined by measuring ionization in the sodium iodide crystal. Shown are the magnetic lines of force that intersect Earth's surface at geomagnetic latitudes of 50, 55, 60, 65 and 70 deg. The horizontal hatching denotes the outer belt; the area of black dots the inner belt. Translations: a—Earth; b—thousands of km; numbers along the trajectory indicate mean time in the trajectory, given in hr and min

very steeply along the magnetic lines of force as distance from Earth increases. This constitutes experimental proof that the particles comprising the radiation belts oscillate within Earth's magnetic field, i.e., travel back and forth from the one hemisphere to the other. In other words, we may consider it demonstrated that Earth's magnetic field represents a trap for these particles. The high level of radiation within the belts is attributed to the fact that the trap is relatively escape proof, i.e., that particles caught within it remain there for some time.

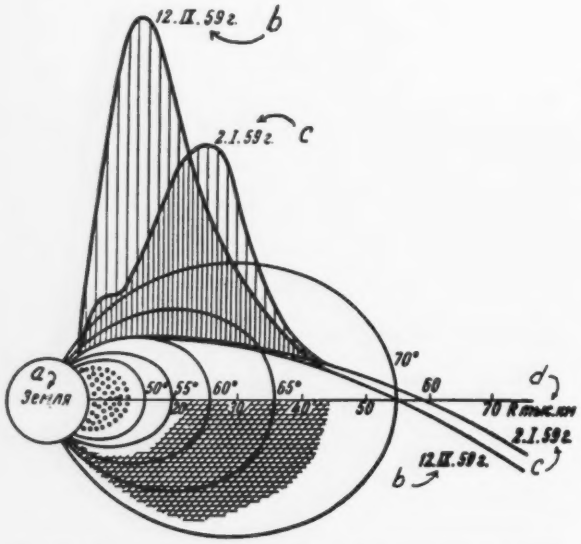

Fig. 10 Respective flight paths of first and second Soviet space rockets and the variation in radiation intensity encountered by each. Translations: a—Earth; b—Sept. 12, 1959; c—Jan. 2, 1959; d—thousands of km

The density of the air at altitudes above 1000 km is extremely low. For this reason, as the particles travel from the Northern to the Southern Hemisphere and back, only a very small amount of energy is consumed by ionization, a total of 0.01 ev. In these circumstances an electron having an energy of one million electron volts is able to complete one hundred million trips from one hemisphere to the other.

Thus, it is actually possible for particles to exist for a considerable length of time within the radiation belts.

The magnetic line of force that intersects Earth's surface at latitude 70 deg extends outward in the equatorial plane to a distance of 55,000 km from Earth's center. If, as we have shown in the foregoing, the particles travel back and forth along the lines of force, it must be that they do this traveling at great distances from Earth because, as we have seen, as our radiation belt approaches Earth's surface, it exhibits a marked decrease in radiation intensity, there being no radiation belt at all near Earth at latitudes above 70 deg. These considerations are valid, of course, only in a case in which, with reasonable accuracy, we may represent Earth's magnetic field as a dipole field. Experimental studies of the radiation belts at great distances from Earth were made during the flights of the space rockets.

Some results obtained during the flight of the first Soviet space rocket are depicted in Fig. 9. We see there the rocket's flight path and the change in radiation intensity with increasing distance from Earth. The highest radiation intensity was encountered at a distance from Earth's surface of 20,000 km. The figure shows also the lines of force of Earth's magnetic field. Comparative evaluation of the respective measurements made by the different instruments in the Sputniks and space rockets does indeed indicate that the boundaries of the outer radiation belt are lines of force of Earth's magnetic field. The configuration of the two belts as plotted from data provided by the U. S. satellites is shown in the figure by the horizontal hatching (outer belt) and the area of black dots (inner belt).

That the radiation level in the outer belt exhibited a very marked variation with time, had already been established during the flight of Sputnik III. What rendered this most

clearly evident was our comparative evaluation of the respective sets of data provided by the first and second Soviet space rockets.

Fig. 10 shows the respective flight paths of the two rockets and the variation in radiation level encountered by each. During the flight of the second rocket the radiation level in the outer belt was found to be much higher, and the peak level was encountered nearer Earth.

The inconstancy of the outer belt is attributed to the fact that it is subjected to bombardment by streams of corpuscles erupting from the sun. These streams depend upon the state or condition of the sun, and their intensity fluctuates very greatly.

The gas discharge and scintillation counters installed in the space rockets enabled us to determine the composition of the radiation in the outer belt. As I have said already, a count was made of the number of x-ray and gamma-ray quanta and high energy particles able to penetrate large thicknesses of matter. To find the energy spectrum of the particles, we placed our counters under absorbers of differing thicknesses. The absorber materials used were lead, copper and aluminum. The lower the atomic number of the absorber material, the more easily was it penetrated by soft x-rays. Thus, by using filters made of different materials we can determine the spectral makeup of the impinging x-rays.

Fig. 11 gives results of measurements made during the flight of the first Soviet space rocket; it shows the variation with distance from the center of Earth: 1 of the total ionization caused by all types of radiation; 2 of the number of impinging x-ray and gamma-ray quanta and penetrating particles. At distances from Earth's center above 70,000 km all instruments showed the impinging cosmic rays to consist solely of high energy particles. At distances within the outer belt of less than 70,000 km additional radiation was encountered. The most sensitive indicator of the presence of the radiation belts is an instrument that measures the x-rays produced when matter is bombarded by electrons. With the aid of this instrument it is possible to detect the presence of a radiation belt at distances exceeding 10 Earth radii. Comparative evaluation of the curves in Fig. 11 leads to the conclusion that the radiation present in the outer belt consists in a current or flux of electrons. Those electrons possess energies of tens, hundreds and millions of electron volts.

More detailed data on the composition of the radiation in the outer belt were obtained from the second Soviet space rocket. Fig. 12 gives results of some of the measurements that were made during its flight. The bottom curve shows that that belt contains practically no electrons with energies higher than 5 mev. The counters, shielded by copper and lead absorbers, indicate a high radiation level. We may conclude from this fact that in the outer radiation belt there are a large number of electrons having an energy of about one million electron volts.

The distribution of electrons with respect to energy level, therefore, has a very distinctive characteristic: With an increase in the energy of no more than several times (from 1 to 5 mev) the current or flux of electrons decreases by hundreds of thousands of times.

The presence of the outer belt of electrons with energies of 1 mev complicates greatly the task of providing shielding against harmful radiation effects in that belt. To provide such shielding, we shall have to use absorbent materials of great thickness.

The total number of electrons there is so great that their motion within Earth's magnetic field produces a demagnetization of the field. During the flight of the first Soviet space rocket N. V. Pushkov and Sh. Sh. Dolginov discovered anomalies in the distribution of Earth's magnetic field. This phenomenon is evidence of the fact that in the outer belt the energy density of the radiation approaches its maximum possible value, namely, the energy density of the magnetic field.

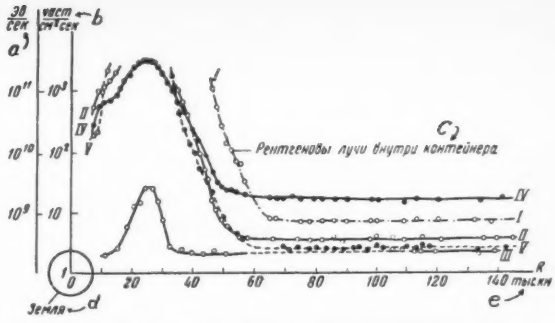

Fig. 11 Variation in radiation intensity as a function of flight altitude of first Soviet space rocket. R = distance from center of Earth. Curves I, II and III denote counting rates for particles having threshold energies of 45 kev, 450 kev and 4.5 mev, respectively. The counting rate is referred to a unit of area of the (19 cm²) cross section of the crystal. Curve IV denotes total ionization, i.e., the total amount of energy released per second inside the crystal. Curve V denotes the counting rate of the gas discharge counters referred to a unit of area of the counter cross sections (4 and 15 cm², respectively). Translations: a—ev per sec; b—particles per cm² per sec; c—x-rays inside container; d—Earth; e—thousands of km from center of Earth

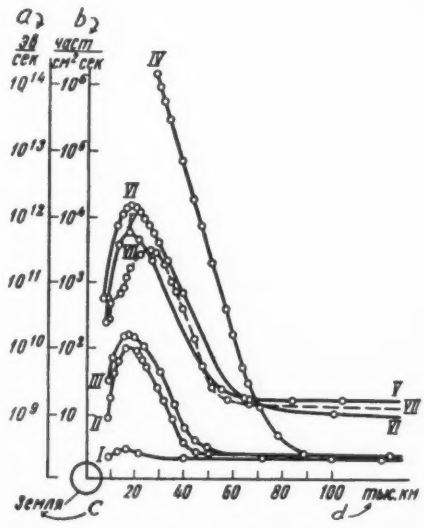

Fig. 12 Variation in radiation intensity as a function of the distance from the center of Earth. Curve I denotes third energy threshold (3.5 mev) of scintillation counter inside container. Curve II denotes readings of a counter shielded by a 3-mm thickness of lead. Curve III denotes readings of a counter shielded by a 1.5-mm thickness of copper inside container. Curve IV denotes readings of a counter having a window consisting of an 0.2-mm thickness of aluminum, the area of the window being considered the counter's effective area of exposure to radiation. Curve V denotes ionization rate in sodium iodide crystal inside container. Curve VI denotes ionization rate in sodium iodide crystal outside container. Curve VII denotes ionization rate indicated by instruments aboard first Soviet space rocket. Translations: a—ev per sec; b—particles per cm² per sec; c—Earth; d—thousands of km from center of Earth

In addition to the outer radiation belt there is an inner radiation belt. Data on the high level of radiation prevailing in the region of the equator at altitudes above 1000 km were first obtained by Van Allen, with the aid of the U. S. satellites "Alpha" and "Gamma." The flight paths of those two satellites traversed a range of latitudes extending 30 deg north and south of the equator. Data indicating that this

intense radiation zone was localized in a small region of space near the equator were first provided by Sputnik III, whose flight path traversed a broader range of latitudes which extended 65 deg north and south of the equator.

As we shall see in material which follows, in the vicinity of Earth the inner belt is observable at geomagnetic latitudes up to 40 deg. The exterior boundaries of that belt, therefore, can be ascertained only with the aid of a satellite whose flight path crosses latitudes above 40 deg. The flight path of Sputnik III met this requirement; the flight paths of "Alpha" and "Gamma" did not.

Fig. 13 shows a sample recording of radio signals from Sputnik III, a recording made aboard the diesel-electric ship "Ob′" off South America. In this way we learned something about the radiation intensity obtaining above that part of Earth. As the satellite vehicle approached the Equator, the radiation intensity was observed to increase by more than 100 times. By then the flight altitude of the vehicle had decreased from 1600 to 1000 km. Fig. 13 shows very clearly that the inner radiation belt lies within the limits of the region of lower latitudes.

Thus, there really does exist an inner belt of radiation, and it is not just a case of an increase in the radiation intensity with increasing altitude, as Van Allen had supposed prior to our reports to the Fifth Assembly of the IGY in 1958, on the results of measurements that we had made during the flight of Sputnik III.

With the aid of Sputnik III we were able to obtain a picture of the distribution of the radiation belts in the space above Earth. To accomplish this, we made use not only of recordings made in different parts of the world of the satellite's radio signals, but we utilized also that peculiar "memory" that a substance retains of its passage through the radiation belts (residual effects). The sodium iodide crystal in the scintillation counter was exposed to intense radiation while passing through the inner belt. As a result, it developed an intense phosphorescence, which remained observable for as long as several hours after the crystal's irradiation. By measuring the intensity of this phosphorescence we were able to determine the radiation intensity in those regions of space traversed by the satellite up to that time.

Experiments have revealed that over America the inner radiation belt starts at an altitude of 600 km, whereas over Australia it does not start until the much higher altitude of 1600 km. This asymmetry with respect to Earth which the radiation belts exhibit is attributed to the fact that the center of Earth's magnetic field does not coincide with the center of the planet. From the experiments that have been undertaken in connection with the study of the radiation belts it has been possible to determine with the utmost precision the extent of the shift involved. It turns out that the center of the dipole of Earth's magnetic field is displaced from the center of Earth, in the direction of Australia, by a distance of 500 km.

The instruments installed in Sputnik III have enabled us to determine the nature of the radiation in the radiation belts. As I have said already, it was through them that we were able to show that relatively low energy electrons are present in the outer belt.

In the inner belt, on the other hand, those same instruments have revealed the presence of high energy particles. The experimental data obtained necessitates the conclusion that the particles of the inner belt possess energies in excess of 10 mev.

But what is the nature of these high energy particles existing near Earth in our inner radiation belt? We have been able to answer this question by studying the phenomena that resulted from irradiation of the satellite vehicle as it passed through the inner belt. It was found that the particles in the inner belt created artificial radioactive substances inside the satellite. Quantitative analysis of the data indicates that, in order to be able to cause such phenomena, the particles

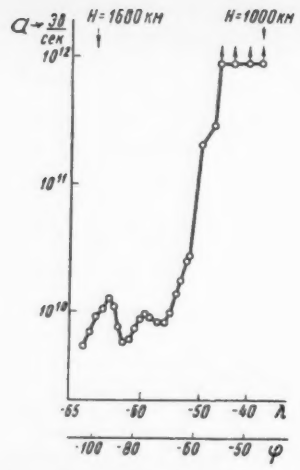

Fig. 13 Typical sample recording of radio signals received from Sputnik III. This recording was made aboard the diesel-electric ship "Ob′" off South America. The satellite's latitude (λ), longitude (φ), and flight altitude (H) are denoted by the horizontal scales. The vertical scale denotes the amount of energy released per second inside the crystal (i.e., the ionization rate, as inferred from measurements of the dynode current). Translations: a—ev per sec

of the inner belt must be protons with energies of about 100 mev.

The experiments carried out with the aid of Sputnik III have afforded evidence also of the presence, in the inner belt, of electrons. Despite the low intensity of the radiation that they produce, it has been possible to detect them along the inner belt's exterior rim, since the region or zone occupied by the electrons is somewhat broader than that occupied by the protons.

Within the inner belt, as our measurements have shown, the radiation intensity along the magnetic lines of force increases sharply with increasing distance from Earth. The energy, especially the momentum of the particles comprising the inner belt, is much greater than that of the particles that comprise the outer belt. But the strength of the magnetic field is greater in the inner belt. As in the outer belt, the particles in the inner belt travel in tightly curved trajectories that wrap themselves around the lines of force. Again, the observed increase in the radiation intensity along the lines of force is experimental proof that the particles of the inner belt also are caught in the trap created by Earth's magnetic field.

In many ways the inner radiation belt differs from the outer one. As I have said, the radiation intensity in the outer belt varies markedly with time, sometimes by a factor of more than 10. In the inner belt, on the other hand, the radiation intensity is very stable, varying by no more than 10–20 per cent.

Fig. 14 shows the structure of the radiation belts that gird Earth. We see there a cross section of the belts made by a meridional plane passing through Earth's geomagnetic poles.

What hypotheses can we offer concerning the origin of the radiation belts that gird Earth? The radiation belts exist, because Earth's magnetic field creates a trap for particles, a trap in which the particles may remain for a very long time. One of the mechanisms proposed by us to explain the origin of the radiation belts is the following. In the upper layers of Earth's atmosphere, under the action of cosmic rays, atomic nuclei are annihilated. Neutrons are emitted as a result. Having no electric charge, these pass unobstructed through Earth's magnetic field. But neutrons are unstable; they

decay spontaneously, giving off not only the neutrino but electrically charged protons and electrons as well. When a neutron decays inside the trap created by Earth's magnetic field, the decay products, i.e., the resulting protons and electrons, will be caught in that trap.

Supported by the results of the cosmic ray studies that have been carried out in the stratosphere, we can calculate reliably the workings of this mechanism. This approach, as we have shown, enables us to account for the existence of Earth's inner radiation belt. I should mention that the protons discovered in the inner belt possess such high energies that it is not likely that they could come from any source other than cosmic rays. Too, the constancy of the inner belt, observed in our experiments, can be explained by the great stability of processes caused by relatively high energy cosmic rays.

The fact that the inner belt is localized in a small region of space in the vicinity of the Equator indicates that in the higher latitudes the trap is not quite escape proof, and that particles there do escape from it in a relatively short time. It is natural to seek the cause of this in those fluctuations of the magnetic field that we observe at the higher latitudes. It is true, and should be stated, that in order to account for what has been observed in the experiments we must assume that the fluctuations of the magnetic field increase greatly in intensity with increasing distance from Earth (see following material).

The origin of Earth's outer radiation belt is something more of a riddle. We can put forward any number of hypotheses, but we cannot, at present, translate any one of them into quantitative calculations. It is natural to seek the origin of Earth's outer belt in the streams of corpuscles emitted by the sun. But the energy of the electrons in corpuscular streams is incomparably less than that of those in the outer radiation belt. We must assume, therefore, that when corpuscular streams collide with Earth there occurs among their particles a substantial redistribution of energy, and that this is the origin of the outer belt's radiation.

There may exist traps that travel or migrate through space, and these migrating traps may contain within them electrons having energies up to one million electron volts. If they exist, these phenomena must be rare, for during the flights of our Soviet space rockets, over a period of nearly 20 days, we were unable to detect that the instruments abroad were ever in contact with any such trap. Yet, the experiments conducted with sounding balloons (discussed in the following) suggest that there do exist traps that migrate through space.

We cannot rule out the possibility that a unique accelerator of some kind is operating near Earth, creating electrons with energies up to several million electron volts.

An acceleration of the particles would occur, actually, if the fluctuations in the strength of the magnetic field were large enough—as we had to assume in the foregoing that they are.

The specific mechanism for acceleration of the particles proposed by A. Ye. Chudakov requires that we assume the existence of a highly variable magnetic field component. The mechanism consists in the increasing of a particle's energy due to collisions of the particle with those previously described oscillating "magnetic stoppers," i.e., with the points or places on the line of force, in the higher latitudes, at which the particle is stopped and bounced back (see λ_{max} in Fig. 8). True, the lifetime of a particle inside the trap would not increase, but decrease, as the result of an acceleration of this type, because then there would be an increase in its velocity component along the line of force. That would increase the amplitude of its back-and-forth oscillations along the line of force, and it would be absorbed in the atmosphere. The existence of such an acceleration mechanism could account for the fact that the inner belt is localized in the region of low geomagnetic latitudes, for the fluctuations of the magnetic field increase with increasing latitude. In the lower latitudes the lifetime of particles is very long, being determined solely by the energy losses that they sustain in collisions with atoms. In the higher latitudes, because of the indicated mechanism, particle lifetime is shortened, and there is a corresponding decrease in the radiation intensity. For this reason, naturally, the greatest attenuation of radiation intensity will be observed in the vicinity of Earth, where only those particles are present that have large oscillation amplitudes, i.e., whose journeys from hemisphere to hemisphere are quite long. Comparison of our own results with those yielded by the flights of the U. S. space rockets tends to confirm these suppositions.

According to measurements made during the flight of Sputnik III, in the interval of space between the two belts the ionization that occurs in the sodium iodide crystal is 1000 times less than that which occurs within it inside the inner belt. Data yielded by the U. S. rocket Pioneer III indicate that in the vicinity of the Equator the radiation intensity decreases by no more than 10 times. Thus, the predicted effect actually is observed.

With the aid of the same mechanism we can try to account for the origin of the outer radiation belt. For this purpose we have to assume that in the outer belt the fluctuations in the magnetic field strength are so great that not only is there an increase in particle energy owing to the oscillations of the said "magnetic stoppers," but that a change occurs in the very nature of the particles' motion along the lines of force, namely, that the magnetic moment of the particles (the so-called adiabatic invariant) ceases to be constant. Under these conditions, notwithstanding the acceleration of the particles, it may be that the amplitude of their back-and-forth oscillations along the lines of force does not increase, but decreases. This would result in a relatively long particle lifetime.

In this way the electrons injected into the outer belt as a result of neutron decay and from corpuscular streams would receive an added acceleration. The fact, discovered by Winkler, that for several days after a magnetic storm the radiation in the outer belt exhibits an increased intensity, may be taken as confirmation of our assumptions. Actually, during a magnetic storm the oscillations of the plasma around Earth reach their very greatest intensity. This could substantially accelerate the particles, and increase at the same time their magnetic moment.

The factors operating to produce the radiation belts around our planet must also be operating to produce similar belts around other celestial bodies—provided those bodies have sufficiently strong magnetic fields.

We have undertaken special experiments designed to tell us whether radiation belts exist around the moon. During the flight to the moon of the second Soviet space rocket no such belts were detected. At distances from the moon of greater than 1000 km the intensity of the supplementary radiation was less than one millionth of the radiation intensity in Earth's outer radiation belt. Even nearer to the moon

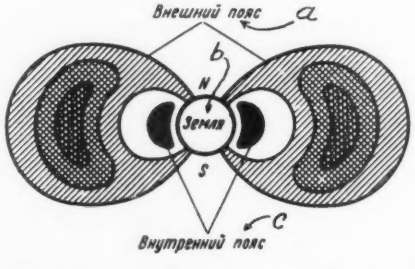

Fig. 14 Structure of radiation belts girding Earth. The density of the hatching in the outer belt affords some idea of the relative radiation intensities prevailing in that belt. Translations: a—outer belt; b—Earth; c—inner belt

there cannot exist any belt of radiation with an intensity of as much as one ten-thousandth of the radiation intensity of Earth's belts.

Radiation belts consist of particles revolving around Earth. Those belts have come into being because of a change in the properties of space near Earth, a change resulting from the presence of the magnetic field. We deem it reasonable, therefore, to call this phenomenon "terrestrial corpuscular radiation." The data yielded by the flight around the moon show that there is no lunar corpuscular radiation. This fact, experimentally established, means either that the moon has no magnetic field at all, or that, if it does have one, it is at least 1000 times weaker than Earth's.

Unquestionably, the existence of magnetic fields in different parts of cosmic space must result in concentrations of radiation in certain regions of it, concentrations in the form of unique radiation belts.

There is reason to believe that there exist in outer space gigantic reservoirs of particles, and that, possibly, these reservoirs travel or migrate. We have been led to this belief by the cosmic ray studies undertaken in the stratosphere during the IGY. For the purpose of those studies our own A. N. Charakhch'yan developed a special radiosonde. With that instrument, installed in sounding balloons, cosmic ray measurements were carried out in the stratosphere daily over three different parts of the Soviet Union. Approximately 1500 ascents were made in all.

As a result of those experiments we were able to discover that fairly often, on an average of once a month, the sun becomes a source of cosmic rays. At those times explosion-like processes occur on the sun, and an acceleration of particles takes place. Many of the particles become caught in the unique traps that fly out from the sun. During these periods the entire solar system also becomes a huge trap for particles. On such occasions the intensity of the cosmic rays becomes so great that, without special shielding, man could not survive in interplanetary space.

We are not able yet to predict when those explosion-like processes will occur on the sun. Meanwhile the state or condition of the sun—the "solar weather," as it is called—can be dangerous for space travelers. Fortunately, though, the scale of those troublesome processes is not insuperably great. Hence the cosmic rays that originate on the sun all have relatively low energies, and it is possible, with special shields, to protect against them. It is true, of course, that the presence of such shields will add greatly to the weight of space vehicles.

The great successes of our Soviet rocket designers assure that we shall have at our disposal whatever is needed for the assault upon the universe.

Before us lies the task of studying the structure of space and of the celestial bodies within it.

Cosmic radiation should be used to help us learn the secrets of matter.

Investigation of Basic Characteristics of Combustion of a Homogeneous Mixture of an Open Turbulent Stream

E. A. PETROV and A. V. TALANTOV

Kazan' Aviation Institute

Many experimental and theoretical papers are devoted to the investigation of combustion of a homogeneous mixture in a turbulent stream.

The theory of turbulent combustion makes use of both the "surface" and "volume" mechanisms of the process (1–4 and others).[1] The question of the mechanism of flame propagation is still moot.

The results of the experimental investigations on the study of the velocity of flame propagation (u_t)(5–9 and others) are somewhat contradictory, this being partially due to different experimental procedures, and also to a certain arbitrariness in the definition of u_t itself. The latter is defined as the rate of displacement of an average surface, corresponding to a certain fraction of the reacted substance. In papers by different authors, this fraction ranges from 0, corresponding to the initial ignition boundary (the most rigorous assumption), to 50 per cent, corresponding to the midpoint of the combustion zone.

Only a few investigations have been devoted to the combustion time (t) and to a quantity corresponding to it, namely the extent of the combustion zone along the stream lines (L)(4–6, 9,10). The latter quantities are of great interest in practice of construction of combustion chambers and for the advancement of our knowledge concerning the combustion mechanism in a turbulent stream.

In the present paper we report the results of an experimental investigation of these fundamental characteristics of

Translated from *Izvestiia Vysshikh Uchebnykh Zavedenii, Seriia Aviatsionnaia Tekhnika* (Bull. of Institutions of Higher Learning, Aviation Technology Series), no. 3, 1959, pp. 91–100. Translated by J. George Adashko.

[1] Numbers in parentheses indicate References at end of paper.

the combustion process (u_t, t, L) in a turbulent stream of a homogeneous mixture, using a procedure proposed in (11).

The experiment was performed with a setup shown schematically in Fig. 1. Air was fed by the centrifugal compressor of the ASh-73 engine, driven by a 240-kw motor. The air from the compressor went through a heat exchanger and was heated to the required temperature by gas from a special combustion chamber. The flow of air could be varied by a throttle valve ahead of the heat exchanger, and was measured by a standard measuring orifice located a certain distance past the heat exchanger. Two fuel jets located some 10 m from the cut section of the tube produced atomization in a direction opposite to the stream. The fuel flow was regulated by the pressure in the main line, which in turn was monitored by a standard manometer and measured with the aid of a sampler.

The object of investigation was an "inverted" flame cone at a section of a tube 150 mm in diameter.

The flame was stabilized with an acetylene-oxygen burner, placed at the center of the tube section. The flow of gas through the burner was very small, and consequently the igniting flame did not introduce any noticeable changes in the main stream and did not distort the combustion in the latter. The combustion process was monitored by measuring the CO_2 fields at different distances from the burner.

The turbulence of the stream was measured with the aid of screens placed at a distance of half the diameter from the section of the tube. The turbulizing screens consisted of two series of mutually perpendicular cylindrical rods. The distances between the axis of the rods (a) and the diameters of the rods (b) were as follows in different gratings

$$N1 - a = 12 \text{ mm}, b = 4 \text{ mm}$$

$$N2 - a = 16 \text{ mm}, b = 8 \text{ mm}$$

$$N3 - a = 8 \text{ mm}, b = 4 \text{ mm}$$

The principal experiments were performed with a benzene-air mixture with initial temperature 100 C at atmospheric pressure. There were carried out at four velocities of the incident stream w (20, 40, 60 and 80 m per sec) and different excess-air coefficients α (1, 1.2, 1.4, 1.6, 1.8 and 2).

To disclose the effect of the type of fuel, experiments were also performed in a kerosene-air mixture. The normal velocity of flame propagation under laminar conditions u_n was determined by means of special experiments, using the Bunsen-burner method with gas sampling from the tube of the principal installation. This made it possible to determine u_n accurately for the mixture used in the principal experiment.

The principal experiment consisted of finding the internal and external boundaries of the "inverted" cone of the flame. The outer boundary was determined by photographing on high sensitivity film. The inner boundary of the combustion zone was determined with the aid of a GEUK-21 gas analyzer. Gas was sampled by means of a water-cooled gas sampler, the small diameter and cooling of which made it possible to gather a sample from a selected point without distorting the stream and "to freeze" the sample. The plotting of the CO_2 fields was in several transverse cross sections of the flame, in a series of points spaced 2–5 mm apart along the section.

The value of u_t was determined in the interval from the burner to a section located 120 mm from the burner. The choice of such a section was dictated by the fact that, under all operating conditions, the outer boundary of the flame did not leave the core of the stream within the confines of this distance. The core of the stream was determined from the analysis of the velocity profiles for different cross sections. The degree of turbulence under these conditions was 0.07 and 0.115 for screens no. 1 and 2 respectively.

The true velocity of flame propagation, which is the velocity of the displacement of the forward ignition boundary relative to the fresh mixture, was determined in accordance with the Michelson law by the method described in (11).

The procedure proposed made it possible to plot the stream lines, which yielded the extent of the combustion zone defined as the distance from the outer boundary of the flame to the inner one. The time of combustion was calculated by dividing the extent of the zone by the velocity of the incident stream, the latter being assumed constant, since the process took place in a free jet. The extent of the zone was investigated for an initial stream line located 4 mm from the tube axis. The choice of this stream line was dictated by the requirement that it should not leave the core of the stream at the instant of completion of the combustion.

The normal flame propagation velocity for benzene-air and

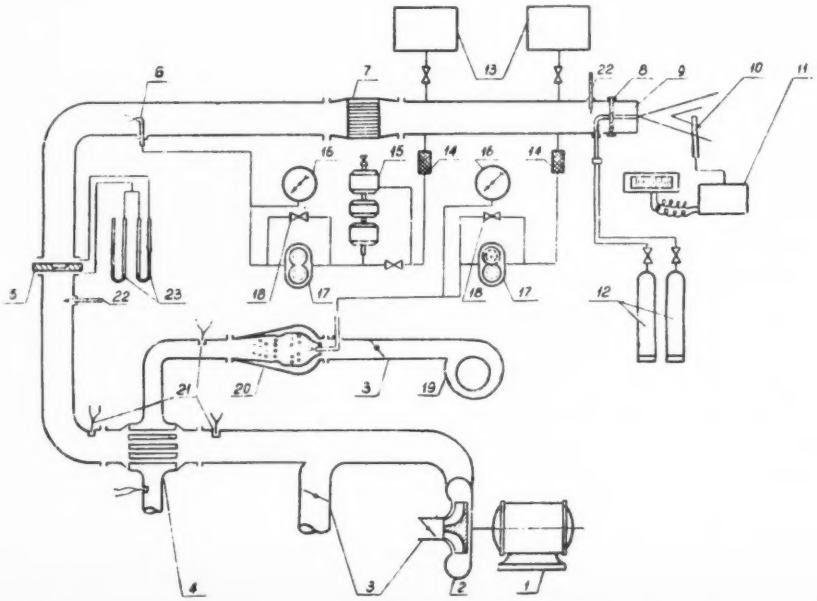

Fig. 1

kerosene-air mixtures was found to be experimentally the same (Fig. 2). This is in satisfactory agreement with the data published in the literature (12).

The rate of flame propagation in a turbulent stream, for gratings nos. 1 and 2, as obtained in this experiment, are shown in Figs. 3 and 4 as functions of u_n for different values of w. The curves obtained show that the normal velocity retains its significance up to large ratios of the pulsational velocity (w') to the normal velocity, which agrees with conclusions of other authors (4–8). Fig. 3 shows also the values of u_t for a kerosene-air mixture. It is seen that the values of the rate

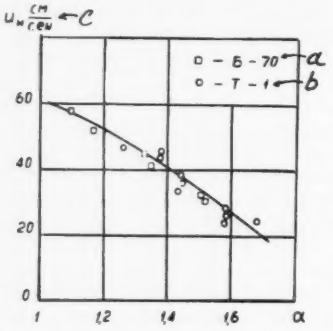

Fig. 2 Translations: a—benzene-air; b—kerosene-air; c—u_n, cm/sec

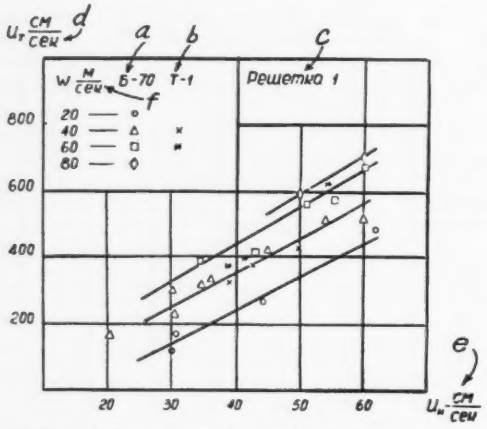

Fig. 3 Translations: a—benzene-air; b—kerosene-air; c—screen; d—u_t, cm/sec; e—u_n, cm/sec; f—m/sec

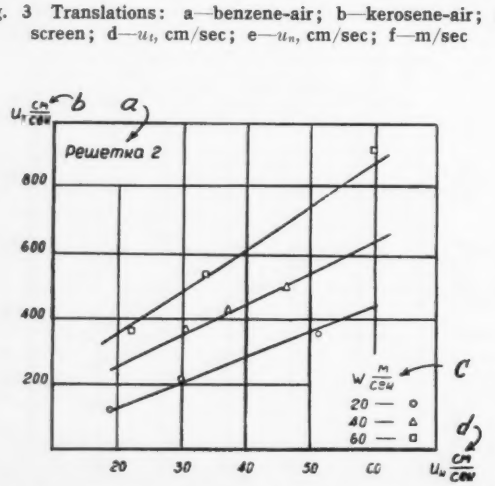

Fig. 4 Translations: a—screen; b—u_t, cm/sec; c—w, m/sec; d—u_n, cm/sec

of propagation of the flame hardly differ from those for the benzene-air mixture. Considering that the normal velocities of flame propagation are the same for these mixtures, this result is in good agreement with the theory of "surface" combustion in a turbulent stream. At the same time, from the point of view of the "volume" theory, it does not necessarily follow that the value of u_t should be equal, for the kinetics of the chemical reactions in the kerosene and benzene mixtures, and the corresponding durations of these processes, may be different.

Fig. 5 shows a plot of u_t vs. w' for different normal velocities, obtained by recalculation from the preceding curves. At the same normal velocity, the quantities u_t, as functions of the pulsational velocities, fit on the same curve for both screens, which have different rod dimensions. Consequently, under these conditions u_t depends only on u_n and on w' and is independent of the method by which the value of w' is obtained. The curves obtained in the experiments with turbulizer no. 3 also fall on the same curve.

In accordance with the theory of "surface" combustion, the rate of propagation of a flame in a turbulent stream can be represented in dimensionless form in the form of a ratio

$$\frac{u_t}{u_n} = f\left(\frac{w'}{u_n}\right)$$

A curve of this relation, obtained experimentally (Fig. 6), is evidence of the existence of this relation, starting with certain values of the ratio $w'/u_n(>20)$. At smaller values of w'/u_n the values of u_t/u_n increase with the normal velocity, in agreement with (6). This is evidence that the process is influenced by certain additional factors, which are not taken into account in the theory (thermal, kinetic, self-turbulization, etc.).

The relative increase in the rate of propagation of the flame due to turbulence $[(u_t - u_n)/w']$ (Fig. 7) increases with the normal velocity for unchanged w'/u_n. With increasing w'/u_n, these quantities decrease, tending to a constant value of 0.5 for different u_n. The only exception is $u_n = 20$ cm/sec, for which $(u_t - u_n)/w'$ is practically constant. This character of the curves $(u_t - u_n)/w' = f(w'/u_n)$ may be explained from the point of view of the "surface" mechanism of flame propagation. An analytic relation for the rate of flame propagation (6), following from the theory based on premises by K. I. Shchelkin, leads to the expression

$$\frac{u_t - u_n}{w'} = \frac{1}{\sqrt{\ln \frac{w'}{u_n}}}$$

It is easy to see that with increasing w'/u_n, the right-hand side, and consequently also the left-hand side, decreases.

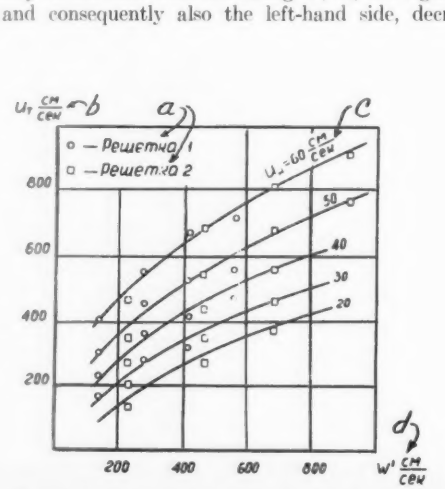

Fig. 5 Translations: a—screen; b—u_t, cm/sec; c—u_n = 60 cm/sec; d—w', cm/sec

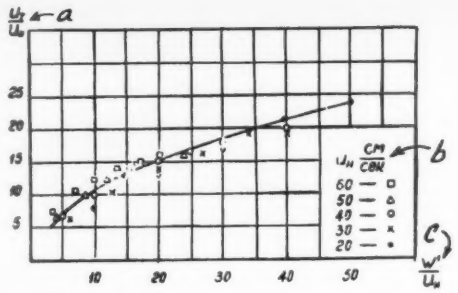

Fig. 6 Translations: a—u_t/u_n; b—u_n, cm/sec; c—w'/u_n

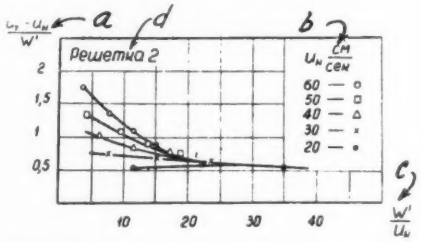

Fig. 7 Translations: a—$(u_t - u_n)/w'$; b—u_n, cm/sec; c—w'/u_n; d—screen

Also the decrease in the value of $(u_t - u_n)/w'$ may not be due to self-turbulization, the role of which increases at small w'/u_n.

The experimental results can be described approximately by the following relation

$$\frac{u_t}{u_n} = A\left(\frac{w'}{u_n}\right)^a \qquad [1]$$

where $A = 2.7$ and $a = 0.6$.

The exponent a in this expression is of the same order as the value obtained by others (5–7). The coefficient A, however, is different from that given in (6).

It is known that the rate of flame propagation under laminar conditions, at a flame-front radius of curvature of the same order as its thickness, decreases substantially when the front is convex toward the fresh mixture. In the "inverted cone" under consideration, the thickness of the front is also of the same order as the radius of curvature. Thus, the reduction in the value of u_t in the case of an axially symmetrical process can be attributed, in analogy with the preceding, to the deterioration of the flame propagation conditions. In addition, the photography results will be somewhat different for a plane and axially symmetrical flame, owing to the greater depth of the flame front in a direction perpendicular to the plane of the photograph.

Figs. 8 and 9 show the dependence of the extent of the zone (L) on the speed of the stream for different normal speeds. It is seen that the extent of the zone increases with increasing speed of the stream. Its increase, however, which is intense in the range of small w, slows down at sufficiently large w. The same curves are evidence that the dimensions of the combustion zone are inversely proportional to the normal velocity.

The extent of the zone, given in dimensionless form

$$\frac{L\epsilon}{d} = f\left(\frac{w'}{u_n}\right)$$

for both screens, is shown in Fig. 10. From an examination of the curve one can conclude that all the points, with a cer-

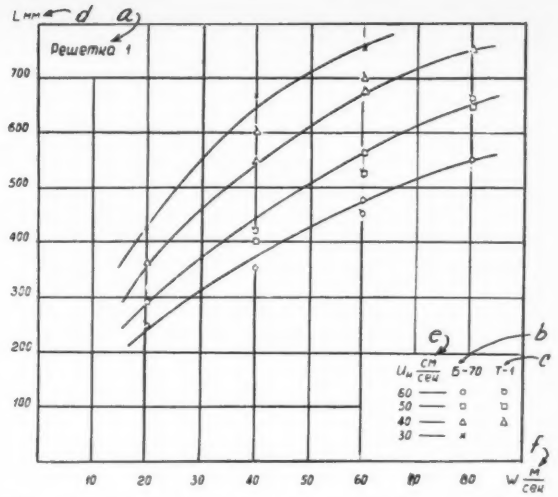

Fig. 8 Translations: a—screen; b—benzene-air; c—kerosene-air; d—Lmm; e—u_n, cm/sec; f—w, m/sec

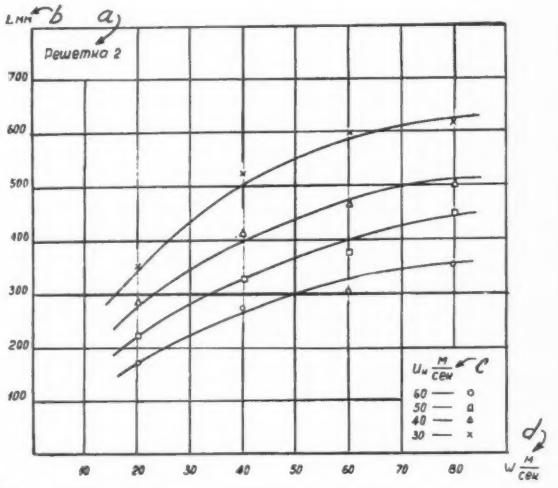

Fig. 9 Translations: a—screen; b—Lmm; c—u_n, m/sec; d—w, m/sec

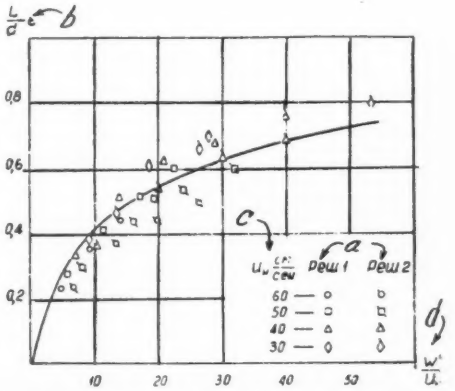

Fig. 10 Translations: a—screen; b—$(L/d)\epsilon$; c—u_n, cm/sec; d—w'/u_n

tain dispersion, fit a single curve, whose equation can be written

$$L = 0.18 \frac{d}{\epsilon} \ln \left(1 + \frac{w'}{u_n}\right) \quad [2]$$

Here

$\epsilon = w'/w$ = degree of turbulence at inlet to zone
d = tube diameter at the section

It is interesting to establish the connection between the size of the zone and the scale of turbulence at the inlet to the zone (l_0), as determined in (13). A plot of the experimental results in coordinates $L\epsilon/l_0$ and w'/u_n causes the points to separate into two individual groups, so that each turbulizer has its own curve. These relations can be represented as follows:

For screen no. 1

$$L = 19.6 \frac{l_0}{\epsilon} \ln \left(1 + \frac{w'}{u_n}\right) \quad [3]$$

For screen no. 2

$$L = 13.6 \frac{l_0}{\epsilon} \ln \left(1 + \frac{w'}{u_n}\right) \quad [4]$$

The combustion time calculation (4–6), based on the premises of K. I. Shchelkin, leads to the following relation

$$t = \frac{l_0}{w'} \ln \left(1 + \frac{w'}{u_n}\right) \quad [5]$$

The extent of the zone, if the stream velocity does not change in the zone, is given by

$$L = \frac{l_0}{\epsilon} \ln \left(1 + \frac{w'}{u_n}\right) \quad [6]$$

By comparing the theoretical equations with the experimental results, one can judge the extent to which the theory accounts for the effect of the principal factors ϵ, w and u_n. An exception is the effect of the turbulence scale on the dimensions of the zone. The experimental data have shown no such connections for screens with substantially different turbulence scales, as determined in (13) (1.5 and 2 mm). Equation [2] is evidence that the extent of the zone is proportional to the tube diameter. The point is that the dimension that determines the combustion time assumes the same value as that for a tube. One can imagine that at a certain distance from the turbulizer, the scale of the greatest perturbations in the stream is determined by the size of the tube, although the eddies generated by the screen continue to exist in the stream. At the particular scale of turbulence prevailing behind the screen in this case, these eddies may be less than for a tube.

An argument in favor of the foregoing assumption is the size of the coefficient in Equation [2], which is close to the coefficient obtained in a similar formula in an experiment without screens, with tubes measuring 40, 25 and 8 mm (5,6). Actually, the dependence obtained in (5 and 6) is of the form

$$L = 0.16 \frac{d}{\epsilon} \ln \left(1 + \frac{w'}{u_n}\right) \quad [7]$$

which is close to Equation [2].

If we replace in Equations [2 and 7] the tube diameter by the turbulence scale, in accordance with the equation $l_0 = 0.04d$ (14), then the extent of the zone becomes

$$L = B \frac{l_0}{\epsilon} \ln \left(1 + \frac{w'}{u_n}\right) \quad [8]$$

where B takes on values of 4.5 and 4, respectively.

The value greater than unity for the coefficient B can be ascribed to the fact that the dimensions of the zone are determined by characteristic dimensions that exceed the average ones by several times. This is quite feasible.

The dimensions of the combustion zone and of the combustion time, obtained in experiments with kerosene-air and benzene-air mixtures, are the same (Figs. 7 and 8). This too is a confirmation of the "surface" model of the process.

The dependence of the combustion time on the different factors can be obtained from the preceding relations by dividing the extent of the zone by the stream velocity. Analytic relations on the results of the performed experiments assume the form

$$t = B_1 \frac{d}{w'} \ln \left(1 + \frac{w'}{u_n}\right) \quad [9]$$

or

$$t = B_2 \frac{l_0}{w'} \ln \left(1 + \frac{w'}{u_n}\right) \quad [10]$$

where

$$B_1 = 0.18 \qquad B_2 = 4.5$$

and l_0 = turbulence scale for the tube.

It is interesting to note that as the stream velocity increases, the extent of the zone increases and the combustion time decreases, owing to intensification of the combustion process. The relations obtained show that the combustion time in the turbulent stream can be reduced by increasing the intensity and reducing the turbulent scale, and also by increasing the normal velocity, i.e., both as a result of hydrodynamic and chemical factors.

References

1 Shchelkin, K. I., *Zhur. Tekhnicheskoi Fiziki* (Journal of Technical Physics), vol. XIII, p. 520, 1943.

2 Shchetnikov, E. S., "Collection of Articles on Turbulent Combustion of a Homogeneous Mixture," Oborongiz (State Publishing House of Defense Industry), 1956.

3 Summerfield, M., Reiter, S., Kebel, A. and Mascolo, R., JET PROPULSION, vol. 25, no. 8, 1955, pp. 377–384.

4 Talantov, A. V., Trudy KAI (Trans. of Kazan' Aviation Institute), vol. 31, 1956.

5 Talantov, A. V., Dissertation, Institute of Chemical Physics, Acad. Sci. USSR, 1953.

6 Talantov, A. V., Trudy MAP (Trans. Ministry of Aviation Industry), no. 8, 1955.

7 Vlasov, K. P. and Inozemtsov, N. N., *Izvestiia Vysshikh Uchebnykh Zavedenii, Seriia Aviatsionnaia Tekhnika* (Bull. of Institutions of Higher Learning, Aviation Technology Series, no. 1, 1959.

8 Shchetnikov, E. S. and Vlasov, K. P., "Collection of Articles on Turbulent Combustion of Homogeneous Mixture," Oborongiz (State Publishing House of Defense Industry), 1956.

9 Lushpa, A. I., Trudy MAP (Trans. of Ministry of Aviation Industry), no. 265, 1955.

10 Doroshenko, V. E. and Nikitskii, A. I., Trudy MAP (Trans. of Ministry of Aviation Industry), no. 282, 1956.

11 Petrov, E. A. and Talantov, A. V., *Izvestiia Vysshikh Uchebnykh Zavedenii, Seriia Aviatsionnaia Tekhnika* (Bull. of Institutions of Higher Learning, Aviation Technology Series, no. 1, 1959.

12 Inozemtsov, N. N., *ibid.*, no. 4, 1958.

13 Baines, W. and Peterson, S., Trans. ASME, vol. 73, no. 5, 1951.

14 Prudnikov, A. G., "Collection of Articles on Turbulent Combustion of Homogeneous Mixture," Oborongiz (State Publishing House of Defense Industry), 1956.

—Original received April 7, 1959

Reviewer's Comment

The "surface" combustion mechanism is well known as the "wrinkled laminar flame" concept; the "volume" combustion mechanism is usually termed the "distributed reaction zone." Several years ago there was disagreement as to which mechanism was valid. It has been recognized that turbulent combustion involves many interrelated physical and chemical processes. One or more processes may dominate for a certain range of conditions. For example, when the ratio $(\delta/u_n)/$

(λ/w') which is known as the Kovasznay parameter,[1] is small, the wrinkled laminar flame appears to be an adequate model. The dominant process then becomes the mechanism of turbulent combustion.

Experiments to determine the numerous variables require careful technique. In this paper the scale and intensity of turbulence were apparently determined using the well-known correlations for these quantities in terms of x/M (the distance downstream from a screen or grid divided by the screen mesh) as reported by Townsend and Batchelor. However the approach stream is a fully developed turbulent flow, since it extends for at least 70 diam upstream of the screens and has a Reynolds number of 10^5 to 10^6. Also the turbulent flame was stabilized at about $x/M = 6$. Values of x/M of at least 15 are necessary for use of the Townsend-Batchelor results.

Another experimental pitfall may be the sampling technique used to ascertain the extent of the CO_2 fields. The tube was stated to be "small." The inside and outside diameters are not given. Results also depend on the sampling rate.

The assumption that the velocity does not change through the combustion zone is used at several points. The density may decrease by a factor of 5 to 10 across a flame; application of the continuity equation shows that the velocity must change. Comparison of Equations [3 and 4] with Equation [6] shows that there is a factor of 19.6 or 13.6 missing. Perhaps half of this missing factor in the equation based on theory, i.e., Equation [6], is due to the variable velocity.

This paper presents data on kerosene-air and benzene-air system. Data on these fuels are scarce since experimenters frequently work with gaseous fuels, e.g., propane. The results presented in Figs. 8, 9 and 10, concerned with the turbulent flame thickness, are valuable additions to the store of knowledge on turbulent combustion. These data may contribute to the development of a satisfactory turbulent flame theory.

Explanation of flame behavior illustrated in the dimensionless plots of Fig. 7 remains a challenge. Qualitatively the curves exhibit trends consistent with the phenomenological theory proposed by Povinelli and Fuhs at the Eighth Combustion Symposium. It will be interesting to apply that theory to obtain numerical results.

The use of the tube diameter d in Equation [2] does not appear justified at first glance. Only one tube size was used and the only geometrical variations were the change in screens. However, the empirical formula does correlate the results for all screens. Use of the scale of turbulence as the reference length requires a different empirical constant for each screen. As the authors state, the tube diameter has an influence on the distribution of eddy sizes.

—Allen E. Fuhs
Physical Research Laboratory
Aerospace Corporation

[1] L. S. G. Kovasznay, "A Comment of Turbulent Combustion" Jet Propulsion, vol. 24, 1956, p. 485.

Digest of Translated Russian Literature

The following abstracts have been selected by the Editor from translated Russian journals supplied by the indicated societies and organizations, whose cooperation is gratefully acknowledged. Information concerning subscriptions to these publications may be obtained from these societies and organizations. Note: Volumes and numbers given are those of the English translations, not of the original Russian.

SOVIET PHYSICS-SOLID STATE (Fizika Tverdogo Tela). Published by American Institute of Physics, New York.

Vol. 2, no. 1, July 1960.

Electrokinetic Effects in Liquid Semiconductors, by V. B. Fiks and G. E. Pikus, pp. 58–59.

Secondary Electron Emission From Thin Metal Films on an Activated Base, by I. M. Bronshtein and R. B. Segal', pp. 84–86.

Thermally Stimulated Conductivity in Semiconductors, by I. I. Boiko, É. I. Rashba and A. P. Trofimenko, pp. 99–107.

Abstract: A theory of thermally stimulated conductivity is constructed on the basis of a quite general model of a semiconductor. It is shown that an analysis of plots of thermally stimulated conductivity for various heating rates allows one to determine the depth of localized levels. A preliminary comparison of theory and experiment is made.

Characteristic Temperature and Spectrum of Thermal Lattice Vibrations, by A. P. Zvyagina and V. I. Iveronova, pp. 108–111.

Concerning the Theory of Inelastic Electron Scattering in Solids, by A. Ya. Vyat-skin, pp. 112–122.

Introduction: In the preceding papers, in the first Born approximation of perturbation theory, the problem of the inelastic scattering of electrons with nonrelativistic energy in metals due to their coulomb interaction with the lattice electrons, was examined. The lattice electrons were described by means of the approximation for the case of weak bonds. The results of the solution refer basically to the electrons in the wide Fermi band of metals, under the conditions of a sufficiently accurate approximation for the case of weak bonds. It is interesting to examine the same problem for the case of strong bonds between the lattice electrons. The results of such a solution, as distinct from the results obtained using the weak bond approximation, are better applicable to the electrons of the narrower filled bands of metals. They may likewise be applied to the electrons of the upper bands of dielectrics and semiconductors, of course, for

the case where the latter may be described by means of the weak bond approximation.

The Absorption of Light in Germanium, by M. I. Kornfel'd, pp. 163–164.

Introduction: The absorption of light in germanium in the region of wave lengths below 2.5μ depends principally on the internal photoeffect. The theory of this phenomenon, developed by Hall, Bardeen and Blatt, leads to complex expressions for the dependence of the absorption coefficient on the wave length of light and the temperature. Between them, as we shall see, this

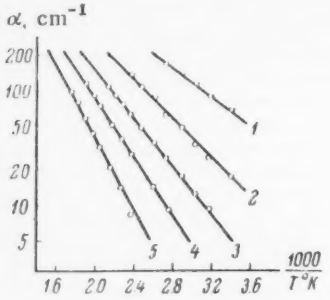

Fig. 1. 1) 1.6μ; 2) 1.7; 3) 1.8; 4) 1.9; 5) 2.0μ.

dependence is extremely simple in any case, at temperatures above 200 K. The results of the measurements we performed on the absorption coefficient of monocrystalline germanium (about 50 ohm · cm), are shown in Fig. 1.

TELECOMMUNICATIONS (*Elektrosviaz'*). Published by Pergamon Institute, New York, in conjunction with Massachusetts Institute of Technology, Cambridge, Mass.

No. 10, 1959.

The Geometric Structure of Optimum Codes, by B. M. Pushnoi, pp. 1047–1061.

Abstract: The possibilities of constructing codes of increased noise immunity are considered. It is shown that the points of optimum code signals coincide with the vertexes of certain perfect solids. Also some imperfect solids, the vertexes of which may serve as points of optimum code signals are examined.

Introduction: It is evident that the optimum code is the one which is not only in harmony with the statistics of the messages, but which also guarantees the maximum probability of correct reception of each signal. The common (noncorrective) binary code provides a comparatively low noise immunity at the given ratio of signal power to noise power. In the present article the questions linked with the problem of constructing codes providing a higher noise immunity will be considered. All investigations were conducted on the ground of geometrical representation of code combinations, in the form of points situated in a space, the number of dimensions of which n equals the quantity of signs in the combination, generally accepted at present.

The Spectrum of Phase Keyed Signals, by F. V. Yelizarov and Iu. A. Iurkov, pp. 1062–1074.

Introduction: Recently the phase manipulation of carrier frequencies is finding ever increasing applications in telegraphy and also in telemetering and telecontrol systems.

In solving a series of problems in connection with the application of phase keying, an investigation into the character of phase manipulated signals is of considerable importance.

In the present article the problem of determining the spectra of pulsed and continuous signals, phase manipulated in a complicated form, will be presented. The problem is formulated as follows. The spectrum of a single pulse, or of a chain or a periodic sequence of pulses, with durations τ for each of them, and with the harmonic external oscillations has to be found. Here, during the time τ the locking phase may go through q step changes (reckoning a step also at the beginning of the pulse) but remain constant between the subsequent jumps for a duration τ_k. In the general case, the value of the initial phase after each step might be described in the form $\Theta_k = i\Theta$, where i may assume any positive or negative value, the total number of these values being equal to q. In case of a periodic phase keyed signal, the values of i recur in each pulse in the same order of succession.

If in a periodic sequence the frequency of pulse recurrence f is selected so as to equal $1/\tau$, then, evidently, this pulse sequence transforms into a continuous phase manipulated signal.

It will be found that, depending on the class of functions into which the signals considered can be regarded as periodic or aperiodic, either the method of Fourier series or the method of Fourier integral could be employed in order to determine their spectrum.

For the sake of clarity, the examples considered in this article will contain signals of rectangular envelope and step changes of phase, the values assigned to i being 0, 1, 2, ..., q. The general formulas, however, deduced in the article, will enable us to find the spectrum of phase manipulated signals with any shape of envelopes and with any nonrandom law of phase manipulation.

Operation of a Single-Cycle Magnetic Shift Register With Synchronous Magnetic Polarity Reversal of Complementer, by A. K. Romanov, pp. 1106–1120.

Abstract: The operation of a single-cycle shift register, using a core with rectangular hysteresis loop, is examined. An account of the circuit from an engineer's viewpoint is included.

No. 11, 1959.

On the Character of Signal Distortion in a Single Sideband Telephony System in Tropospheric Communication Links, by M. P. Dolukhanov, pp. 1180–1188.

Abstract: The character of the steady-state signal distortion in tropospheric communication links, due to the method of propagation, has been theoretically analyzed. An idealized case of interference between two rays, which then propagates into the real troposphere, has been investigated. It has been proved that there is no distortion in an SSB telephony system, which is due to the method of propagation of transients. The types of distortion present are: Fading; the Doppler frequency shift.

On the Stability of Single-Circuit Tuned Amplifiers Using Transistors, by Yu. L. Simonov, pp. 1221–1232.

Abstract: An analysis of the stability of tuned amplifiers using transistors is presented. The stability conditions and relationships giving the limit of stable amplification with different numbers of stages are developed.

Some Applications of Bessel Functions in the Technique of Communication Line Protection, by Kao. Iu-kan, pp.1252–1264.

Abstract: This article gives a generalized mathematical approach according to the theory of Earth currents and the theory of mutual inductance between Earthed circuits, and a generalization of the theories of Pollaczek and Carson according to the theory of mutual inductance. A formula in a new form, with the introduction of the Struve and Neumann functions from complex quantities and formulas for determining the effect of Earth currents, is also given.

On One Possibility of Increasing the Efficiency of a Tuned Transistor Amplifier in the Communication System, by A. Magazanik, pp. 1293–1301.

No. 1, 1960.

The Synthesis of an Amplitude-Frequency Characteristic From Its Series Expansion Coefficients, by N. K. Ignat'yev, pp. 1–13.

Introduction: The need is encountered, in systems designed for the compression of a speech spectrum, of obtaining frequency characteristics of a given wave form to electronic control. This is in particular the system of the band vocoder and the harmonic synthesis system.

In the band vocoder system a set of oscillatory circuits with mutually shifted resonant frequencies is used for this purpose. This system does not, however, secure the accurate addition of

the amplitude-frequency characteristics of the separate circuits on account of the difference in their phase-frequency characteristics. The result is that the synthesis of a frequency characteristic is accompanied by specifiable distortions.

The synthesizing system proposed by Pirogov does not have this drawback and can provide a more exact reproduction of the given frequency characteristic.

Both Pirogov's method and some other possible methods also devoid of the above mentioned drawback are analyzed.

The Investigation of a Push-Pull Frequency Divider, by S. I Yevtianov and B. A. Snedkov, pp. 14–31.

Abstract: Push-pull frequency divider (PPFD) circuits, their theory and calculation on the basis of a polynomial approxima-

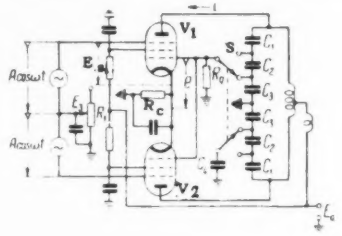

FIG. 1

tion of the anode current characteristics, are described in previous articles. The present article deals with a PPFD circuit based upon pentodes, the external drive being fed to the suppressor grids. Such a circuit is calculated for repeated divisions n = 2–5 using the lumped linear approximation of the characteristics of the anode and grid currents. The grid self-bias is taken into account. The results of the calculation are compared with those obtained experimentally.

The Use of the Simplest Four-Poles With Inductive Couplings in Electrical Filters, by Kh. I. Cherne, pp. 91–101.

Introduction: In a previous work the problem of the use in electrical filters of two-terminal networks with inductive couplings between the elements was examined. It was shown that with the use of two-terminal networks of this kind one can gain certain advantages; for example, one can decrease the number of elements of the filter circuit, make the parameters of the elements more convenient for production, and so forth.

Moreover, with the use of similar two-terminal networks in electrical filters of balanced circuits, for example, in the longitudinal branches of ladder circuits, the value of these advantages is decreased, as it is necessary to double the number of elements.

In such cases it is essential to use not two-terminal networks but four-terminal networks with inductive couplings between the elements.

Cases of the use in electrical filters of separate circuits of the simplest four-terminal networks with inductive couplings are known. The properties of such circuits have not been examined in print, and the formulas for the design of their elements have not been published.

The task of this work is to investigate some of the simplest four-poles with inductive couplings with a view to using them in balanced electrical filters as opposed to simplest four-poles without inductive couplings in balanced filters.

No. 2, 1960.

Integrator for an Apparatus for Measuring the Absorption of Radio Waves in the Ionosphere, by B. P. Potapov and Z. Ts. Rapoport, pp. 156–162.

Abstract: An integrator has been described with anode grid capacity for an instrument for measuring the absorption of waves in the ionosphere.

After gating (in a medium frequency amplifier), detection and amplification, the impulse was delivered to the integrator, whose circuit is represented in Fig. 1.

The storage element in the circuit is the capacity C_2. To prevent the discharge of the accumulated signals through the charging circuit the charge is introduced through a diode for which purpose half of the double diode V_1 (6X 6S) is employed. Only the

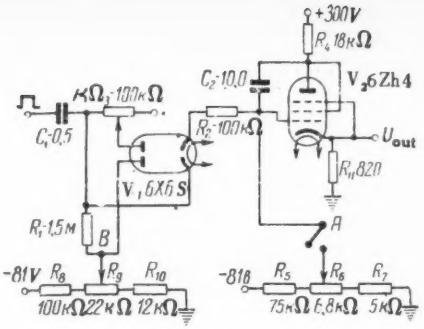

Fig. 1

positive impulses are integrated. The second half of the diode is used as a level-fixer. In view of the real characteristics of the diode, the potential of the anode of the charging diode is re-established by means of the potentiometer R_8, R_9, R_{10} at approximately 0.5 v lower than the potential of the controlling grid of the valve 6Zh4. In fixing this level it is necessary to make sure that it is not too low, since in this case only the tops of the impulses would be integrated. Integration was carried out for 50 sec. Then the grid V_2 was connected (by means of a relay) to the divider R_5, R_6, R_7 and the previous potential was re-established on it. At the beginning of the following minute integration was recommenced. The output voltage was taken from the cathode resistance R_{11}: Here

$$U_{out} \approx \int_v^t U_{in} dt + U_0$$

The voltage U_0 was regulated by the divider R_5, R_6, R_7 and was chosen at about 0.3 v.

A Divider for Low Frequencies, by B. S. Andreyev and E. M. Soshnikov, pp. 163–172.

Abstract: The construction, principles and fundamental characteristics of a divider for low frequencies with a switch in the feed back circuit have been described. As selective element a selective RC amplifier is used with a double T-form bridge. With this circuit a stable division of frequency by 10 or more is possible.

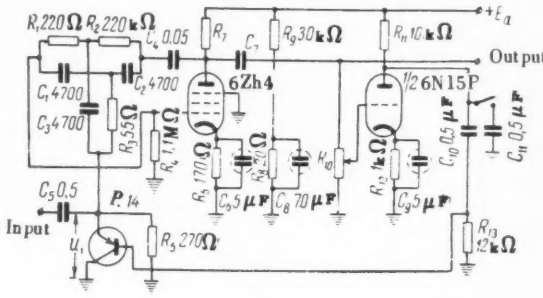

Fig. 1

The essential circuit of an experimental frequency divider of the RC type with a switch in the feed back network is represented in the figure.

Determination of the Fundamental Parameters of Multichannel Amplifiers with Semiconducting Triodes for Trunk Cable Lines, by A. I. Borisov, pp. 182–194.

Abstract: Relations have been deduced and analyzed, connecting the values of the fundamental parameters of intermediate amplifiers and the parameters of a cable trunk line with the necessary values of protection against thermal and nonlinear interference at the end of the line. On this basis an order is suggested for the determination of the necessary requirements of the fundamental parameters of multichannel intermediate amplifiers with semiconducting triodes.

Conclusion: The analytical relations (6,9,10,11) between the fundamental parameters of the intermediate multichannel amplifiers and the parameters of the line, calculated under the condition

that the norm with respect to thermal and nonlinear noise is fulfilled, make it possible to calculate directly such fundamental parameters of the amplifier as the maximum and minimum permissible level of transmission of intermediate amplifiers, the values of the nonlinear damping, etc., as they depend on the chosen values of the amplification factor (or the length of the amplifying portion). Investigation of the relations found has made it possible to construct trunk lines of multichannel communication which satisfy the norms as to noise, with very different parameters for the intermediate amplifiers in relation to the chosen length of the amplifying portion.

In particular, it has been shown that the least requirements as to the values of the nonlinear damping of an intermediate amplifier are obtained with an amplification factor (or a damping of the amplifying portion), equal to 1 nep, and the least requirements as to the magnitude of the transmission level are obtained with an amplification factor equal to 0.5 nep. It has also become clear that on change of the amplification of the intermediate amplifier within the limits 0.5–2 nep, requirements as to the magnitudes of the remaining parameters of the amplifier change comparatively little, and with further increase in the amplification factor the required magnitudes of the parameters (especially the level of transmission and the nonlinear damping) begin to increase very quickly.

Analysis of the difference between the requirements as to nonlinear damping of the intermediate amplifier for different laws of summation (by voltage or by power) of the products of nonlinearity of the third order and the first kind has shown that when the value of the amplification factor lies within the limits 0.5–2 nep this difference is inconsiderable, but on further increase of the amplification factor it begins to increase rapidly.

The established fact of the considerable reduction of the demands as to the values of the fundamental parameters of intermediate multichannel amplifiers with reduction of the damping of the amplifying portion (or reduction of the amplification factor) to values of 1–2 nep indicates that semiconducting multichannel amplifiers in this case can be made considerably simpler both in form and construction than for greater lengths of the amplifying portion, and the plane triodes used in them need not be subjected to especially difficult demands as to nonlinear properties and set noise.

The usefulness of choosing the values indicated for the damping of the amplifying portions must be verified from the economic point of view, and the values of the fundamental parameters of the intermediate amplifiers as determined by this method must be rendered more exact by taking into account the influence of the automatic amplification control apparatus and the possible variation in the lengths of the amplifying portions and the control sections.

Analysis of the Double T-Form Filter With a Single Tuner, by Yu. A. Andreyev, pp. 195–203.

Abstract: A double T-form filter turned by a single resistance has been investigated. Expressions have been obtained for the transmission factor, the quasi-resonance frequency and the goodness of the filter. The conditions for obtaining a symmetrical amplitude-phase characteristic of the filter has been deduced. Its possible applications have been discussed.

Brief Communications—The Discretization of Signals With Unlimited Spectrum, N. K. Ignat'ev, pp. 220–223.

Abstract: In papers referenced, the errors arising in the discretization of signals with unlimited spectrum are investigated, and proofs are given of the magnitudes of these errors. We suggest a very simple variant of the investigation of this question, based on the use of a purely spectral method. (Discretization is understood to be the process of transformation of a continuous signal into a series of pulses discrete in time.)

No. 3, 1960.

Multiplication of Voltages by Means of the Hall Pickup, by V. C. Kobzev, pp. 253–264.

Abstract: Experimental data of the multiplication of two voltages by means of the Hall pickup are presented.

Conclusion: The investigations which have been carried out confirm the theoretical prediction as to the practical possibility of using Hall pickups for the linear multiplication of two voltages with any form of curve. With appropriate choice of the magnetic system a nonlinearity of the product of less than 1% can be obtained.

With n-type germanium Hall pickups using a core of ordinary electrotechnical steel, with an air gap of 0.6 mm, and a field of 1000 oersted, with a magnetizing power of 150–200 mva, it is possible to obtain an output voltage on open circuit of the order of 30–50 mv. In this case the nonequipotential voltage does not exceed 50 μv.

The best results are obtained by using low frequency signals in the magnetizing circuit, and higher frequency signals in the input circuit of the pickup.

The construction of practical apparatus consisting of several identical multipliers is at present difficult owing to the large variation both in the geometrical dimensions and also in the electrical parameters of the Hall pickups. Obviously undertakings which design and market Hall pickups should at the same time as they design new types extend their work on the reduction of the variety both in parameters and also in dimensions of the types of pickup marketed.

Hall pickups already offer wide possibilities in the construction of a large class of new radio electronic circuits, including: Apparatus for measuring the intensity of constant and variable magnetic fields; apparatus for measuring power in d-c and a-c circuits; for measuring the coefficients of correlation of processes investigated, the modulation and detection of alternating voltages, the multiplication and division of voltages, etc. Hence it is necessary to develop in every possible way the branch of semiconductor technology which is concerned with the designing and the production of Hall pickups.

Transitional, Amplitude-Frequency and Phase-Frequency Characteristics of Flying Spot Television Cameras, by L. T. Perevezentsev, pp. 265–278.

Abstract: A theoretical and experimental analysis is given of the influence of the aperture of the ray and the aftershine of the phosphor of a scanning tube on the modulation of the light flux in a flying spot transmitter.

Introduction: The principal feature of television transmitters which use the principle of flying spot is the decomposition of the transmitted image into elements by means of a color raster in the scanning tube. In this case the process of decomposition is accompanied by specific distortions of the video signal, depending on the particular properties of the phosphor used. During the movement of the electron ray over the screen of the scanning tube, owing to the inertia of the processes of lighting-up and extinction of the phosphors, there arises a distortion of the aperture of the luminous point. The dimensions of the luminous spot on the screen are, so to speak, increased in the horizontal direction, leading to the diminution of the coefficient of modulation of the light flux for small details and to an increase in the length of the fronts over which the brightness diminishes. A distortion of the light flux thus arises similar to the distortions which occur in the video-signal when it passes through a low frequency filter.

In the analysis of the processes of formation of the video signal, great interest attaches to the amplitude-frequency, phase-frequency and transition characteristics of flying spot cameras. The calculation of these characteristics can be carried out on the basis of data as to the light aperture of scanning tubes.

Conclusion: The analysis of the formation of the video signal in cameras using the principle of the flying spot has enabled us to obtain expressions for their transitional, amplitude-frequency and phase-frequency characteristics. The theoretical data quoted in this paper have been used in the designing of different types of flying spot cameras, intended for color television. The practical results obtained have confirmed the theoretical calculations.

Determination of the Roots of the Characteristic Polynomial for Chebyshevskii Filters, by A. S. Ufel'man, pp. 307–318.

Abstract: An analytical method has been worked out for determining the roots of the characteristic polynomial of Chebyshev filters by means of conformal transformation of the plane of the complex frequency, which makes it possible to determine the approximate values of the roots from the zeros of the Chebyshev fractions and two characteristic frequencies.

Introduction: In another paper it was shown that the roots of the characteristic polynomial of the Chebyshev filters are disposed in the left-hand half of the plane of the complex frequency at the point of intersection of the line of equal damping of the filter where the characteristic damping is equal to

$$A_N = Ar \sin h \frac{1}{\sqrt{e^{2A_{max}} - 1}} \qquad [1]$$

with the lines of equal phase which join the poles of the filtration function with its zeros.

The line of equal damping $A_C = A_N$ on which the roots of the characteristic polynomial $g(\Lambda)$ are situated will be called for brevity the characteristic line, and the points of intersection of this line with the axes of coordinates will be called the characteristic frequencies. Thus, the characteristic frequencies are the imaginary frequency Σ_N and the real frequency Ω_N, at which the damping of the equalizing filter is equal to A_N.

In the case of polynomial filters, when all the poles of damping lie at infinity and the filtration function is a Chebyshev polynomial, the roots of the characteristic polynomial are situated in the plane of the complex frequency on an ellipse, the semiaxes of which correspond to the characteristic frequencies Σ_N and Ω_N. Hence we obtain simple calculation formulas for the determination of the roots of the characteristic polynomial.

In the case where throughout the whole attenuation band of the filter the same high working damping is required and the filtration function is a Zolotarev function, it is also possible to obtain simple calculation formulas for the roots of the characteristic polynomial from the zeros of the Zolotarev fractions and the imaginary characteristic frequency Σ_N.

In the general case, where different requirements are made as to the working damping in the attenuation band of the filter, and the filtration function is a Chebyshev fraction, it is impossible to obtain exact formulas for the determination of the roots of the characteristic polynomial (for degrees of the fraction higher than 4).

The difficulty of determining the roots in this very important general case is a serious obstacle to the introduction into engineering practice of more adequate methods of calculating filters from their working parameters.

At the present time electrical modelling apparatus specially designed for finding the roots, the so-called root-finders, have been worked out. But the results they give are not sufficiently accurate for the calculation of filters, and electronic calculating machines are very rarely available as yet. The graphical, mechanical and electrolytic methods of finding complex roots are cumbersome and insufficiently exact.

In this paper a method is given for determining the roots of the characteristic polynomial of Chebyshev filters by means of the conformal transformation of the plane of the complex frequency, which enables us to determine the approximate values of the roots by a purely analytical method with a sufficient degree of accuracy.

Conclusion: By means of the conformal transformation of the plane of the complex frequency we have obtained simple formulas of calculation which make it possible to determine the approximate values of the roots of the characteristic polynomial for given zeros of the Chebyshev fraction and the two characteristic frequencies Σ_N and Ω_N. In calculations with the approximate formulas by means of a slide rule, the error oscillates within the limits 0.5–5 per cent, depending on the degree of nonuniformity of the required conditions as to the working damping in the attenuation band of the filter.

If this nonuniformity is not great ($\mu < 0.05$), the roots must be calculated by the exact formulas [12], by means of an arithmometer or by the formulas [10 and 11] by means of tables of elliptical functions. In this case it is possible to obtain an accuracy up to the fourth or fifth figure, and subsequent operations to render the roots more exact are not required.

JOURNAL OF APPLIED MATHEMATICS AND MECHANICS (Prikladnaia Matematika i Mekhanika). Published by Pergamon Institute, New York, in conjunction with American Society of Mechanical Engineers.

Vol. 23, no. 5, 1959.

The Equations of the Precessional Theory of a Gyroscope in the Form of Equations of Motion of the Pole in the Phase Plane, by A. Iu. Ishlinskii, pp. 1153–1163.

Abstract: This paper gives a rigorous justification of the equations of motion of a gyroscope in the form of equations of the representative point in a certain plane, the so-called phase plane. It turns out that these well-known equations are valid only if the forces acting on the gyroscope satisfy a number of limitations.

The Theory of a Gyrocompass, by V. N. Koshliakov, pp. 1164–1173.

Introduction: In this paper the author investigates the equations of the perturbed motion of a gyrocompass with two rotors, which does not have the properties of the space (free) gyrocompass of Geckeler-Anschutz.

Without dwelling on the properties of a space gyrocompass in detail, we shall mention only that the natural, undamped vibrations of its sensing element have equal periods with respect to all three principal axes of inertia and that this period approximately equals the Schuler period that is $T_0 = 1\ \pi\ \sqrt{R/g}$ (R is Earth's radius, g is the gravitational acceleration).

The above mentioned property is imparted through a spring, which couples the two gyroscopes and creates a moment about the vertical axis of each inner ring, given by the formula

$$N = \lambda \sin 2\epsilon \qquad [0.1]$$

where λ is a certain proportionality factor, 2ϵ is the angle between the axes of rotation of the two rotors. The theory of the space gyrocompass in simplified term is given in the books of Geckeler, Grammel and Bulgakov.

The equations derived in the work of Ishlinskii could be applied to a gyrocompass which does not possess the properties of a spatial gyrocompass, as, for example, the two-rotor compass of Anschutz, and also certain domestic two-rotor gyrocompasses.

This paper contains an investigation of the unperturbed motion of the above described gyrocompass on the assumption that it is mounted on a ship travelling at high latitudes (70–80 deg).

Conditions for the Existence of Limit Cycles, by B. A. Barbashin and V. A. Tabueva, pp. 1185–1197.

Abstract: A qualitative investigation of a nonlinear differential equation of the second order is carried out. This equation, in particular, describes the motion of a particle along a closed curve subject to a pushing force. Under certain additional conditions the presence of a pushing force assures the existence of at least one stable limit cycle.

A simple illustrative example is a pendulum, subject to the action of a pushing force.

The Vibration Theory of Quasilinear Systems With Lag, by S. N. Shimanov, pp. 1198–1208.

Abstract: This article generalizes the vibration theory of quasilinear systems whose motion is described by ordinary differential equations to systems with a time lag. The case of resonance in quasilinear non-autonomous systems with a lag is considered.

Application of the Residue Theory to Transformation of Automatic Control Systems Equations to Canonic Variables, by O. I. Komarnitskaia, pp. 1209–1217.

Abstract: In stability investigations of automatic control systems canonic variables are frequently used; sometimes it is not only necessary to transform the equations to canonic forms but also to know the transformation matrix.

Lur'e developed formulas for transformation of variables for the case of simple roots of the characteristic equation; applications may be found in the paper by Letov.

In this paper we propose a method of constructing the transformation matrix, based on the residue theory and permitting us to determine transformation coefficients for any structure of the roots of the characteristic equation.

Oscillations of a Quasilinear Non-Autonomous System With 1 Degree of Freedom Near Resonance, by A. P. Proskuriakov, pp. 1218–1232.

Abstract: In an earlier paper, there was developed a method for the construction of periodic solutions of a non-autonomous system with 1 deg of freedom for the case of simple roots of the equations of fundamental amplitudes. In this work there is considered the general case when the roots of these equations may be multiple roots. A solution containing secular terms is constructed for the case when resonance with unlimited amplitude of oscillations occurs.

Small Harmonic Oscillations of a Cylindrical Shell Along the Axis of Which an Ideal Gas Flows With Supersonic Velocity, by B. I. Rabinovich, pp. 1255–1262.

Abstract: A circular cylindrical shell is considered to have a flat bottom at one end where a system of uniformly distributed

supersonic sources is located. The other end of the shell is open and through it flows a uniform supersonic stream of an ideal gas originating at the bottom. On the assumption that the shell performs small harmonic oscillations in a certain plane, the dynamic interaction between the gas and the shell walls is investigated. The gas compressibility leads to the appearance of nonstationary forces whose role in the general scheme depends upon the Strouhal number; in other words, the principal vector of the gasdynamic forces manifests itself during the shell oscillation as displacement and rotation relative to the longitudinal axis.

Statistical Method in the Theory of Stability of Shells, by I. I. Vorovich, pp. 1263–1272.

Introduction: We consider a shell, subjected to a loading which increases proportionally to some parameter λ. We assume that the boundary conditions of the shell admit for $\lambda = 1$ a membrane state of stress. In this case, for a large class of shells, the following picture of the change of the number of equilibrium shapes of the shell and their properties will be typical.

There exists a certain number λ_0, such that for $\lambda < \lambda_0$ there exists a unique membrane equilibrium shape of the shell which corresponds to an absolute minimum of the energy of the system, composed of the shell and external forces. Further, there exists a number $\lambda_1 \geq \lambda_0$, such that for $\lambda_0 \leq \lambda < \lambda_1$ the shell possesses, in addition to the membrane equilibrium shape, also a bending equilibrium shape; however, the membrane equilibrium shape of the shell will have a lower energy level than an arbitrary bending state. Further, there exists a number $\lambda_{00} \geq \lambda_1$, such that for $\lambda_1 < \lambda < \lambda_{00}$ the membrane equilibrium shape of the shell, even though it is associated with a relative minimum of the energy, is accompanied by at least one bending equilibrium shape, associated with lower energy level. Finally, for $\lambda > \lambda_{00}$ the membrane equilibrium shape of the shell, in general, ceases to be associated with an energy minimum.

Such a change of equilibrium shapes was factually established in a series of investigations (see bibliographies given) for a spherical and cylindrical shell on the basis of application of approximate methods. The same finding received a strong justification for a rather large class of shells and boundary conditions.

From what has been mentioned, it becomes clear that even if it were possible to completely surmount all mathematical difficulties associated with the solution of the basic equations of the nonlinear theory of shells, the problem could still not be considered as solved completely, since the degree of reality of each of the possible equilibrium shapes of the shell for $\lambda_0 < \lambda < \lambda_{00}$ would still not be determined.

The selection of the most real equilibrium shape of the shell must be made, taking additional considerations into account. It is rational to introduce as a measure of reality of a certain equilibrium shape of the shell the probability of finding the shell in that shape.

The idea of introducing the probability considerations into stability problems of shells was expressed by Feodos'ev and Vol'mir. The introduction of probability considerations in our opinion will significantly advance the solution of such important questions as:

1 Determination of admissible loads on the shell in studying stability, taking into account the conditions of its behavior and the irregularities in its manufacture.

2 The determination of inaccuracies with regard to basic shell parameters. Of most importance in this regard, the most important factor we have in mind is the analysis of the necessary accuracy in manufacturing the middle surface of the shell.

The development of the statistical theory of stability of shells must in our opinion include the following items:

1 Methods of statistical description of factors which determine the random characteristics of deformation of the shell. Methods and technique of experimental determination of statistical characteristics of indicated factors.

2 Methods of statistical description of parameters which characterize the deformation of the shell. Methods and techniques of experimental determination of statistical characteristics of indicated parameters.

3 Relations between the statistical characteristics of the parameters, which describe the deformation of the shell, and the statistical characteristics of factors which determine the accidental character of the deformation of the shell.

An approximate approach to the construction of such a theory will be presented.

A Particular Solution of the Problem of the Motion of a Gyroscope on Gimbals, by A. A. Bogoiavlenskii, pp. 1365–1369.

Abstract: A particular solution of the problem of motion of a heavy gyroscope on gimbals is investigated, for the case in which the axis of rotation of the outer ring is horizontal.

Accelerated Placing of a Gyroscopic Compass in a Meridian, by Ia. N. Roitenberg, pp. 1370–1374.

Abstract: The gyroscopic compass represents an instrument with a large period of natural vibrations, of the order of one hour and a half. For the damping of the natural vibrations which may occur because the gyrocompass in starting was not along a meridian, a considerable time will be required, equal to three to four periods of natural vibrations. There is an interest, therefore, in studying methods of an accelerated placing of the gyrocompass in the meridian. Usually, the latter is accomplished by an application to the gyrocompass of additional external forces. The problem regarding the selection of the law of control of these forces is discussed.

Investigation of the Stability of a Gyroscope Taking Into Account the Dry Friction on the Axis of the Inner Cardan Ring (Gimbal), by V. V. Krementulo, pp. 1382–1386.

Abstract: Lately, the exact theory of gyroscopic systems based on the application of the direct method of Liapunov, has been greatly developed; in particular, see the works of Chetaev, Rumiantsev and Magnus.

With regard to the works of other authors who, in their investigations of the differential equations of motion of the gyroscope, often rejected certain terms without any proper justification. In the papers mentioned the exact solutions of the differential equations are given, and the properties of the solutions are studied by means of construction of Liapunov's functions. Rumiantsev solved the question of viscous friction on the axes of suspension rings. In the paper under consideration an attempt is made to apply the direct method of Liapunov for the investigation of stability of certain motions of a gyroscope in a Cardan suspension, assuming dry friction on the axis of the gimbal.

RADIO ENGINEERING AND ELECTRONICS (*Radiotekhnika i Elektronika*). Published by Pergamon Institute, New York, in conjunction with Massachusetts Institute of Technology, Cambridge, Mass.

Vol. 4, no. 9, 1959.

Relative Duration of a Nonstationary Random Process, by C. M. Rytov, pp. 1–6.

Abstract: In this article the ergodicity condition is introduced for the process $f[X(t)]$, where f is a determined function and $X(t)$ is a nonstationary random process. When condition (1) is fulfilled, the relative duration of $X(t)$ in the interval $(x,x + dx)$ is given by the one-dimensional distribution function of the process $X(t)$, averaged in time. Examples of average distribution are given.

Binary Storage Systems With Dual-Threshold Analysers, by A. E. Basharinov, B. S. Fleischman and M. A. Samokhina, pp. 7–19.

Abstract: This article is a consideration of binary storage systems for detecting signals in noise, constructed according to the method of sequential analysis. Calculatory and experimental data are given for the distribution function for the length of the accumulating process. For the case of Rayleigh fluctuating signals of low intensity, relationships are obtained for the selection of the optimum discrimination threshold, and the "losses" of a binary system in comparison with a corresponding system of continuous optimum processing are calculated.

Application of the Laplace Transform to the Theory of Rectangular Cavity Resonators and Wave Guides, by M. I. Kontorovich, pp. 93–101.

Abstract: The problem is examined of the exciting of rectangular resonators and wave guides. The application of the Laplace transform enables a solution to be obtained, not in the form of series as is usually done, but in the form of multiple integrals in the complex domain. The usual form of solution can be obtained by computing the integrals from the theorem of residues.

Experimental Investigation of a Backward-Wave Spiratron, by G. A. Bernashevskii and T. A. Novskova, pp. 135–144.

Abstract: The results are given of an experimental investigation of a backward-wave tube with centrifugal electrostatic focusing, operating in the 10-cm band. Thirty % continuous frequency tuning was obtained by varying one voltage, while, by varying

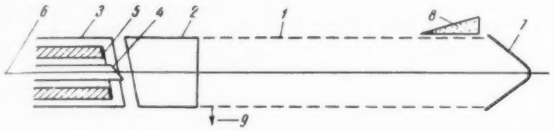

Fig. 1 Schematic diagram of a backward-wave spiratron: 1 delay system; 2 anode; 3, 4 external and internal focusing electrodes; 5 cathode, oxide layer; 6 focusing rod; 7 collector; 8 absorber; 9 energy pickup

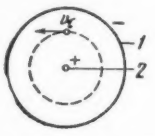

Fig. 2 Transverse cross section of a spiratron (v_T is the electron tangential velocity): 1 delay system; 2 focusing rod

two voltages simultaneously, a band was obtained with lower and upper cutoff frequencies in the ratio 1–1.7 (11.5–6.7 cm). The maximum generated power level was 50 mw. "Spiratron"-type oscillations were observed, the existence of which is not explained by present theories.

Germanium Diodes for Parametric Amplification, by S. N. Ivanov, N. E. Skvortsova and Yu. F. Sokolov, pp. 199–206.

Abstract: The basic requirements to be met by semiconductor diodes for use in parametric amplifiers are formulated. A simple approximate method of analysis is given which permits an estimation to be made of the necessary values of specific resistance, areas of contacts, and crystal thickness for a semiconductor diode to be used in a parametric amplifier. On the basis of this analysis diodes were designed which enabled parametric amplification to be obtained in the centimeter wave band.

Conclusion:

1 A simple approximate method is described for calculating the parameters of diodes for use in parametric amplifiers.

2 Satisfactory agreement was obtained between the calculated and the measured parameters of diodes made in accordance with the theory.

Measurement of the Noise Spectrum of Germanium Photodiodes Over a Wide Frequency Range, by T. M. Lifshits and L. Ya. Pervova, pp. 207–214.

Abstract: The method and results are given of an investigation

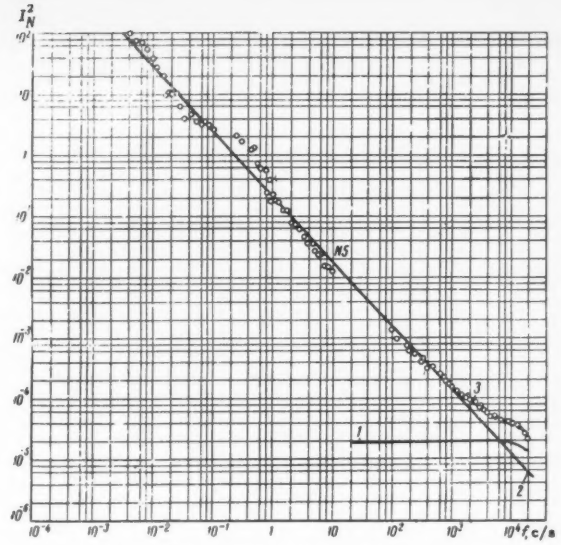

Fig. 3 Noise spectrum (photodiode no. 5)

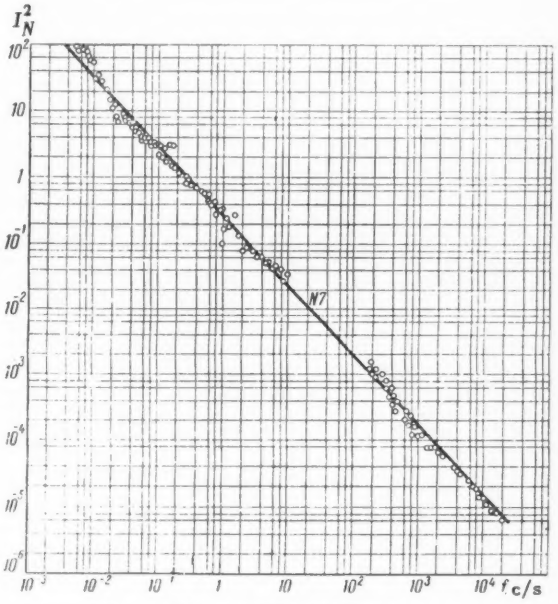

Fig. 4 Noise spectrum (photodiode no. 7)

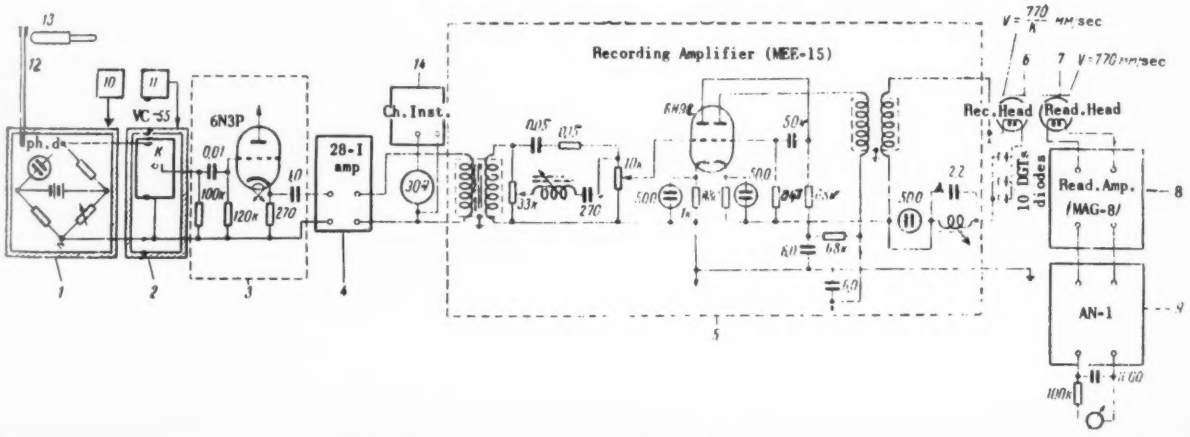

Fig. 1 Diagram of apparatus for analyzing noise spectrum

of the spectral distribution of noise in germanium junction photodiodes over a frequency range 2×10^{-3} to 2×10^{4} c/s. The magnetic recording method was used for the measurements, the low frequencies being transformed into audio frequencies by varying the tape speed. It is shown that the spectral density of the noise retains the form $1/f^m$ right down to the lowest frequencies, where m is a constant approximately equal to unity over the entire frequency range examined.

The Energy Variation of a Particle or System Under the Action of External Forces, by V. I. Gaiduk, pp. 158–180.

Abstract: It is shown that the total energy of a particle or system of particles which varies with time under the action of nonconservative forces applied from without can be determined directly from the solution of a system of differential equations of the first order. It is not required in this connection to determine preliminarily the dependence of the coordinates of the particles upon time from the equations of motion. The expressions obtained are formally simple and are valid for an arbitrary motion of the particles. When the external action is a weak one, it is possible to use well-established methods for constructing approximate solutions. As an example of application of the method outlined, the interaction of electrons with HF oscillations in a strophotron is considered.

In the case of a complicated motion of the particles the transformation described of the equations of motion (Lagrange's equations) is advantageous not only for the determination of the energy of the particles but also for finding approximately their law of motion.

Algorithm for the Statistical Selection of Highly Probable Symbols in a Self-Adjusting System With Limited Memory Faculty, by V. L. Epstein, pp. 237–241.

Vol. 4, no. 5, 1959.

Radar Detection of a "Fluctuating Target" in the Presence of Correlated Noise. Pt. I—A Coherent Packet of Signals, by L. A. Vainshtein, pp. 1–15.

Abstract: A theoretical examination is made of the optimum radar receiver for the detection of a packet of coherent signals reflected off a "fluctuating target," i.e., signals subjected to fluctuation as a result of small changes in the orientation of a complex reflecting target. Detection occurs in the presence of normal interference having intraperiodic (for the duration of each signal) and interperiodic (for the duration of a whole packet) correlations. The coefficient of likelihood is calculated, and the optimum intraperiodic and interperiodic processing of the mixture of useful signals and noise appearing at the receiver input, is examined. The probabilities of spurious and correct detection are calculated for a receiver realizing interperiod subtraction.

Introduction: An interesting question in the statistical theory of reception is the question of the radar detection of a fluctuating target, i.e., the detection of a useful signal of random phase and amplitude, or a packet of such signals. The question arises in connection with the fact that targets reflecting radar signals usually have a complex shape, and that a useful signal fluctuates at the receiver input with small changes in their orientation. A signal reflected off a complex object is formed as a result of the superimposition of fields of many "luminous dots," distributed more or less at random in relation to the radar, and therefore the signal fluctuates according to the normal law, the parameters of which are determined by the reflecting object, the character of its movement, and by the main signal.

It is quite natural to assume that the fluctuation of a useful signal is normal, and the supposition is usually accepted in calculations, although in a number of cases it is only qualitatively valid. Collation of theoretical results, relating to signals with fixed amplitude, and to signals fluctuating normally, gives quite a full representation of the problem of radar detection as a whole. According to the classification in article [1], the detection of fluctuating signals is a complicated process, inasmuch as there are unknown, random parameters present—the phase and amplitude of each signal in the packet. Later we will examine the optimum receiver which detects a fluctuating target by a packet of coherent main signals in the presence of correlated noise. The simpler problem of an incoherent packet will be examined in the second part of the work.

Conclusion: In this work we have carried out an investigation of an optimum receiver, detecting a fluctuating target in normal correlated noise, conditioned by random reflections from numerous neighboring targets, in conjunction, possibly, with the usual receiver noise. The coefficient of likelihood, found in paragraphs 2 and 3, shows in which case an optimum receiver ought to carry out a subtraction, and in which a coherent or incoherent addition, and so on. Calculation of the probabilities of a false alarm, and correct detection for two-channel or single-channel receivers giving an interperiod difference permits a comparison to be made of the effectiveness of the detection of a constant and a fluctuating target in the presence of strongly correlated noise.

Optimum Signal Detection in the Presence of Correlated Gaussian Noise, by V. G. Sragovich, pp. 16–28.

Abstract: A solution is given of the problem of finding the best method of detecting a gaussian signal of special form in the presence of correlated gaussian noise, and its probability characteristics are calculated.

Introduction: The aim of this work is to find and to examine the best method of detecting a signal in a sequence $\vec{\Sigma}_k$ ($k = 0, 1, \ldots, n-1$) of vectors, which are the sums $\vec{s}_k + \vec{\Delta}_k$, where $\vec{s}_k$ and $\vec{\Delta}k$ are, respectively, the signal and noise vectors. The sequence $\vec{s}_k$ is based on an initial random vector $\vec{s}$, which is rotated through a given angle ϕ and modulated by the set of numbers g_k: $\vec{s}_k = g_k U^k \vec{s}$ (U is the matrix of rotation through the angle ϕ). It is assumed that the random vector $\vec{s}$ is distributed normally. The sequence of noise vectors $\vec{\Delta}_k$ is also distributed normally, in which the unlike components are independent, and each of the groups of like components is connected by the same correlation link.

The model described here can be interpreted in terms of the problem of detecting a moving target. The projections of the vectors $\vec{s}_k$ and $\vec{\Delta}_k$ are interpreted as components of corresponding electrical voltages. The rotation of the signal vectors $\vec{s}$ through the angle ϕ occurs as a result of the Doppler effect; the numbers g_k— the envelopes of a sequence (packet) of signals—describe the form of the directivity pattern of an antenna. The noise vectors $\vec{\Delta}_k$ are the result of the combination of two types of noise: Internal noise in the receiving apparatus, shown as a sequence of normal, independent, random vectors $\vec{N}_k$ ("white noise"), and correlated random noise $\vec{\Pi}_k$, arising from the presence of a cloud of reflectors.

The method by which the best means of separating signal from noise can be determined is based on the employment of the statistical theory of verifying the Neumann-Pearson hypotheses. For this it is necessary to know the probability density of the noise and of the mixture of signal and noise. Their relationship, called in statistics the coefficient of likelihood, indicates the functional form of the operations by means of which the signal may best be detected. A further problem consists of calculating the probability of mistakes of the first and second kinds, made in checking the hypotheses and interpreted, respectively, as the probabilities of the signal being lost and of the noise being taken for the signal.

Some Properties of Media With Periodically Time Varying Parameters ϵ and μ, by A. M. Markovkin, pp. 72–81.

Abstract: The concept of parametric phenomena is extended to media with variable parameters. The emission (absorption) conditions are formulated for electromagnetic waves propagated or localized, in the absence of external electric and magnetic forces, in media with time varying parameters.

Examples of the design of some systems based on the application of the energy relationships are given.

Conclusion: Generalizing the results given in the article it is possible to draw several conclusions about the properties of a medium whose parameters vary with time. Systems with lumped and distributed parameters can be emitters if the variation of the parameters is brought about according to a certain law and the necessary phase relations and modulation depth of the parameter are observed. It is possible to assume, for example, that the emission of electromagnetic waves which occurs with the movement of bodies in the troposphere is caused to some extent by parametric emission by virtue of strong excitation of the dielectric constant of the medium.

Design of a Two-Mirror Radiotelescope, by A. E. Salomonovich and N. S. Soboleva, pp. 92–100.

Abstract: An approximate evaluation is given of the effect of diffraction at the edges of the secondary mirror of a two-mirror, Cassegranian radiotelescope on the field distribution in the aperture of the principal mirror. It is shown that, essentially, the diffraction at the secondary mirror does not deteriorate the resulting polar diagram of the radiotelescope.

Introduction: Many important problems in radio astronomy can be solved only by means of high resolution radiotelescopes. In the microwave band a mirror with dimensions of some tens of meters is necessary to obtain a resolving power of a few minutes of arc. If the diameter of the mirror is increased, then in order to make better use of the surface of the mirror the focal length must be made correspondingly larger. Moreover, it is well known that, other conditions being equal, increasing the focal length reduces the extra-axial aberration. At the same time the construction of systems with long focal lengths is fraught with a number of design and operational drawbacks. In fact, if only the receiving aerial (element) is placed at the focus of the mirror, there then arise the difficulties of channelling the energy from the focus to the receiver. If a long length of standard-section transmission line is used a considerable fraction of the energy is lost in it. Widening the wave guides, however, gives rise to waves of higher modes, and this also is connected with a loss of energy. Moreover, when working on different microwave bands it is necessary to replace the whole high frequency channel or to lay parallel or combined transmission lines of great length. If, however, the whole receiver (or the h. f. and mixer stages) is placed at the focus, then operating drawbacks arise connected with the necessity of servicing the outlying receiver.

One of the possible ways of increasing the focal length of the whole system while eliminating the design and operating difficulties mentioned above is to use a two-mirror radiotelescope, with dimensions analogous to those in the Cassegran-type system, which is well known in astronomical optics. In this system, as we know, the principal mirror is parabolic and the secondary mirror is hyperbolic. One of the foci of the latter (0_1) coincides with the focus of the principal mirror, and the other (0_2) is situated close to its pole (Fig. 1). With such an arrangement the receiver can be placed directly behind the principal mirror.

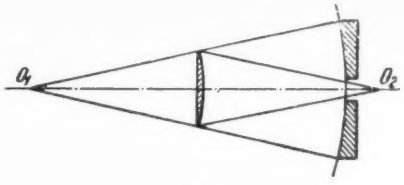

Fig. 1

Apart from the advantages mentioned, the presence of the secondary mirror guarantees the possibility of correcting the principal mirror, the preparation of which in exact conformity to a given profile can prove (on account of the large dimensions) a technically difficult task to carry out. An indication of the use of this possibility is given.

In a two-mirror radiotelescope, besides the usual geometric calculation there also arises the question of the effect of the secondary mirror on the polar diagram of the whole system.

In this article, we will not examine this problem in its entirety, but limit ourselves to the particular question of the effect of diffraction at the edges of a secondary mirror placed near the focus of the principal mirror on the field distribution in the aperture of the latter.

Conclusion: The calculation we have made shows that the diffraction at the secondary mirror introduces distortion into the field distribution of the principal mirror; however, by using the method described it is possible with a given wave length to select such geometrical dimensions and positioning of the secondary mirror that (to the required accuracy) the resultant polar diagram of the radiotelescope will not be worsened.

The approximate formula (9) obtained can apparently prove useful in a number of other cases where the assumptions made in its derivation are valid.

Universal Binary Switch for Electronic Digital Computors, by M. I. Yelinson, D. V. Zernov and A. M. Kharchenko, pp. 162–169.

Abstract: This article calls attention to and investigates a new electronic device with a plane deflected beam, which can operate as a universal binary switch. A distinctive feature of the device is the use of secondary emission. The article examines the design, parameters and operating conditions of the device, which can be used in computor engineering circuits.

Measurement of the Time Resolution of an Electronic Multiplier With a Large Output Current, by L. V. Artemenkova and B. M. Stepanov, pp. 199–205.

Abstract: A short discussion is given of the factors which determine the time resolution of electronic multipliers. A method is described for measuring the time resolution of an electronic multiplier by means of velocity oscillograms of the output current pulse when rectangular current pulses are delivered at the input. The time of growth is worked out for an output pulse of 1 *A*.

Experimental Results: Further development of the electron gun, as mentioned, made it possible to obtain a lower growth time of the output pulse. Fig. 4 shows the oscillogram of the output pulse. The triggering pulse of the gun, shaped by the line, can be seen in Fig. 5. The frequency of the calibrating sinusoid, shown in Figs. 4 and 5, was 104.5 Mc/s.

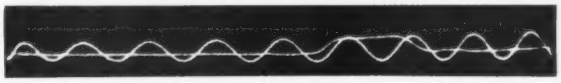

Fig. 4 Oscillogram of output pulse; frequency of sinusoid = 104.5 Mc/s

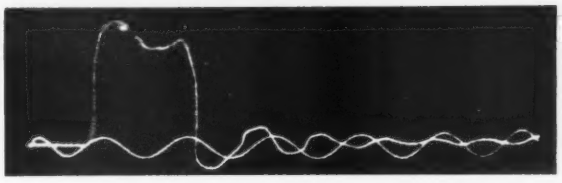

Fig. 5 Oscillogram of the triggering pulse of gun

About a hundred oscillograms were taken from three models of the multiplier. The oscillograms were measured and on the basis of the average of the results obtained the conclusion was drawn that the mean value of the growth time (measured at the level of 0.1 to 0.9 of the amplitude value of the pulse) for the output pulse of the electron multiplier was 2.5×10^{-9} sec with an accuracy of 15 to 20%, coinciding well with the calculated value.

Inversion of Zeeman-Split Levels, by F. B. Bunkin, pp. 219–225.

Abstract: The effect is considered of transverse magnetic-field perturbations on the inversion of Zeeman-split levels for a reversal of the longitudinal field. Estimates are obtained of the required velocity of the particles for certain concrete manners of reversing the magnetic field.

Speed of the Inversion of Zeeman-Split Levels, by M. I. Rodak, pp. 226–227.

Introduction: The object of the present communication is to observe that estimates suitable in practice and close to the estimates by Bunkin can also be established without performing the quantum mechanics calculations for each concrete method of reversal of the magnetic field: We need only interpret somewhat differently the condition of non-adiabaticity of the perturbation (jump) of the field, taken, for example, in the form

$$\left|\frac{d\mathbf{H}}{dt}\right| \gg \gamma H^2 \qquad [1]$$

where **H** is the total magnetic field and γ is the gyromagnetic ratio.

***RADIO ENGINEERING* (*Radiotekhnika*). Published by Pergamon Institute, New York, in**

conjunction with Massachusetts Institute of Technology, Cambridge, Mass.

Vol. 14, no. 12, 1959.

Calculation of the Losses in Hyperbolic Lenses Irradiated by a Hertzian Dipole, by I. P. Dobrovol'skii and V. P. Smirnov, pp. 1–8.

Abstract: The losses owing to the reflection of energy from the surfaces of a hyperbolic lens and the thermal losses in the material of which the lens is made are examined. A calculation is carried out for the case of the irradiation of the lens by a Hertzian dipole. The graphs given serve as a guide to the selection of those parameters of lens antennas which ensure the least energy losses.

Conclusion: It will be seen that the thermal losses in the hyperbolic lenses are extremely small and do not exceed a few score decibels even in the worst case. If artificial and natural dielectrics are available with a loss tangent less than 0.003 it is doubtful whether, in practice, when the problem of the losses becomes very acute the necessity will arise of using dielectrics with large losses for the lenses.

It follows from these results that in hyperbolic lenses the losses owing to the scattering of the reflected energy are basic. If the refraction factors vary in reasonable limits (1.4 to 2.0) the reflection losses will not exceed 20–25 per cent even when the geometry of the lens is unfavorable (i.e., when f/D is of the order 0.5).

Evaluation of the Channel Capacity of Some Communication Channels With Randomly Varying Parameters, by Ia. I. Khurgin, pp. 25–36.

Abstract: The channel capacities of single-channel and multichannel communication lines are evaluated on the assumption that the transmitted signal, the transmission factor for the medium, the propagation time and the added noise are mutually independent stationary random processes. As an example, the channel capacity of a single-channel line is calculated taking into account the fluctuations of the propagation time and the added noise.

Analysis of Complex Electronic Circuits, by L. Ia. Nagornyi and V. P. Sigorskii, pp. 37–50.

Abstract: Formulas are derived for the analysis of electronic circuits using the node voltage and contour current methods for the basic magnitudes of the equivalent four-terminal network to which most circuits can be reduced. The expressions for the basic quantities are studied by conformal transformations. The method is illustrated by an example.

Effect of the Quartz Resonator Load Upon the Frequency Stability of Quartz Oscillators, by G. B. Al'tshuller, pp. 62–69.

Abstract: It is shown that the quartz resonator load has a substantial effect upon the frequency stability of quartz oscillators. Formulas are given which permit the temperature owing to self-heating of the high frequency resonator plates to be determined, and a method for taking into account the frequency instability of a quartz oscillator is given.

The method of calculating the influence of the quartz resonator load on the frequency stability is as follows:

1 The voltage change in the quartz resonator owing to action of the destabilizing factor is determined.

2 A change in the power dissipated in the plate of the quartz resonator is determined when the voltage change in the quartz resonator is known, according to formula (4).

3 In accordance with the change in the power dissipated in the plate, from formula (10) the change in the temperature of self-heating of the quartz plate is determined.

4 From the change in the temperature of self-heating of the quartz plate according to formula (12) the relative change in the frequency of the quartz oscillator owing to the change in the thermal regime of the quartz resonator is determined.

The effect of the change of the thermal regime of the quartz resonator may be reduced by reducing the temperature coefficient of the frequency in the region of the working temperature and increasing the heat dissipation coefficients of the quartz resonators.

Conclusion: We quote, in conclusion, data for the instability of the frequency of the quartz oscillator for various values of the power dissipated in the plate of the quartz oscillator. The Shembel' circuit has been investigated with an internal circuit in the form of a capacitive Hartley oscillator using a 6P6S tube. The anode circuit is tuned to the second harmonic of the quartz oscillator frequency. The averaged data of the experimental investigations are given in the table.

The Theory of a Radio Thermal Direction Finder With Conical Scanning, by Iu. V. Pavlov, pp. 70–79.

Abstract: Expressions are derived for the maximum and angular sensitivity of a modulation-type radio thermal direction finder with conical scanning. A formula is derived for the equivalent temperature of the antenna which is true for a radio thermal direction finder with any noise factor including quantum noise.

Introduction: The problem of direction finding for radio thermal sources which produce signals having a complex spectrum has acquired great interest in recent years. The spectral density of the weak signals in the frequency interval of the radio thermal direction finder is lower than the spectral density of its natural noise. Nonterrestrial sources (the sun, moon, radio stars) and the ratio thermal radiation of terrestrial objects constitute the sources of these signals.

Modulation-type radio thermal direction finders are frequently used to receive such signals. A radiometer, the theory of which has been examined in many articles, is a component part of the radio thermal direction finder.

In [5,6,7] the concept of the radiometer sensitivity is given greater precision, and the sensitivity is calculated taking into account the fluctuations of the amplification factor at high frequencies.

In this paper the properties of a radio thermal direction finder with conical scanning designed to operate in an automatic radio thermal coordinator are examined.

The Maximum Sensitivity of a Radio Thermal Direction Finder With Conical Scanning.

The block diagram of the direction finding part of a radio thermal direction finder of the modulation type is represented in the figure. In investigating this arrangement we make the following assumptions:

1 The signal $u(t)$ and the noise $n(t)$ of the radio thermal direction finder are random independent quantities which have a stationary Gaussian amplitude distribution with zero average values and effective values σ_c^2 and σ_n^2, respectively.

2 The linear part of the radiometer and the low frequency amplifier have an ideal rectangular frequency characteristic with a power pass band Δf and ΔF_x, respectively.

3 The low frequency filter also has an ideal rectangular characteristic with power pass band ΔF.

4 The phase detector transforms the signal according to the law $w(t) = v(t) \sin \Omega t$, where $v(t)$ is the output voltage of the low frequency amplifier.

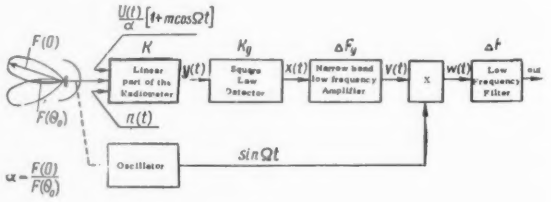

Conclusion: It appears from formula (34) that the angular sensitivity of the radio thermal direction finder is proportional to the maximum sensitivity ΔT_a and inversely proportional to the coefficient K_m and the antenna temperature T_a. To increase the angular sensitivity we must raise the sensitivity of the radiometer and choose parameters of the antenna system, such that the modulation transmission factor K_m is a maximum.

MEASUREMENT TECHNIQUES (Izmeritel'naya Teknika). Published by Instrument Society of America, Pittsburgh, Pa.

No. 7, July 1959.

Efficiency of Automatic Control Devices, by A. V. Vysotskii, pp. 495–496.

Introduction: When appraising the economic efficiency of auto-

matic inspection machines, it is necessary to know the number of articles scrapped because the automatic machine makes measurement errors, owing to which some of the good products are scrapped and some of the faulty articles are passed. A large amount of work in rechecking articles scrapped by the automatic machine lowers its efficiency. A knowledge of the number of good articles among those rejected by the automatic machine, as well as the number of faulty articles among those passed, will enable the machine's efficiency to be determined. Study of the measuring devices of automatic inspection machines equipped with electrical contact and pneumatic transducers showed that the distribution of random measurement errors follows the normal distribution law very closely.

The distribution law, which sometimes deviates from the normal, and the expected percentage of actual scrap should be determined experimentally, for the preliminary calculations, from the operation of the equipment under consideration. We shall quote some calculations of the rechecking required for an automatic machine which checks one parameter for two limits. Approximate data for multidimensional automatic machines can be obtained by adding the data obtained for each parameter, since the probability of simultaneous incorrect rejection with respect to several parameters is small.

Experimental Determination of Errors in Piston Manometers at High Pressures, by M. K Zhokhovskii, pp. 505–509.

Abstract: The theoretical errors in manometers caused by strains in the piston and cylinder have been determined for all types of instruments. The solution of this intricate problem was obtained by making certain approximations which require experimental checking. The correction formulas were successfully confirmed experimentally by V. N. Samoilov for various types of manometers for pressure up to 2500 kg per cm². In the present work the previously obtained solutions are checked experimentally over a substantially larger range.

Conclusion: The suggested method of comparing piston manometers of high pressures by means of a differential instrument is also applicable for determining experimentally the differences between the errors as functions of pressure. The experiments carried out up to pressures of 7000 kg per cm² confirmed the previously obtained formulas of corrections for strains in manometers with different piston systems.

Dynamics of a Self-Balancing Manometer for Measuring Low Gas Pressures, by V. I. Bakhtin, pp. 511–515.

Static Calibration of Accelerometers and Accelerographs by Means of a Centrifugal Device, by F. A. Markhevka, pp. 516–517.

Decatron Computer with a Preset Time or Pulse Count, by I. Ya. Breido, pp. 531–533.

Introduction: The use of gas discharge decimal counting tubes, known as decatrons, proves economical in thermionic, semiconductor and other elements in computer design. That fact, plus their compactness and economy in use, makes decatrons successful replacements for tube circuits as well as mechanical registers. Decatrons are extensively employed in various devices of commercial and scientific value, such as telemetering devices, computers for experimental nuclear physics, memory units of digital computers, electrical measuring instruments with digital displays, electronic tachometers, frequency dividers, precision timers (producing time pips), etc. A brief description is given of a computer which operates with Soviet-made mass produced decatrons and contains a unit for presetting the required counting time or pulse count. The block schematic of the instrument is given in Fig. 1. It performs the following operations: Counting of pulses over an arbitrary time with manual starting and stopping; counting pulses with automatic stopping after a given time (time presetting); and automatic measurement of the duration of counting of a set number of pulses (pulse count presetting).

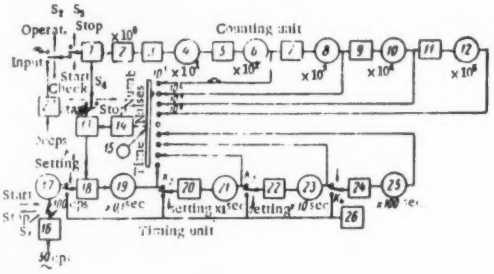

Fig. 1

Experimental Investigation of a Molecular Generator, by A. Ya. Leikin, pp. 543–546.

Introduction: The molecular generators whose investigation results are given in this article were constructed in the Khar'kov State Institute of Measures and Measuring Instruments in 1956 and 1957. In both generators the main electrical features developed by N. G. Basov in the P. N. Lebedev Physics Institute of the Academy of Sciences USSR were preserved with a number of constructional modifications. A grid with long channels (1.3–1.5 mm with a diameter of 0.05 mm) was used as a source of the beam.

Conclusion: Tests have shown that the molecular generator has a highly stable frequency and good operational properties. For any given absolute frequency the resonator should be tuned with respect to variations in the ammonia gas pressure. The accuracy of the absolute frequency of a molecular generator obtained by this means and the effect of various factors on it will be further investigated. A. I. Samoilovich participated in designing our molecular generator model. He also suggested the technique and carried out the construction of the grid with long channels. M. I. Klyus took part in the construction of the generator, and E. Z. Orlov in the tests described.

No. 8, Aug. 1959.

Gold-Platinum Thermocouple, by A. M. Sirota and B. K. Mal'tsev, pp. 611–612.

Abstract: In research work it is often necessary to use thermocouples for precise measurements below 630 C, for instance,

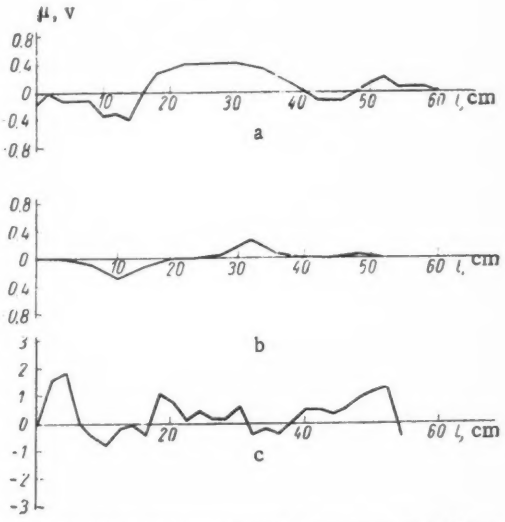

Analysis of the thermoelectric homogeneity of thermocouple materials: a) platinum; b) gold; c) platinorhodium.

Calibration of a Gold-Platinum Thermocouple with the Cold Junction at 0°C

Temperature of the hot junction, °C	Thermal emf, μv
200	1839.2
300	3133.4
400	4622.1
500	6285.4
550	7180.1

for measuring small temperature differences, or when it is necessary to decrease the dimensions of the sensitive elements, thus precluding the use of platinum resistance thermometers. The accuracy of measurement will in this case be limited by the thermoelectric homogeneity and stability of the materials forming the thermocouple. Platinorhodium-platinum thermocouples do not possess these properties to the full. Purified platinum is a very homogeneous and stable material, but platinorhodium is usually insufficiently homogeneous; instances of instability of platinorhodium at 400–600 C are described. It is known that the thermoelectric homogeneity of pure metals is higher than that of alloys. Hence, it was decided to investigate in the temperature range under consideration the platinum-gold thermocouple in order to see what the advantages are of this pure metal thermocouple as compared with the normal platinorhodium-platinum one.

Application of the Phase Detector for Measuring Weak Signals, by V. S. Voyutskii, pp. 629–631.

System for Comparing the Frequency of a Molecular Generator With a Crystal Standard, by A. Ya. Leikin, pp. 632–633.

Calibration of Infrasonic Hydrophones by the Reciprocity Method in Small Water Chambers, by A. G. Golenkov, pp. 637–641.

Abstract: An experimental apparatus is described for calibrating infrasonic piezoelectric hydrophones by the reciprocity method, which was developed by the All-Union Scientific Research Institutes of Physicotechnical and Radiotechnical Measurements (VNIIFTRI).

A Set for Measuring Ultrasonic Fields in Liquids, by I. N. Kanevskii, pp. 642–645.

Introduction: At present one often encounters problems in the measurement technique involving the establishment and analysis of ultrasonic fields with a complex form, including those produced by focusing radiators and focusing systems. For a detailed investigation of such fields it is necessary to have a receiver whose dimensions are smaller than the wave length in the medium and an accurate coordinate measuring device for its displacement. Moreover, for working in the range of small amplitudes, to which the linear theory can be applied, it is necessary to have an amplifying channel with a high gain, since the signals received from a miniature receiver are weak.

B. D. Tartakovskii and G. I. Kaminir, under the guidance of L. D. Rozenberg produced, in the Physics Institute of the Acad. Sci. USSR, a model of an apparatus by means of which the distribution of ultrasonic fields in liquids could be obtained manually point by point. On the basis of the experience gained with this coordinate measuring device the equipment described in this article was made; in its development attention was mainly paid to increasing accuracy of measuring linear and angular coordinates, decreasing the size of the receiver, and making its operation automatic.

No. 9, Sept. 1959.

Optical Method of Checking Kinematic Accuracy Without a Prototype, by V. P. Korotkov, pp. 678–682.

Abstract: The most important factor which determines the operational qualities of any mechanism is its kinematic accuracy, i.e., the accuracy with which the mechanism reproduces a given law of movement in the absence of external interference.

Introduction: Described is the theoretical basis of an optical method developed by the author for controlling kinematic accuracy. The essence of the method consists in observing the coordinated displacement of the driving and the driven control mechanism elements which are interconnected during operation by appropriate scales. The optical images of the scales are made to coincide in the field of vision of a double microscope.

Conclusion: This method can be used for checking the kinematic accuracy of various mechanisms, such as kinematic pairs, metal working lathes, screws, worm gears and other devices. This optical method of nonprototype checking of the kinematic accuracy was used in practice in checking the accuracy of the chain feed of a gear-hobbing machine, which was constructed to the design of the author of this article by the gear transmission section of TsNIITMASh. The tests showed that the instrument can be recommended for use in industry.

Measurement of Angular Displacements of Machine Details With Reversible Rotation, by L. I. Solov'ev, pp. 694–695.

Balanced Voltmeter With a Crystal Diode, by D. N. Livshits, pp. 703–707.

Introduction: When in a conventional balanced voltmeter circuit the thermionic diode was replaced by a crystal one, it was found that the stability of the voltmeter with time was relatively good and its reading little affected if the crystal diodes were changed. It is also known that other crystal diode voltmeter circuits do not possess these properties, since their readings depend to a considerable degree on the deviations of the diode parameters when the diodes are changed and also depend on temperature variations.

A large number of germanium diodes of various types, whose volt-ampere characteristics were previously plotted, were tested in a model of this instrument. Despite the large deviations in the parameters of several diodes of the same type, the readings of the voltmeter only differed from each other on an average by ±1%. Tests have shown the possibility of using crystal diodes for relatively accurate measurements of a-c voltages over a wide frequency range.

Effect of the Internal Temperature of a Conductor on the Accuracy of Determining Its Electrical Resistance, by F. N. Nikolaev, pp. 708–713.

Conclusion:

1 When the resistance of homogeneous cylindrical conductors of 6.5 mm diameters for copper and 3.3 mm for manganin are determined at a current density of 1.5 amp per mm², the error of measurement owing to temperature differences inside the conductor and at its surface can be ignored owing to their small values.

2 When the resistance of cylindrical conductors with diameters greater than 6.5 cm for copper and 3.3 cm for manganin are determined, the errors owing to the cause mentioned must be corrected according to formula.

3 The given formula holds for sufficiently long homogeneous cylindrical conductors with a temperature coefficient whose sum of higher power terms is not larger than the first term.

Lowering of the Bottom Limit for Measuring Inductances by a Bridge Method Combined With Substitution, by G. Ya. Gurovich, pp. 716–717.

Introduction: The accuracy of measurement by the bridge method at audio frequencies drops rapidly when small inductances are measured or when the Q factor of the inductance is low. In the practical application of bridges in this country the wide possibilities offered by a combination of the bridge and substitution methods are not fully utilized. The substitution method, however, with the use in this case of inductor boxes, provides a considerable extension of the bridge range for the lower inductance values. Moreover, the range of the bridge is also extended with respect to low Q factors, which is another equally valuable advantage of this method. In fact, by connecting in series with the unknown inductance an inductor box, it becomes possible to bring the total inductance connected to the bridge terminals within the range of the bridge. In addition, the high Q factor of the box inductors provides a measurable Q-factor value for the total inductance, even if a direct measurement of the unknown inductance is impossible owing to its low Q factor.

Method of Extending the Range of emf Measurements by d-c Potentiometers, by E. P. Maslov, pp. 718–719.

Introduction: At present d-c potentiometers are being widely used in many spheres of electrical engineering. The high accuracy and stability of readings, the possibility of measuring the emf or voltages without distortion, make these instruments irreplaceable in many instances. The top limit of the potentiometer ranges seldom exceeds 2v, which in many cases is not high enough. If a potential divider is used, the measured circuit is closed by a resistance, thus losing one of the advantages

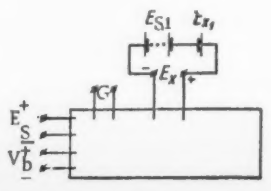

of the compensation method. We give a method of extending the top limit of a potentiometer range and at the same time preserving all the advantages of compensation. It will be seen from the schematic that in this method a standard cell (or a group of cells) E_{S1} is connected in series opposing the unknown emf E_{X1}.

Thus, the potentiometer terminals are fed with the difference of

$$E_{X1} - E_{S1} = E_X$$

where E_{X1} is the unknown emf.

Naturally, the number of standard cells is chosen to make the difference E_X smaller than the top measuring limit of the potentiometer. E_X is measured in the normal manner, i.e., the measuring current is first calibrated against E_S and then E_X is measured. Moreover, the standard cell E_S can be used as E_{S1} for obtaining the difference E_X.

This method is essentially a differential one, since the potentiometer is used for measuring the difference between an unknown quantity and a standard measure whose value is known with great precision. The use of the differential method raises considerably the accuracy of measurement as compared with that of the instrument itself. Another advantage of this method is the possibility of keeping the measuring current of the potentiometer low when measuring the emf; a high current in certain cases is highly undesirable. This method can be used for measuring the emf of the order of several volts. Although theoretically any extension of the potentiometer range is possible by this means, the connection of a large number of standard cells is undesirable.

The Limiting Q Values of Crystal Resonators, by E. D. Novgorodov, pp. 720–722.

Introduction: This article describes the results of research carried out at the Khar'kov State Institute of Measures and Measuring Instruments on the dissipation of energy in 100 kc quartz slices oscillating longitudinally (x-axis) at the second overtone. The crystal slices were excited by means of electrodes with air gaps, thus eliminating energy losses in the metallized layers. The surfaces of all the slices had an optical polish finish. For the sake of convenience, instead of the Q factor, its reciprocal, the damping ratio, was measured.

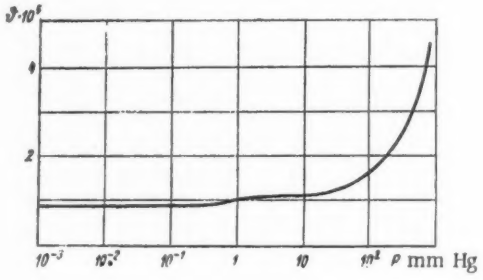

Tests of the relation between the damping ratio and ambient medium pressure (Fig. 1) showed that in order to avoid any appreciable effect of the latter on the former, it is sufficient to place the quartz slice in a container with a pressure in it maintained at about 10^{-3} mm Hg. Numerous tests have shown that at this pressure the medium increases the damping ratio only by a value of the order of 10^{-8}.

BULL. ACAD. SCI. USSR, GEOPHYSICS SERIES (Izvestiya Akademii Nauk SSSR, Seriia Geofizicheskaya). Published by American Geophysical Union, Washington, D. C.

No. 1, Jan. 1959.

Duhamel's Principle and Asymptotic Solutions of the Dynamic Equations of Elasticity Theory, I, by G. A. Skuridin, pp. 1–4.

Abstract: An application of Duhamel's principle to the construction of asymptotic solutions of the dynamic equations of elasticity theory is given. It is shown that, if a system of finite discontinuities is present in the impulse solution, then the solution of the dynamic equations of elasticity theory can be represented in the form of a series expansion with regard to reciprocal powers of $i\omega$ (assuming a harmonic source of oscillation). The discontinuities of the impulse solution and the discontinuities of its time derivative appear as coefficients of this expansion. For $\omega \to \infty$, the expansion which one obtains for the components of the displacement vector becomes an asymptotic one. The domain of convergence of this expansion has not been investigated.

Rocket Investigations of Short Wave Solar Radiation, by G. S. Ivanov-Kholodny, pp. 65–73.

Abstract: This is a review of researches into short wave solar radiation by means of rocket borne instruments. Since the publication of Mandelsfam's survey of short wave radiation from the sun, several other papers have appeared describing further progress in this field up to the year 1954. These have now become outdated, however, owing to the rapid development of research techniques with rocket borne instruments and the

Table 1

Spectral Distribution of Solar Radiation Energy

λ	H_λ	P_λ	λ	H_λ	P_λ	λ	H_λ	P_λ	λ	H_λ	P_λ	λ	H_λ	P_λ
0.22	0.0030	0.02	0.36	0.116	5.47	0.50	0.198	23.5	0.68	0.151	46.7	2.6	0.00445	96.90
0.225	0.0042	0.03	0.365	0.129	5.89	0.505	0.197	24.2	0.69	0.148	47.8	2.7	0.00390	97.21
0.23	0.0052	0.05	0.37	0.133	6.36	0.51	0.196	24.9	0.70	0.144	48.8	2.8	0.00343	97.47
0.235	0.0054	0.07	0.375	0.132	6.84	0.515	0.189	25.6	0.71	0.141	49.8	2.9	0.00303	97.72
0.24	0.0058	0.09	0.38	0.123	7.29	0.52	0.187	26.3	0.72	0.137	50.8	3.0	0.00268	97.90
0.245	0.0064	0.11	0.385	0.115	7.72	0.525	0.192	26.9	0.73	0.134	51.8	3.1	0.00230	98.08
0.25	0.0064	0.13	0.39	0.112	8.13	0.53	0.195	27.6	0.74	0.130	52.7	3.2	0.00214	98.24
0.255	0.010	0.16	0.395	0.120	8.54	0.535	0.197	28.3	0.75	0.127	53.7	3.3	0.00191	98.39
0.26	0.013	0.20	0.40	0.154	9.03	0.54	0.198	29.0	0.80	0.1127	57.9	3.4	0.00171	98.52
0.265	0.020	0.27	0.405	0.188	9.65	0.545	0.198	29.8	0.85	0.1003	61.7	3.5	0.00153	98.63
0.27	0.025	0.34	0.41	0.195	10.3	0.55	0.195	30.5	0.90	0.895	65.1	3.6	0.00139	98.74
0.275	0.022	0.43	0.415	0.192	11.0	0.555	0.192	31.2	0.95	0.0803	68.1	3.7	0.00125	98.83
0.28	0.024	0.51	0.42	0.192	11.7	0.56	0.190	31.8	1.0	0.0725	70.9	3.8	0.00114	98.91
0.285	0.034	0.62	0.425	0.189	12.4	0.565	0.189	32.5	1.1	0.0606	75.7	3.9	0.00103	98.99
0.29	0.052	0.77	0.43	0.178	13.0	0.57	0.187	33.2	1.2	0.0501	79.6	4.0	0.00095	99.05
0.295	0.063	0.98	0.435	0.182	13.7	0.575	0.187	33.9	1.3	0.0406	82.9	4.1	0.00087	99.13
0.30	0.061	1.23	0.44	0.203	14.4	0.58	0.187	34.5	1.4	0.0328	85.5	4.2	0.00080	99.18
0.305	0.067	1.43	0.445	0.215	15.1	0.585	0.185	35.2	1.5	0.0267	87.6	4.3	0.00073	99.23
0.31	0.076	1.69	0.45	0.220	15.9	0.59	0.184	35.9	1.6	0.0220	89.4	4.4	0.00067	99.29
0.315	0.082	1.97	0.455	0.219	16.7	0.595	0.183	36.5	1.7	0.0182	90.83	4.5	0.00061	99.33
0.32	0.085	2.26	0.46	0.216	17.5	0.60	0.181	37.2	1.8	0.0152	92.03	4.6	0.00056	99.38
0.325	0.102	2.60	0.465	0.215	18.2	0.61	0.177	38.4	1.9	0.01274	93.02	4.7	0.00051	99.41
0.33	0.115	3.02	0.47	0.217	19.0	0.62	0.174	39.7	2.0	0.01079	93.87	4.8	0.00048	99.45
0.335	0.111	3.40	0.475	0.220	19.8	0.63	0.170	40.9	2.1	0.00917	94.58	4.9	0.00044	99.48
0.34	0.111	3.80	0.48	0.216	20.6	0.64	0.166	42.1	2.2	0.00785	95.20	5.0	0.00042	99.51
0.345	0.117	4.21	0.485	0.203	21.3	0.65	0.162	43.3	2.3	0.00676	95.71	6.0	0.00021	99.74
0.35	0.118	4.63	0.49	0.199	22.0	0.66	0.159	44.5	2.4	0.00585	96.18	7.0	0.00012	99.86
0.355	0.116	5.04	0.495	0.204	22.8	0.67	0.155	45.6	2.5	0.00509	96.57			

Notes: λ – wavelength in μ; H_λ – spectral density of stream of solar radiation energy at the Earth's surface in w/cm λμ; P_λ – fraction of solar constant included in the wave length interval O – λ, in percentages.

Table 2
Lines of Radiation in The Ultraviolet Region of The Spectrum 1000–1900 A

λ	Identification	λ	Identification	
1892.2	Unidentified	1355.4	OI	
1817.1*	SiII	1335.7*	CII	150
1808.2	SiII	1334.4	CII	120
1670.9*	FeII	1309.5	SiII	13
1659.7	FeII	1306.0*	OI	64
1657.8	CI	1304.9	OI	59
1657.0*		1302.1	OI	39
1656.6		1288.1	Unidentified	—
1654.4	FeII	1265.0	SiII	20
1649.1		1260.2	SiII	12
1643.3		1258.8*	SII	88
1640.4	HeII	1238.9	NV	10
1574.3	FeII	1236.0	Unidentified	—
1570.3	FeII	1229.5	»	—
1563.8	FeII	1218.5	»	—
1561.2	CI	1215.5	HI	6000
1560.3		1206.5	SiIII	160
1558.9	FeII	1201	Unidentified	—
1550.9	CIV	1176.0	CIII	
1548.2	CIV	1174.9		
1542.1	PII	1037.6	OVI	
1533.4	SiII	1031.9	OVI	
1526.7	SiII	1025.7	HI	
1402.8	SiIV	977.0	OIII	
1393.8	SiIV			

*Resonance lines

Table 3

Window	Thickness	Filling	Response band, A
Beryllium	0.75 mm	Helium or neon + methyl formate	0-4
Beryllium	0.13 mm		0-10
Aluminum	0.0063 mm		8-18
Nitro-cellulose			10-60
Mylar	0.75 mg/cm^2		40-60
Glyptal	0.0005 mm		15-100
Lithium fluoride		Neon + chlorine or nitric oxide	1050-1350
Calcium fluoride			1250-1350
Sapphire		Neon + bromine	1450-1500
Quartz		Argan + ethylene	1750-1900

Table 4
Solar X-Radiation Measured by Photon Counters

Rocket	Date	Filter mg/cm^2	Region of spectral sensitivity	No. of pulses per cm^2 sec	Energy in ergs/cm^{2}sec within the given spectral region
V-2	9/29/1949	Be 13	7-12	1.0×10^4	0.0015
Aerobee-9	5/1/1952	Be 47	5-9	495	0.0017
Aerobee-10	5/5/1952	Be 47	5-9	125	0.0005
Viking-9	12/15/1952	Be 13	7-12	1.5×10^3	0.0006
		Al 1.59	8-20	2.9×10^6	0.2
Aerobee-14	11/15/1953	Be 13	7-12	40	6.7×10^{-6}
		Al 1.59	8-20	3×10^4	0.0015
		Lithium	44-100	5.9×10^7	0.035
Aerobee-15	11/25/1953	Be 13	7-12	332	2.9×10^{-6}
		Al 1.59	8-20	2.6×10^4	0.0013
Aerobee-16	12/1/1953	Be 13	7-12	0	
		Al 1.59	8-20	4.5×10^4	0.0004
		Maylar	44-60	2.8×10^6	0.014
		Lithium	44-100	4.9×10^7	0.029
Aerobee 34	10/18/1955	Be 13	7-12	0	-
		Al 1.59	8-20	1.4×10^5	0.0012
Aerobee 43	11 1957	Al 1.59	8-20		0.003

findings of a large number of recent experiments. The reviews given do not contain any account of the latest information obtained during the 1957–1958 IGY. This paper is an attempt to fill the gap.

The Slow Motion of Conducting Medium in a Stationary Magnetic Field, by A. N. Tikhonov and A. G. Sveshnikov, pp. 30–34.

Abstract: Discussed are phenomena which occur as a result of a conducting medium moving in a stationary magnetic field. The authors derived at the relationships between the sea currents velocity and the intensity of an electric field induced by the magnetic field of Earth, taking into account the finite width of the flow and the nonzero value of the sea bed conductivity.

Properties of Earth's Mantle and the Physical Nature of the Transition Layer, by V. A. Magnitsky and V. A. Kalinin, pp. 49–54.

Abstract: We investigate whether it is possible to explain the properties of the *C*-layer by assuming a transition from a predominantly ionic bond type in the upper part of the mantle to a predominantly covalent bond type in deeper layers. This will be done without adopting a specific hypothesis regarding the chemical composition of the material of the mantle.

Distribution of Aurora Polaris in the Circumpolar Region, by Ya. I. Feldstein, pp. 110–111.

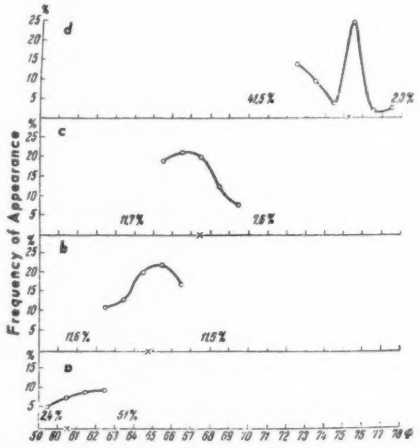

Fig. 1. Distribution of polar aurorae in terms of geomagnetic latitudes

a. Tadibe – Yaga (70.4°N, 74.1°E; Φ = 60.5°N) b. Cape Vykhodnoi (73.2°N; 56.7°E; Φ = 64.8°N) c. Krasnoflotskii Island (78.6°N; 98.7°E; Φ = 67.3°) d. NP-5 (86.5°N; 100°E; Φ = 75.2°N) Key. 1 – b 2 – c 3 – d 4 – Frequency of Appearance

Comparison of Various Equations of the Freezing of Supercooled Water Aerosols, by L. G. Kachurin, pp. 74–79.

Abstract: Various forms of computations of the freezing of supercooled water aerosols are considered. The role of separate parameters entered into the equations of freezing is discussed. It is demonstrated that for the purpose of final selection of the method of computations of the freezing it is necessary to measure the speed of freezing of the highly dispersible water aerosols.

Conclusion: The discussed data of meteorological observations show that the range of the temperatures most characteristic of an intensive formation of the ice particles in the clouds and fogs is limited by temperatures −10 to −20 C. Approximately the same temperatures limit the computed range of intense freezing of the supercooled water aerosols, if for the surface energy on the boundary between ice and water are assumed the values of [10 or 11], corrected in [12]. It is significant that a pronounced temperature relation ω in the temperature range interesting to us assures sufficient reliability of the computed interval, in spite of comparative roughness of determination of the constants entering into the respective equations.

The data of meteorological observations do not make it possible to have final selection of the method of computations of the freezing of supercooled water aerosols. Such a selection can be made on the basis of the results of measurements of the speed of freezing of highly dispersible supercooled water aerosols, and then even the comparatively rough measurements of the speed of freezing would permit a sufficiently accurate judgement of the extent of the reliability of various equations for ω.

Primeval Temperature of Earth, by V. S. Safronov, pp. 85–89.

Conclusion: We have considered a mechanism of evolution of Earth which is based upon the assumption that the latter evolved, in an embryonic state, as the result of the accretion of material from a protoplanetary cloud. This led to the conclusion that Earth was practically completely created during the elapse of the first 10^8 years of its existence. At the end of this time, the temperature at the center of Earth reached 1000 K. The heating was basically caused by the decay of radioactive elements and by the compaction of the material during the process of Earth's growth. The heating owing to the impacts of the captured bodies was relatively small. The later warming of Earth took place on account of the liberation of radioactive heat. The radioactive elements were able to heat the interior of Earth after 5 billion years to a temperature of some thousands of degrees. This heating demonstrates that it represents an essential influence upon the evolution of Earth and, in particular, creates necessary conditions for the processes that are connected with Earth's crust.

Possibilities of Developing an Apparatus for Making Gravimetrical Measurements While in Motion, by V. V. Fedynsky, pp. 93–97.

Conclusion. Elementary theoretical considerations confirm the feasibility of elaborating an apparatus for gravimetric prospecting while in motion. No doubt a number of other promising schemes can be suggested, but the time has now come for experimental treatment of the many problems which involve great precision.

No. 2, Feb. 1959.

Natural Radioactivity of Atmospheric Precipitates, by L. D. Solodikhina, pp. 180–185.

Abstract: The natural radioactivity and precipitation rate of atmospheric precipitates was measured. It was found that the magnitude of the specific activity of precipitates decreased as their precipitation rate increased. The data which were obtained show that in terms of the magnitude of specific activity the precipitates fall into the following sequence: graupel snow, heavy rain, snowflakes and steady rain. Analysis of samples gathered simultaneously at two different altitudes showed that, as the rain falls, it cleans out radioactive particles from the lower layers of the atmosphere.

Interpolation Polynomials Applied to the Study of Earth's Figure, by V. A. Kazinsky, pp. 199–200.

Abstract: We have many uses for interpolation polynomials in various applied disciplines, particularly for solving problems in exploratory geophysics. For example, many searching and exploratory problems are most clearly outlined and solved only by resorting to interpolation polynomials. A no less representative example is the use of interpolation polynomials for solving geodesic problems, and, in the first place, the problem of studying Earth's figure.

Disturbances of the Force of Gravity by the Atmosphere, by V. A. Romanyuk, p. 214.

Introduction: In recent years the accuracy of measurement of variations of the force of gravity at one and the same point has grown substantially. The number of these observations is also growing. For practical use of observational data it is quite important to exclude, from the observed value of the force of gravity, the greatest possible number of disturbing factors. One of the disturbing factors, which has not been taken into consideration in recent times, is the attraction of the atmosphere. As simple calculations show, the variation of this attraction can attain values which compare with the values of the lunar-solar attraction.

Photoelectrical Measurements of Luminescence of a Nocturnal Sky, by A. D. Bolyunova and V. M. Morozov, pp. 215–218.

Introduction: The basic purpose of photoelectrical investigations of nightglow is a study of emissions λ 5577, 5893, 6300 Å and of the OH bands.

An interpretation of results of photoelectrical observations is complicated by the fact that photometers, simultaneously with the investigated radiations in lines, record radiation in the adjacent lines, and also record such components as stellar light, the continuous spectrum of the night sky, zodiacal light, and diffused light in the lower layers of the atmosphere. The total level of these components is relatively high. As a result of this, accuracy

in observing the investigated emissions is considerably lowered, and an indeterminacy is introduced into the absolute calibration of the photometers.

Comparison of Various Methods of the Harmonic Analysis of the Tidal Deformations of Earth, by B. P. Pertsev, N. N. Parisky and M. V. Kramer, pp. 159–160.

Abstract: Comparison of four methods of the harmonic analysis of elastic tides is given. It was made by analyzing the theoretical values of the tide generating potential; the results of the comparison show that with respect to the amount of work involved, all four methods are approximately equivalent. Regarding the degree of accuracy of the attained results, however, Pertsev's method has a slight advantage.

		M_2	S_2	N_2	K_1	O_1
I. DOODSON'S METHOD						
First approximation	R, %	1.3	0.9	4.1	0.6	5.7
	Δδ	-0°55	+0°13	+2°10	+1°14	-0°25
Second approximation	R, %	0.2	0.5	0.7	0.2	2.3
	Δδ	-0°28	+0°45	+2°50	+0°15	-0°32
II. LENNON'S METHOD						
	R, %	1.4	1.6	2.6	1.1	5.7
	Δδ	-0°50	+0°2	-0°6	+1°2	-0°5
III. LECOLAZET'S METHOD						
	R, %	0.2	0.9	0.3	1.5	2.3
	Δδ	0°0	-0°9	+1°2	+0°9	+0°3
First approximation	R, %	1.2	1.5	5.5	2.0	5.5
	Δδ	+0°7	-2°6	+1°1	-1°4	+0°6
Second approximation	R, %	0.2	1.2	0.7	1.5	2.3
	Δδ	+0°1	-2°0	+1°4	-0°9	+0°4
IV. PERTSEV'S METHOD						
First approximation	R, %	0.3	0.6	2.5	0.03	7.7
	Δδ	+0°2	-1°3	+1°2	+0°2	-0°2
Second approximation	R, %	0.5	0.3	0.3	0.14	0.9
	Δδ	-0°2	-0°7	+1°2	+0°2	+0°2

No. 3, March 1959.

Duhamel's Principle and the Asymptotic Solution of the Equations of Motion of the Theory of Elasticity. II, by G. A. Skuridin, pp. 227–230.

Abstract: General solutions of the equations of motion from the theory of elasticity are used to obtain equations for the "jumps" of discontinuous (impulse) solutions and for the "jumps" of their derivatives with respect to time. The results are applied to obtain expressions for the coefficients of the asymptotic series derived in the first part of the study. The equations obtained are identical to the conditions for the application of Duhamel's principle to the equations of elasticity theory. This fact proves that it is possible to use Duhamel's principle to obtain asymptotic solutions of the equations of motion of the theory of elasticity.

High Frequency Filtering as a Means of Eliminating Multiple Reflections, by A. M. Epinat'eva and L. A. Ivanova, pp. 244–252.

Abstract: Certain types of multiple reflections can be eliminated by means of high frequency filtering, whereby a better and more detailed study of the profile is possible than with the commonly used medium frequency seismic apparatus.

Conclusion:

1 High frequency filtering decreases the intensity of certain multiple reflections considerably. The application of high frequency filters (f_{res} = 105 cycles; $S \approx 6.0$) eliminated almost completely the most intensive second-stage reflections and some of the partially multiple waves. The present filter combinations of medium frequency stations are inadequate for the elimination of multiple reflections. It will be necessary to either add some filters to the medium frequency station or to use high frequency instruments.

One of the reasons for the attentuation of multiples through high frequency filtering might be found in the different frequency spectra of primary and multiple waves.

2 The use of high frequency apparatus improves the recording conditions of primary waves within the plotting range of the multiples. High frequency filtering can add detail and depth to seismic cross sections in regions of the occurrence of intensive multiple reflections, compared with the detail and depth achieved with medium frequency instruments. The improved registration of primary waves with high frequency filtering can be linked with the following reasons:

The different frequency spectra of primary and multiple waves; the primary waves, being of higher frequency, plot with greater relative amplitudes than multiple waves if high frequency filtering is employed.

Better wave separation on the record if high frequency filters are used. Primary waves, also primary and multiple waves interfering with one another on records obtained with medium frequency filtering, plot separately with high frequency filters.

The possibility for more widespread application of high frequency seismic methods is pointed out. Previous publications mention the use of high frequency instruments for elimination of certain wave types (surface, converted, refracted) which are impeding seismic reflection shooting. The paper demonstrates the applicability of high frequency instruments to the elimination of one kind of disturbing waves, i.e., of certain types of multiples.

Theory of Thermal Deformations of Earth's Surface, by S. N. Kabuzenko, pp. 300–303.

Introduction: An investigation of indications that might be used in forecasting earthquakes showed that observations of the slope of Earth's surface gave encouraging results. The slope of Earth's surface, however, is related to various other phenomena, such as the variation of atmospheric pressure and temperature, the amount of precipitation, etc. This fact greatly complicates the problem of relating the slope of Earth's surface to earthquakes, especially since up to the present there has been practically no development of any quantitative theory of slopes having an external origin. A theory is given of the relation between the deformation of Earth and the daily temperature variations.

***SOVIET PHYSICS-SOLID STATE* (*Fizika Tverdogo Tela*). Published by American Institute of Physics, Inc., New York.**

Vol. 2, no. 3, Sept. 1960.

Electrical Properties of an Equimolecular InSb–GaSb Alloy, by V. I. Ivanov-Omskii and B. T. Kolomiets, pp. 363–368.

Introduction: Investigation of the electrophysical properties of semiconductor alloys is of great importance, since it increases the number of known semiconductors and helps to provide materials with optimum properties for various applications. For example, the laws governing the carrier mobility in substitution solid solutions are of considerable interest. It is to be expected that alloy formation results in variation in the nature and energy of the chemical bond, and additional scattering of the carriers owing to the statistical distribution of the dissolved atoms among the lattice sites of the solvent, provided, of course, that this does not result in the formation of "fine structure." Whereas it is difficult to predict the effect of the former, it is clear that the latter will result in a decrease in carrier mobility.

Up to the present, only the Ge-Si system has been thoroughly investigated, and, in this case, the experimental data are easily interpreted on the basis of scattering in the disordered arrangements of the atoms in the alloy lattice (disorder scattering). Disorder scattering was also investigated by Nordheim and Brooks who obtained the following expression for the mobility

$$u_{\text{alloy}} = \frac{u_0 T^{-0.5}}{\alpha(1-\alpha)}$$

where u_{alloy} is the mobility owing to disorder scattering, u_0 is a material constant, α is the molar fraction of the second component and T is the absolute temperature.

The carrier free path length for disorder scattering is independent of the carrier velocity, with the particular result that it is impossible to separate this scattering mechanism from scattering at acoustic phonons by the use of the Nernst-Ettinghausen (N-E) effect, thermal emf, etc. Preliminary results recently published concerning an investigation of the equimolecular InSb-GaSb alloy indicated that our own results differ from those of Blakemore. In the present work, we attempt, first, to determine certain parameters of the equimolecular InSb-GaSb alloy, and secondly to explain the effect of alloy formation on carrier mobility.

and Evaluating the Valence-Band Parameters for Semiconductors of the $A^{III}B^{V}$ Type, by A. A. Nran'yan, pp. 439–446.

Abstract: In finding the valence bands of specific $A^{III}B^{V}$ compounds, as well as crystals of the diamond type, it is necessary to evaluate the integrals of interaction of the equivalent orbitals connected with the valence bonds; such is the purpose of this paper. The equivalent orbitals are chosen in the form of a linear combination of the two oppositely oriented sp^3 functions of neighboring atoms. The atomic functions are chosen as indicated. With the help of the values of the integrals thus determined, the effective masses of three kinds of holes, the widths of the valence and additional forbidden bands of the various $A^{III}B^{V}$ compounds are calculated. Regularities in the variations of these parameters of the band structure upon transition from certain substances to others are analyzed.

Generalized Fresnel Equations for the Surface of a Crystal, Taking Account of Anisotropy in the Effective Exciton Mass, by B. E. Tsekvava, pp. 447–453.

Abstract: The Fresnel equations for the transmission of light through a vacuum-crystal boundary are generalized. Equations are obtained for the reflectivity of light from the surface of the crystal, as well as expressions for the coefficients of transparency, reflection, and attenuation of the light intensity in passing through a plane-parallel plate. Experiments are discussed for the purpose of verifying the optical anisotropy of cubic crystals that is obtained.

Theory of Electron Plasma in a Magnetic Field, by V. L. Bonch-Bruevich and A. G. Mironov, pp. 454–463.

Abstract: The behavior of a nondegenerate electron plasma in a constant magnetic field is investigated by the method of Green's functions. The spectrum of plasma oscillations is obtained; in particular the limiting wave number of the vibration is determined and the damping constant calculated taking full account of the quantum correction. The external electric field shielding law (in the presence of a magnetic field) is also investigated.

Vol. 2, no. 4, Oct. 1960.

The Hole-Capture Cross Section of Defects Produced in Germanium by γ-Irradiation, by R. F. Konopleva, S. M. Ryvkin and I. D. Yaroshetskii, pp. 533–535.

Introduction: In a series of papers concerned with investigation of the structure of defects appearing in *n*-type germanium exposed to various kinds of radiation, in particular for the cases of irradiation by neutrons and γ-rays, the observed values of the hole-capture cross sections for the radiation centers q_p differ by an order of magnitude. Thus, for neutron irradiation the values of q_p that were found were 3×10^{-15}, 1.5×10^{-15} and 1.6×10^{-15} cm². For comparison, the magnitude of q_p in the case of γ-radiation as reported was 4.10^{-16} cm². The reason for such a difference is not clear as yet.

It is shown that one reason for the indicated difference is associated with the fact that in a paper given, on the basis of another, it was assumed that to each defect produced as a result of γ-irradiation there correspond two acceptor levels in the forbidden band. As was recently shown, however, in reality there

Electrical Properties of the InSb-GaSb Alloy and Its Starting Binary Components

Property	InSb	InSb·GaSb	GaSb
Electron mobility*, $cm^2/v \cdot sec$	80,000	30,000	5000
Hole mobility*, $cm^2/v \cdot sec$.	≃ 800	≃ 600	≃ 800
Forbidden zone width at 0°K	0.27	0.42 ± 0.02	0.78
Forbidden zone width*	0.17	0.33 ± 0.01	0.70
$d\Delta E/dT$, ev/°C	$-4.0 \cdot 10^{-4}$	$-(4.0 \pm 0.5) \cdot 10^{-4}$	$-4.0 \cdot 10^{-4}$
Effective electron mass	0.013 m_0	(0.04 ± 0.01) m_0	≃ 0.1 m_0
Effective hole mass	0.18 m_0	(0.25 ± 0.5) m_0	≃ 0.3 m_0

* Data for room temperature

Conclusion: The parameters of the equimolecular InSb-GaSb alloy obtained together with the corresponding values for the starting binary components are given in the table.

Injection Heat Transfer, by V. I. Stafeev, pp. 406–412.

Abstract: This paper investigates the mechanism for the onset of the Peltier effect in a semiconductor diode with a p-n junction under various conditions of recombination. It is shown that for recombination in the space charge layer, and for recombination at the contacts between a metal and the semiconductor, the nature of the thermal processes is different in each case. The transfer of heat by injected nonequilibrium carriers is considered. From the usual thermodynamic relations, the Peltier coefficient and differential thermal-emf for a diode with a through current are written. The temperature difference arising in the diode is evaluated, and the possible applications of injection heat transfer for the design of cooling equipment is examined.

Computing the Integrals in the Method of Equivalent Orbitals

are four acceptor levels associated with each defect in the case of γ-radiation. The results of an experimental investigation of the dependence of lifetime on γ-ray irradiation and calculation of the hole-capture cross section are presented. (The source of γ-rays was a preparation of Co-60 whose activity was 400 g-eq. Ra.)

Quantum Efficiency of CdTe p-n Junctions in the Ultraviolet Part of the Spectrum, by G. B. Dubrovskii, p. 536.

Introduction: Preliminary results of measurements of spectral sensitivity of photocells made by diffusing gold into n-type CdTe have previously been presented. It develops that the shape of spectral response curves depends on the method of preparation of the photocells, and that it can change over wide limits, but for all the observed photocells there occurred an increase in sensitivity at incident quantum energies of $h\nu > 2E_g$. Detailed measurements were made of the spectral sensitivity of a large number of CdTe photocells for the purpose of establishing whether electron multiplication occurs when the cells are illuminated by short wave-length light. The figure shows the product of quantum efficiency of the material Q and the collection coefficient α on the energy of the incident photons for several photocells. The spectral dependence of the transmission through the thin metallic layer on the cell surface which served as removable current electrode was taken into account. As is evident from the curves, $Q\cdot\alpha$ falls with increasing photon energy in the region from 2.5 to 3.5 ev.

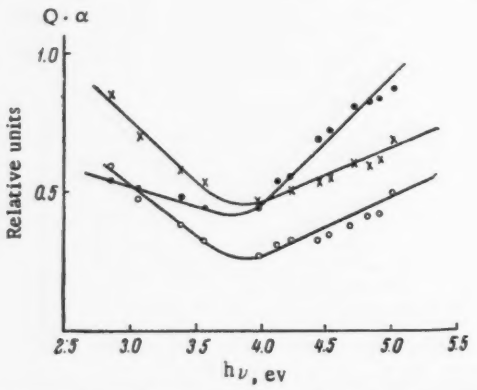

Dependence of $Q\cdot\alpha$ on h ν for three CdTe photocells.

Effect of Heat Treatment on the Electrical Properties of p-Type Silicon, by I. D. Kirvalidze and V. F. Zhukov, pp. 537–540.

Introduction: On the basis of the totality of data appearing in the literature, it can be concluded that the effect of heat treatment on the electrical properties of silicon has not been studied sufficiently. The mechanism of formation of donors under the influence of oxygen in the temperature region from 400 to 500 C and the process of decrease of donor concentration on heating to 500 C has not been sufficiently investigated. We present our experimental results of a study of the effect of heat treatment on the specific resistance and carrier concentration in p-type monocrystalline silicon.

Surface Properties of Silicon, by V. G. Litovchenko and O. V. Snitko, pp. 554–565.

Abstract: Investigated is the effect of an external electric field on the electrical conductivity, the "field-effect mobility" and its kinetics, the surface recombination, and the capacitor photo-emf in silicon. Comparison of the results with theory yielded information on the densities, the energy positions and the capture cross sections of the surface levels in silicon treated with a standard etcher.

Introduction: Properties of real germanium surfaces have been thoroughly investigated. In contrast there are few papers on the surface properties of silicon, and only one of them reports an estimate of the surface level density. We deduced the surface properties of silicon from a study of the following characteristics of a thin plate of silicon: The dark conductivity; the "field-effect mobility" and its "fast" kinetics; the minority carrier lifetime; and capacitor photo-emf. An external electric field was used to vary the surface curvature of the energy bands in silicon within the limits of 0.6 ev. The experimental dependences of the measured quantities on the surface potential were compared with the theoretical dependences in order to obtain the parameters of the surface levels.

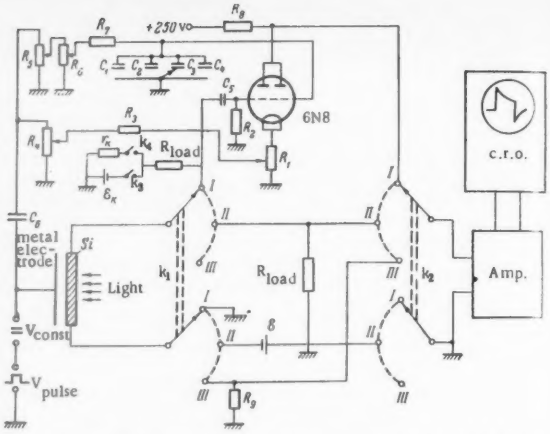

Fig. 1. The circuit used to study the field-effect kinetics (k_1 and k_2 in the position I), photoconductivity (k_1 and k_2 in the position II) and capacitor photo-emf (k_1 and k_2 in the position III). C.r.o. is an oscilloscope 25I or Éo-53; Amp. is an amplifier; R_1 = 1 kohm; R_2 = 1 meg; R_3 = 4 kohm; R_4 = R_5 = 3 kohm; R_6 = 70 kohm; R_7 = R_8 = 2.5 kohm; R_9 = 10^8 ohm; C_1 = 50 $\mu\mu$f; C_2 = 500 $\mu\mu$f; C_3 = 5000 $\mu\mu$f; C_4 = 0.05μf; C_5 = 1 μf; C_6 = 2.0 μf.

Discussion: The results obtained show that chemically treated silicon surfaces possess a complex system of surface levels—five fast and three slow levels. The most important of the fast levels are the uppermost and the lowest levels lying about 10 kT per e above and below the middle of the forbidden energy band, whose densities are $1\text{–}3 \times 10^{12}$ cm^{-2}. These two levels are chiefly responsible for surface recombination. Densities of the other fast levels are one order smaller ($2\text{–}4 \times 10^{11}$ cm^{-2}) and at least one of them takes part in surface recombination. The estimated values of the capture cross sections of the recombination levels are listed in given tables. The slow level densities are $2\text{–}7 \times 10^{11}$ cm^{-2} in vacuum. These levels are probably the hole trapping levels which affect the capacitor photo-emf.

The etched silico nsurface differs from a similar germanium surface in the following respects: The higher (by one order of magnitude) density of the fast surface levels, which may be of multi-charge type; energy positions of the uppermost and lowest levels further from the middle of the forbidden bands; and the presence of surface trapping levels. The density of slow levels in silicon in vacuum is of the same order of magnitude as the density of similar levels in germanium.

The change of the surface level parameters produced by each new etching of silicon samples is not very great ($\Delta E \simeq 1\ kT$ per e), so that the values reported are typical for the type of surface treatment used. The fairly large difference between properties of samples with different resistivities probably results from the effect of the bulk (volume) properties on the surface ones. Since the densities of the fast surface levels are three orders of magnitude smaller than the theoretical predicted densities of the Tamm levels ($\simeq 10^{15}$ cm^{-2}) and the method of surface treatment affects the surface properties, we may conclude that the fast surface states of silicon result from structure defects and foreign atoms at the boundary between silicon and its oxide. The slow surface states result from adsorbed atoms and defects at the outer surface of the oxide, and possibly in the oxide itself.

Absorption of Infrared Radiation by Semiconductor in an Electric Field, by N. V. Fomin, pp. 566–568.

Abstract: The dependence of the absorption of infrared radiation by current carriers in nondegenerate semiconductors on the angle between the directions of polarization of light and the electric field is considered. It is shown that when $eEl \ll kT$ (where E is the field, and l is the carrier mean free path), the effect becomes squared with respect to the field.

Certain Peculiarities of Photoconductivity of Mercuric Sulfide, by N. I. Butsko, pp. 585–587.

Abstract: The wide use of semiconductors in current technology has stimulated an intense search for new semiconducting materials, suitable for practical application, and a detailed study of their properties. This paper describes an investigation of the electrical and photoelectric properties of "pure" crystals of mercuric sulfide prepared artificially.

Transitional d-c Conduction Processes in Ceramic Barium Titanate, by V. M. Gurevich and I. S. Rez, pp. 624–628.

Abstract: Very few investigations have dealt with the d-c conductivity of piezoelectric materials. Thus, out of a total of 278 works cited, Sachse's monograph gives only eight references to work dealing with the conductivity of barium titanate. While investigating the conductivity of barium titanate, we observed the gradual development of current flow through the specimen, termed here the transitional processes of conduction (transitional processes). A similar phenomenon has been observed previously, but has not been specially investigated and discussed.

Summary: The passage of direct current through ceramic barium titanate was investigated.

1 It was observed that the current flow through the specimen was not instantaneous, but was gradually developed over a period of minutes during which the transition conduction processes take place.

2 It was established that these transitional processes are piezoelectric in character.

3 The transitional conduction processes may be employed in the investigation of piezoelectric polarization (polarization energy, coercive fields and in the search for new dielectrics).

4 A difference was observed in the electrical conductivity of polarized and unpolarized piezoelectric barium titanate. This difference was used to calculate the percentage of domains responsible for the remanent polarization in polarized material (13%).

5 The effect of a transverse electric field on the forward conductivity is presumably piezoelectric in nature.

The Possibility of Investigating the Phonon Density Distribution in a Noncubical Crystal With the Help of the Noncoherent Scattering of Neutrons, by V. S. Oskotskii, pp. 647–649.

Introduction: Placzek and van Hove have shown that the differential cross section of noncoherent inelastic scattering of neutrons by cubical crystals is proportional to the phonon density distribution $g(\omega)$. For noncubical crystals, the cross section depends on the polarization of the phonons, which is unknown. In this paper it will be shown that one may exclude consideration of the polarization of the phonons from the cross section by using a composite sample.

We obtain an expression for the cross section by the usual, given method (taking into consideration single-phonon processes)

$$\frac{d\sigma^{\text{inc}}}{d\sigma'} = \frac{\Omega}{2(2\pi)^5\hbar^6}\frac{m}{M}\frac{1}{p}\sum_s \exp\left[-\frac{\overline{(\Delta \mathbf{p}\mathbf{u}_s)^2}}{\hbar^2}\right]\times \left[\overline{\Delta A_s^2}+\frac{1}{4}\overline{B_s^2 J_s(J_s+1)}\right]\sum_j\int d\mathbf{q}\,|\mathbf{e}_{sj}(\mathbf{q})\,\Delta\mathbf{p}|^2\times \frac{n[\omega j(\mathbf{q})]+\frac{1}{2}(1\pm 1)}{\omega j(\mathbf{q})}\,\delta[|E_{p'}-E_p|-\hbar\omega_j(\mathbf{q})]$$

$\mathbf{p}$ and $\mathbf{p}'$, E_p and $E_{p'}$ are the momenta and energies of the neutrons up to and after scattering; $\Delta\mathbf{p}$ equals $\mathbf{p}'-\mathbf{p}$; m and M are the masses of a neutron and elementary crystal cell; Ω is the volume of the crystal; s is the number of the atom in the elementary cell; A_s and B_s are the interaction constants of a neutron with atom s; J_s is the spin of nucleus s; $\overline{\Delta A_s^2}$ and $\overline{B_s^2 J_s(J_s+1)}$ are mean squares of the deviation of the quantity A_s from its mean value and the mean value of the quantities $B_s^2 J_s(J_s+1)$ for the given isotropic composition of atoms of type s; $\mathbf{u}_s$ is the deviation of the atom of type s from equilibrium position; $(\Delta\mathbf{p}\mathbf{u}_s)$ is this mean value of the quantity $(\Delta\mathbf{p}\mathbf{u}_s)^2$ at the given crystal temperature; j, $\mathbf{q}$, $e_{sj}(\mathbf{q})$, $\omega_j(\mathbf{q})$ are the number of the oscillatory branch, the quasi-wave vector, the polarization vector and the phonon oscillation frequency; $n[\omega_j(\mathbf{q})]$ is the number of phonons of frequency $\omega j(\mathbf{q})$, determined by the Planck distribution. The signs "±" refer respectively to the cases of emission and absorption of phonons.

Thermal-Electron Emission From Barium Tungstate, by A. I. Mel'nikov, A. V. Morosov, R. B. Sobolevskaya and A. R. Shul'man, pp. 650–654.

Introduction: In recent years, impregnated cathodes in which the active material consists of barium compounds (aluminates, tungstates, etc.) have found wide application, since they possess certain advantages in comparison with carbonates. In this connection, therefore, an investigation of the thermal emission from these compounds would appear to be of interest. Up to the present, no complete explanation of the mode of functioning of impregnated cathodes has been available. In order to decide whether these cathodes are semiconductors, film conductors or a combination of both, further investigation is necessary with particular reference to the thermal electron properties of the barium compounds.

Certain characteristics of barium tungstate have already been investigated by the authors. The results showed that the thermal electron properties of directly heated barium tungstate cathodes investigated differed considerably from the corresponding properties of impregnated cathodes. However, in this case, comparison is made difficult owing to the fact that this variation in properties may be caused both by the considerable difference in the heat treatment and activation regimes as between our cathodes and impregnated cathodes, and by the fact that the best results were obtained with partially damaged cathodes, where there was direct participation of tungsten from which the heavy coating of barium tungstate had been removed. Thus, it appeared desirable to investigate the properties of barium tungstate under approximately the same conditions as when used in impregnated cathodes. Compressed barium tungstate tablets were used, the difference from actual cathodes being that the tablets were prepared from pure barium tungstate, no metal being present. Thus the subject of the present investigation consisted of cathodes for which the starting conditions were determined by the properties of barium tungstate only.

Discussion of Results: The results obtained indicate that the investigated cathodes possess properties peculiar to semiconductor emitters. This is particularly evidenced by the low values of the Schottky temperature as given in a table. The investigated cathodes are characterized by high thermal-emission current densities which have not previously been obtained during investigations of incompletely activated, directly heated cathodes. Comparison of the present data with that obtained previously shows that the activation regime has a very important effect on the emission properties of the cathode.

We indicated that important changes occur at the emitter surface during activation, especially during current activation. This is confirmed by the change in color of the cathode surface accompanying prolonged passage of current, and by the variation in emission as a result of activation indicated by the electron projector. In every case the emission conditions were more homogeneous after activation than before. The reasons for the high emission from barium tungstate remain obscure. It remains to be determined whether the comparatively high emission of the investigated cathodes is owing to the barium tungstate itself or whether during activation the tungstate decomposes with the formation of barium oxide or some other compound.

If the present results are compared with previous data, it appears that cathodes of compressed Ba_3WO_6 powder only, without metallic powder, give emission currents comparable with those obtained from Ba_3WO_6 impregnated cathodes. The maximum current value obtained was 2 amp/cm² at 950 C, whereas in another paper the current obtained at 980 C and the same anode voltage was 3.5 amp per cm². This unimportant difference can be explained on the basis that the cathodes in that investigation were better activated (T_{act} = 1200 C, current activation), and also by the fact that the tablets in our case were prepared under a pressure of 7 tons per cm², whereas in the previous investigation the optimum pressure was found to be 15 tons per cm². This type of comparison, and also the fact that the static current emission of Ba_3WO_6 impregnated cathodes is independent of the percentage contents of the metal component and Ba_3WO_6, supports the view that the metallic component of an impregnated cathode is of secondary importance only in regard to the emission mechanism.

Influence of the Temperature Dependence of Physical Parameters on the Efficiency of Thermoelectric Generators and Refrigerators, by B. Ya. Moizhes, pp. 671–680.

Abstract: When solving problems dealing with the temperature distribution in the arms of heat generators, it is assumed that the

heat conduction current is many times larger than the Joule heat. For refrigerators operating over a small temperature range, a variation of physical parameters is treated as a perturbation.

Method for Growing Uniform Monocrystals of Alloyed Semiconductor Materials, Solid Solutions, and Intermetallic Compounds of a Given Composition Determined by the Composition of the Melt, by S. V. Airapetyants and G. I. Shmelev, pp. 689–696.

Theory of a Plasma Thermoelement, by B. Ya. Moizhes and G. E. Pikus, pp. 697–714.

Abstract: Physical processes in a plasma thermoelement (thermocouple) are treated in the case of: Local thermodynamic equilibrium; neglect of regeneration and recombination inside the body of the plasma. It is demonstrated that in the second case, which is apparently of the greatest practical interest, the current is determined by carrier diffusion and the load voltage mainly by the contact potentials. We calculate the volt-ampere characteristic and the efficiency in the limiting cases: In the absence of exchange energy between electrons and atoms; in the case of an isothermal plasma.

Discussion of Results: In conclusion we state briefly the principal results.

1 In the case of moderate Cs vapor pressures and comparatively small interelectrode spacings, the current in the plasma thermocouple is determined by the diffusion of electrons and ions from the hot cathode to the cold anode. At the same time the electrons are not able to either recombine nor exchange energy with atoms. Therefore the current is mainly determined by n_1, the electron concentration at the cathode, and D_{ea}, the electron diffusion coefficient at the anode. At the condition of maximum power the current is

$$j_e = \simeq q D_e \frac{n_1}{d}$$

The thermoelectric emf arising in the element is mainly determined by the difference between μ_k, the position of the plasma chemical-potential level at the cathode, and χ_a, the anode work function. For a sufficiently large magnitude of this difference, the kinetic part of the thermoelectric emf is essentially small, and at the condition of maximum power the voltage drop is $v_l \simeq \frac{\mu_k - \chi_a}{q}$. At the same time the kinetic part of the thermo-emf is negative because the electron gas at the anode is warmed up.

2 Inasmuch as the current output $\sim D n_1/d$, $n_1 \sim \exp[-(qV_l/2kT_k)]$, first and foremost it is necessary to have a sufficiently high cathode temperature ($T_k \gtrsim 2100$ K) in order to produce noticeable power. Upon increasing T_k, the relative role of radiation losses, which are proportional to T_k^4, also decreases.

The current output increases approximately inversely with the interelectrode spacing, which also corresponds with the increase in power output. At the same time the efficiency increases until the radiation losses play a substantial role, after which the efficiency tends to saturation. The current depends comparatively little on pressure, because the product $D n_1 \sim P_{Cs}^{-1/2}$ holds for scattering by atoms and almost does not depend on pressure in the case of scattering by ions.

3 In order to increase the voltage output, it is necessary to lower the anode work function as much as possible, and in order to increase the efficiency, one must increase its reflection coefficient. It is profitable to have a higher anode temperature with a view toward subsequent utilization of the heat which it liberates. In addition however, the anode emission current ought to be rather small, approximately $\gtrsim 0.1$ of the current output. At the condition of maximum power the reverse current from the anode decreases because of the anode sheath voltage drop $q\varphi_a$, which retards the electrons. In the example we considered ($\chi_a - 1.2$ ev, $\varphi_a = 0.2$ v) the anode temperature can be raised to approximately 800 K.

4 A calculation given demonstrates that, when operating in the plasma condition in which the diffusion current constitutes only a small part of the cathode emission current, the cathode work function can be varied over rather wide limits, without substantially decreasing the power output. Thus, in the example discussed, when χ_k changes from 2.3 to 3.6 ev, the power varies but 10% in comparison with the maximum (for $\chi_k = \mu_k = 3.2$ ev). Because the power output, as shown, depends relatively little on the Cs vapor pressures, one can select a pressure in order to obtain the necessary values of χ_k by using given curves. This allows us to use in the apparatus a tungsten cathode which has a minimum vapor pressure. Also, the rate of evaporation at the cathode will be considerably less than in a vacuum, because it is determined by the diffusion of tungsten vapors through the plasma.

5 By increasing the Cs pressure and enlarging the interelectrode spacing, one can bring about the condition close to the case of an isothermal plasma. Apparently this condition is not preferred in practice, because some increase in the power on account of the kinetic part of the thermo-emf is compensated by a decrease in current owing to a decrease in the diffusion coefficient and an increase in d.

6 The condition of thermodynamic plasma equilibrium can be realized only in case of a substantial pressure increase and enlargement of the interelectrode distance. Besides the connection with this diminution in current, this condition requires a considerable anode temperature increase, which leads to a decrease in the thermodynamic efficiency. In the case of a high cathode temperature, at a certain distance from the cathode the plasma can also exist in thermodynamic equilibrium; however, also in this case at low anode temperature, diffusion from this "hot" region to the anode will play a basic role. The formulas obtained are valid at all times in the condition of small temperature drops. This method can be utilized in order to investigate the thermoelectric properties of a plasma.

7 The conditions which were discussed are idealized limiting cases. By gradually decreasing the gas pressure and the interelectrode spacing or by lowering the temperature, one can gradually pass from the condition of thermodynamic equilibrium through the isothermal condition to the nonisothermal plasma, and further to the vacuum thermocouple with compensation of volume charge, by passing through various intermediate conditions.

After completion of the present work and article by Lewis and Reitz, "Thermoelectric properties of a plasma diode" was published. The authors of this paper started from the hypothesis that a plasma exists in a state of complete thermodynamic equilibrium. This condition, which we briefly discussed, can be realized only in the case of high pressures and large interelectrode distances, and also in the case of a very high plasma temperature, namely, under those conditions which at the present time are apparently not of practical interest.

Appearance of the emf in Lead Sulfide Films on Being Irradiated by Slow Electrons, by O. M. Artamonov and L. P. Strakhov, p. 715.

Introduction: In a number of papers, photoelectromotive forces have been observed in polycrystalline films of lead sulfide obtained by vaporization in vacuum on a glass backing. This photo-emf depended on the angle of incidence of the light beam on the sample and changed sign on both sides of a certain fixed direction, which coincided approximately with the direction of incidence of the molecular beam in the formation of the layer. When such films of PbS are bombarded with slow electrons (3–300 ev), there arise electromotive forces, the magnitude and sign of which depend on both the direction and on the energy of the incident electrons. If the energy of the electrons is greater than 150 ev, the direction of the sign change for electron bombardment approximately coincides with the direction of the sign change for irradiation.

The magnitude of the emf that appears in this case depends on the intensity and angle of incidence of the electron beam, but does not ordinarily exceed a value of a few hundredths of a volt. However, for certain very definite "critical" angles of incidence (of the order 60 deg to the normal), in some samples a startling rise in the emf has been observed, attaining as much as 1 v, where a unique and characteristic transformation of electrical energy took place: With a beam current of $\sim 10^{-8}$ amp and an electron energy of ~ 100 ev, in the film there appeared an emf of the order of 1 v, and the short circuited current reached a value of 10^{-6} amp. On varying the energy of the incident electrons, the magnitude and even the sign of the emf that arises in the film is seen to change. This change in sign, which is connected apparently with a change in the secondary emissivity, usually takes place with electron energies of the order 30–100 ev, whereas at the critical angles of incidence of the beam, it happens at energies less than 10 ev, or it may happen that there is no change of sign at all in this case. If light and electron bombardment act on the film at the same time, the sum total effect approximately corresponds to algebraic addition of the electromotive forces that arise with the separate action of the light and electrons.

TRANSFER RATE (bytes/sec)

(*Continued from page 376*)

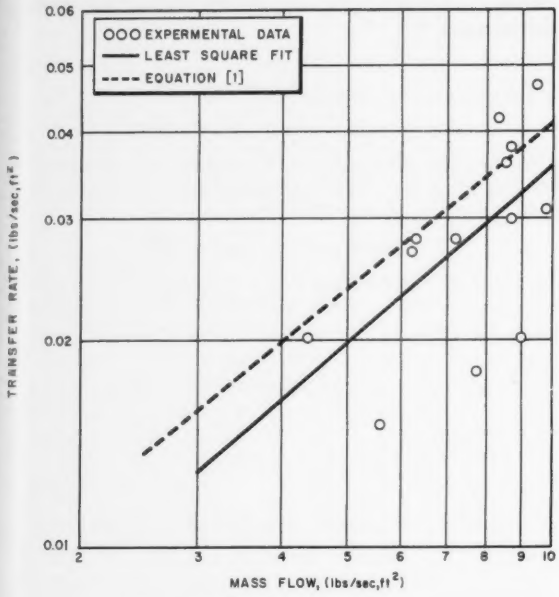

Fig. 3 Transfer rate in section 2

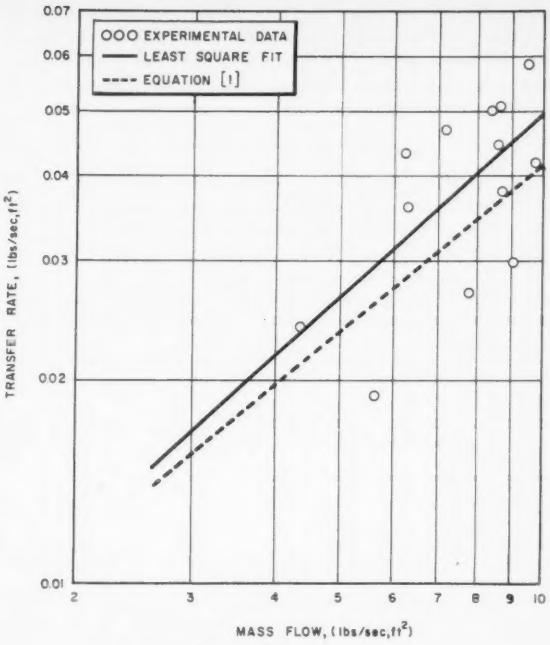

Fig. 4 Transfer rate in section 3

lb per ft, sec which were calculated for the test gas at an enthalpy of 8000 Btu per lb. The experimental data were fitted to equations of the same form by the method of least squares, and the results are given below:

For section 1

$$q/\Delta H = 0.0138G^{0.61} \quad [2]$$

For section 2

$$q/\Delta H = 0.00513G^{0.84} \quad [3]$$

For section 3

$$q/\Delta H = 0.00631G^{0.89} \quad [4]$$

Discussion of the Results

It may be observed that the heat transfer rates in the calorimeter nearest the inlet exceeded those predicted from Equation [1] by approximately 45 per cent. In the middle calorimeter the observed rates were less than predicted, whereas they exceeded the predicted rates in the third calorimeter. This pattern was observed with other gases also, and it was a reproducible effect. It is believed that the heat transfer rate in the third section included a radiative contribution which was absent in the other two sections, and a radiative correction would, therefore, bring the observed and the predicted values closer together. It may be concluded that the turbulent pipe flow equation (Eq. [1]) can predict heat transfer rates correctly, within 15 to 20 per cent, in regions as close to the inlet as 7 to 10 diam for a geometry as shown in Fig. 1. Since the observed results represent average conditions over $2\frac{1}{2}$ diameters it is probable that heat transfer rates considerably greater than those measured in section 1 prevail locally in the upstream portion of this section.

Acknowledgments

We are indebted to C. Brine who assisted with the experimental studies and to T. Munson who carried out the thermodynamic calculations.

Comparison of Some Approximate Methods for Calculating Re-Entry Ablation of a Subliming Material[1]

SHELDON BLECHER[2] and GEORGE W. SUTTON[3]

**Missile and Space Vehicle Dept.,
General Electric Co., Philadelphia, Pa.**

Three different methods are used to calculate the re-entry ablation of a subliming material. The first method is a modification of the Goodman integral method and assumes an exponential temperature profile. The second method is a quasi-steady method, and the third assumes small surface motion. Any of the three methods may be used to calculate the total amount of material ablated within about 15%; however, only the modified Goodman method is useful in predicting temperature profiles.

Received Oct. 3, 1960.

[1] This report is based partially on work performed under the auspices of the U. S. Air Force Ballistic Missile Division, Contract no. AF 04(647)-269.

[2] Mathematician, Magnetohydrodynamic Power Generation, Space Sciences Laboratory.

[3] Manager, Magnetohydrodynamic Power Generation, Space Sciences Laboratory.

IN ORDER to calculate nonsteady ablation rates, it is necessary to calculate the heat conduction within the ablating material and match the energy transfer to the ablating material with that from the gaseous boundary layer. Since the ablation rate varies with time, the boundary condition is nonlinear, and numerical solutions are therefore

required to obtain exact results. However, several approximations may be made which allow the equations to be integrated more easily. The purpose of this note is to compare results obtained from solutions, based upon three different approximate methods, of the heat conduction equation

$$K(\partial^2 T/\partial x^2) = \rho c_p(\partial T/\partial t)$$

The following simplifying assumptions have been made:

1 The material is completely removed from the surface as a gas when it reaches the ablation temperature T_a.

2 The material is initially at uniform temperature T_0.

3 The material has constant thermal properties.

4 The "heat blocking" term $\Delta q/\Delta \dot{m}$, which is the effect of mass transfer, is taken at an average value over the entire re-entry trajectory.

5 The boundary condition for the conduction is as follows

$$q = \rho\left(L - \frac{\Delta q}{\Delta \dot{m}}\right)\frac{ds}{dt} - k\left(\frac{\partial T}{\partial x}\right)\Big|_{x=0} \qquad [1]$$

where q is the aerodynamic heat transfer in the absence of mass transfer. Thus Equation [1] neglects the effect of wall temperature on the heat transfer and the chemical reactions with the ablating material. These effects are usually small for high speed flight.

A discussion of the three approximate methods follows.

I Modification of the Goodman Integral Method (1)[4]

The modification consists of assuming an exponential temperature profile of the form (2)

$$T(x, t) - T_0 = Ve^{-x/\bar{x}} \qquad [2a]$$

since this is exact for the beginning of re-entry or during steady-state ablation of a material with constant thermal properties. The heat balance method then yields the following ordinary differential equations for the e-folding length of the temperature profile $\bar{x}$, and s, the amount of material which has been ablated

$$d\bar{x}/dt = \alpha/\bar{x} - ds/dt \qquad [2b]$$

$$ds/dt = (1/\gamma L)[q(t) - kV/\bar{x}] \qquad [2c]$$

After the end of the heating cycle, the temperature profile in the ablating material may be found by use of the Fourier transform as follows

$$T(x, t) - T_0 = \frac{1}{2}V_a e^{\alpha(t-t_a)/\bar{x}_a^2}\left\{e^{-x/\bar{x}_a}\left[1 + \operatorname{erf}\left(\frac{x}{2\sqrt{\alpha(t-t_a)}} - \frac{\sqrt{\alpha(t-t_a)}}{\bar{x}_a}\right)\right] + e^{x/\bar{x}_a}\left[1 - \operatorname{erf}\left(\frac{x}{2\sqrt{\alpha(t-t_a)}} + \frac{\sqrt{\alpha(t-t_a)}}{\bar{x}_a}\right)\right]\right\} \qquad [3]$$

II Quasi-Steady Method

For this assumption, the ablation rate is given by

$$\frac{ds}{dt} = \frac{\dot{q}}{\rho(L - \Delta q/\Delta \dot{m} + c_p V_a)} \qquad [4]$$

and the temperature profile is given by

$$T(x, t) - T_0 = V_a e^{-(ds/dt)(x/\alpha)} \qquad [5]$$

[4] Numbers in parentheses indicate References at end of paper.

III Assumption of Small Surface Motion

During the beginning of re-entry, the heating rate is given approximately by

$$q = q_0 e^{a^2 t} \qquad [6]$$

and the temperature response is given by

$$T(x, t) - T_0 = q_0 e^{-xa/\sqrt{\alpha}}\, e^{a^2 t}/a\sqrt{k\rho c_p} \qquad [7]$$

After the ablation temperature T_a is reached, the surface temperature will remain at that temperature. The temperature distribution at that time from Equation [7] is

$$T(x, t) - T_0 = V_a e^{-xa/\sqrt{\alpha}} \qquad [8]$$

For the boundary condition $V = V_a$, and the initial condition given by Equation [8], the temperature distribution during ablation is given by the following expression

$$T(x, t) - T_0 = \frac{V_a}{2}\left\{e^{a^2(t-t_a) - ax/\sqrt{\alpha}}\left[1 + \operatorname{erf}\left(\frac{x}{2\sqrt{\alpha(t-t_a)}} - a\sqrt{t-t_a}\right)\right] - e^{a^2(t-t_a) + ax/\sqrt{\alpha}} \times \left[1 - \operatorname{erf}\left(\frac{x}{2\sqrt{\alpha(t-t_a)}} + a\sqrt{t-t_a}\right)\right] + 2\left[1 - \operatorname{erf}\left(\frac{x}{2\sqrt{\alpha(t-t_a)}}\right)\right]\right\} \qquad [9]$$

By taking $(\partial T/\partial x)(x = 0)$ from Equation [9], and making use of Equation [1], one obtains the following expression for the ablation rate

$$\rho\left(L - \frac{\Delta q}{\Delta \dot{m}}\right)\frac{ds}{dt} = q(t) - V_a\sqrt{k\rho c_p}\, a e^{a^2(t-t_a)} \times [1 - \operatorname{erf}(a\sqrt{t-t_a})] \qquad [10]$$

Calculations

The assumed heat pulse (to a nonablating surface) is shown in Fig. 1. Calculations were performed for the three peak heat transfer rates 500, 2000 and 5000 Btu/ft²-sec, for a material with the properties

$L - \Delta q/\Delta \dot{m}$	$= 5.24 \times 10^3$ Btu/lb
k	$= 3.3596 \times 10^{-4}$ Btu/ft-sec-deg F
α	$= 1.0764 \times 10^{-5}$ ft²/sec
ρ	$= 1.3735 \times 10^2$ lb/ft³
V_a	$= 4 \times 10^3$, deg F

The calculated ablation rates are shown in Fig. 2. For high heating rates, method II agrees better with the modified Goodman method, whereas for low heating rates, method III gives better agreement with the modified Goodman method. Method II is always in error at the beginning and end of ablation, since it predicts a finite ablation rate at these times. Hence, the lower the heating rate, the greater this error.

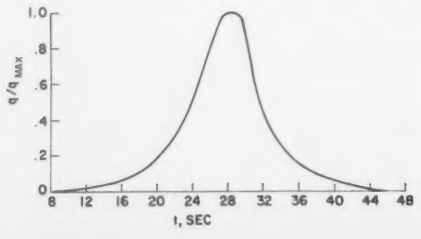

Fig. 1 Re-entry heating pulse to a nonablating surface

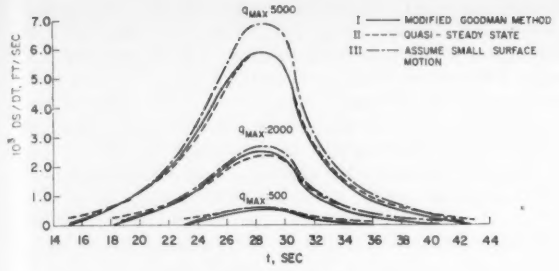

Fig. 2 Calculated ablation rates

Some calculated temperature profiles are shown in Figs. 3 and 4 for a peak heating (29 sec). Methods I and II are in perfect agreement, but method III is in considerable error. However, toward the end of the heating cycle (36 sec) considerable difference develops between methods I and II.

Conclusions

Any of the three methods may be used to calculate the total amount of material ablated within about 15%; however, simple theory, such as methods II and III, will not predict the temperature profiles correctly.

Nomenclature

c_p = specific heat
k = thermal conductivity
L = latent heat of sublimation
$\dot{m}$ = mass transfer, $\rho ds/dt$
q = heat transfer rate
s = distance ablated in x-direction
t = time
T = temperature
V = $T - T_0$
x = distance from instantaneous material surface
$\bar{x}$ = thermal thickness based on exponential profile
α = thermal diffusivity
ρ = density
$\Delta q/\Delta \dot{m}$ = reduction in heat transfer owing to mass transfer

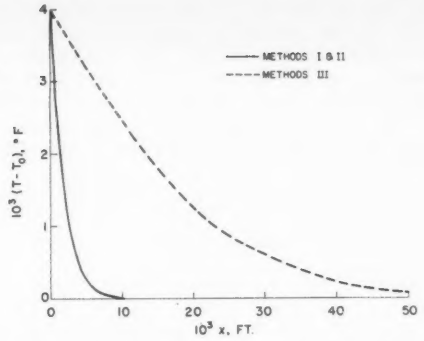

Fig. 3 Temperature profiles for a maximum heating rate of 5000 Btu/ft²-sec at T = 29 sec

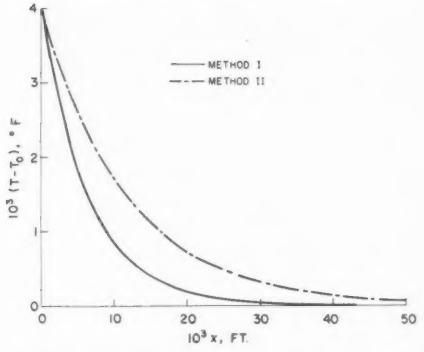

Fig. 4 Temperature profiles for a maximum heating rate of 5000 Btu/ft²-sec at T = 36 sec

Subscripts

a = beginning of ablation
e = end of ablation
0 = initial

References

1 Goodman, T. R., "The Heat Balance Integral and Its Application to Problems Involving a Change of Phase," Heat Transfer and Fluid Mechanics Institute, California Institute of Technology (1957); *also* Trans. ASME, vol. 80, no. 2, Feb. 1958.

2 Sutton, G. W., "Heat Conduction Relations for a Subliming Material During Re-Entry," General Electric Co., Philadelphia, Pa., Rep. TIS 57Sd736, Oct. 1957.

Minimum Time Ballistic Interplanetary Trajectories

VERNON A. LEE[1] and DWIGHT E. FLORENCE[2]

Convair Div., General Dynamics Corp., Fort Worth, Texas

Two equations are developed which, when solved simultaneously by a numerical method, yield minimum time ballistic interplanetary trajectories. Results are presented for transfers from Earth to Mercury, Venus, Mars and Jupiter.

Received Sept. 1, 1960.

[1] Senior Aerodynamics Engineer, Aerosciences Group. Member ARS.

[2] Formerly Aerodynamics Engineer, Aerosciences Group. Now with General Electric MSVD, Philadelphia, Pa.

OF THE infinity of ballistic trajectories which permit transfer between two planetary orbits with a specified total impulse velocity, the path corresponding to minimum transfer time is of particular interest. For example, this path is applicable to the task of placing a scientific payload on or in orbit about another planet, since equipment lifetime and therefore transit time are of direct concern. The round trip case (possibly manned) involves minimum overall mission time, which includes outbound and inbound transit times and stay time on the destination planet. Only the one-way mission is considered here.

Mathematical Model

The basic solar system model employed is a simplified one which has been used in a number of feasibility investigations,

of which that of Vertregt (1)[3] is particularly noteworthy. This model consists of massless planets revolving about the Sun in co-planar circular orbits. The application of two-body (vehicle, sun) relations yields explicit expressions (elliptical case, direct route) for transit time and total impulse velocity (one impulse at each planet). These relations are in terms of eccentricity and perihelion distance (2,3), as is indicated functionally

$$T = F_1(e, q) \quad [1]$$

$$V_0 = G(e, q) \quad [2]$$

The expanded form of Equation [1] is

$$T = F_1(e, q) = \frac{1}{2\pi}\left[\frac{q}{1-e}\right]^{3/2}\left(\cos^{-1}\left[\frac{q-n(1-e)}{qe}\right] - \cos^{-1}\left[\frac{q-(1-e)}{qe}\right] + e\left\{\sin\left[\cos^{-1}\left(\frac{q-(1-e)}{qe}\right)\right] - \sin\left[\cos^{-1}\left(\frac{q-n(1-e)}{qe}\right)\right]\right\}\right) \quad [3]$$

The velocity, V_0, in Equation [2] is for orbit to orbit transfer. It does not include escape from the original planetary field or entry into the destination planetary field. The total impulse required is given by (4) as

$$V = \sqrt{V_{01}^2 + V_{E1}^2} + \sqrt{V_{02}^2 + V_{E2}^2} \quad [4]$$

The expanded form of Equation [4] is

$$V = F_2(e, q) = \sqrt{\left[3 - 2\sqrt{q(1+e)} - \frac{(1-e)}{q}\right] + V_{E1}^2} + \sqrt{\left[\frac{3 - 2\sqrt{\frac{q(1+e)}{n}}}{n} - \frac{(1-e)}{q}\right] + V_{E2}^2} \quad [5]$$

Extremal Equations

Transit time T is extremized (minimized), subject to the total impulse velocity constraint V by the method of Lagrange (5). The extremal equations are

$$\frac{\partial F_1}{\partial q} + \lambda \frac{\partial F_2}{\partial q} = 0 \quad [6]$$

$$\frac{\partial F_1}{\partial e} + \lambda \frac{\partial F_2}{\partial e} = 0 \quad [7]$$

$$V - F_2 = 0 \quad [8]$$

where λ is an undetermined (Lagrangian) multiplier.

By combining Equations [6 and 7] the following set of equations is obtained.

$$\frac{\partial F_1}{\partial e}\frac{\partial F_2}{\partial q} - \frac{\partial F_1}{\partial q}\frac{\partial F_2}{\partial e} = 0 \quad [9]$$

$$V - F_2 = 0 \quad [10]$$

Expressions for the partial derivatives in Equations [9 and 10] are found by differentiating Equations [3 and 5]. Since these expressions are straightforward but lengthy, they are not included here (3).

Results

Equations [9 and 10] were solved simultaneously for e and q, by a numerical method on an IBM 704 computer, for transfers from Earth to Mercury, Venus, Mars and Jupiter. All four missions were first computed neglecting the planetary fields (using zero escape velocities). The Venus and Mars trips were then computed considering the planetary fields (using the surface values of escape velocities).

Fig. 1 presents the values of e and q which were thus obtained. Figs. 2 and 3 present the corresponding minimum transit times as a function of total impulse velocity for the Venus and Mars missions (computed from Equations [3 and 5]). It should be noted that each e, q point of Fig. 1 and each velocity, time point of Figs. 2 and 3 corresponds to a particular planetary configuration angle at launch (date of launch) and that configuration angles repeat every synodic period, 584 days for Venus and 780 days for Mars (2). For the curves which consider the planetary fields, velocity is the sum of the surface impulse velocities required at each planet to launch and soft-land, respectively. The effects of finite rocket burning time, atmosphere, planet axial rotation and planet-sun field interaction are not accounted for.

Two general comments regarding minimum time transfer are appropriate here: It can be shown that the same values of e and q are applicable for the establishment of a near satellite orbit about the destination planet as for soft-landing on it. The total impulse velocity will, of course, be different from that given by Equation [5]. Small deviations in e and q, from those values corresponding to minimum transfer time, will not, in general, significantly increase the time. This occurs as a result of the derivatives of time with respect to e and q being zero at the minimum time point.

The round trip problem is more complex than the one-way case, in that it requires simultaneous numerical solution of four more-involved equations, includes a stay-time discontinuity, and is concerned with various combinations of four possible routes. Preliminary results on direct route round

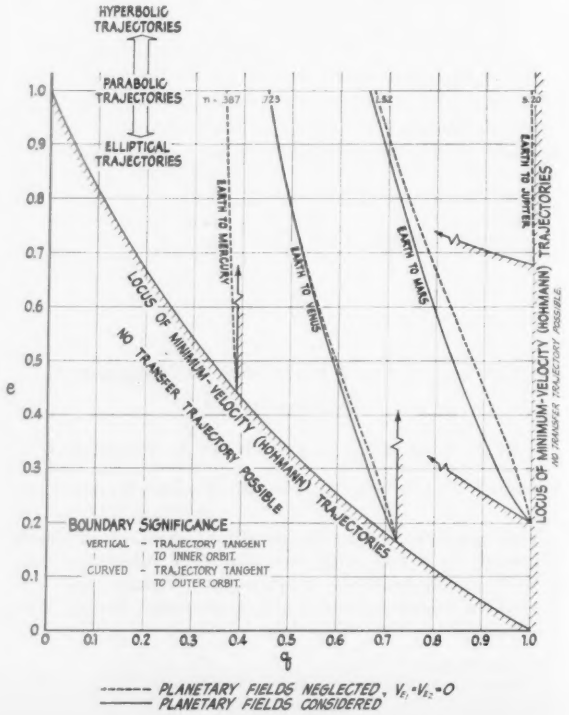

Fig. 1 Minimum-time transfer conics

[3] Numbers in parentheses indicate References at end of paper.

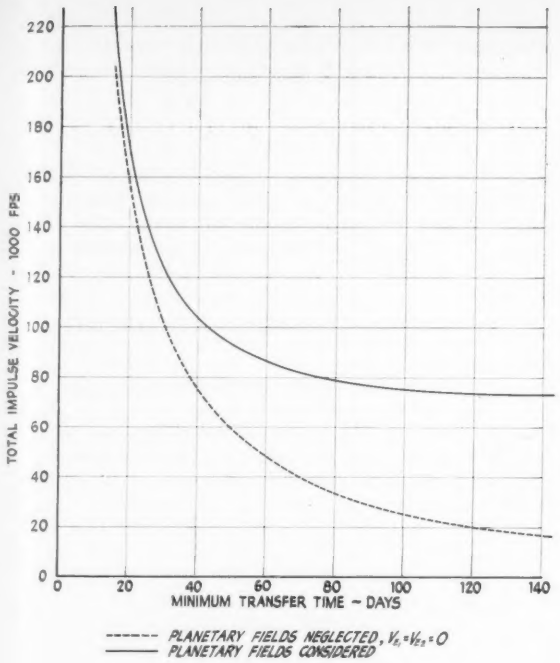

Fig. 2 Earth-Venus trajectories

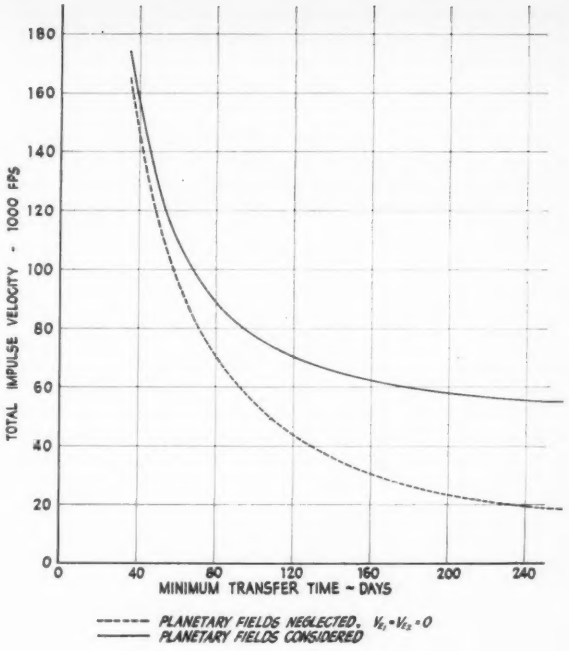

Fig. 3 Earth-Mars trajectories

trip Venus and Mars missions, for relatively low velocities, indicate minimum time paths to be mirror image trajectories lying on the right and left boundaries, respectively, of Fig. 1.

Acknowledgment

The authors are indebted to Jack W. Grigsby, of the Convair-Fort Worth Computation Laboratory, for the IBM-704 computer programming of the procedure, and to J. L. Lindsey, of the Aerosciences Group, for the development of the basic equations.

Nomenclature

- e = eccentricity
- n = ratio of radius of final planetary orbit to radius of initial planetary orbit
- q = perihelion distance, in radii of initial planetary orbit
- T = transit time, in initial planet years
- V = total impulse velocity considering planetary fields, in units of initial planetary orbit circular velocity
- V_0 = total impulse velocity neglecting planetary fields, in units of initial planetary orbit circular velocity
- V_{01} = that part of V_0 applied at initial planetary orbit
- V_{02} = that part of V_0 applied at final planetary orbit
- V_{E1} = surface escape velocity of initial planet, in units of initial planetary orbit circular velocity
- V_{E2} = surface escape velocity of the final planet, in units of initial planetary orbit circular velocity
- λ = Lagrangian multiplier

References

1 Vertregt, M., "Interplanetary Orbits," J. of the Brit. Interplanetary Soc., vol. 16, no. 6, March–April 1958.

2 Lindsey, J. L. and Lee, V. A., "Two-Body Transfer Between Points Moving in Co-Planar Circular Orbits," Convair-Fort Worth, MR-A-1221 Dec. 4, 1959.

3 Lee, V. A. and Florence, D. E., "A Method for Obtaining Minimum Time Two-Body Transfer Trajectories Between Points Moving in Co-Planar Circular Orbits," Convair-Fort Worth, MR-A-1233, Jan. 22, 1960.

4 Karrenberg, Hans K. and Arthur, Paul D., "Interplanetary Ballistic Orbits," ARS Preprint 870-59, 1959.

5 Sokolnikoff, I. S. and Sokolnikoff, E. S., "Higher Mathematics for Engineers and Physicists," second ed., McGraw-Hill Book Co., Inc., New York, 1941, pp. 163–167.

Approximate Velocity, Position and Time Relationship for Ballistic Re-Entry

B. P. MILLER[1]

Defense Electronic Products, RCA, Princeton, N. J.

The general equations of motion for a body re-entering the atmosphere of Earth can be integrated with several constraints to yield an analytical relationship between velocity and position. The results of this analysis can be employed to formulate an approximate expression for the position-time history of the re-entry trajectory.

Analysis

The parametric equations for a body re-entering the atmosphere of Earth as shown in Fig. 1 can be expressed as

$$d^2y/dt^2 = -g + (C_D\rho V^2 A/2m)\sin\theta$$
$$d^2x/dt^2 = (C_D\rho V^2 A/2m)\cos\theta \quad \ldots\ldots [1]$$

These equations can be integrated to form an analytical relationship between the velocity and position, assuming that the

Received Aug. 31, 1960.

[1] Project Engineer, Advanced Projects Analysis Group, Astro-Electronics Division.

drag coefficient and the acceleration of gravity are invariant, that the variation of density as a function of altitude is given by the relation

$$\rho = \rho_0 e^{-\beta y} \qquad [2]$$

where ρ_0 and β are constants, and that the acceleration of gravity is negligibly small compared to the drag effect.[2] Integration of Equations [1] with these constraints yields the following relationship for velocity as a function of position

$$V = V_E e^{-ze^{-\beta y}} \qquad [3]$$

where

$$z = C_D \rho_0 A/2\,\beta\, m \sin\theta \qquad [4]$$

The resulting trajectory is essentially a straight line at the initial re-entry angle.

The results of this classical analysis of the re-entry problem can be used to derive a relationship for the position-time history of the re-entry motion. Velocity and time are related by:

$$dy/dt = -V \sin\theta \qquad [5]$$

Re-arranging terms and substituting for the instantaneous velocity from Equation [3]

$$-dt = dy/V_E \sin\theta\, e^{-ze^{-\beta y}} \qquad [6]$$

The variable in Equation [6] may be transformed by the relationship

$$u = e^{-\beta y}$$
$$dy = -du/\beta u \qquad [7]$$

Substitution of Equations [7] into Equation [6] results in an expression for time that can be directly integrated

$$\int dt = 1/\beta V_E \sin\theta \int e^{u} du/u \qquad [8]$$

$$t = \frac{\ln u + u + (u^2/2\,|2|) + (u^3/3\,|3|) + \dots}{\beta V_E \sin\theta} + \mathrm{K} \qquad [9]$$

$$t = \frac{-\beta y + ze^{-\beta y} + [(ze^{-\beta y})^2/2\,|2|] + [(ze^{-\beta y})^3/3\,|3|] + \dots}{\beta V_E \sin\theta} + \mathrm{K} \qquad [10]$$

If $t = 0$ when

$$V = V_E$$
$$y = y_E \cong 210{,}000 \text{ ft} \qquad [11]$$

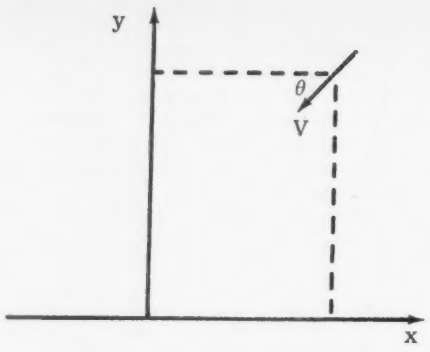

Fig. 1 The re-entry coordinate system

it can be shown that the constant of integration in Equation [10] is approximately equal to βy_E for usual values of z. Thus, the approximate position-time history of the re-entry motion is given by

$$t = \frac{y_E - y}{V_E \sin\theta} + \frac{ze^{-\beta y} + [(ze^{-\beta y})^2/2\,|2|] + [(ze^{-\beta y})^3/3\,|3|] + \dots}{\beta V_E \sin\theta} \qquad [12]$$

The series part of Equation [12] cannot be expressed in a closed form; however, the series is rapidly convergent and can be truncated to about six terms for usual values of z at low altitudes and fewer terms at high altitudes.

Nomenclature

A = reference area for drag evaluation
C_D = drag coefficient
g = acceleration of gravity
K = constant of integration
m = mass
t = time
V = velocity
V_E = velocity at re-entry
x = horizontal distance from impact point
y = vertical distance from impact point
y_E = vertical distance from impact point at re-entry
β = altitude-density function ($\beta = 4.55 \times 10^{-5}$ ft^{-1})
θ = re-entry angle with respect to the horizontal
ρ = density of the atmosphere
ρ_0 = sea level density for altitude-density relationship ($\rho_0 = 0.0034$ slugs-ft^{-3})

[2] Allen, H. Julian, and Eggers, A. J., "A Study of the Motion and Aerodynamic Heating of Ballistic Missiles Entering the Earth's Atmosphere at High Supersonic Speeds," NACA Rep. no. 1381, 1958.

Sputtering Effects on the Moon's Surface[1]

G. K. WEHNER[2]

Mechanical Division of General Mills, Inc., Minneapolis, Minn.

About 40 m of material has probably been sputtered under "solar wind" bombardment from the moon's surface in ~10^9 years. Most of the sputtered atoms have been ejected at such high velocities that they have escaped into space. Sputtered heavy atoms are less likely to have escaped and should have become enriched on the surface. Chemical compounds are dissociated by sputtering, and the lunar surface should be made up predominantly of heavy metal atoms. "Solar wind" bombardment conditions have been simulated in the laboratory at a much accelerated rate (1 hr of laboratory sputtering equivalent to 6000 years of lunar surface sputtering). Experimental evidence confirms that loose dust particles are fused together by sputtered atoms. It may be reasonably assumed that with the help of micrometeoritic activity the

Received Sept. 7, 1960.
[1] In part supported by AFCRC Contract no. AF-19(604)5536.
[2] Senior Physicist. Member ARS.

surface has been converted into a porous but rather solid crust. Sputtering, furthermore, provides an explanation for the smoothness of the lunar surface on a 10-cm scale.

THE MOON'S surface, unprotected by a shielding atmosphere, has been under "solar wind" bombardment for $\sim 10^9$ years. It is interesting to speculate as to the effects of this bombardment on the moon's surface.

As discussed by Reiffel in detail (1,2),[3] who provides many references to other literature, one can assume that the solar wind consists mostly of protons which are traveling away from the sun at an average velocity of 1000 km per sec and whose density in Earth's orbital vicinity is 600/cm³. Thus, the moon's surface is steadily bombarded by 5-kev protons with a particle current density of 6×10^{10}/cm² sec. These values may increase to 10 kev and 1.5×10^{13}/cm² sec during a solar storm. Assuming that the composition of the solar wind plasma is similar to that of the corona itself, the solar wind would contain a 10% He component which, in the moon's vicinity under quiet solar conditions, would amount to ~ 60 He ions per cm³, impinging with 20 kev at a current density of 6×10^9/cm² sec.

Sputtering yields, as determined experimentally for Ag under normal ion incidence, are of the order of 0.04 atoms per ion for 5-kev protons and 0.3 atoms per ion for 20-kev He ions (3). Using these values, one finds that 75×10^{15} atoms per cm² year would be sputtered by protons and 56×10^{15} atoms per cm² year by the He ion component; both combined would yield ~ 130 monolayers of sputtered atoms per year. This value is of the same order as that calculated by Reiffel (1,2) as well as that estimated from the etching rate of meteorites (4). In 10^9 years this would amount to 1.3×10^{26} atoms per cm², or a material thickness of the order of 40 m. Silver has one of the highest sputtering rates. For other materials like Fe, yields are estimated [from argon, neon and mercury sputtering yield data (5,6)] to be lower by a factor of ~ 5. But this lowering of the values is largely compensated for by the fact that sputtering yields increase under oblique ion incidence (7).

It is reasonable to assume that the ejection velocities would be much higher than those of thermally evaporated atoms as was found experimentally for Hg ion bombardment (8). With an escape velocity on the moon of 2.4 km per sec, atoms with $M = 25$ would escape from the moon when their ejection energy is higher than 1 ev, or atoms with $M = 200$ when they are ejected with more than 6 ev. One can conclude that a substantial part of the sputtered material has escaped into space and that the material which has not escaped must have been enriched with heavier constituents.

If chemical bonds are broken in the sputtering process, the sputtered particles would leave a surface mostly as atoms and not as molecules. One would then expect that the moon's surface has become enriched with heavy metal atoms, whereas the oxygen, nitrogen, silicon, etc., constituents of the moon's original compounds or of the meteoric dust collected by the moon have escaped into space.

A considerable number of atoms, especially on rough surfaces, may be trapped again after sputtering and only shift their position during bombardment. This effect is much enhanced by the fact that sputtered atoms under oblique ion incidence are ejected preferentially in forward directions (9). Thus, atoms sputtered from the sides of hillocks or from the sides of dust particles are generally pushed to lower levels and attach themselves in holes and crevices. This has two important consequences:

1 The moon's surface roughness tends to decrease, at least on a macroscopic scale. This provides an explanation for the remarkable smoothness of the lunar surface as found by radar studies on the 10-cm scale.

2 Atoms which are sputtered and then subsequently trapped provide the glue which cold fuses surface particles together or surface particles to underlying particles. Thus, we may reasonably expect that the lunar surface does not consist of a loose dust layer but is rather a porous but relatively solid crust of fused dust particles.

The following experimental studies were performed to support these speculations. A layer of Fe dust supported in a dish was immersed in a low pressure Hg plasma and bombarded with Hg ions of 400-ev energy with 5 milliamp per cm² ion current density, which is equivalent to 30×10^{15} ions per cm² sec. The sputtering yield in this case is 0.5 atoms per ion, 1 hr of laboratory sputtering corresponds roughly to 6000 years of sputtering on the moon's surface. Iron does not react chemically with Hg, and results should provide a reasonably good simulation of lunar conditions on a much accelerated scale. The temperature of the dust layer did not exceed 300 C during the experiments. The appearance of the surface layer following bombardment had changed from that of the dark (iron oxide covered) powder to one with a bright metallic appearance. Microscopic inspection shows that the surface particles have been fused together. One can carry the simulation of lunar surface conditions still further by controlled deposition of dust particles onto the surface during bombardment and thereby build up a whole porous matrix of fused dust particles.

Note added just prior to publication:

Dr. Fred L. Whipple kindly pointed out that meteoric studies set an upper limit of 1-m thickness of material sputtered in 10^9 years. Solar wind intensities have recently been revised downward by one or two orders of magnitude, and we therefore agree that the sputtering rate is more likely to be much lower. This however does not change the conclusions on the modification of the moon's surface.

[3] Numbers in parentheses indicate References at end of paper.

References

1 Reiffel, L., "Structural Damage and Other Effects of Solar Plasmas," ARS JOURNAL, vol. 30, 1960, pp. 258–262.

2 Reiffel, L., "Structural Effects and Particle Content of Interplanetary Space," ARS JOURNAL, vol. 30, 1960, pp. 654–655.

3 Gronlund, F. and Moore, W. J., "Sputtering of Silver by Light Ions with Energies from 2 to 12 kev," *J. Chem. Phys.*, vol. 32, 1960, pp. 1541–1547.

4 Whipple, F. L. and Fireman, E. L., "Calculations of Erosion in Space from the Cosmic-ray Exposure Ages of Meteorites," *Nature*, vol. 183, 1959, p. 1315.

5 Laegreid, N. and Wehner, G. K., "Sputtering Yields of Metals for Ar^+ and Ne^+-Ions with Energies from 50 to 600 ev," to be published in *J. Appl. Phys.*, March 1961.

6 Wehner, G. K., "Low Energy Sputtering Yields in Hg," *Phys. Rev.*, vol. 112, 1948, pp. 1120–1124.

7 Wehner, G., "Influence of the Angle of Incidence on Sputtering Yields," *J. Appl. Phys.*, vol. 30, 1959, pp. 1762–1765.

8 Wehner, G. K., "Velocities of Sputtered Atoms," *Phys. Rev.*, vol. 114, 1959, pp. 1270–1272.

9 Wehner, G. K. and Rosenberg, D., "Angular Distribution of Sputtered Material," *J. Appl. Phys.*, vol. 31, 1960, pp. 177–179.

Celestial Rate Sensing[1]

HANS K. KARRENBERG[2] and ROBERT E. ROBERSON[3]

Systems Corporation of America, Los Angeles, Calif.

THE ANGULAR velocity of a space vehicle can be important to the operations of attitude control and data compensation. Components of angular velocity relative to inertial space resolved along body-fixed axes can be measured by rate gyroscopes fixed in the vehicle with sensitive axes along the prescribed body axes. However, exactly the same components can be determined from the measured velocity of drift of the star field across the fields of view of two or three body-mounted telescopes. This may be called "celestial rate sensing," and may be an attractive alternative to mechanical rate gyros on mechanization grounds.

The purpose of this note is to describe the principle of operation of celestial rate sensors of a particular type, and to derive the relationship between the vehicle's angular velocity in inertial space and the output of such an instrument. Mechanization details are not included, largely because these are proprietary features from the viewpoints of the several companies concerned with such developments.

For this analysis the telescope and its field are analogous to a pinhole camera and its field. The camera's photographic plate or photocathode ("reference surface") and the image of a star produced on it are shown schematically in Fig. 1. A vector directed perpendicularly from the pinhole to the reference surface is denoted by $\bar{r}_0$. The position of a star image on the plate at time t is given by the vector $\bar{r}_1$. The position of the image, a small time increment Δt, later is given by $\bar{r}_2$. The star field is rotating at an angular velocity $-\bar{\omega}$ with respect to the camera pinhole and plate, where $\bar{\omega}$ is the vehicle's angular velocity in inertial space. The vector velocity of the star image at $\bar{r}_1$ is given by $(-\bar{\omega} \times \bar{r}_1)$. The projection of this velocity onto the plate produces $\bar{v}$, the velocity of the star image in the plane of the plate. Note that the projection to the plate is not a perpendicular one but is directed from the pinhole along $\bar{r}_1$ and $\bar{r}_2$. A base vector reference system $\bar{e}_1$, $\bar{e}_2$, $\bar{e}_3$ is presented in the figure; $\bar{e}_3$ is along $\bar{r}_0$ while $\bar{e}_1$ and $\bar{e}_2$ lie in the plane of the reference surface. Polar coordinates ρ and θ may be used to represent the position of the star image in the plane.

The first step is to determine $\bar{v}$ in terms of ρ, θ, $\bar{r}_0$ and $\bar{\omega}$. From the figure it is clear that $(\bar{r}_2 - \bar{r}_0)\cdot\bar{r}_0 = 0$ and that $[\bar{r}_1 + (-\bar{\omega} \times \bar{r}_1)\Delta t] \times \bar{r}_2 = 0$. Expanding the several vectors in the base system and substituting them into these relations, and using the fact that $\bar{v}\Delta t = \bar{r}_2 - \bar{r}_1$, it can be shown that in the limit as $\Delta t \to 0$

$$r_0\bar{v} = -\bar{e}_3 \times [\bar{r}_1 \times (-\bar{\omega} \times \bar{r}_1)] \qquad [1]$$

Introducing

$$\bar{r}_0 = r_0\bar{e}_3 + \rho \cos\theta\bar{e}_1 + \rho \sin\theta\bar{e}_2$$

into Equation [1], one obtains the component form

$$r_0\bar{v} = [-\omega_3\rho r_0 \cos\theta - \omega_2\rho^2 \sin\theta\cos\theta - \omega_1\rho^2\cos^2\theta + \omega_1(r_0^2 + \rho^2)]\bar{e}_2 + [\omega_3\rho r_0 \sin\theta + \omega_1\rho^2 \sin\theta\cos\theta + \omega_2\rho^2\sin^2\theta - \omega_2(r_0^2 + \rho^2)]\bar{e}_1 \qquad [2]$$

in which ω_1, ω_2, ω_3 are respectively the components of $\bar{\omega}$ along $\bar{e}_1$, $\bar{e}_2$, $\bar{e}_3$.

Now the instrument design normally averages (in some sense) the star velocities over the entire field of view. If one assumes that the mechanization operation is equivalent to finding the expected value

$$\langle\bar{v}\rangle = \frac{4}{\pi D^2}\int_0^{2\pi}\int_0^{D/2} \bar{v}\rho d\rho d\theta \qquad [3]$$

where D is the diameter of a circular field of view, then

$$\langle\bar{v}\rangle = [(r_0^2 + D^2/16)/r_0](\omega_1\bar{e}_2 - \omega_2\bar{e}_1) \qquad [4]$$

Since the multiplier involving r_0 and D is simply a constant K of the instrument,

$$\langle\bar{v}\rangle = K(\bar{e}_0 \times \bar{\omega}) \qquad [5]$$

In Equation [5], one can let $\bar{e}_0$ lie respectively along body-fixed axes X_1, X_2, X_3 within the vehicle, in which case

$$\begin{aligned} \bar{e}_0 &= -\bar{X}_3 & \langle\bar{v}\rangle &= K(\omega_{X_2}\bar{X}_1 - \omega_{X_1}\bar{X}_2) \\ \bar{e}_0 &= -\bar{X}_1 & \langle\bar{v}\rangle &= K(\omega_{X_3}\bar{X}_2 - \omega_{X_2}\bar{X}_3) \\ \bar{e}_0 &= -\bar{X}_2 & \langle\bar{v}\rangle &= K(\omega_{X_1}\bar{X}_3 - \omega_{X_3}\bar{X}_1) \end{aligned} \qquad [6]$$

Thus if the telescope is oriented along any body axis, measuring the components of $\langle\bar{v}\rangle$ along the two body axes normal to the telescope axis gives components of the vehicle angular rate in inertial space resolved along these axes. Two telescopes suffice to measure all three components ω_{X_i} if both components of $\langle\bar{v}\rangle$ can be measured in each telescope, but if the mechanization permits the measurement of only one such component in each telescope, then three telescopes are required. Note that ω_{X_i} is precisely the output that would have been obtained from a rate gyro with sensitive axis along X_i.

Consider the case of a "body-centered" attitude reference system in which vehicle body axes $\bar{X}_1$, $\bar{X}_2$, $\bar{X}_3$ are to be kept respectively "forward," "lateral" and "vertical" as the vehicle traverses an orbit with angular frequency ω_0. Follow-

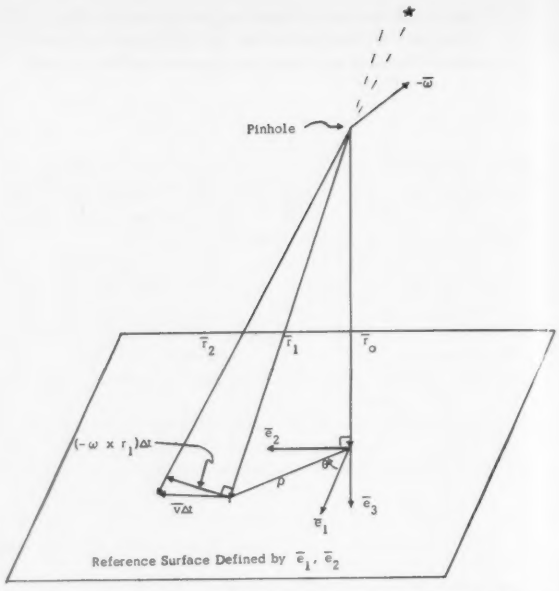

Fig. 1 Schematic presentation of the motion of star field in the sensor

Received Aug. 31, 1960.

[1] This work was supported by the Flight Control Laboratory of Wright Air Development Div. under Contract AF 33(616)-6674.

[2] Now Member of the Technical Staff, Aerospace Corp., Los Angeles, Calif.

[3] Now Consultant in Astronautics, Fullerton, Calif.

ing (1),[4] describe small angular deviations by θ_1, θ_2, θ_3, these being respectively roll, pitch and yaw. It is shown in (1) that

$$\omega_{X_1} = \dot{\theta}_1 + \omega_0\theta_3$$

$$\omega_{X_3} = \dot{\theta}_3 - \omega_0\theta_1$$

from which it is clear that one or more properly mounted telescopes indirectly give information about the deviation angles θ_1 and θ_3 themselves as well as about the angular deviation rates. In particular, θ_3 (yaw) can be inferred from ω_{X_1} provided $\dot{\theta}_1$ can be ignored or compensated using additional sensing information about θ_1 obtained by independent means. In this case the celestial rate sensor would play precisely the role of a single-axis yaw gyrocompass such as would result from the two-axis instrument described in (2) by freezing the roll freedom of the instrument and introducing damping into the remaining (yaw) axis.

However, it should be noted that the normal use of angular rate information is for attitude control system damping, in which case the entire signals for ω_{X_1}, ω_{X_3} and $\omega_{X_2} - \omega_0$ might be used rather than attempting first to infer the values of $\dot{\theta}_1$, $\dot{\theta}_3$ and $\dot{\theta}_2 - \omega_0$. This again is precisely the same situation that exists if the sensing is done by body-mounted rate gyros, so the latter are conceptually equivalent to the celestial rate sensors.

[4] Numbers in parentheses indicate References at end of paper.

References

1 Roberson, R. E., "Attitude Control of Satellites and Space Vehicles," in "Advances in Space Science, Vol. II," Academic Press, New York, 1960, pp. 351–436.

2 Roberson, R. E., "Gyroscopic Sensing of Satellite Yaw," presented at the First International Congress on Automatic Control, Moscow, June, 1960.

Graphical Method for Prediction of Time in Sunlight for a Circular Orbit

G. B. PATTERSON[1]

Grumman Aircraft Engineering Corp., Bethpage, N. Y.

THE COMPUTATION of the percentage time that a satellite will spend in sunlight for any given orbit and Earth-sun orientation is a relatively straightforward procedure. However, the investigation of how time in sunlight changes owing to orbital precession and Earth's motion about the sun, and how it is affected by changing the instant of launch requires tedious repetiton of these calculations. The following, a simple graphical procedure for predicting the percentage time in the sunlight of a satellite in a circular orbit, will rapidly show the effect of variation in launch date or launch instant. The method is accurate for as long a period of time as the satellite's precession rate can be predicted.

For a circular orbit, the percentage time in sunlight t_s is given by

$$t_s = \frac{90 + \sin^{-1}\left|\frac{\sin\alpha}{\sin\eta}\right|}{180} \times 100\% \qquad [1]$$

where

α = $\cos^{-1}[R/(R+h)]$
R = radius of Earth
h = orbital altitude
η = angle between Earth-sun line and normal to orbit

Using an equatorial coordinate system, with the X-axis in the equatorial plane pointing to the vernal equinox, we can find:

Direction cosines of Earth-sun line

$$(\cos\theta, \cos\phi\sin\theta, \sin\phi\sin\theta) \qquad [2]$$

Direction cosines of normal to orbit

$$(\sin i\sin\psi, -\sin i\cos\psi, \cos i) \qquad [3]$$

Received Aug. 10, 1960.

[1] Applied Research Engineer, Propulsion Section. Member ARS.

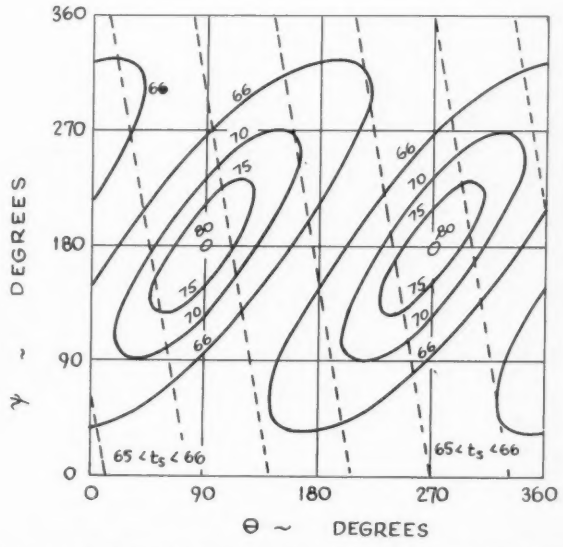

Fig. 1 Contour plot of per cent time in sunlight vs. θ and ψ for 500 nautical mile circular orbit inclined 32 deg to the Equator

where

i = inclination of orbit to Equator
θ = angle between X-axis and Earth-sun line
ψ = angle between X-axis and ascending node of orbit

The dot product of [2 and 3] yields

$$\cos\eta = \sin i\sin\psi\cos\theta - \sin i\cos\psi\cos\phi\sin\theta + \cos i\sin\phi\sin\theta \qquad [4]$$

It can be seen from expressions [1 and 4] that for an orbit of fixed altitude and inclination to the Equator t_s is solely a function of θ and ψ. t_s may now be plotted as a contour map vs. θ and ψ. Fig. 1 shows such a plot for an altitude of 500 miles and inclination of 32 deg. To facilitate the computations for obtaining a t_s plot it should be observed that the curves repeat in intervals of 2π in ψ and π in θ. Further

$$t_s(\theta, \psi) = t_s(\pi - \theta, -\psi)$$

Therefore, it is sufficient to compute values of t_s in the range

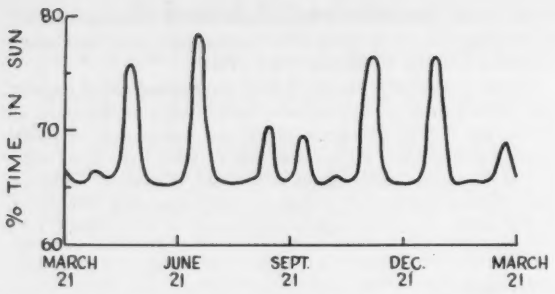

Fig. 2 Time history of per cent time in sun—from dashed line overlay in Fig. 1

$0 \leq \theta \leq \pi/2, 0 \leq \psi \leq 2\pi$, and develop the remainder of the plot from this portion. Data for a complete set of such curves may be computed in about ten minutes on an IBM 704.[2]

It is now only necessary to plot a trace on Fig. 1 representing the change of θ and ψ with time. θ, which locates the sun, is essentially a linear measure of the date. This relationship is given approximately by

$$\theta \times \frac{365.25}{360} = \text{days past March 21}$$

The initial value of ψ, ψ_0, which locates the initial orbital ascending node is set by the selection of the launch instant on any given launch date. Once the vehicle is in orbit, ψ will change owing to orbital precession. A simplified expression for precession of a circular orbit is

$$\frac{d\psi}{dt} = -10\left(\frac{R}{R+h}\right)^{3.5} \cos i \frac{\text{deg}}{\text{day}}$$

However, more accurate expressions for precession are available. Since the accuracy of this method requires precise location of the line of nodes, it is best to use the most recent and complete method for evaluation of precession rate.

Since both ψ and θ change at known, constant rates, the trace showing time history of t_s will be a straight line of slope

$$\frac{d\psi}{d\theta} = \frac{d\psi/dt}{d\theta\ dt}$$

In order to investigate the effects of changing the launch date or launch instant, this trace can be plotted on a transparent overlay so that the starting point may be shifted to different values of ψ_0 and θ_0. The trace plotted in Fig. 1 was intentionally selected to avoid the peak values of t_s. The resulting time history of t_s is shown in Fig. 2.

Although it is generally sufficient, for the purposes of an analysis, to work in terms of ψ_0 without conversion to actual values of time (recognizing that a 24-hr period produces a 2π cycle in ψ_0), if an exact correspondence between ψ_0 and launch time is required the following procedure should be followed.

From the geometry of the launch trajectory, determine the longitude of the ascending node based on the instantaneous orbit at injection. The longitude west of Greenwich of the ascending line of nodes plus ψ_0 is the hour angle (longitudinal displacement) of the vernal equinox from Greenwich. Consult the American Ephemeris and Nautical Almanac to determine at what Greenwich mean time this occurs on the date of launch and convert to local time for the launch site.

[2] Patterson, G., "A Graphical Method for the Prediction of Time in Sunlight for a Circular Orbit," Grumman Aircraft Engng. Corp. Rep., PM-17, Sept. 1960.

Aerodynamic Influences on Satellite Librations[1]

D. M. SCHRELLO[2]

North American Aviation, Inc., Columbus, Ohio

The equations governing the rolling, pitching and yawing motions of a rigid, axisymmetric satellite under the combined influence of aerodynamic and gravitational torques are derived. Atmospheric rotation and motion on an elliptical orbit are considered. Qualitative aspects of the vehicle's angular motion are discussed, and numerical results are presented to show that the aerodynamic torques may exceed those due to gravity gradients by several orders of magnitude at altitudes below 400 miles.

THE PROBLEM of determining the angular motion of a rigid satellite about its mass center under the influence of gravitational torques has been treated extensively in the recent literature, e.g., see Frye and Stearns (1).[3] However, the corresponding problem when other torques also act has not been as thoroughly examined. In particular, satellite motion under the combined influence of aerodynamic and gravitational torques has received only preliminary consideration, e.g., DeBra (2), in spite of the fact that, for altitudes below about 400 miles, aerodynamic torques may exceed those resulting from gravity gradients by several orders of magnitude. Since these aerodynamic influences are determined by the external configuration of the satellite, just as the gravitational torques are determined by its internal mass distribution, the formulation of rational satellite design criteria requires that the interaction of these two torques be studied in detail. It is the purpose of this note to present an analytical framework within which the analysis and subsequent utilization of these aerodynamic torques may be performed.

Received Sept. 6, 1960.

[1] This work is being sponsored by the Flight Dynamics Laboratory, Wright Air Development Division, under Air Force Contract no. AF 33(616)-7100, Project no. 1366, Task no. 13967.

[2] Group Leader, Engineering Research Group.

[3] Numbers in parentheses indicate References at end of paper.

Equations of Motion

Consider a rigid satellite moving on an elliptical orbit. Define a right-handed, orthogonal triad x_0,y_0,z_0 with origin at the vehicle's mass center such that z_0 is directed downward along the geocentric radius vector and x_0 lies in the instantaneous orbit plane, pointing in the direction of motion. Next define body-fixed principal axes of inertia x,y,z oriented with respect to x_0,y_0,z_0 by small Euler angles ϕ, θ, ψ which denote the roll, pitch and yaw position of the vehicle, respectively.

Denote the components of the angular velocity vector along x,y,z by p,q,r. Then, neglecting squares and products of the small angles and their time derivatives, one finds that $p = \dot{\phi} + \psi\dot{v}$, $q = \dot{\theta} - \dot{v}$ and $r = \phi\dot{v} - \dot{\psi}$ where v is the true anomaly. The angular velocity contribution of perturbations on the orbit resulting from oblateness and atmospheric drag may be shown to be negligible compared with $\dot{v}$ for orbits of small eccentricity, and hence the orbit may be regarded as space-fixed and known.

Neglecting all torques except those resulting from aerody-

namic or gravitational effects, the linearized differential equations governing the angular motion are readily found from the well-known Euler equations of a rigid rotator (3). If x is an axis of rotational symmetry of the satellite, these equations simplify to read

$$\ddot{\phi} = L_{A_x}/I_x - \dot{v}\psi$$
$$\ddot{\theta} + 3M\dot{v}^2\sqrt{\frac{n}{\dot{v}}}\,\theta = L_{A_y}/I + \ddot{v}$$
$$\ddot{\psi} - \dot{v}^2M\psi = -L_{A_z}/I + \dot{v}(M+1)\dot{\phi} \qquad [1]$$

where

$I_x, I_y = I_z = I$	=	satellite's principal moments of inertia
$L_{A_x}, L_{A_y}, L_{A_z}$	=	aerodynamic torque components
n	=	Keplerian mean motion
M	$\equiv$	$(I_x - I)/I$

The term involving n stems from the gravitational torque (3) which, for small angles and axisymmetric shapes acts only about the y-axis. When the orbit is sufficiently circular so that $n \cong \dot{v}$, Equations [1] become identical to those of Roberson (3).

The aerodynamic torques acting on the satellite may be found once the velocity vector of the vehicle relative to the atmosphere is oriented with respect to the body. Owing to atmospheric rotation, this relative velocity vector may differ appreciably from the inertial velocity vector. Retaining the conventional aerodynamic representation, the angle of attack α and the sideslip angle β may be found for small angles as $\alpha \cong (\theta - \gamma)$ and $\beta \cong (\psi - \Lambda)$, where γ and Λ are the angles between the relative velocity V_R and the x_0-axis; γ is measured in the orbit plane and Λ is perpendicular to it.

The aerodynamic torques may be represented in terms of dimensionless moment coefficients as

$$\begin{bmatrix} L_{A_x} \\ L_{A_y} \\ L_{A_z} \end{bmatrix} = \frac{1}{2}\,\rho V_R^2 Ab \begin{bmatrix} C_l \\ C_m \\ C_n \end{bmatrix} \qquad [2]$$

where

ρ	=	atmospheric density
A	=	reference area
b	=	reference length
C_l, C_m, C_n	=	dimensionless rolling, pitching and yawing moment coefficients

It is conventional to expand these coefficients about the equilibrium position as Taylor series in the variables α, β, p, q, r and their time derivatives. When the angular deviations of the body from equilibrium are small, only the leading terms in the series need be retained, and when only bodies of revolution are considered, a number of these leading terms may be shown to vanish. In the present analysis, the following linearized representation is employed[4]

$$C_l = C_{l_p}(pb/2V_R)$$
$$C_m = C_{m_\alpha}\alpha + C_{m_q}(qb/2V_R)$$
$$C_n = -C_{m_\alpha}\beta + C_{m_q}(rb/2V_R) \qquad [3]$$

where C_{m_α} is the initial slope of the pitching moment curve, and the terms involving the angular velocity components p, q and r represent the aerodynamic damping in roll, pitch and yaw, respectively. These terms constitute the only natural damping present in the system. Because of the assumed rotational symmetry, it is permissible to assign the same aerodynamic characteristics to both the pitching and yawing motions. Although the stability derivatives C_{l_p}, C_{m_α} and C_{m_q} generally depend upon altitude, velocity, etc., they are regarded as constant in this analysis.

Using Equations [2 and 3] together with the small angle expressions for α, β, q and r allows Equations [1] to be rewritten as

$$\ddot{\phi} + R\dot{v}\dot{\phi} = -[\ddot{\psi} + R\dot{v}\psi]\dot{v}$$
$$\ddot{\theta} + Q\dot{v}\dot{\theta} + [3(n/\dot{v})^{1/3}M + P]\dot{v}^2\theta = [P\gamma + Q]\dot{v}^2 + \ddot{v}$$
$$\ddot{\psi} + Q\dot{v}\dot{\psi} + [P - M]\dot{v}^2\psi = [P\Lambda + Q\phi]\dot{v}^2 + (M+1)\dot{v}\dot{\phi} \qquad [4]$$

where the functions P, Q and R are defined by

$$P \equiv -C_{m_\alpha}\frac{Ab}{2I}\frac{\rho V_R^2}{\dot{v}^2}$$
$$Q \equiv P\,\frac{C_{m_q}}{C_{m_\alpha}}\left(\frac{b\dot{v}}{2V_R}\right)$$
$$R \equiv \frac{Q}{M+1}\,\frac{C_{l_p}}{C_{m_q}}$$

Equations [4] constitute the complete equations of small angle motion for an axisymmetric satellite. It should be noted that the pitch equation is completely uncoupled from the roll and yaw equations.

Equations for Small Eccentricity Orbits

The aerodynamic damping parameters Q and R are generally several orders of magnitude less than the moment parameter P; hence it is permissible to neglect products of Q and R with any small angle or its rate. With this simplification, the first of Equations [4] becomes merely $\ddot{\phi} = -\dot{v}\dot{\psi}$, which may be integrated to yield $\dot{\phi} = k_1 - \dot{v}\psi$, second-order products having again been neglected. Note that if initial conditions are such that $\dot{\phi}(0) \neq -\dot{v}\psi(0)$ then the roll rate $\dot{\phi}$ will possess a (small) secular term k_1 which will cause ϕ to eventually become large. Using these results, the remaining two of Equations [4] become

$$\ddot{\theta} + [3(n/\dot{v})^{1/3}M + P]\dot{v}^2\theta = (P\gamma + Q)\dot{v}^2 + \ddot{v}$$
$$\ddot{\psi} + [1+P]\dot{v}^2\psi = [P\Lambda + (M+1)k_1/\dot{v}]\dot{v}^2 \qquad [5]$$

It is now necessary to express the coefficients of Equations [5] in terms of v and the constants of the motion. For example, Sterne (5) has developed the expressions necessary to relate the angles γ and Λ to the known orbital elements, considering the atmosphere to rotate as a rigid body with Earth. For small orbital eccentricities ϵ, one finds $\gamma \cong \epsilon \sin v$ and $\Lambda \cong d \cos(v + \omega)$, where ω is the argument of perigee and d is a small atmospheric rotation parameter, defined by $d = \Omega_E \sin i/n$; Ω_E is Earth's angular velocity of daily rotation and i the orbital inclination. Likewise, from the equations for the elliptical orbit, to terms of order ϵ, $\ddot{v} \cong -2\epsilon\dot{v}^2 \sin v$ and $(n/\dot{v})^{1/3} \cong 1 - \epsilon\cos v$.

Finally, transforming to v as the independent variable in place of time (noting that $\ddot{v}/\dot{v}^2$ multiplied by any angle or its rate is a second-order product) and employing the foregoing, Equation [5] becomes

$$\theta'' + [3M(1 - \epsilon\cos v) + P]\theta \cong \epsilon(P-2)\sin v + Q$$
$$\psi'' + [1+P]\psi \cong Pd\cos(v+\omega) + k(M+1) \qquad [6]$$

where primes denote differentiation with respect to v and $k = k_1/\dot{v}$, $\phi' \cong k - \psi$.

It remains to express P and Q in terms of v. Assume an exponential density variation (an acceptable approximation for $\epsilon < 0.05$) of the form $\rho = \rho_P \exp[-H(h - h_P)]$, where H is a constant, h is the true altitude over a spherical Earth, and

[4] A clear discussion of the definition and interpretation of the aerodynamic stability derivatives is contained in (4), and need not be repeated here.

the subscript P denotes perigee conditions. From the equation of the conic section, it is found, to terms of order ϵ, that $\rho \cong \rho_P \exp [C(\cos v - 1)]$ where $C \equiv Hr_P\epsilon$; r_P is the geocentric radius to perigee. When $v = \pm\pi/2$, the satellite is at the semi-latus rectum of the ellipse, and the density at this point is $\rho_l \cong \rho_P \exp [-C]$. Thus, $\rho \cong \rho_l \exp [C \cos v]$, and it may then be shown that

$$P \cong \mathcal{P}_P e^{C \cos v}[1 + 2\epsilon(1 - \cos v)]$$
$$Q \cong \mathcal{Q}_P e^{C \cos v}[1 + \epsilon(1 - \cos v)] \quad \ldots\ldots [7]$$

where $\mathcal{P}_P$ and $\mathcal{Q}_P$ are constants, defined by

$$\mathcal{P}_P \equiv -C_{m_\alpha}(Ab/2I)(1 - d \cot i)^2 r_P^2 \rho_l$$
$$\mathcal{Q}_P \equiv (\mathcal{P}_P/1 - d \cot i)(C_{m_q}/C_{m_\alpha})(b/2r_P) \quad \ldots\ldots [8]$$

Equations [6–8] constitute the first-order equations of angular motion of an axisymmetric satellite moving on an elliptical orbit of small eccentricity and subject to aerodynamic and gravitational torques. In order to proceed, it is convenient to expand the period coefficients in Equations [6] as Fourier series. The procedure is straightforward but laborious, and frequent use must be made of the integral representation of the modified Bessel functions of the first kind and order ν (5)

$$I_\nu(C) = \frac{1}{\pi}\int_0^\pi e^{C \cos t} \cos \nu t \, dt$$

The final results may be expressed in the form

$$\theta_i'' + [\kappa_i + 4\lambda_i \cos v + \ldots]\theta_i =$$
$$\delta_i + \eta_i \cos v + \zeta_i \sin v + \ldots \quad [9]$$

where

$$\theta_1 = \theta$$
$$\theta_2 = \psi$$

and where, neglecting second-order terms

$$\kappa_1 = \mathcal{P}_P I_0(C) + 3M$$
$$\lambda_1 = \tfrac{1}{2}\mathcal{P}_P I_1(C) - \tfrac{3}{4}\epsilon M$$
$$\delta_1 = \mathcal{Q}_P I_0(C)$$
$$\eta_1 = 2\mathcal{Q}_P I_1(C)$$
$$\zeta_1 = 2\epsilon[(\mathcal{P}_P/C)I_1(C) - 1]$$
$$\kappa_2 = \mathcal{P}_P I_0(C) + 1$$
$$\lambda_2 = \tfrac{1}{2}\mathcal{P}_P I_1(C)$$
$$\delta_2 = 2\mathcal{P}_P d I_1(C) \cos \omega + k(M + 1)$$
$$\eta_2 = \mathcal{P}_P d[I_0(C) + I_2(C)] \cos \omega$$
$$\zeta_2 = -2(\mathcal{P}_P/C)d I_1(c) \sin \omega \quad \ldots\ldots [10]$$

Discussion of Equations

Consider Equations [9] for circular orbits (i.e., $\epsilon = C = 0$). If $\mathcal{P}_P > -3M$ or $\mathcal{P}_P > -1$ (whichever is larger), these equations have the solutions of a forced, undamped oscillator

$$\theta = K_1 \cos [(\mathcal{P}_P + 3M)v + c_1] + \mathcal{Q}_P/(\mathcal{P}_P + 3M)$$
$$\psi = K_2 \cos [(\mathcal{P}_P + 1)v + c_2] + d \cos (v + \omega) + k[(M + 1)/(\mathcal{P}_P + 1)] \quad \ldots\ldots [11]$$

where K_i and c_i are constants determined by initial conditions. The equilibrium pitch angle $\mathcal{Q}_P/(\mathcal{P}_P + 3M)$ arises because a static moment is required to balance the damping moment produced by the satellite's inertial pitch rate. At equilibrium, this rate is equal to the mean motion n. For $M \geq 0$, the equilibrium pitch angle is very small, but if the satellite is slender (i.e., $M < 0$), the angle will become prohibitively large at some altitude.

A forced harmonic yawing motion of amplitude d exists, produced by atmospheric rotation. The maximum amplitude of this motion occurs for polar orbits, being of the order of 4 deg for altitudes below 500 miles. Since d vanishes only for $i = 0$, it follows that for nonequatorial orbits, yaw (and hence roll) equilibrium is generally impossible.

When the orbit is not circular, Equations [9] are nonhomogeneous Hill equations, since the series multiplying θ_i will generally contain more than the two terms shown. For very small eccentricities, only κ_i and λ_i need be retained, and the equations become of the Mathieu type, a result also found by Baker (6), who was considering only gravitational torques. However, inclusion of the aerodynamic influences further complicates the problem. For example, the first term in δ_2, which vanishes only for orbits symmetric about the Equator, represents a net average yawing torque over one orbit, produced by atmospheric rotation. Since $I_1(C)$ grows essentially as $\exp [C]$, this constant term rapidly becomes large as ϵ increases. Moreover, owing to the roll-yaw coupling, the secular drift of the equilibrium roll position also increases exponentially with ϵ. Similar behavior is seen in the other terms of Equations [10]. In general, extensive numerical calculations are required to study Equations [9] for the case of an elliptical orbit.

An approximate free molecular aerodynamic theory (7) has been used to calculate $\mathcal{P}_P$ vs. circular orbit altitude for three homogeneous 100-lb conical satellites. A mass density of 0.5 slug per ft^3 is assumed, and the molecular reflection is taken to be diffuse with complete accommodation to a surface temperature of 550 R. The results are shown in Table 1. Although no special effort has been made to select an optimum configuration, $\mathcal{P}_P$ still dominates $3M$ for altitudes below about 400 miles, suggesting that by proper design, aerodynamic stabilization may be readily rendered more effective than gravity gradient stabilization for moderately sized, near-Earth satellites.

Table 1. $\mathcal{P}_P$ vs. h for conical satellites of constant mass

$3M$	Semi-vertex angle, deg	Base diam, ft		h, miles 100	200	300	400	500
−2.50	8.59	1.93	$\mathcal{P}_P$	824	25.8	2.34	0.361	0.080
0	26.6	2.88	$\mathcal{P}_P$	2,370	74.4	6.73	1.04	0.230
+2.50	59.2	4.30	$\mathcal{P}_P$	2,030	63.8	5.77	0.891	0.198

References

1 Frye, W. E. and Stearns, E. V. B., "Stabilization and Attitude Control of Satellite Vehicles," ARS JOURNAL, vol. 29, no. 12, Dec. 1959, pp. 927–931.

2 DeBra, D. B., "The Effect of Aerodynamic Forces on Satellite Attitude," *J. Astron. Sci.*, vol. 6, no. 3, Autumn 1959, pp. 40–45.

3 Roberson, R. E., "Attitude Control of a Satellite Vehicle—An Outline of the Problem," ARS preprint no. 485-57, 1957.

4 Tobak, M. and Wehrend, W. R., "Stability Derivatives of Cones at Supersonic Speeds," NACA TN 3788, Sept. 1956.

5 Sterne, T. E., "Effect of the Rotation of a Planetary Atmosphere Upon the Orbit of a Close Satellite," ARS JOURNAL, vol. 29, no. 10, Oct. 1959, pp. 777–782.

6 Baker, R. M. L., Jr., "Librations on a Slightly Eccentric Orbit," ARS JOURNAL, vol. 30, no. 1, Jan. 1960, pp. 124–126.

7 Schrello, D. M., "Approximate Free Molecule Aerodynamic Characteristics," ARS JOURNAL, vol. 30, no. 8, Aug. 1960, pp. 765–767.

Radiated Power From a 2-In. Sphere of High Temperature Air at Pressures to 50 Atm

DOMENICO RAGUSA[1]

MHD Research, Inc., Newport Beach, Calif.

RADIANT energy losses in high temperature plasma jet operation can become quite significant at elevated pressures.

A calculation has been performed, and is illustrated in Fig. 1, which gives the power in kilowatts radiated by a spherical volume of ionized air two inches in diameter. In the calculation the reflected emissive power is not accounted for, since the reflectivity is small and the re-absorption of power by the plasma is also small.

The calculations were performed for enthalpy values of 4000, 8000 and 16,000 Btu per lb at pressures up to 50 atm.

The radiated power P_r has been expressed as follows

$$P_r = VE\,\sigma T^4$$

P_r = radiant power, watts
V = volume of the sphere, cm^3
E = air emissivity, per cent per 1 cm
σ = Stefan-Boltzman constant, 5.67×10^{-12} joules, cm^{-2} deg^{-4}·sec^{-1}
T = average plasma temperature, deg K

The calculations were based on the emissivity values of air[2] at various temperatures and pressures and Mollier Diagram for equilibrium air.[3]

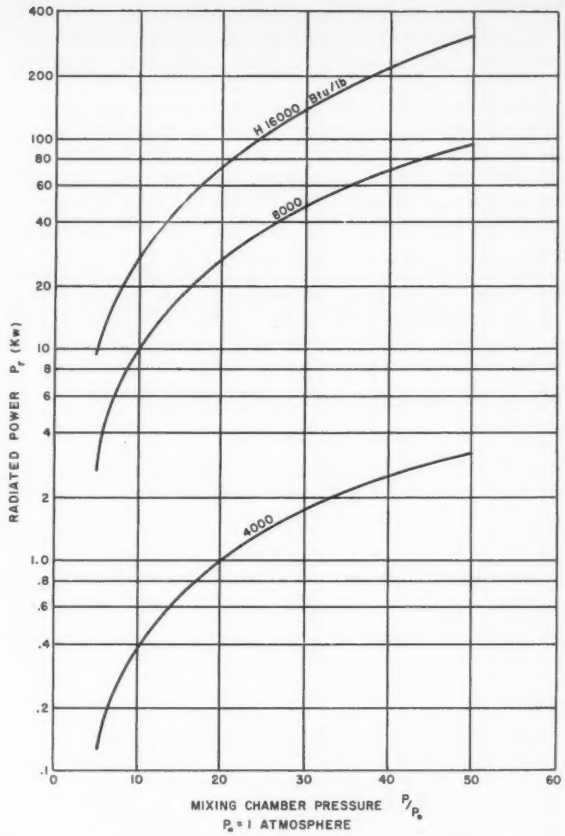

Fig. 1 Power in kilowatts radiated by a spherical volume of ionized air 2-in. in diameter

Received Sept. 1, 1960.
[1] Research Scientist.
[2] Rose, P. H., Avco Res. Rep. no. 9, July 1957.
[3] Felman, S., Avco Res. Rep. no. 40, Jan. 1957.

Effect of Two-Dimensional Heat Transfer on Wall Temperatures in a Tubular Thrust Chamber

JOHN P. SELLERS Jr.[1]

Rocketdyne Div., North American Aviation, Inc., Canoga Park, Calif.

THE TUBULAR type thrust chamber is primarily constructed of a *large* number of tubes; hence, there are many wall extensions into a coolant flowing through these tubes. These extensions normally serve as cooling fins because of the thinness of the tubes ($\sqrt{k/h_L d} > 1.0$). Since the wall thickness, wall material, and the number of tubes is left to the discretion of the designer, it would seem that an optimum tube configuration would exist for maximum utilization of this intrinsic cooling potential.

Analysis

Referring to Figs. 1, assume that:

1 The coolant-side heat transfer coefficient is constant around the interior contour of the tube.

2 Adjacent tubes are symmetrical with respect to heat transfer conditions.

3 No heat is transferred to the environment.

4 Thermal conductivity is not a function of temperature.

5 Tubes are constructed of homogeneous and isotropic materials.

6 The heat flux over the gas-side surface of the tube a is uniform.

7 Heat flow is the x and y directions only.

8 Tube is of uniform wall thickness d.

For a tube made from a single material

$$\frac{T_{max} - T_L}{(Q/A)_a} = \alpha\left(\frac{1}{h_L} + \frac{d}{k}\right) + \beta \qquad [1]$$

where α and β are the correction factors introduced to account for two-dimensional heat conduction. It can be shown (1)[2] that approximate expressions for α and β are

$$\alpha = \frac{1}{2}\frac{1}{(1 + b/a)} \qquad [2]$$

$$\beta = \frac{2(a+b)}{k}\sum_{n=1}^{n=\alpha}\left[\sin\frac{n\pi a}{2(a+b)}\right]\left\{\frac{\frac{n\pi}{(a+b)}\cosh\frac{n\pi d}{(a+b)} + \frac{h_L}{k}\sinh\frac{n\pi d}{(a+b)}}{n^2\pi^2\left[\frac{h_L}{k}\cosh\frac{n\pi d}{(a+b)} + \frac{n\pi}{(a+b)}\sinh\frac{n\pi d}{(a+b)}\right]}\right\} \qquad [3]$$

Received Aug. 30, 1960.
[1] Senior Research Engineer, Combustion Devices Section. Member ARS.

[2] Numbers in parentheses indicate References at end of paper.

Results

It can be shown (2), with a uniform liquid-side heat transfer coefficient, that there is a "critical" width that can be exposed to the hot gas (Fig. 2). When this critical width is exceeded, increases in the thickness of the wall will always result in higher wall temperatures. If the exposed length is less than critical, it is possible to determine an optimum wall thickness for lowest wall temperatures. In both cases the calculated wall temperatures will be less than one-dimensional values, but especially so when in or near the second region.

By differentiating Equation [1] with respect to d, setting the result equal to zero, and solving d_{opt} by iteration, Fig. 2 may be constructed. It can be seen that the values of d_{opt}, except at very large values of h_L/k, are large in relation to present thrust chamber usage.

Comparison With One-Dimensional Results

According to one-dimensional theory

$$\frac{(T_{max} - T_L)_{1-D}}{(Q/A)_G} = \frac{1}{h_L} + \frac{d}{k} \qquad [4]$$

comparing Equation [1] with Equation [4]

$$\frac{(T_{max} - T_L)}{(T_{max} - T_L)_{1-D}} = \alpha + \frac{\beta}{1/h_L + d/k} \equiv \text{fin factor}$$

If the fin factor is plotted versus the heat input ratio a/d for constant values of the parameter $h_L d/k$ then the family of curves shown in Fig. 3 is obtained. This method of presenting the data is excellent for comparing particular examples and is a universal plot of the calculated data. It obviates the need for a detailed calculation with each new problem under consideration.

An obvious conclusion from Fig. 3 is that, with relatively low values of the ratios $h_L d/k$ and a/d, the effect of two-dimensional heat transfer on the maximum wall temperature is pronounced. The effect will have engineering significance when (a) k is high, (b) h_L is low, or (c) spacing between side walls is small. All of these requirements would be realized

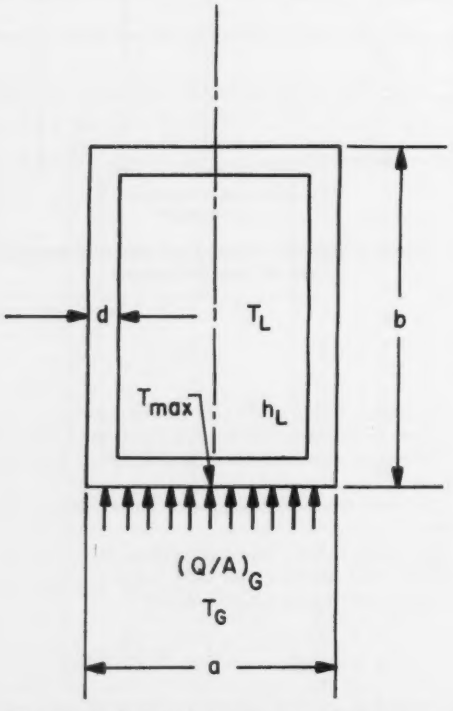

Fig. 1a Typical tubular thrust chamber problem

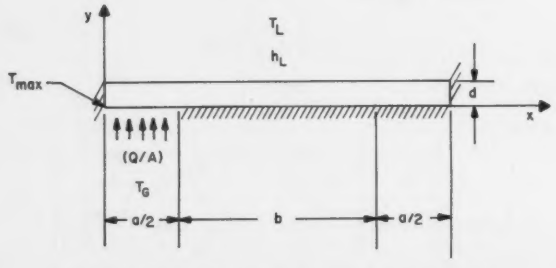

Fig. 1b Model used in Lieberman's (1) analysis

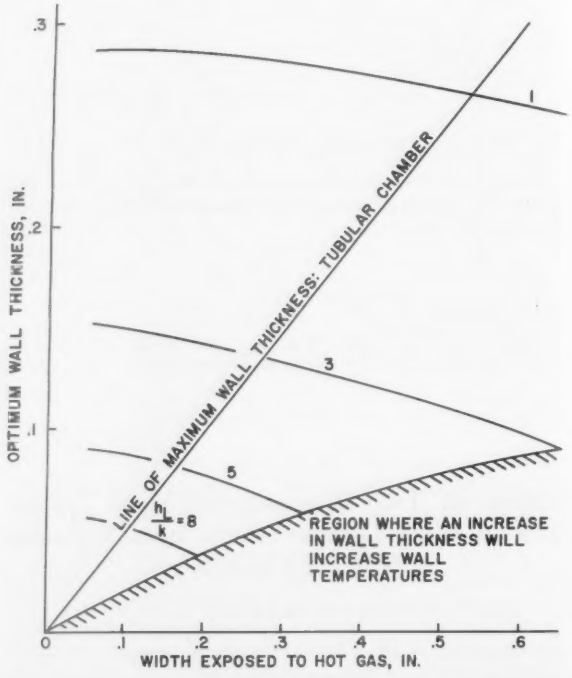

Fig. 2 Optimum wall thickness vs. width of tube exposed to the hot gas for various values of h_L/k

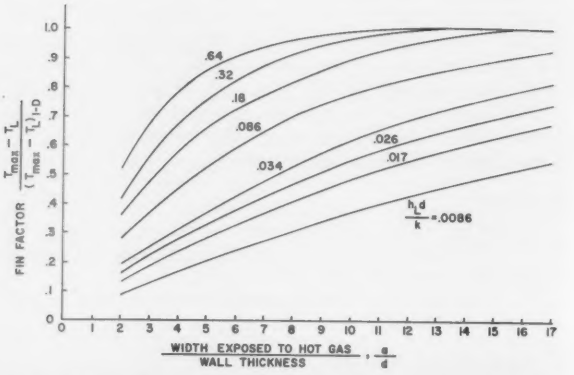

Fig. 3 Comparison of one- and two-dimensional heat transfer

with a motor containing a large number of copper or aluminum tubes and a coolant flowing through the tubes at relatively low velocities.

Similar studies have been carried out for composite materials (1,2).

Nomenclature

a = width of tube subjected to a heat flux
b = height of tube
d = tube wall thickness
h = heat transfer coefficient defined by $Q/A = h\Delta T$
k = wall thermal conductivity
Q/A = heat flux
T = temperature
α, β = correction factors for two-dimensional heat transfer; defined by Equations [2 and 3].

Subscripts

G = gas
L = liquid
max = maximum
opt = optimum
1-D = one-dimensional

References

1 Lieberman, D., "Heat Transfer in Tubular Wall Thrust Chambers," Rocketdyne Internal Rep., DDM 718-5022, May 1957.
2 Sellers, J. P., Jr., "The Conduction of Heat in the Walls of Thrust Chambers," Rocketdyne Internal Rep., CER 922-2010, Nov. 1959.

Hydraulic Analog Investigation of a Plug Nozzle

R. H. PAGE[1] and A. P. MEYER[2]
Stevens Institute of Technology, Hoboken, N. J.

ALTHOUGH the use of the hydraulic analog to gasdynamics is well known (1, 2),[3] it is interesting to point out some of the results of its application to a plug nozzle configuration. It has already been emphasized (3) that many steady and transient gasdynamic flows about and through fixed and time varying geometries can be conveniently, quickly and economically studied by means of the hydraulic analog. This brief note further demonstrates the versatility of the analog as a research tool.

A model of a two-dimensional, Mach three, plug nozzle with a throat width (each side) of 1.00 in. was designed, fabricated and tested (4) in the water table facility of the Fluid Dynamics Laboratory of the Stevens Institute of Technology (Fig. 1). Static testing conditions (i.e., without a nacelle and without external flow about a nacelle) were simulated. Shadowgraph techniques combined with dye tracers and color motion picture photography permitted direct observations of the flow field. Coupled with the model thrust data (obtained from water height measurements) these techniques enabled an overall description of the flow field to be obtained from the experiments. The adjustment of the flow field to off-design pressure ratios (under- and over-expanded) was of primary interest (4), and this could be conveniently recorded during transients by means of slow

Received Oct. 4, 1960.
[1] Professor of Mechanical Engineering.
[2] George Westinghouse Fellow in Mechanical Engineering.
[3] Numbers in parentheses indicate References at end of paper.

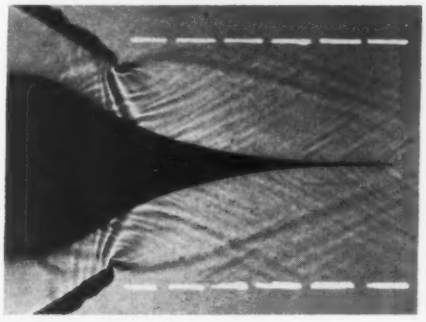

Fig. 2 Flow at design pressure ratio

Fig. 1 Water table facility

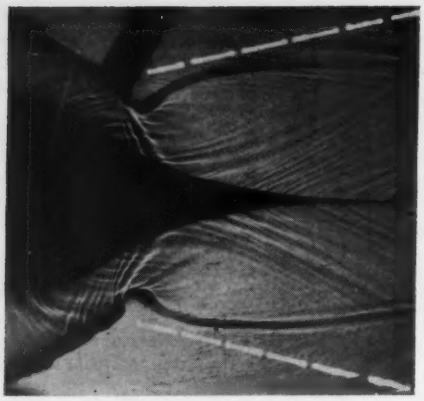

Fig. 3 Flow with surrounding pressure less than design exit pressure

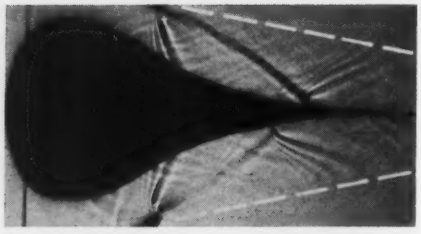

Fig. 4 Flow with surrounding pressure greater than design exit pressure

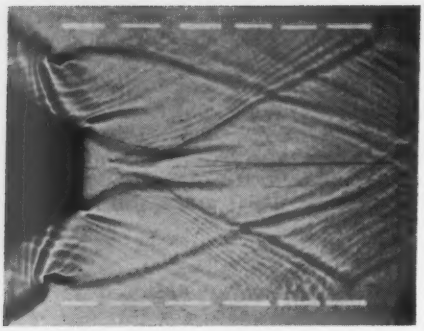

Fig. 5 Flow with shortened exit spike at design pressure ratio

speed (8 frames/sec) short exposure ($\frac{1}{14}$ sec) motion picture photography.

A typical shadowgraph of the "on design" condition is shown in Fig. 2. The boundary of the nozzle flow (as shown by the dashed white line) is aligned with the nozzle axis. Shadowgraphs of the flow field with pressure ratios (stagnation to surroundings) above and below design are reproduced in Figs. 3 and 4. In Fig. 3 the jet boundary turns away from the nozzle (underexpanded) and in Fig. 4 turns toward the nozzle axis. Finally the flow field accompanying a shortened exit spike is shown in the shadowgraph of Fig. 5. Note that the separated flow at the end of the spike follows the normal pattern for supersonic base flow.

References

1 Loh, W. H. T., "Hydraulic Analogy for Two-Dimensional and One-Dimensional Flows," *J. Aero/Space Sci.*, vol. 26, no. 6, June 1959.

2 Bryant, R. A. A., "The Hydraulic Analogy for External Flow," *J. Aero/Space Sci.*, vol. 27, no. 2, Feb. 1960.

3 Page, R. H., "Solution of Gas Dynamics Problems via the Hydraulic Analogue," Lecture, Applied Mechanics Seminar, Stevens Institute of Technology, Hoboken, N. J., Dec. 1958.

4 Meyer, A. P., "An Investigation of Plug Nozzles for Rocket Propulsion," Undergraduate Honors Rep., Mech. Engng. Dept., Stevens Institute of Technology, Hoboken, N. J., May 1960.

Divergence From Equilibrium Glide Path at Supersatellite Velocities

RAYMOND MORTH[1] and JASON L. SPEYER[1]

Boeing Airplane Co., Seattle, Wash.

At supersatellite speeds, velocity greater than circular satellite speed, equilibrium glide paths are unstable because lift must be directed toward Earth to maintain the equilibrium. An approximate formulation for the rate of divergence away from the equilibrium glide path is derived. Measured as time to double amplitude, this rate of divergence is

$$T_2 = \frac{\ln 2}{[g(V^2/V_S{}^2 - 1)\beta]^{1/2}}$$

This rate of divergence depends only on velocity, scale height $\beta = (1/\rho)(d\rho/dh)$, local value of gravity and satellite velocity. To a first-order approximation, the divergence rate is independent of wing-loading, drag coefficient and lift to drag ratio. This time to double amplitude is slow, varying from 20 sec at 35,000 fps to 70 sec at 26,500 fps.

Received Sept. 29, 1960.

[1] Research Engineer.

IN (1)[2] equilibrium glide with negative lift as one possible phase of a re-entry at supersatellite speeds is discussed. At these speeds the equilibrium glide path is unstable, since the negative lift required to balance the normal forces will tend to cause the vehicle to leave the path with any perturbing force. The equilibrium condition is

$$C_L \frac{\rho V^2}{2} A - mg + m \frac{V^2}{R} = 0 \qquad [1]$$

Owing to the inverse relation of altitude and dynamic pressure q, a decrease in altitude at negative lift will cause still more negative lift and hence divergence. An increase in altitude at negative lift will cause less negative lift and again divergence.

To formulate this phenomenon, perturbation equations in the Laplace variable will be derived and the characteristic roots corresponding to these equations will be found.

The equations of motions for a lifting vehicle on a spherical nonrotating Earth are written (see Fig. 1)

$$m\dot{V} + C_D(\rho V^2 A/2) + mg \sin \gamma = 0 \qquad [2a]$$

$$\dot{\gamma} - C_L \frac{\rho V A}{2m} + \left(\frac{g}{V} - \frac{V}{R}\right) \cos \gamma = 0 \qquad [2b]$$

[2] Numbers in parentheses indicate References at end of paper.

$$h - V \sin \gamma = 0 \qquad [2c]$$

Variation of density with altitude is assumed to be exponential

$$\rho = \rho_0 e^{-\beta h} \qquad [3]$$

Perturbation equations are then written for Equations [2], making use of the fact that $\delta\rho = -\beta\rho\delta h$ and neglecting perturbations resulting from changes in R

$$\delta\dot{V} - C_D \frac{V^2}{2m} A\rho\beta\delta h + C_D \frac{\rho VA}{m} \delta V + g \cos \gamma\delta\gamma = 0$$

$$\delta\dot{\gamma} + C_L \frac{VA\rho\beta}{2m} \delta h - C_L \frac{\rho A}{2m} \delta V - \left(\frac{g}{V^2} + \frac{1}{R}\right) \cos \gamma\delta V + \left(\frac{V}{R} - \frac{g}{V}\right) \sin \gamma\delta\gamma = 0$$

$$\delta\dot{h} - \sin \gamma\delta V - V \cos \gamma\delta\gamma = 0 \qquad [4]$$

These perturbation equations are Laplace transformed and in matrix notation are

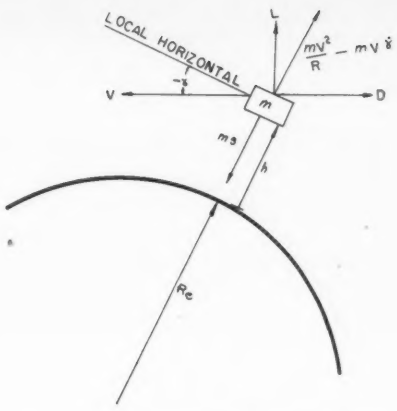

Fig. 1 Forces on re-entering lifting vehicle

$$\begin{bmatrix} S + C_D \frac{\rho VA}{m} & g \cos \gamma & -C_D \frac{AV^2\rho\beta}{2m} \\ -\frac{C_L\rho A}{2m} - \left(\frac{g}{V^2} + \frac{1}{R}\right) \cos \gamma & S + \left(\frac{V}{R} - \frac{g}{V}\right) \sin \gamma & C_L V \frac{\rho\beta A}{2m} \\ -\sin \gamma & -V \cos \gamma & S \end{bmatrix} \begin{Bmatrix} \delta V \\ \delta\gamma \\ \delta h \end{Bmatrix} = 0 \qquad [5]$$

The characteristic equation is third order and is shown to be

$$S^3 + a_2S^2 + a_1S + a_0 = 0 \qquad [6]$$

where

$$a_2 = \left(\frac{V}{R} - \frac{g}{V}\right) \sin \gamma + \frac{C_D\rho VA}{m}$$

$$a_1 = \frac{C_D\rho VA}{m} \left(\frac{V}{R} - \frac{g}{V}\right) \sin \gamma - \frac{C_DV^2\rho\beta A}{2m} \sin \gamma + \left[C_L \frac{\rho A}{2m} + \left(\frac{g}{V^2} + \frac{1}{R}\right) \cos \gamma\right] g \cos \gamma + \left(C_L \frac{V^2\rho\beta A}{2m} \cos \gamma\right)$$

$$a_0 = -g \frac{C_LV\rho\beta A}{2m} \sin \gamma \cos \gamma - \left(C_D \frac{V^2\rho\beta A}{2m}\right)\left[\frac{C_L\rho A}{2m} + \left(\frac{g}{V^2} + \frac{1}{R}\right) \cos \gamma\right] V \cos \gamma - \left(\frac{V}{R} - \frac{g}{V}\right) \sin^2 \gamma \left(\frac{C_DV^2\rho\beta A}{2m}\right) + \left(\frac{C_LAV\rho\beta}{2m}\right)\left(\frac{C_DA\rho V}{m}\right) V \cos \gamma$$

Simplifications of these coefficients are possible with expected values of $L/D > 0.2$, and with consideration of the equilibrium glide path where $\sin \gamma \cong 10^{-3}$ and $\cos \gamma \cong 1$. By neglecting higher order terms, the order of magnitude of $a_2 \cong 10^{-4}$, $a_1 \cong 10^{-3}$ and $a_0 \cong 10^{-6}$. Since $a_0 \ll a_1$, then the cubic can be factored as

$$\left(S + \frac{a_0}{a_1}\right)\left[S^2 + \left(a_2 - \frac{a_0}{a_1}\right) S + a_1\right] \qquad [7]$$

where

$$a_2 \cong C_DA\rho V/2m$$

$$a_1 \cong V^2C_L\rho\beta A/m$$

$$\frac{a_0}{a_1} \cong -\left[\frac{1}{\beta(\rho V^2/2)(C_LA/m)}\right]\left\{\beta \left(\frac{C_DA}{m}\right)\left(\frac{\rho V^2}{2}\right)\left[\left(\frac{C_LA}{m}\right) \frac{\rho V}{2} + \left(\frac{g}{V} + \frac{V}{R}\right)\right] - \left(\frac{C_LA}{m}\right)\left(\frac{C_DA}{m}\right)\left(\frac{\rho V^2}{2}\right) \rho\beta V\right\}$$

The root of the first-order term $S = -a_0/a_1$ is associated with the perturbation in velocity. This root can be simplified by using the equilibrium equation [1]. By this method the root was found to be

$$\frac{a_0}{a_1} \cong + \frac{C_D}{C_L} \frac{2V}{R}$$

This same result can be obtained by introducing the equilibrium equation [1] into Equation [2a] and then perturbing the velocity.

The quadratic term is associated primarily with divergence in altitude and in flight path angle. The damping term of

this factor is negligibly small, so that the characteristic roots of this unstable mode can be written as

$$\omega = \pm \left(\frac{\rho}{2} V^2 \frac{C_L A \beta}{m} \right)^{1/2} \quad [8]$$

This can be further simplified by using Equation [1] to eliminate $(\rho V^2/2)(C_L A/m)$

$$\omega = \pm [g(V^2/V_S^2 - 1)\beta]^{1/2} \quad [9]$$

The result can be obtained differently by perturbing the altitude of Equation [2b], substituting in $\delta\rho = -\beta\rho\delta h$, and then introducing the equilibrium equation. The time to double amplitude can be defined from the positive root of Equation [9]

$$T_2 = \frac{\ln 2}{[g(V^2/V_S^2 - 1)\beta]^{1/2}} \quad [10]$$

Equation [10] is plotted in Fig. 2. The divergence rates shown are slow, ranging from 20 to 70 sec in time to double amplitude. It is particularly interesting to note that this time to double amplitude is independent of all vehicle parameters (W/AC_L and L/D) and dependent only on velocity and on β.

Analog computer studies on the basic equations (Eqs. [2]) show a close agreement with Equation [10]. It was noted that divergence of a unit displacement from equilibrium was about twice the time to double amplitude indicated by Equation [10]. Equation [10] shows the divergence characteristic of the positive real root, whereas a unit initial condition will include the negative real root and be approximately $\frac{1}{2} e^{+\omega t} + \frac{1}{2} e^{-\omega t} + \epsilon_1 e^{-(a_0/a_1)t}$ where ϵ_1 is negligibly small. This expression will take about twice the time shown in Equation [10] to reach double amplitude. Also, the formulation of Equation [10] will not hold for very low lift to drag ratios, $L/D < 0.2$. At these low L/D's the vehicle passes through the superorbital velocity region so fast that a divergence to double amplitude cannot be observed.

It should also be noted that Equation [10] shows fair agreement in predicting the characteristic frequency for path perturbations at less than satellite speed.

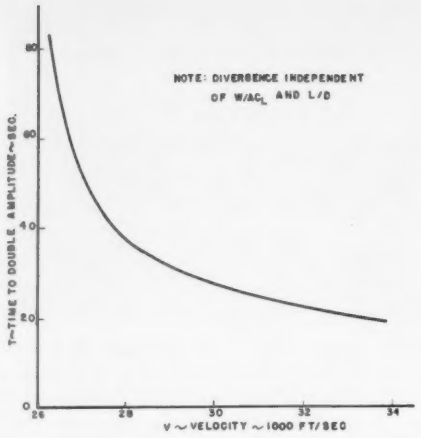

Fig. 2 Time to double amplitude

Nomenclature

A = reference area
C_D = drag coefficient $\equiv D/qA$
C_L = lift coefficients $\equiv L/qA$
D = aerodynamic drag
g = local acceleration of gravity
h = altitude
L = aerodynamic lift
m = vehicle mass
q = dynamic pressure $\equiv \frac{1}{2}\rho V^2$
S = Laplace operator
R = $R_e + h$
R_e = radius of Earth
V = velocity
V_S = circular satellite velocity $\equiv \sqrt{gR}$
β = atmospheric density decay parameter
γ = flight path angle, measured with respect to the local horizontal
ω = frequency of divergence
T_2 = time to double amplitude
ρ = density

References

1 Hildebrand, R. B., "Manned Return From Space," presented at the International Congress for Aeronautical Sciences for the International Council of the Aeronautical Sciences (ICAS), Sept. 1960.

2 Hildebrand, R. B., "Manned Re-Entry at Supersatellite Speeds," IAS preprint no. 60-83, June 1960.

Multistage Rocket Optimization

ROBERT V. RAGSAC[1] and PAUL L. PATTERSON[2]

Lockheed Aircraft Corp., Missiles and Space Div., Palo Alto, Calif.

THE GENERAL problem of optimizing the performance of a multistage rocket vehicle, as treated by Hall and Zambelli (1)[3] and Vertregt (2), requires that a minimum gross weight to payload ratio be found under the condition that the vehicle attains a prescribed burnout velocity. Using the technique of Lagrange multipliers, the proper choice of the mass ratios may be found by solving a transcendental equation for the multiplier λ. This method holds for any number of stages, each with different exhaust velocity and structural factors, and under the simplifying assumptions of constant thrust direction (no turning), no drag or gravity losses and constant specific impulse throughout any stage.

The results of (1 and 2) have been widely applied to preliminary designs of various types of rocket vehicles and have proved to be quite useful. After applying this method to several vehicle designs, two observations become apparent which when analyzed yield further information as to how one may facilitate the optimization procedure. First, it becomes evident that only after several calculations of Equation [1] for each set of exhaust velocities C_i, structural factors β_i and number of stages J, is it possible to establish the proper range of values for λ

$$V = \sum_{j=1}^{J} C_j \ln \left(\frac{1 + \lambda C_j}{\lambda C_j \beta_j} \right) \quad [1]$$

What would be helpful, therefore, is a restriction on λ, so that an initial choice will minimize the iterations necessary to obtain the correct value. Second, it is not clear that there is

Received Sept. 14, 1960.

[1] Senior Scientist, Advanced Systems Research. Member ARS.

[2] Advanced Study Scientist, Advanced Systems Research.

[3] Numbers in parentheses indicate References at end of paper.

one and only one solution to Equation [1] which results in mass ratios that yield an absolute minimum for the gross weight to payload ratio. In fact, examination of Equation [1] shows that there are multiple roots to this equation.

It is the purpose of this paper to show that from physical considerations of the vehicle parameters an upper bound can be placed on λ which greatly facilitates the iteration procedure. As a consequence of this result, upper and lower bounds are established on the total burnout velocity obtainable with a given set of C_j, β_j and J. Use of this restriction on total burnout velocity in conjunction with the gross weight to payload ratio equation involving only the Lagrange multiplier, exhaust velocities and structural factors will be shown to be an expedient method of determining design optima.

The following discussion uses the nomenclature and simplifying assumptions of (1) with the obvious physical restrictions on exhaust velocity, mass ratio and structural factor. The stages are indicated by the index j, and the total number of stages considered is J. For convenience the nomenclature of (1) is repeated here:

V = burnout velocity of last stage
C_j = effective exhaust velocity of jth stage
P = payload weight
W_{pj} = propellant weight burned in jth stage
W_{0j} = gross weight of vehicle at ignition of jth stage
W_{sj} = weight of material staged off following burnout of jth stage
μ_j = mass ratio of jth stage, $W_{0j}/(W_{0j} - W_{pj})$
β_j = disposable structure factor, fraction of jth step which is not burnable propellant, $W_{sj}/(W_{sj} + W_{pj})$

Physical limitations: $C_j > 0$, $\mu_j > 1$, $0 < \beta_j < 1$ and $\mu_j \beta_j < 1$.

Analysis of Bounds and Minimality

As given in (1 and 2), the minimum of

$$\ln\left(\frac{W_{01}}{P}\right) = \sum_{j=1}^{J} \ln\left[\mu_j\left(\frac{1-\beta_j}{1-\mu_j\beta_j}\right)\right] \qquad [2]$$

can be found by solving Equation [1] for λ and finding the necessary mass ratios from

$$\mu_j = (1 + \lambda C_j)/\lambda C_j \beta_j \qquad [3]$$

Using the fact that the product $\mu_j\beta_j$ is less than one, together with Equation [3], we find that λ must be negative. With this result and knowing the mass ratio must be greater than one, we see from Equation [3] that λ must be less than $-1/C_j(1-\beta_j)$ for every j. If this is true for any j, it must in particular be true for that stage which gives the smallest value for this upper bound. Hence, the upper bound may be stated as

$$\lambda < -1/\min\,[C_j(1-\beta_j)] \qquad [4]$$

where the minimum of the bracketed quantity over all the j's is indicated.

Examination of Equation [1] indicates that it is continuous for all values of λ as given by Equation [4]. In addition, the derivative of Equation [1] in respect to λ is always negative, as given in Equation [5]

$$\frac{dV}{d\lambda} = \sum_{j=1}^{J} -\frac{1}{\lambda^2\mu_j\beta_j} \qquad [5]$$

These two observations lead to the following conclusions. First, the velocity V must lie between the limiting velocity as λ approaches minus infinity and the velocity given by the upper bound, Equation [4]; and second, there is one and only one value of λ corresponding to every velocity within this range. Evaluating these two limits by Equation [1] yields the range of possible values for the total velocity

$$\sum_{j=1}^{J} C_j \ln\frac{1}{\beta_j} > V > \sum_{j=1}^{J} C_j \ln\left\{\frac{1}{\beta_j}\left[1 - \frac{\min\,[C_j(1-\beta_j)]}{C_j}\right]\right\} \qquad [6]$$

Equation [6], therefore, is a necessary and sufficient condition on the velocity for a solution of Equation [1] to exist and to be unique.

To show that the solution to Equation [1] gives a minimum to Equation [2] we investigate the derivatives of Equation [2] with respect to the mass ratios. Taking the second derivative with respect to the same mass ratio μ_j we find that

$$\frac{\partial^2[\ln(W_{01}/P)]}{\partial\mu_j^2} = (\lambda C_j)^2\frac{\beta_j}{\mu_j} \qquad [7]$$

Furthermore, we find that the second derivative with respect to any other mass ratio, say μ_k, is always zero, i.e.

$$\frac{\partial^2[\ln(W_{01}/P)]}{\partial\mu_j\,\partial\mu_k} = 0 \qquad (j \neq k) \qquad [8]$$

It can be shown that these conditions satisfy the criteria for a relative minimum (3). Since there is only one value of λ, it yields an absolute minimum to Equation [2].

Discussion of Results

Using the added information presented here in conjunction with the optimizing method of either (1) or (2), the number of iterations required to find the correct λ in Equation [1] is reduced. For a given set of C_j's and β_j's one need find the minimum bracketed quantity of Equation [4], and use a value very close to this as a first guess for the interpolation. This choice is justified by inspecting the sensitivity of the velocity to changes in λ, Equation [5]. For values of λ close to its upper limit, it can be seen that the derivative is quite large, and hence, slight changes in λ will cause large changes in the computed velocity. Note that if this upper bound was used as a trial, the resulting velocity is simply that given on the right-hand side of the inequality in Equation [6].

It is instructive to note what happens as the Lagrange multiplier approaches its lower limit of minus infinity. By referring to Equation [3], we find that in this case the mass ratio equals the reciprocal of the structural factor. Using this result in Equation [2] shows that either the payload is zero or the gross weight of the vehicle is infinitely large.

An important point must be considered when attempting to optimize a given vehicle to meet a velocity requirement. Although experienced designers may be aware of it intuitively, it is not immediately obvious that a given velocity requirement can be met with a certain combination of exhaust velocities, structural factors and number of stages. It is just this information that may be obtained from Equation [6]. By evaluating each bound of V for a given set of parameters, one can note whether the required velocity is attainable (i.e., falls within the limits) and, if it is, whether a reduction in the number of stages or a change in any of the other parameters will also satisfy the desired performance.

Although a certain design may fall within the limits stated, the gross weight to payload ratio will probably be the deciding criteria. If we substitute out the mass ratio in Equation [2] by use of Equation [3] and rewrite the summations as products to eliminate the natural log, then

$$\frac{W_{01}}{P} = \prod_{j=1}^{J}\left[\left(1-\frac{1}{\beta_j}\right)(1+\lambda C_j)\right] \qquad [9]$$

This relationship offers a ready calculation for W_{01}/P, allowing the designer to discontinue calculating a certain case if it appears that the gross weight to payload ratio is becoming prohibitively large.

References

1 Hall H. H. and Zambelli E. D. "On the Optimization of Multistage Rockets" JET PROPULSION vol. 28 no. 7 July 1958 pp. 463–465.

2 Vertregt M. "A Method for Calculating the Mass Ratios of Step Rockets" *J. British Interplan. Soc.* vol. 15 March–April 1956 pp. 95–97.

3 Taylor A. E. "Advanced Calculus" Ginn and Co. N. Y. 1955 p. 232.

Effect of Scale Size on a Rocket Engine With Suddenly Frozen Nozzle Flow[1]

RONALD WATSON[2]

California Institute of Technology, Pasadena, Calif.

Recent analytical work by Bray indicates that single element, chemically reacting systems, e.g., $H_2 \rightleftharpoons 2H$, may suddenly freeze their composition at some point in a high speed nozzle and then remain at fixed composition throughout the remainder of the expansion. This sudden freezing or "quenching" phenomenon was also apparent in some theoretical calculations reported by Hall et al. and has been verified experimentally by Wegener. It is the purpose of this note to show qualitatively how Bray's sudden-freezing criterion is related to engine size by the scale factor for geometrically similar engines having nonequilibrium nozzle flows and in which a propellant system is used for which Bray's analysis is valid.

Theory

USING Lighthill's model for an "ideal" dissociating diatomic gas (1),[3] Bray (2) calculated properties of initially dissociated oxygen and nitrogen systems during expansion through a hypersonic nozzle. His results showed that the flow was near equilibrium in the upstream region of the nozzle but that a relatively sudden[4] freezing of composition occurred downstream of the throat. He attributed the sudden freezing to the effective vanishing of atom recombination because of the low densities; i.e., he assumed, the recombination rate depends on density cubed (since it is a three-body collision process) and thus is very low at low gas densities.

Since in near-equilibrium flow, the rates of both recombination and dissociation are of comparable magnitudes, and since in near-frozen flow the dissociation rate is negligibly small, Bray reasoned that the quench point must be in the neighborhood where the dissociation rate is comparable to the time rate of change of the mass fraction of the atomic species during an equilibrium expansion. That is

$$\left|\frac{d\alpha}{dt}\right| \ll r_D \text{ (for near-equilibrium)}$$

$$\left|\frac{d\alpha}{dt}\right| \gg r_D \text{ (for near-frozen)}$$

Therefore

$$\left|\frac{d\alpha}{dt}\right|_Q \cong r_D \text{ (for the quench point)} \qquad [1]$$

where

α = mass fraction of the atomic species
r_D = dissociation reaction rate
Q = subscript signifying sudden freezing point

Subsequent calculations by Bray showed that Equation [1] was indeed a satisfactory criterion for the quench point. Calculations by Hall et al. (3) and experiments by Wegener (4) confirm the essentials of Bray's conclusions.

Following Penner [see (5), chaps. 17 and 18], the quench point criterion may be rewritten in a form which is more easily related to the size of the engine, namely

$$\left|\frac{d\alpha}{dx}\right|_Q = \frac{k_R P K_P (1-\alpha)}{2u\,R^2\,T^2} \qquad [2]$$

where

x = distance along the nozzle
k_R = specific recombination rate constant
P = static pressure
K_P = pressure equilibrium constant
u = gas velocity
R = universal gas constant
T = static temperature

Application to Geometrically Similar Engines

The shape of the downstream section of the nozzles of a set of geometrically similar rocket engines may be characterized by the formula

$$A_i = A_0^*(C_i^2 + bx_i^2) \qquad [3]$$

where

A_i = nozzle area of the ith engine at any distance from the throat
A_0^* = throat area of the reference engine which is constant for a set of similar engines
C_i = scale size factor for the ith engine (see Eq. [4])
b = shape factor, which is constant for a set of similar engines
x_i = distance from the throat in the ith engine

At large distances from the throat, the nozzle geometry of Equation [3] corresponds to a cone of half-angle $\sqrt{bA_0^*/\pi}$. The distance from the throat is then

$$x_i = C_i\sqrt{(1/b)(A_i/A_i^* - 1)} \qquad [4]$$

where A_i^* = throat area of the ith engine.

Thus, for a common nozzle area ratio, a characteristic length in any two of these similar engines is related by the ratio of their scale factors, C_i/C_j.

For a given set of chamber conditions, the performance of a quenched flow engine would depend only upon the area ratio at which the flow is frozen, since this fixes the exhaust conditions. Since the distances from the throat to a given quench point area ratio for geometrically similar engines are related through the scale factors C_i, C_j, etc., and since the gas conditions at these quench points are all the same (same area ratio and equilibrium flow up to the quench point), then the slopes of the equilibrium mass fractions at these quench points are all related through Equation [4] by

$$C_1\frac{d\alpha}{dx_1} = C_2\frac{d\alpha}{dx_2} = \ldots$$

Received Sept. 29, 1960.

[1] This work was carried out in part under Air Force Contract AF 04(647)-309 at Space Technology Laboratories, Inc., Los Angeles, Calif.

[2] NSF Fellow, Daniel and Florence Guggenheim Jet Propulsion Center.

[3] Numbers in parentheses indicate References at end of paper.

[4] The "suddenness" of the freezing depends on both the reaction rate constants and geometry. In a personal communication Bray pointed out that for nozzles with very small expansion angles, the freezing stretches out over quite some length and is far from sudden.

or

$$C_i \frac{d\alpha}{dx_i} = \text{constant (for same area ratio quench point)} \quad [5]$$

Then from Equation [2], for these engines to have the same exhaust conditions would require that

$$C_1 k_{R_1} = C_2 k_{R_2} = \ldots$$

or

$$k_{R_i} = (C_j/C_i)k_{R_j} \quad [6]$$

Equation [6] shows that a smaller specific recombination rate constant is required to quench the flow in a large engine at the same area ratio as in a small engine. Conversely, for the same rate constant, Equations [2 and 4] indicate that the quench point would be delayed to a lower $|d\alpha/dx|_Q$ (with resulting higher specific impulse values) in a large engine by very roughly the scale factor C_i, although no "clean" analytical expression shows this.

Bray's quenching criterion thus reinforces the intuitive feeling that recombination should proceed further in a large engine because of the longer gas residence time in the nozzle (which coincidentally increases linearly with the scale factor C_i for engines with the flow completely in equilibrium or completely frozen throughout).

Thus from the point of view of chemical kinetics only, it appears that for a given total thrust, there would be an improvement in specific impulse obtained by using one large engine rather than by "stacking" several small ones, if sudden freezing occurred somewhere in the nozzle.

References

1 Lighthill, M. J., "Dynamics of a Dissociating Gas." *J. Fluid Mech.*, Jan. 1957, vol. 2, pp. 1–32.

2 Bray, K. N. C., "Atomic Recombination in a Hypersonic Wind-Tunnel Nozzle," *J. Fluid Mech.*, July 1959, vol. 6, pp. 1–32.

3 Hall, J. G., Eschenroeder, A. Q. and Klein, J. J., "Chemical Nonequilibrium Effects on Hydrogen Rocket Impulse at Low Pressures," ARS JOURNAL, Feb. 1960, vol. 30, no. 2, pp. 188–190.

4 Wegener, P. P., "Experiments on the Departure from Chemical Equilibrium in a Supersonic Nozzle," ARS JOURNAL, April 1960, vol. 30, no. 4, pp. 322–329.

5 Penner, S. S., "Chemistry Problems in Jet Propulsion," Pergamon Press, N. Y., 1957, chaps. 17, 18.

Book Notes

A Compendium of Spherical Astronomy, with Its Applications to the Determination and Reduction of Positions of the Fixed Stars, Newcomb, Simon, Dover Publications, Inc., New York, 1960, 444 pp. Paperback reprint, $2.25.

Chapters: 1. Introductory; 2. Differences, Interpolation and Development; 3. The Method of Least Squares; 4. Spherical Coordinates; 5. The Measure of Time and Related Problems; 6. Parallax and Related Subjects; 7. Aberration; 8. Astronomical Refraction; 9. Precession and Nutation; 10. Reduction of Mean Places of the Fixed Stars; 11. Reduction to Apparent Place; 12. Method of Determining the Positions of Stars by Meridian Observations; 13. Methods of Deriving the Positions and Proper Motions of the Stars from Published Results of Observations.

This book, first published in 1906, is a standard work in its field. It has the double purpose of developing the elements of practical and theoretical astronomy for the student of astronomy, and of serving as a handbook of convenient reference for the use of the working astronomer in applying methods and formulas.

The books listed here are those recently received by the ARS from various publishers who wish to announce their current offerings in the field of astronautics. The order of listing does not necessarily indicate the editors' opinion of their relative importance or competence.

Principles of Feedback Control, Wilts, C. H. (Professor of Electrical Engineering, California Institute of Technology), Addison-Wesley Publishing Company, Inc., Reading, Mass., 1960, 271 pp. $8.75.

Chapters: 1. Introduction; 2. Selected Topics in Linear Differential Equation Theory; 3. The Response and Error Functions of Feedback Systems; 4. Stability of Feedback Systems; 5. Root-Locus Diagrams; 6. The Nyquist Criterion; 7. Elementary Compensation Techniques; 8. Multiple-Loop Control Systems; 9. Some General Stability Considerations; 10. The Response of a Closed-Loop System; 11. Sampled-Data Control Systems; 12. Nonlinear Analysis Using the Describing Function. *Appendixes*: The Second-Order Contactor Feedback System; The Convolution Integral of the Sampling Theorem.

The author claims to present a carefully balanced choice of methods and viewpoints, with the frequency-response and the root-locus points of view employed in alternate solutions. It is intended for use as a textbook for seniors, graduate students and practicing engineers who wish to study the principles of feedback control; it assumes a good background in ordinary differential equations and complex variable theory.

Linear Circuits, Scott, R. E. (Professor of Electrical Engineering, Northeastern University), Addison-Wesley Publishing Company, Inc., Reading, Mass., 1960. In two volumes:

Part 1 – Time-Domain Analysis, 510 pp. $6.75.

Chapters: 1. Introduction; 2. The 2*b* Equations of Electrical Networks; 3. Mesh Currents and Node Voltages; 4. Methods of Characterizing One-Terminal-Pair Resistive Networks; 5. Methods of Characterizing Two-Terminal-Pair Resistive Networks; 6. Power and Energy in Resistive Circuits; 7. An Introduction to Energy Storage in Electric Circuits; 8. Differentiation, Integration and Singularity Functions; 9. The Differential Equations of Electric Circuits; 10. The Time Response Functions of Single Elements; 11. The Time Response Functions of *R–L* and *R–C* Circuits; 12. The Time Response Functions of *L–C* and *R–L–C* Networks; 13. Time-Domain Solutions for Arbitrary Exciting Functions; 14. Power and Energy in Circuits with Energy-Storage Elements. *Appendix:* Transients in More Complex Circuits.

Part 2 – Frequency-Domain Analysis, pp. 511–928. $6.75.

Chapters: 15. Introduction to Sine Waves and the Frequency Domain; 16. Frequency-Domain Networks; 17. Mutual Inductance, Unity-Coupled Coils, and Transformers; 18. Magnitude and Phase Response Curves; 19. Power and Energy in Alternating-Current Circuits; 20. Signal Analysis in the Frequency Domain; 21. Network Response to Complex Waves of Excitation; 22. Problems Solved

by Laplace Transforms; 23. Power and Energy Relationships in Networks Excited by Arbitrary Functions.

The complete book, in two volumes, is designed to achieve a maximum of depth in the circuit-theory area in the minimum possible time. To this end, circuits are presented as linear models and the circuit theory as a branch of applied mathematics. The book is intended as a first course for electrical engineering students.

Introduction to the Statistical Dynamics of Automatic Control Systems, Solodovnikov, V. V. (translation edited by Thomas, John B. and Zadeh, Lotfi A.), Dover Publications, Inc., New York, 1960, 307 pp. Paperback, $2.25.

Chapters: 1. Frequency Characteristics, Transfer Functions and Impulsive Responses of Dynamic Systems; 2. Some Auxiliary Data from the Theory of Probability; 3. Stationary Random Processes; 4. Dynamic System Analysis for Random Inputs; 5. Methods of Approximation of Spectral Density Functions by Meromorphic Functions; 6. Determination of the Minimum Mean-Squared Error and the Formula for the Optimum Transfer Function; 7. Optimum Statistical Prediction, Smoothing and Differentiation; 8. Calculation of the Optimum Transfer Function for a Finite Time of Observation and for a Useful Signal Containing a Component in the Form of a Prescribed Function of Time.

First published in the Soviet Union in 1952, this book constitutes one of the first comprehensive treatments of the subject and is of value as a self-contained exposition of the principles of the analysis of linear systems, the statistics of random signals, and the theory of linear prediction and filtering. The editors have attempted to correct the many instances of improper terminology that appeared in the original translation.

An Engineering Approach to Gyroscopic Instruments, Siff, Elliott J. (Head of Advanced Research, Kearfott Div., General Precision, Inc.), and Emmerich, Claude L. (Head of Stabilization and Navigation Branch, Norden Div., United Aircraft Corporation), Robert Speller & Sons, Publishers, Inc., New York, 1960, 120 pp. $7.50.

Chapters: 1. Basic Gyroscopics; 2. Basic Gyro Configurations; 3. Special Gyro Designs; 4. Some Instrument Gyroscope Applications.

This book is intended to fill the gap, for the average engineer, between the most elementary explanations of gyroscopic effects and the complicated purely mathematical derivations associated with gyroscopic motion. A forward by Professor C. S. Draper of MIT introduces this book.

Modern Flight Dynamics, Kolk, W. Richard, (Systems Engineer, United Aircraft Corporation), Prentice-Hall, Inc., Englewood Cliffs, New Jersey, 1961, 288 pp. Trade edition, $10. Text edition for classroom use, $7.50.

Chapters: 1. Mechanics and Equations of Motion; 2. Direction Cosines and Eulerian Angles; 3. Aerodynamic Forces and Moments; 4. Modes of Motion; 5. Longitudinal Motion; 6. Lateral Motion; 7. Roll Coupling; 8. Flying Qualities; 9. Reversible Control System; 10. Irreversible Control System; 11. Aero-Structure-Control Interactions; 12. Rockets: As they Tumble and Spin; 13. Celestial Mechanics. *Appendixes:* Vector Differentiation; Lin's Method of Factoring; Longitudinal Response to Step Elevator; Neutral Points and Maneuver Points; Routh Stability Criterion.

This book originated from a series of lectures on dynamics given in the Education Department of The Martin Company, and from a subsequent course given United States Naval Test Pilot School, Patuxent River, Maryland. The volume emphasizes the analytic foundations of dynamic motion and indicates the assumptions and approximations necessary to any analytic solution.

Small Particle Statistics, Herdan, G. (Lecturer in Statistics, University of Bristol), Academic Press, Inc., New York, Second Revised Edition, 1960, 418 pp. $14.50.

Chapters: 1. Particles in the Sieve and Sub-Sieve Size Range; 2. Some Fundamental Concepts of Statistics; 3. The Units of Particle Statistics and the Principles of Particle Size Measurement; 4. The Distributions of Particle Size and Their Averages; 5. Sampling Procedures for Particle Size Determinations; 6. Some Standard Forms of the Distribution Function; 7. Graphical Representation; 8. Statistical Testing Analysis of Differences between Determination Results; 9. Methods for Ascertaining the Relations between Variable Characteristics of Materials; 10. Testing the Dependence of Properties of Materials upon Particle Size by Correlation Methods; 11. Fundamental Relations between Particle Size and Other Characteristics of Materials as Particulate Matter; 12. Physical and Chemical Properties of Materials in Their Dependence upon Characteristics of These Materials as Particulate Universes; 13. Attainment of a Specified Fineness; 14. Attainment of Homogeneity in Coarse Disperse Systems (Industrial Mixing); 15. The Inhomogeneity of Polymers; 16. Principles of Statistical Theory of Coarse Disperse Systems; 17. Statistical Design of Investigations of Particulate Materials; 18. Microscope Method of Determining Size Distribution; 19. Automatic Counting and Sizing of Particles; 20. Sedimentation Methods of Determining Particle Size Distribution; 21. Centrifugal Sedimentation; 22. Radiometric Techniques; 23. Size Distribution of Dispersions in Gases; 24. Permeability Method for the Determination of Surface Area; 25. Photo-Extinction Method of Determining Surface Area; 26. Adsorption Methods of Determining Surface Area.

This book, by means of statistical mathematics, bridges the gap between the type of information desired about systems of small particles and the available experimental methods of measurement. It should prove of use to those working with solid propellant oxidizers, catalysts, solid deposits, sprays, smokes, emulsions and dispersions, in their search for adequate means of quantitative measurement.

Photoelasticity: Principles and Methods, Jessop, H. T. (Senior Lecturer, Department of Civil and Municipal Engineering, University College, London) and Harris, F. C. (Lecturer, Department of Mathematics, University College, London), Dover Publications, Inc., New York, 1960, (first published by Cleaver-Hume Press, Ltd., London, 1949), 182 pp. Unabridged paperback reprint, $2.

Chapters: 1. Stresses; 2. Strain and Stress-Strain Relations; 3. Optics; 4. Polarization and Double Refraction; 5. Theory of Photoelasticity; 6. Reduction and Interpretation of Observations; 7. Stresses in Three Dimensions; 8. The Photoelastic Bench; 9. Materials and Procedure; 10. Examples. *Appendixes:* The Stress-Quadric; Use of Laplace's Equation in Two-Dimensional Stress Problems; The Use of Quarter-Wave Plates; The Effect of Errors in Quarter-Wave Plates in Stress Optical Observations; Use of Quarter-Wave Plate as Compensator; A Composite Quarter-Wave Plate.

This volume is an introduction to general and recent developments in two- and three-dimensional stress analysis techniques, written for the engineer or designer who wishes a primarily physical and practical survey of photoelasticity. College undergraduate mathematics should suffice to follow the authors' derivations and examples. For mathematically expert readers, however, more advanced mathematical treatment is given in appendixes.

Weight-Strength Analysis of Aircraft Structures, Shanley, F. R. (Professor of Engineering, University of California), Dover Publications, Inc., New York, 1960, 396 pp. Paperback edition, $2.45.

Contents: Part I. Principles of Optimum Structural Design; Part II. Structural-Weight Equations; Part III. Material Properties and Behavior.

This book focuses on the principles of design for minimum weight of aircraft, missile and space structures. This new edition is a reprint of the first edition published by the McGraw-Hill Book Company in 1952, to which has been added a new preface, and bibliographies on optimum design of structures and creep buckling.

AGARD Aeronautical Multilingual Dictionary, edited by Frenot, G. H. and Holloway, A. H., Pergamon Press, New York, 1960, 146 pp. $20.

This volume constitutes a glossary of aeronautical and astronautical terms and definitions, in eight different languages, namely, Dutch, French, German, Italian, Spanish, Turkish, Russian and English. The Documentation Committee of the NATO Advisory Group for Aeronautical Research and Development (AGARD) intends to keep the dictionary up to date and intends to issue revisions as they become necessary.

New Patents

George F. McLaughlin, *Associate Editor*

Meteor particle impact sensing apparatus (2,944,250). J. R. Outt, Malvern, Pa., assignor to General Electric Co. (ARS corporate member).

Solar batteries on the surface of a high velocity missile exposed to the impact of particles and coupled to transmitting channels. Output is proportional to the integrated eroding effect of very small velocity particles.

Jet propelled aircraft (2,944,764). R. J. Lane and R. F. Sargent, Bristol, England, assignors to Bristol Siddeley Engines, Ltd.

Two elongated bodies interconnected by a double powerplant body with wings facing away from the powerplants.

Thermal stability additive in hydrocarbon fuels (2,945,342). R. M. Schirmer, Bartlesville, Okla., assignor to Phillips Petroleum Co.

Fuel containing as an additive from 1 to 1000 parts per million of the hydrocarbon soluble extract from an oily carbon black which, before extraction, had a photelometer reading less than 50.

Charge (2,945,343). C. A. Gongwer (ARS member), Glendora, Calif., assignor to Aerojet-General Corp. (ARS corporate member).

Propulsion device. Body of solid metallic lithium with an exposed reacting face within a housing. Water is applied from a ram water duct to the reacting face.

Gas generator adapted for on-off operation (2,945,344). W. M. Hutchinson, Barlesville, Okla. assignor to Phillips Petroleum Co.

Rocket motor with solid propellant grain between a holder and spring bias. A cutter severs the grain to stop burning at a predetermined distance from the holder.

Reverse thrust brake (2,945,346). H. E. Arnzen, Amityville, N. Y., assignor to Republic Aviation Corp. (ARS corporate member).

Movable doors in the exhaust pipe are opened for unrestricted passage of gases, and closed to divert the gases to effect reverse operation through curved vanes at the sides of the exhaust.

Accelerometer (2,945,379). F. R. Barnes and L. R. Greenaway, Seattle., Wash., assignors to Boeing Airplane Co. (ARS corporate member).

Lineal displacement transducer. Two pairs of flat magneto-resistive grids are in co-planar alignment with the two grids of each pair in superimposed registry.

Inertial guidance device (2,945,380). H. W. Pope, P. F. Hayner and R. B. Henderson, Nashua, N. H., assignors to Sanders Associates, Inc.

A member having a natural resonant frequency requiring damping; its motion with respect to an axis provides an indication of movement of the device with respect to a set of reference coordinates.

Rocket launcher (2,945,420). H. W. Babcock, Pasadena, Calif., assignor to the U. S. Navy.

Reaction turbine rotatably mounted on the launcher, and operable by the blast of the rocket. A coupling initially transmits rotation to the rocket.

Spin rocket and rotating screw-type launching apparatus (2,945,421). N. W Pion, Covina, Calif., assignor to North American Aviation, Inc. (ARS corporate member).

Screw threaded into the after end of a rocket. A torque member threaded upon the screw is adapted to cause the rocket to spin.

Explosive separation device (2,945,442). B. R. Adelman (ARS member) and J. D. Burke, Altadena, Calif., assignor to the U. S. Army.

Piston urged forwardly upon ignition of an explosive powder train by burning of a propellant liner to separate and propel an inert missile from a mount.

Aircraft with wings containing lifting jets (2,945,641). E. Pribram, Hays, England, assignor to Fairey Aviation, Ltd.

Horizontal thrust generator to propel the aircraft forward. A vertical thrust generator in the wing. Elongated ducts extending spanwise of the wing are supplied with high velocity gaseous fluid.

Static lift wing plane (2,945,642). P. Nofi, Farmingdale, N. Y.

Ring-shaped static wing having an airfoil section on its upper profile. Air is forced down through a central opening. A pair of hinged wings is mounted on the static wing.

Control System (2,945,643). J. M. Slater, Fullerton, Calif., assignor to North American Aviation, Inc. (ARS corporate member).

Rate gyroscopes, each having an operable angular velocity over a range from the magnitude of missile angular velocities to Earth angular velocity.

Ignition system for rocket motors (2,949,006). K. C. Halliday Jr., Port Washington, N. Y., assignor to the U. S. Army.

Method of using a nonfluid organic hypergole having a viscosity of greater than 250 centistokes at 70 deg F for igniting nonhypergolic hydrocarbon fuels.

Rocket engine feed system (2,949,007). D. E. Aldrich and A. P. Bignon, Reseda, Calif., assignors to North American Aviation, Inc. (ARS corporate member).

Normally closed valve opens upon attainment of a predetermined monopropellant pressure. Liquid propellant valve opens upon attaining a predetermined pressure in the thrust chamber.

Variable thrust solid propellant rocket motor (2,949,009). C. L. D'Ooge, Citrus Heights, Calif., assignor to the U. S. Navy.

Pressurizing section containing a multiperforated gas generator grain; extremely rapid pressure is developed when squib firing voltage is applied.

Low drift gyro-stabilized platform (2,949,785). H. E. Singleton (ARS member) and H. F. Erdley, Los Angeles, Calif., assignors to Litton Industries, Inc. (ARS corporate member).

For inertial guidance systems. Purely inertial means for operating free of any external reference, to stabilize an element rotatably connected to a reference frame.

Tracking device (2,950,395). J. B. O' Maley and J. W. Barnes, Floral Park, N. Y., assignors to Kollsman Instrument Corp.

Continuously tracks a target the sighting of which is periodically interrupted. A. C. signals yield correctional data to azimuth and elevation orienting motors.

Missile guiding system (2,950,474). R. M. Page, Camp Springs, Md.

Energy is supplied to a highly directive transducer system for radiation centered about the axis of directivity.

System for synchronization and range measurement with radar guided missiles (2,950,477). F. C. Alpers, Riverside, Calif., assignor to the U. S. Navy.

Launching aircraft having a highly directive radar transmitter and receiver. Missile having a semidirective radar transmitter and receiver mounted in the tail.

Method of guiding missiles (2,950,880). B. Chance and D. T. Griggs, Chevy Chase, Md., assignors to the U. S. Navy.

Pulses of electromagnetic energy transmitted to a target. Means on a missile for receiving reflections of the pulses and for amplitude modulating received signals in accordance with the direction of their reception.

Balloon and gondola (2,950,881). R. L. Schwoebel, Minneapolis, Minn., assignor to General Mills, Inc.

Supporting surface mounted on a keel, and enclosing a passenger in a gas-tight shell. An attaching means runs through the shell for attachment to a lifting cell.

Balloon gondola (2,950,882). P. E. Yost, Hugo, Minn., assignor to General Mills, Inc.

The top of a flexible bag is attached to a lifting cell. The weight of a passenger support inside the bag is carried by the walls of the bag.

Stable propellants (2,951,335). L. A. Stengel, Terre Haute, Ind., assignor to Commercial Solvents Corp.

Fluid mixture consisting of monomethylamine unsymmetrical dimethylhydrazine and hydrazine.

Chamber wall casting process (2,951,336). H. E. Mueller (ARS member), Lockport, N. Y., assignor to the U. S. Air Force.

Wall structure for a rocket motor consisting of stainless steel tubes in side by side relation, flattened adjacent the restricted nozzle section.

Missile (2,952,207). M. M. Kamimoto, China Lake, Calif., assignor to the U. S. Navy.

Directional flight control and roll control. Flexible gas pressure chambers operate four fins for controlling the direction of flight.

Detonation circuit (2,952,208). B. J. Wagoner, Riverside, Calif., assignor to the U. S. Navy.

Multiple sensitivity fuze for a missile having an air to water trajectory. Switches actuate sequentially in response to acceleration forces.

EDITOR'S NOTE: Patents listed above were selected from the Official Gazette of the U. S. Patent Office. Printed copies of patents may be obtained from the Commissioner of Patents, Washington 25, D. C., at a cost of 25 cents each; design patents, 10 cents.

Technical Literature Digest

M. H. Smith, *Associate Editor*
The James Forrestal Research Center, Princeton University

Propulsion and Power (Combustion Systems)

Temperature Survey Using Fast-response Thermocouples (J34-WE-48 engine), *Westinghouse Electric Co., Rep. A2677Z,* May 18, 1960, 43 pp.

Mechanical Design and Operation of Turbine Rotors for the Air-Turborocket Engine, by T. L. Tyson, *Experiment Inc., TM-1127,* Aug. 22, 1959, 34 pp.

The E-D Nozzle, by G. V. R. Rao, ASTRONAUTICS, vol. 5, Sept. 1960, p. 28.

Plug-Nozzle Flexibility, by Kurt Berman and Bruce Neuffer, ASTRONAUTICS, vol. 5, Sept. 1960, p. 30.

A Study of the Propellant Specific Impulse-Density Trade-offs of Solid Propellant Rocket Motors, by E. R. Flemig and J. R. Carnes, *Air Force Flight Test Center, Engng. Div., Edwards AFB, Calif., AFFTC-TN-60-29,* July 1960, 49 pp.

Hypersonic Flow, edited by A. R. Collar and J. Tinkler, *Proceedings of the 11th Symposium of the Colston Research Society,* Univ. of Bristol, April 6–8 1959, Academic Press, Inc., N. Y., 1960, 432 pp.

Hypersonic Air Breathing Engines, by R. R. Jamison, pp. 391–408, discussion pp. 409–428.

Auxiliary Systems, by C. K. Trotman, *Aircraft Engng.,* vol. 32, Sept. 1960, pp. 246–254.

Combustion performance Characteristics of a Laboratory Subsonic Ram-jet, by Louis A. Povinelli, *Royal Aero Soc. J.,* vol. 64, Sept. 1960, p. 564.

High Altitude Testing of Propulsion Systems, by B. H. Goethert and D. Taylor, *Zeitschrift für Flugwissenschaften,* vol. 8, no. 7, July 1960, pp. 202–211.

A Preliminary Investigation on the Destruction of Solid-Propellant Rocket Motors by Impact from Small Particles, by David J. Carter Jr., *NASA Tech. Note* D-422, Sept. 1960, 25 pp.

Static Thrust of an Annular Nozzle with a Concave Central Base, by Blake W. Corson Jr. and Charles E. Mercer, *NASA Tech. Note* D-418, Sept. 1960, 18 pp.

Performance of Several Conical Convergent-Divergent Rocket-Type Exhaust Nozzles, by C. E. Campbell and J. M. Farley, *NASA Tech. Note* D-467, Sept. 1960, 31 pp.

Turbulence Studies of a Rectangular Slotted Noise-Suppressor Nozzle, by James C. Laurence, *NASA Tech. Note* D-294, Sept. 1960, 85 pp.

Flight Performance of a Spin-Stabilized 20-Inch-Diameter Solid-Propellant Spherical Rocket Motor, by Jack Levine, C. William Martz, Robert L. Swain and Andrew G. Swanson, *NASA Tech. Note* D-441, Sept. 1960, 38 pp.

The Effect of Catalyst-Bed Arrangement on Thrust Buildup and Decay Time for a 90 Per cent Hydrogen Peroxide Control Rocket, by Conrad M. Willis, *NASA Tech. Note* D-516, Sept. 1960, 25 pp.

Rocket Testing in the AEDC Propulsion Wind Tunnel, by R. W. Hensel, *AEDC Tech. Note* 60-136, July 1960, 42 pp.

Ramjet Preliminary Design a Rapid, Accurate Graphical Method, by C. C. E. Heobich, *ABMA Redstone Arsenal, Alabama, Rep. no.* RA-TR-I-60, Aug. 23, 1960, 42 pp.

Propellant Vaporization as a Design Criterion for Rocket Engine Combustion Chambers, by Richard J. Priem and Marcus F. Heldmann, *NASA Tech. Rep.* R-67, 1960, 55 pp.

Altitude Performance Investigation of a High-temperature Afterburner, by S. C Huntley, Carmon M. Auble and James W. Useller, *NACA Res. Mem.* E53D22, June 1953, 28 pp. (Declassified by authority of *NASA Tech. Pubs. Announcement* no. 33, Nov. 24, 1960.)

Experimental Investigation of Direct Control of Diffuser Pressure on 16-inch Ram-jet Engine, by William R. Dunbar, George Vasu and Herbert G. Hurrell, *NACA Res. Mem.* E55D15, June 1955, 68 pp. (Declassified by authority of *NASA Tech. Pubs. Announcement* no. 33, Nov. 24, 1960.)

The Performance of Ram-jet Combustion Systems, by S. W. Greenwood, *Royal Aeron. Soc. Journal,* vol. 64, Nov. 1960, p. 699.

Liquid Rockets, by Martin Goldsmith, ASTRONAUTICS, vol. 5, Nov. 1960, p. 38.

Solid Rockets, by G. Daniel Brewer, ASTRONAUTICS, vol. 5, Nov. 1960, p. 45.

Testing the Saturn Booster Motors, *Rivista Aeronautica,* vol. 36, no. 9, Sept. 1960, pp. 1445–1447. (In Italian.)

Propulsion and Power (Non-Combustion)

The Magnetic Induction Plasma Engine, *Space Tech. Labs., Inc.,* TN no. 60-0000-0263, by Milton U. Clauser, Aug. 19, 1960, 37 pp.

Heavy Particle Propulsion Research, by Douglas M. Jamba, *Thiokol Chem. Corp., Reaction Motors Div.,* 155–83, April 30, 1960, pp. 34.

Superfast Pinch Studies, by Lee O. Heflinger and Stanley L. Leonard, *Space Tech. Labs., Inc., Physical Res. Lab.,* TR 60-0000-09226, Aug. 1960, 60 pp.

The Neutron Producing Mechanism in Transverse Pinches, by V. Josephson, M. H. Dazeu and R. F. Wuerker, *Space Tech. Labs., Inc.,* TR no. 60-0000-19258, Aug. 9, 1960, 11 pp.

The Super-Fast Longitudinal Pinch, by Burton Fried, *Space Tech. Labs., Inc., Physical Res. Lab.,* ARL-7-60 Nov. 12, 1957, 40 pp.

Gas Dynamics Symposium, 3rd, Northwestern University, 1959, Dynamics of conducting gases, edited by Ali Bulent Cambel and John B. Fenn, Evanston, Northwestern University Press, 1960, 212 pp.

Space Propulsion Engines—A Problem in Production of High Velocity Gases, by M. L. Ghai, pp. 168–175.

The Electromagnetic Pinch Effect for Space Propulsion, by Alfred E. Kumen and William McIlroy, pp. 176–189.

The Plasma Acceleration by Guided Microwaves, by Robert V. Hess and Karlheinz, pp. 190–200.

Techniques for producing Plasma Jets, by James A. Browning, pp. 226–238, 55 refs.

Optimum Power Generation using a Plasma as the Working Fluid, by Joseph L. Neuringer, pp. 153–167.

Considerations in the Design of a Steady DC Plasma Accelerator, by George P. Wood and Arlen F. Carter, pp. 201–212.

Direct Conversion of Nuclear to Electric Energy, by Nguyen Van Dong, *France, Commissariat a l'Energie Atomique, Bulletins d'Informations,* no. 41, June 1960, pp. 14–27. (In French.)

Experiments on Electrodynamic Acceleration of Plasmas, by I. F. Kvartskhava and R. D. Meladze, *Soviet Physics, Tech. Physics,* vol. 5, Sept. 1960, pp. 266–273.

Magnetohydrodynamic Propulsion, by G. Sargent Janes, *Avco Everett Res. Lab., Res. Rep.* 90, *AFOSR Tech. Note* 60-955, Aug. 1960, 62 pp.

Performance of a T-Tube Plasma Accelerator Fired into a Vacuum, by P. Gloersen, B. Gorowitz, G. Bethke and W. Palm, *General Electric Co., Missile and Space Vehicle Dept.,* T.I.S. R60-SD454, Oct. 1960, 22 pp.

Analysis of Constant Velocity Pulsed Plasma Accelerator, by Z. J. J. Stekly, *Avco-Everett Res. Lab., Everett, Mass.,* July 1960, 19 pp.

The Use of Low Impedance Transmission Lines in Plasma Heating and Confinement Studies, by M. H. Dazey, V. Josephson and R. F. Wuerker, *Space Tech. Labs., Inc., Physical Res. Lab.,* STL/TR-60-0000-09255, Aug. 1960, 29 pp.

Dynamic Stabilization of a Plasma Column, by Erich S. Weibel, *Space Tech. Labs., Inc., Physical Res. Lab.,* STL/TR-60-0000-6R269, Aug. 1960, 55 pp.

International Astronautical Congress, 10th, London, 1959 proceedings, edited by F. Hecht, Vienna, Springer Verlag, 1960, 2 vols., pp. 1–504 and 505–946.

Some Remarks on the Optimum Operation of a Nuclear Rocket, by G. Leitmann, vol. 1, pp. 83–89.

Problems of Magnetic Propulsion Plasma, by Ralph W. Wanick, Vol. 1, pp. 131–137.

EDITOR'S NOTE: Contributions from Professors E. R. G. Eckert, E. M. Sparrow and W. E. Ibele of the Heat Transfer Laboratory, University of Minnesota, are gratefully acknowledged.

Two types of Electric Propulsion, by Juliusz Vlam, vol. 1, pp. 228–244. (In French.)

Ion Rocket Efficiency Studies, by Guntis Kuskevics, vol. 1, pp. 409–425.

Nuclear Rocket Missions and Associated Power Plants, by John J. Newgard and Myron M. Leroy, vol. 1, pp. 445–458.

Recent Developments and Designs of the Ion Rocket Engine, by Robert H. Boden, Vol. 1, pp. 463–482.

Thermoelectronic Converters of Thermal Energy into Electric Energy, by L. N. Dobretsov, *Soviet Physics, Tech. Physics,* Vol. 5, Oct. 1960, pp. 343–368.

Propulsion Side Effects May Endanger Man in Space, by F. G. McGuire, *Missiles and Rockets,* vol. 6, no. 17, April 25, 1960, pp. 44–46.

Constant Thrust Engines, by R. Ainsworth, *The Iowa Engr.,* vol. 60, no. 6 March 1960, pp. 24–26, 46.

Non-Propulsive Power for Advanced Vehicles-III, by R. W. Curran, *Space/Aeron.,* vol. 33, no. 5, May 1960, pp. 52–54.

Solar Sail: Key to Interplanetary Voyaging, by B. W. Powell, *Spaceflight,* vol. 2, no. 4, Oct. 1959, pp. 116–118.

Arc-Jet and Photon Rockets: Propulsion for Near and Far Future, by K. R. Stehling, *Space/Aeron.,* vol. 33, no. 5, May 1960, pp. 42–45.

Sunpower, by J. Oostermeyer, *Industrial Res.,* vol. 2, no. 2, April-May 1960, pp. 46–52.

Summarization of Studies on Nuclear Heat Engine Systems, by F. G. Hammitt, *University of Michigan,* Ann Arbor, *IP-275,* April 1958.

A Parametric Study of Certain Low-Molecular-Weight Compounds as Nuclear Rocket Propellants. IV. Lithium Hydride, by F. J. Krieger, *Rand Corp.,* Santa Monica, Calif., *RM-2403,* Aug. 29, 1959.

Weight Optimization of a Solar or Nuclear Mechanical Conversion System, by L. Schipper, *Wright Air Devel. Center,* WADC TN 59-180, June 1959.

Solar-Thermoelectric Generator Program: General Results, Boeing Airplane Co., D7-3041, Jan. 1960.

Collection of Solar Thermal Energy for Space Power System Application, by N. R. Griswold, *Boeing Airplane Co.,* D2-5523, Jan. 11, 1960.

Solar Power for Space Vehicles, A Summary of Recent Boeing Research, *Boeing Airplane Co.,* D7-3040, Sept. 4, 1959.

NASA Research on the Hydrodynamics of the Gaseous Vortex Reactor, by Robert G. Ragsdale, *NASA TN-288,* Sept. 1960, 41 pp.

Grid Electrode Ion Rockets for Low Specific Impulse Missions, by J. Howard Childs and William R. Mickelsen, *Symposium on Advanced Propulsion Concepts, 2nd. Boston,* Oct. 7–8, 1959, 20 pp., 22 figs.

Cesium Ion Motor Research, by R. C. Speiser and C. R. Dulgeroff, *Symposium on Advanced Propulsion Concepts, 2nd, Boston,* Oct. 7–8, 1959, 9 pp.

High Speed Shock Waves in a Magnetic Annular Shock Tube, by Richard M. Patrick, *Symposium on Advanced Propulsion Concepts, 2nd, Boston,* Oct. 7–8, 1959, 36 pp.

Fast Interplanetary Missions with Low-thrust Propulsion Systems, by W. E. Moeckel, *NASA Tech. Rep. R-79,* 1960, 56 pp.

A Thermal Energy Storage System for Solar Powered Earth Power Plants, by Curtis L. Walker and James D. Matchett, *General Motors Engng. J.,* vol. 7, no. 3, July–Sept. 1960, pp. 10–12.

Electric Propulsion-Measurements with a Small Thrust Plasma Generator, by B. W. Harned, *SAE Trans.,* vol. 68, 1960, pp. 85–92.

Non-Air-Breathing Auxiliary Powerplants, by D. L. Cochran, A. T. Biehl, D. R. Sawle, M. R. Gustavson and A. M. Taylor, *SAE Trans.,* vol. 68, 1960, pp. 111–119.

High-Energy Accelerators, by Keith R. Symon, *SAE Trans.,* vol. 68, 1960, pp. 157–164.

Electric Propulsion Systems, by Victor P. Kovacik and Daniel P. Ross, *SAE Trans.,* vol. 68, 1960, pp. 380–389.

Nuclear Rockets for Interplanetary Propulsion, by Frank E. Rom and Paul G. Johnson, *SAE Trans.,* vol. 68, 1960, pp. 600–608.

Conversion of Thermal Energy Into Electricity With the Aid of Thermoelectric Emission, by N. D. Morgulis, *Soviet Physics: Uspekhi,* vol. 3, no. 2, Sept.–Oct. 1960, pp. 251–259.

Effect of Interelectrode Spacing on Cesium Thermionic Converter Performance, by R. L. Hirsch, *J. Appl. Phys.,* vol. 31, Nov. 1960, pp. 2064–2065.

Effect of Magnetic Fields on Thermionic Power Generators, by Alfred Schock, *J. Appl. Phys.,* vol. 31, Nov. 1960, pp. 1978–1987.

Electric Propulsion, by David B. Langmuir, ASTRONAUTICS, vol. 5, Nov. 1960, p. 33.

Nuclear Propulsion, by C. J. Wang, ASTRONAUTICS, vol. 5, Nov. 1960, p. 41.

Power Systems, by A. M. Zarem, ASTRONAUTICS, vol. 5, Nov. 1960, p. 43.

Underwater Propulsion, by George F. Wislicenus, ASTRONAUTICS, vol. 5, Nov. 1960, p. 49.

NASA-Industry Program Plans Conference, 1st, July 28–29, 1960.

Space Propulsion and Power Generation, by Emerson W. Conlon, pp. 29–33.

Chemical and Electrical Propulsion, by Elliot Mitchell, pp. 50–53.

Nuclear Energy for Advanced Space Missions, by Harold B. Finger, pp. 54–57.

Solar and Chemical Power Generation Systems, by William C. Cooley, pp. 92–95.

Analysis of Magnetic Triodes for Direct-Energy Conversion Having Flat-Plate Cathodes and Anodes At an Arbitrary Angle, by James E. Hatch, *NASA TN* no. D-575, Nov. 1960, 22 pp.

An Exploratory Study of Thermoelectrostatic Power Generation for Space Flight Applications, by B. H. Beam, *NASA TN* no. D-336, Oct. 1960, 35 pp.

Experimental Performance of a Pulsed Gas Entry Coaxial Plasma Accelerator and Applications to Space Missions, by B. Gorowitz and P. Gloersen, *General Electric Co., Missile and Space Vehicle Dept. TIS Rep.* R60SD-456, Oct. 1960, 14 pp.

Generalized Pinch Dynamics in Nondimensional Form, by William J. Guman, *Republic Aviation Corp., Plasma Propulsion Laboratory,* PPL-TR-60-7, May 1960, 12 pp.

Decennial Symposium, Proceedings, *Toronto University, Institute of Aerophysics,* Oct. 14–16, 1959, 3 parts, 512 pp.

Plasma Propulsion for Space Vehicles, by H. Preston-Thomas, pp. 478–490.

Reports on Progress in Physics, A. C. Strickland, ed., London, The Physical Society, 1959, vol. XXII, 634 pp.

Physical Problems of Thermoelectricity, by A. G. Joffe and L. S. Stil'bans, pp. 167–203.

International Astronautical Congress, 10th, London, 1959, Proceedings, F. Hecht, ed., Springer-Verlag, Vienna, 1959, 2 vols. 946 pp.

Study of Convection and Radiation for a Thermal Fission Propulsion System, by P. Perrier, vol. 2, pp. 625–638. (In French.)

Space Power, by W. W. T. Crane, vol. 2, pp. 749–75.

On the Directing of Intense Photonic Beams by Means of Electron Gas Mirrors, by E. Sanger, vol. 2, pp. 828–834.

Design Compromises in Space Power Systems, by M. A. Zipkin and E. Schnetzer, vol. 2, pp. 560–575.

Reactor Neutron Activation Cross Sections for a Number of Elements, by W. S. Lyon, *Nuclear Science and Eng.*, vol. 8 Nov. 1960, pp. 378–380.

Power Sources for Satellites and Space Vehicles, by H. A. Bahl and H. K. Ziegler, *Solar Energy*, vol. 4, no. 1, Jan. 1960, pp. 32–38.

Space Missions and Auxiliary Power Demands, by J. D. Burns and W. R. Menetrey, *Western Aviation*, vol. 40, no. 10, Oct. 1960, pp. 20–23.

Unconventional Power Converters, by C. M. Celent, *Electronic Industries*, vol. 19, no. 9, Sept. 1960, pp. 101–116.

Space Power Systems, *Electromechanical Design*, vol. 4, no. 9, Sept. 1960, pp. 30–36.

Methodology for Determination of Performance Characteristics of Spectrally Selective Absorbers, by R. O. Whitaker, *Solar Energy*, vol. 4, no. 2, April 1960, pp. 40–45.

Volumetric Assary of Ammonium Perchlorate, by Eugene A. Burns and R. F. Muraca, *Stanford Res. Inst., Poulter Labs.* (reprinted from *Analytical Chemistry*, vol. 32, Sept. 1960), 3 pp.

Alignment Charts for Transport Properties; Viscosity, Thermal Conductivity, and Diffusion Coefficients for Nonpolar Gases and Gas Mixtures at Low Density, by Richard S. Brokaw, *NASA Tech. Rep.* R-81, 1960, 34 pp., 28 refs.

A High Intensity Explosive Light Source, by Zev. Pressman, *Stanford Res. Inst., Poulter Labs., Tech. Rep.* 009–60, Sept. 1960, 5 pp.

Kinetics of Condensation from the Vapor Phase, by Welby G. Courtney, *Texaco Experiment Inc.*, Richmond, Va., *Tech. Mem.* 1212, quarterly report for the period ending Aug. 5, 1960, 47 pp.

Radiation Chemistry of N-pentane: Mechanism for the Formation of Lower Molecular Weight Products, by Jean H. Futrell, *Aeron. Res. Labs., Air Force Research Div.*, Wright-Patterson Air Force Base, Ohio (*ARL TN* 60–139), Aug. 1960, 10 pp.

Supersaturation of Oxygen in Aqueous Hydrogen Peroxide Solutions, by Charles N. Satterfield, *MIT, Dept. of Chem. Eng., rep.* no. 57, Oct. 1960, 12 pp.

Propellants and Combustion, by Peter L. Nichols Jr., ASTRONAUTICS, vol. 5, Nov. 1960, p. 44.

Propellants and Combustion

Experimental Performance of the Mixed-oxides of Nitrogen-ammonia Propellant Combination with Several Injection Methods in a 1000-Pound-Thrust Rocket Engine, by William A. Tomazic and George R. K. Kinney, *NACA Research Memorandum* E55A07, March 1955, 30 pp. (Declassified by authority of *NASA Tech. Pubs. Announcement* no. 33, Nov. 24, 1960.)

Advances in Spectroscopy, H. W. Thompson, ed., Interscience Publishers, N.Y., 1959, 1 vol. 363 pp.

The Spectra of Polyatomic Free Radicals, by D. A. Ramsay, pp. 1–55, 185 refs.

Conference on Applied Gas Dynamics Proceedings, *Alma-Ata, Akad. Nauk Kazakhskoi SSR*, 1959, 235 pp. (In Russian.)

Investigation of Characteristic Turbulence in Free Nonisothermal Jets and Open Flames, by G. S. Antonova, pp. 45–55, 16 refs.

Some Questions of the Aerodynamics of Two-Phase Flow in Cyclone Combustion Chambers, by E. V. Volkov, pp. 142–152, 7 refs.

Problems of Working Processes in Cyclone Chambers, by A. V. Tonkonogii and I. P. Basina, pp. 152–158, 9 refs.

Mechanism of Combustion in Gaseous Jets, by A. S. Telegic, pp. 160–167, 18 refs.

On James' Type of Wave Functions for Hydrogen Molecular Ion, by Yatendra Pal Varshni and Ramesh Chandra Shukla, *Canadian J. Phys.*, vol. 38, Nov. 1960, pp. 1547–1551.

Monopropellant Stability, by Ted A. Erikson, *Illinois Inst. Tech., Armour Res. Foundation*, ARF 3180–4 (Quarterly no. 1), Oct. 1960, 16 pp.

Experimental Investigation of Heat-transfer Characteristics of Liquid Nitrogen Tetroxide, by D. E. Birdseye, *Calif. Inst. Tech., Jet Prop. Lab., Technical Rep.* no. 32–37, Oct. 1960, 20 pp.

Research on the Hazards Associated with the Production and Handling of Liquid Hydrogen, by Michael G. Zabetakis and David S. Burgess, *Wright Air Development Div., Technical Rep.* no. 60–141, June 1960 (ASTIA AD-239,644), 76 pp.

A Preliminary Experimental and Analytical Evaluation of Diborane as a Ram-jet Fuel, Benson E. Gammon, Russell S. Genco and Melvin Gerstein, *NACA Research Memorandum*-E50J04, Dec. 22, 1950, 39 pp. (Declassified by authority of *NASA Tech. Pubs. Announcement* no. 33, Nov. 24, 1960.)

Experimental Performance of Liquid Fluorine-Liquid Ammonia Propellant Combination in 1000-pound-thrust Rocket Engines, by Howard W. Douglass, *NACA Research Memorandum* E54C17, May 1954, 32 pp. (Declassified by authority of *NASA Tech. Pubs. Announcement* no. 33, Nov. 24, 1960.)

Ignition of Ammonia and Mixed Oxides of Nitrogen in 200-pound-thrust Rocket Engines at 160°F., by Glen Hennings, Dezso J. Ladanyi and John H. Enders, *NACA Research Memorandum* E54C19, May 1954, 18 pp. (Declassified by authority of *NASA Tech. Pubs. Announcement* no. 33, Nov. 24, 1960.)

Pentaborane Combustion Performance in 9.75-inch-diameter Ram-jet Engine in Connected-pipe Altitude Facility, by Herschel J. Fivel, Leonard K. Tower and James B. Gibbs, *NACA Research Memorandum* E54116, March 1957, 47 pp. (Declassified by authority of *NASA Tech. Pubs. Announcement* no. 33, Nov. 24, 1960.)

Solid Propellants, by B. F. Greek, C. F. Dougherty and W. J. Mundy, *I/EC Ind. Eng. Chem.*, vol. 52, Dec. 1960, pp. 974–984.

How Does Nitric Oxide Affect Reactions of Aqueos Nitrogen Dioxide, by E. Koval, and M. S. Peters, *I/EC Ind. Eng. Chem.* vol. 52, Dec. 1960, pp. 1011–1026.

Boltzmann Equation and Inverse Collisions, by J. T. O'Toole and J. S. Dahler, *J. Chem. Phys.*, vol. 33, Nov. 1960, pp. 1487–1495.

Microwave Spectrum, Structure, and Dipole Moment of Propane, by David R. Lide Jr., *J. Chem. Phys.*, vol. 33, Nov. 1960, pp. 1514–1518.

Metastable Hydrogen Molecules, by William Lichten, *Phys. Rev.*, vol. 120, Nov. 1, 1960, pp. 848–853.

Analysis of Steady-state Supported One-dimensional Detonations and Shocks, by W. W. Wood and Z. W. Salsburg, *Phys. Fluids*, vol. 3, July–Aug. 1960, pp. 549–566.

Photoelastic Study of Powder Pellets for Rockets, by J. Nicolas, *La Recherche Aeronautique*, no. 78, Sept.–Oct. 1960, p. 55. (In French.)

The Effect of Fluorine on the Electronic Spectra and Ionization Potentials of Molecules, by R. Bralsford, P. V. Harris and W. C. Price, *Royal Society, London, Proceedings*, vol. 258 A, Nov. 8, 1960, pp. 459–469.

The Vapor Pressure of Nitrogen and Hydrogen at Low Pressures, by E. S. Borovik, S. F. Grishin and E. Ya. Grishina, *Soviet Physics: Tech. Physics*, vol. 5, no. 5, Nov. 1960, p. 506.

The Critical Temperatures of Forty Organic Compounds, by D. Ambrose, J. D. Cox and R. Townsend, *Faraday Society Trans.*, vol. 56, Oct. 1960, p. 1452.

An Analytical Investigation of Three General Methods of Calculating Chemical-equilibrium Compositions, by Frank J. Zeleznik, *NASA TN* D-473, Sept. 1960, 35 pp.

Propagation of Free Flames in Laminar and Turbulent Flow Fields, by Ray E. Bolz and Henry Burlage Jr., *NASA TN* D-551, Sept. 1960, 66 pp.

The Adhesion of Molten Boron Oxide to Various Materials, by W. R. Witzke, *NACA Res. Memo* E57L11, April 1958, 13 pp. diagrs.

Investigation of Conditions for Spontaneous Ignition and Combustion Efficiency of Pentaborane in a Small-scale Combustor, by Albert M. Lord and James F. Morris. *NACA Res. Memo.* E54K05, April 1957, 20 pp. (Declassified by authority of *NASA Tech. Pubs. Announcement* no. 29.)

Preliminary Performance Evaluation of Blends of Pentaborane and JP-4 Fuel in a Full-scale Turbojet Engine, by C. R. King, Roland Britwieser and J. N. Sivo, *NACA Res. Memo.* E54J05, Jan. 1957, 29 pp. (Declassified by authority of *NASA Tech. Pubs. Announcement* no. 29.)

An Investigation of Effects of Flame-Holder Gutter Shape on Afterburner Performance, by S. Nakanishi, W. W. Velie and L. Bryant, *NACA Res. Memo.* E53J14, Feb. 1954, 49 pp. (Declassified by authority of *NASA Tech. Pubs. Announcement* no. 29.)

Preliminary Investigation of the Altitude Performance of Pentaborane-JP-4 Blend in an Experimental 9.5-inch-diameter Tubular Combustor, by Warner B. Kaufman and J. Robert Branstetter, *NACA Res. Memo.* E53J19, April 1957, 37 pp. (Declassified by authority of *NASA Tech. Pubs. Announcement* no. 29.)

Annual Review of Physical Chemistry, vol. 11, 1960, edited by H. Eyring, C. J. Christensen and H. S. Johnston, *Annual Reviews, Inc.*, Palo Alto, Calif. 1960, 588 pp.

Thermochemistry and Thermodynamic Properties of Substances, by John P. McCullough, pp. 1–20.

Combustion and Flames, by S. S. Penner and T. A. Jacobs, pp. 391–406.

Advances in Catalysis, vol. 12, 1960, by D. D. Eley, P. W. Selwook, and Paul B. Weizz, eds., Academic Press, N. Y. 1960, 324 pp.

Base-catalyzed Reactions of Hydrocarbons, by Herman Pines and Luke A. Schaap, pp. 117–148.

An Alignment Chart for the Direct Determination of the Weight of Gun Charges in Interior Ballistic Calculations, by R. C. Strittmater, *Ballistic Res. Labs. Rep.* no. 1299, Aug. 1960.

Theoretical Performance of Selected Propellant Systems, IV, Survey of Thermochemical Data, by R. S. Scheffee, J. A. Simmons, K. E. Woodcock, C. B. Henderson and K. E. Rumbel, *Atlantic Research Corp.*, April 1959, 79 pp. (Contract NORD-15536). (Declassified by authority of *Bureau of Naval Weapons letter DSC-42:-GEC* **585**, *Aug.* **29, 1960.**)

Materials and Structures

Structural Considerations of Inflatable Reentry Vehicles, by Robert W. Leonard, George W. Brooks and Harvey G. McComb Jr., *NASA TN* D-457, Sept. 1960, 23 pp.

Some Measurements of Noise Transmission and Stress Response of a 0.020-inch Duralumin Panel in the Presence of Air Flow, by George T. Kantarges, *NASA TN* D-459, Sept. 1960, 25 pp.

Temperature Effects on Material Characteristics, by A. J. Murphy and A. J. Kennedy, *Cranfield, College of Aeron., Rep.* no. 135, Aug. 1960, 27 pp.

Formation of Thin Polymer Films by Electron Bombardment, by R. W. Christy, *Space Tech. Labs., Physical Res. Lab.* PRL-90-30, Dec. 17, 1959, 15 pp.

Theory of Magnetism, Magnetic Properties of Materials and Use of Magnetic Materials in Instrumentation, by Dorothy I. Sweitzer, *Calif. Inst. Tech., Jet Prop. Lab., Literature Search* no. 186, Jan. 1960, 356 pp.

Materials for Re-entry Heat Protection of Satellites, by Leo Steg, ARS JOURNAL, vol. 30, Sept. 1960, pp. 815–822.

Thermal and Electrical Properties of Armco Iron at High Temperatures, by M. J. Laubitz, *Canadian J. Phys.*, vol. 38, July 1960, pp. 887–907.

Creep Deformation and Stresses in Pressurized, Long Cylindrical Shells, by M. P. Bieniek and A. M. Freudenthal, *J. Aero/Space Sci.*, vol. 27, Oct. 1960, pp. 763–766.

A Comparison of Transient and Quasi-steady Performance of Melting-type Reentry Shields, by Ernst Wilhelm Adams, *J. Aero/Space Sci.*, vol. 27, Oct. 1960, p. 791.

Utilization of Similarity Considerations for the Improvement of the Convergence of a Process of Successive Approximation in Shell Analysis, by I. V. Svirskii, *PMM: J. Appl. Math. and Mech.* (trans. of *Prikladnaia Matematika i Mekhanika*), vol. 24, no. 1, 1960, pp. 177–190.

Characteristics of a 60-inch Arc-image Furnace and Application to the Study of Materials, by Roger W. Peters, R. Gale

Wilson and Milton A. Wallio, *NASA TN* D-505, Oct. 1960, 19 pp.

Materials Problems in Chemical Liquid-Propellant Rocket Systems, by L. L. Gilbert, *NASA Tech. Memo.* X-89, August 1959, 41 pp. (Declassified by authority of *NASA Tech. Pubs. Announcement* no. 29.)

Surface Effects on Materials in Near Space, by Francis J. Clauss, *Aero/Space Engng.*, vol. 19, Oct. 1960, pp. 16–19.

A Theory for the Small Rotationally Symmetric Deformations of Cylindrical Shells, by Edward L. Reiss, *Communications Pure Applied Math.*, vol. 13, no. 3, Aug. 1960, pp. 531–545.

A Note on Rigid Body Displacements in the Theory of Thin Elastic Shells, by P. M. Naghdi, *Quarterly Applied Math.*, vol. 18, Oct. 1960, pp. 296–298.

Bonded and Sealed External Insulations for Liquid-hydrogen-fueled Rocket Tanks During Atmospheric Flight, by V. H. Gray, T. F. Gelder, R. P. Cochran and J. H. Goodykoontz. **(Appendix B: Strength of Insulations and Bond to Aluminum at Cryogenic Temperatures,** by Morgan P. Hanson, **Appendix C: Step Method of Approximate Numerical Calculation of One Dimensional Transient Heat Conduction with Variable Thermal Properties,** by William Lewis), *NASA TN* D-476, Oct. 1960, 51 pp.

Fluid Dynamics, Heat Transfer and MHD

Force and Pressure Tests of an AGARD Calibration Model B at a Mach Number of 8, by L. D. Kayser and C. R. Fitch, *Arnold Engng. Dev. Center, TN* 60-34, July 1960, 39 pp.

A Two-stage Driver for Shocktubes and Shock Tunnels, by Z. I. Slawsky and A. E. Seigel, *NAVORD Rep.* 5669, Jan. 5, 1960, 9 pp.

Nonlinear Problems in Thermodynamics of Irreversible Processes, by Thor A. Bak, *Wright Air Dev. Div., TN* 60–102, April 1960, 31 pp.

Electron Density Distribution in a Cylinder, by H. D. Weymann, *Univ. Maryland, Inst. Fluid Dynam. & Appl. Math., TN* BN 214, July 1960, 7 pp. (*AFOSR TN* 60–704.)

Magnetohydrodynamic Simple Waves (Supplement), by Y. M. Lynn, *Calif. Inst. Tech., Galcit,* May 1960, 23 pp. (*AFOSR TN*-59-1302.)

Some Optical Investigations of a High-power Pulsed Gas Discharge in Hydrogen, by P. A. Kireev and A. A. Iuzefovich (*transl. of Vestnik Moskov. Univ. Seriia Mat. Mekh., Astron., Fiz., Khimii,* no. 5, 1958, pp. 105–110), *Johns Hopkins Univ., Appl. Phys. Lab., Transl.* no. TG 230-T 163, May 26, 1960, 7 pp.

The Kinetics of Gases, by *Gas Dynamics Lab., Northwestern Univ.,* (*AEDC-TN*-60-130), July 1960. 1 vol.

Experimental Studies on Plasma Dynamics, by Winston H. Bostick, John Nankivell, Samuel Koslov and George Schmidt, *ARS Preprint* 904–59, Aug. 1959, 9 pp.

Ion Wave Instabilities, by Ira B. Bernstein and R. M. Kulsrud, *Princeton Univ., Proj. Matterhorn, MATT*-39, April 13, 1960, 28 pp.

Heat Transfer and Fluid Mechanics Institute, Stanford University, June 1960. **Proceedings,** ed. by D. M. Mason, W. C. Reynolds and W. G. Vincenti, Stanford Univ. Press, Calif., 1960, 259 pp.

Magnetohydrodynamically Driven Vortices, by W. S. Lewellen, pp. 1–15.

Behavior of Solutions of the Navier-Stokes Equations for a Complete Class of Three-dimensional Viscous Vortices, by C. duP. Donaldson and R. D. Sullivan, pp. 16–30.

An Experimental Study of Gas Dynamics in High Velocity Vortex Flow, by J. J. Keyes Jr., pp. 31–46.

The Behavior of Vortex Motion in an Emptying Container, by P. Dergarabedian, pp. 47–61.

Some Applications of Crocco's Integral for the Turbulent Boundary Layer, by D. A. Spence, pp. 62–76.

Heat Transfer in the Unsteady Compressible Laminar Boundary Layer on a Flat Plate, by N. A. Evans, pp. 77–91.

Boundary Layer Transition Induced by a Vibrating Ribbon on a Flat Plate, by F. R. Hama, pp. 92–105.

A New Analytical Model for Boundary Layer Transition, by K. G. Sewell, pp. 106–119.

Hot Wire Exploration of Transition on Cones in Supersonic Flow, by V. A. Sandborn and R. J. Wisniewski, pp. 120–134.

Explosive Decompression of Water, by E. A. Brown Jr., pp. 135–149.

Heat Transfer Around Blunt Bodies with Non-equilibrium Boundary Layers, by P. M. Chung and A. D. Anderson, pp. 150–163.

Weak, Nonequilibrium, Diffusive Waves in a Dissociated Gas, by F. K. Moore and J. T. Curtis, pp. 164–178.

Separated Supersonic Flows, by J. J. Ginoux, pp. 179–191.

Some Effects of Particle-particle and Particle-fluid Interaction in Two Phase Flow Systems, by R. L. Peskin, pp. 192–207.

An Experimental Study of the Transition from Nucleate to Film Boiling under Zero Gravity Conditions, by N. H. Steinle, pp. 208–219.

A Method of Measuring Total Hemispherical Emissivities at Low Temperatures–Results for Pure Iron from 200 to 500 Degrees Rankine, by J. A. Brandt, T. F. Irvine Jr. and E. R. G. Eckert, pp. 220–228.

Minimum Mass Thin Fins for Space Radiators, by J. E. Wilkins Jr., pp. 229–243.

Weight Optimizations of Heat Rejection Systems for Space Applications, by C. L. Walker, C. R. Smith and D. G. Gritton, pp. 244–259.

Measurement of Screen-size Effects on Intensity, Scale, and Spectrum of Turbulence in a Free Subsonic Jet, by Charles D. Howard and James C. Laurence, *NASA TN* D-297, Aug. 1960, 38 pp.

Experimental and Theoretical Studies of Axisymmetric Free Jets, by Eugene S. Lov, Carl E. Grigsby, Louis P. Lee and Mildred J. Woodling, *NASA Tech. Rep.* R-6, 1959, 292 pp.

Radiation Oxidation of Nitrogen, by M. T. Dmitriev, *Johns Hopkins Univ., Appl. Phys. Lab., Transl.* TG230-T 149 (*transl. of Zhurnal Fiz. Khimii,* vol. 32, no. 10, 1958, pp. 2418–2423), July 7, 1960, 9 pp.

Propagation of Magnetohydrodynamic Waves Without Radial Attenuation, by Harold Grad, *AEC, NYO*-2537, Jan. 15, 1959, 48 pp.

Avionics Research: Satellites and Problems of Long Range Detection and Tracking; Papers Presented at the AGARD Avionics Panel Meeting, Copenhagen, Oct. 20–25, 1958, *NATO, AGARD,* ed. by E. V. D. Glazier, E. Rechtin and J. Voge, Pergamon Press, New York, 1960, 257 pp.

The Electrostatic Field About an Ion Moving Slowly Through a Highly Ionized Gas, by S. Rand, pp. 68–74.

Plasma Motions Induced by Satellites in the Ionosphere, by Lester Kraus and Kenneth M. Watson, pp. 75–91.

International Symposium on High Temperature Technology, Asilomar Conference Grounds, Calif., Oct. 5–9, 1959, McGraw-Hill Book Co., New York, 1960, 348 pp.

Experiments with High Intensity Electric Discharges, by G. M. Giannini, A. C. Ducati, W. F. von Jaskowsky and D. Ragusa, pp. 21–32.

Extended Hypervelocity Gas Dynamic Charts for Equilibrium Air, by Richard W. Ziemer, *Space Tech. Labs., Phys. Res. Lab., Tech. Rep.* 60–0000–09093, Apr. 14, 1960, 38 pp.

Experiments on Supersonic Plasma Flow Along Magnetic Fields, by D. Finkelstein, M. Ehrlich, I. Livingston and D. Wetstone, *Atomic Energy Comm. NYO*-7981, March 27, 1958, 48 pp.

A Magnetically Insulated Shock Tube, by Richard G. Fowler and Eugene B. Turner, *Space Tech. Labs., Phys. Res. Lab., Tech. Rep.* 60–0000–09180, 1960, 44 pp.

A Method for Calculating the Thermal Irradiance Upon a Space Vehicle and Determining Its Temperature, by T. L. Altshuler, *General Electric Co., Missile & Space Vehicle Dept., TIS* R60SD386, Aug. 1960, 51 pp.

Analytic Study of Induced Pressure on Long Bodies of Revolution with Varying Nose Bluntness at Hypersonic Speeds, by Vernon Van Hise, *NASA TR* R-78, 1960, 37 pp.

A Viscous Magnetohydrodynamic Boundary Layer, by A. Sherman, *General Electric Co., Flight Propulsion Lab. Dept.,* R-60-FPD-443, Aug. 1960, 16 pp.

Three-dimensional Boundary Layer Equations of an Ionized Gas in the Presence of a Strong Magnetic Field, by Ching-Sheng Wu, *Calif. Inst. Tech., Jet Prop. Lab.,* TR. no. 32-17, May 27, 1960, 24 pp.

Measurement of the Characteristics of the Compressible Turbulent Boundary Layer with Air Injection, by James E. Danberg, *NavOrd Rep.* 6683, Sept. 3, 1959, 13 pp.

Blunt Body Heat Transfer at Hypersonic Speed and Low Reynolds Numbers, by Antonio Ferri, Victor Zakkay and Lu Ting, *Brooklyn Polytechnic Inst. Dept. Aeron. Engng. and Appl. Mech., PIBAL Rep.* no. 611, June 1960, 70 pp.

Blunt Body Heat Transfer at Hypersonic Speed and Low Reynolds Numbers, by Antonio Ferri, Victor Zakkay and Lu Ting, *Brooklyn Polytechnic Inst. Dept. Aeron. Engng. and Appl. Mech., PIBAL Rep.* no. 611, June 1960, 70 pp.

The Structure of a Centered Rarefaction Wave in an Ideal Dissociating Gas, by J. P. Appleton, *Southampton Univ. Dept. of Aeron. and Astron., U.S.A.A. Rep.* no. 136, April 1960, 43 pp.

On Convected Turbulence and Its Relation to Near Field Pressure, by J. E. F. William, *Southampton Univ. Dept. Aeron. and Astron., U.S.A.A. Rep.* no. 109, June 1960, 51 pp.

Real-gas Correction Factors for Hypersonic Flow Parameters in Helium, by Wayne D. Erickson, *NASA TN* D-462, Sept. 1960, 13 pp.

Subsonic Hydromagnetic Flow in a

Two-dimensional Channel, by F. D. Hains, *Boeing Scientific Labs.*, DI-82-0057, March 1960, 20 pp.

An Experimental Study of the Ionization of Low-Density Gas Flows by Induced Discharges, by R. I. Barger, J. D. Brooks and W. D. Beasley, *NASA TN* D-432, Sept. 1960, 21 pp.

Experimental Determination of Statistical Properties of Two-phase Turbulent Motion, by S. L. Soo, H. K. Ihrig and A. F. El Kouh, *Princeton Univ., Project Squid, Tech. Rep.* PR-82-P, Sept. 1958, 19 pp. 2 figs.

Longitudinal Ion Oscillations in a Hot Plasma, by Burton Fried and Roy Gould, *Space Tech. Labs., Physical Res. Lab., Tech. Rep.* No. 60-0000-GR 185, June 28, 1960, 24 pp.

Gas Dynamics Symposium, 3rd, Northwestern University, 1959. Dynamics of Conducting Gases: Ali Bulent Cambel and John B. Fenn, eds., Northwestern Univ, Press, Evanston, 1960, 212 pp.

The Conductivity of an Ionized Gas in a Magnetic Field, by W. P. Allis and S. J. Buchsbaum, pp. 3–14.

Some Properties of a Hydrogen Plasma, by R. A. Gross and C. L. Eisen, pp. 15–24.

The Statistical Mechanics of the Approach to Equilibrium in Gases, by I. Prigogine, pp. 25–31.

Irreversible Processes in a Plasma: Effect of Long Range Forces, by Radu Balescu, pp. 32–35.

Relaxation Processes in Plasma, by H. F. Calcote, pp. 36–47, 66 refs.

Some Solutions of the Microscopic Equations of Magneto-hydrodynamics, by W. R. Sears, pp. 51–63.

A Microscopic Analysis of Magneto-gas-dynamics, by E. E. Covert, pp. 64–79, 45 refs.

Magnetohydrodynamics in the Limit of Small Inertial Forces, by Rudolf X. Meyer, pp. 80–85.

Axially Symetric Hydromagnetic Channel Flow, by F. D. Hains and Edward Ehlers, pp. 86–103.

Experimental Studies on Plasma Dynamics, by Winston H. Bostick, John Nankivell, Samuel Koslov and George Schmidt, pp. 107–111.

Applied Magnetohydrodynamics at Avco, by M. Camao and G. S. Janes, pp. 112–125.

Electromagnetic Shock Tubes, by Rickard W. Ziemer, pp. 139–149.

Particle Impacts on the Melt Layer of an Ablating Body, by E. W. Ungar, ARS JOURNAL, vol. 30, Sept. 1960, pp. 799–805.

Ablation of Glassy Material Around Blunt Bodies of Revolution, by Henry Hidalgo, ARS JOURNAL, vol. 30, Sept. 1960, pp. 806–814.

Analysis of the Ablation of Plastic Heat Shields That Form a Charred Surface Layer, by R. J. Barriault and J. Yos, ARS JOURNAL, vol. 30, Sept. 1960, pp. 823–829.

Measurements of Heat Transfer and Friction Coefficients for Helium Flowing in a Tube at Surface Temperatures up to 5900 R, by Maynard F. Taylor and Thomas A. Kirchgessner, ARS JOURNAL, vol. 30, Sept. 1960, pp. 830-891.

Extension of the Transient Heating Charts, by A. N. Baxter, ARS JOURNAL, vol. 30, Sept. 1960, p. 904.

Insulation Temperature for the Transient Heating of an Insulated Finite Metal Slab, by William H. Holter and John H. Grover, ARS JOURNAL, vol. 30, Sept. 1960, p. 907.

Location of Frontal Wave in Asymmetrical Flow of Gas at High Supersonic Speed over a Pointed Body, by A. L. Gonor, ARS JOURNAL, vol. 30, Sept. 1960, *Russian Suppl.*, pp. 841–842.

Problem of Nearly Self-Similar Unsteady Motion, by T. G. Koldobskaya, ARS JOURNAL, vol. 30, Sept. 1960, *Russian Suppl.*, pp. 853–858.

Dependence of Internal Energy of Air on the Pressure and Density at High Temperatures, by S. S. Kvashnina, ARS JOURNAL, vol. 30, Sept. 1960, *Russian Suppl.*, pp. 875–876.

Velocity Autocorrelations of Charged Particles in a Magneto-ionic Medium with Applications to Turbulent Diffusion, by R. C. Bourret, *Canadian J. Phys.*, vol. 38, Sept. 1960, pp. 1213–1223.

Spectroscopic Temperature Measurements in a Shock Tube Using CN as a Thermometric Molecule, by W. H. Parkinson and R. W. Nicholls, *Canadian J. Phys.*, vol. 38, June 1960, pp. 715–719.

An Hypothesis Concerning Turbulent Diffusion, by R. Bourret, *Canadian J. Phys.*, vol. 38, May 1960, pp. 665–676.

Use of Analog Memory for Simulation of a Melting Slab, by Maxwell C. Gilliland and Hiroshi H. Hara, *Instruments and Control Systems*, vol. 33, Sept. 1960, pp. 1545–1550.

Heat Transfer, Recovery Factor, and Pressure Distributions around a Circular Cylinder Normal to a Supersonic Rarefied-air Stream, by O. K. Tewfik and A. H. Giedt, *J. Aero/Space Sci.*, vol. 27, Oct. 1960, pp. 721–729.

Second-order Theory of Unsteady Supersonic Fow Past Slender, Pointed Bodies of Revolution, by James D. Revell, *J. Aero/Space Sci.*, vol. 27, Oct. 1960, pp. 730–740.

On the Response of the Laminar Boundary Layer to Small Fluctuations of the Free-stream Velocity, by Nicholas Rott and Martin L. Rosenzewig, *J. Aero/Space Sci.*, vol. 27, Oct. 1960, pp. 741–747.

Dynamics and Thermodynamics of Reentry, by W. H. T. Loh, *J. Aero/Space Sci.*, vol. 27, Oct. 1960, pp. 748–762.

A Comparison of Blunt-body Flow-field Results, by Herbert W. Ridyard, *J. Aero/Space Sci.*, vol. 27, Oct. 1960, pp. 789–790.

Plane Flows of an Ideal Gas with Infinite Electrical Conductivity, in a Magnetic Field Not Parallel to the Flow Velocity, by M. N. Kogan, *PMM: J. Appl. Math. & Mech.* (transl. of *Prikladnaia Matematika i Mekhanika*), vol. 24, no. 1, 1960, pp. 129–143.

Some Solutions of the Equations of One-dimensional Magneto-hydrodynamics and Their Application to Problem of Shock Wave Propagation, by V. P. Korobeinikov and E. V. Raizanov, *PMM: J. Appl. Math. & Mech.* (transl. of *Prikladnaia Matematika i Mekhanika*), vol. 24, no. 1, 1960, pp. 144–158.

Application of Integral Relationships in Problems of Propagation of Strong Shock Waves, by G. G. Chernyi, *PMM: J. Appl. Math. & Mech.* (transl. of *Prikladnaia Matematika i Mekhanika*), vol. 24, no. 1, 1960, pp. 159–165.

On a Solution to the Equation of Magneto-gasdynamics, by I. M. Lur'ev, *PMM: J. Appl. Math. & Mechs.* (transl. of *Prikladnaia Matematika i Mekhanika*), vol. 24, no. 1, 1960, pp. 233–237.

Magnetohydrodynamic Effects Observed in Pulsed Contraction of a Plasma, by I. F. Kvartskhava, K. N. Kervalidze et al., *Soviet Physics: Tech. Physics* (transl. of *Zhurnal Tekhnicheskoi Fiziki*), vol. 5, no. 3, Sept. 1960, pp. 274–281.

High-frequency Oscillations in a

Bounded Plasma, by R. A. Demirkhanov and A. K. Gevorkov et al., *Soviet Physics: Tech. Physics* (transl. of *Zhurnal Tekhnicheskoi Fiziki*), vol. 5, no. 3, Sept. 1960, pp. 282–289.

Interaction of a Beam of Charged Particles with a Plasma, by R. A. Demirkhanov and A. K. Gevorkov, *Soviet Physics: Tech. Physics* (transl. of *Zhurnal Tekhnicheskoi Fiziki*), vol. 5, no. 3, Sept. 1960, pp. 290–294.

Radiation Energy Losses in a Plasma, by V. D. Kirillov, *Soviet Physics: Tech. Physics* (transl. of *Zhurnal Teknicheskoi Fiziki*), vol. 5, no. 3, Sept. 1960, pp. 295–304.

Stability of a Thin Circular Plasma Conductor in a Magnetic Field, by Yu. V. Vandakurov, *Soviet Physics: Tech. Physics* (transl. of *Zhurnal Teknhicheskoi Fiziki*), vol. 5, no. 3, Sept. 1960, pp. 305–312.

Nonstationary Flow of a Conducting Fluid in a Flat Tube in the Presence of a Transverse Magnetic Field, by I. B. Chekmarev, *Soviet Physics: Tech. Physics* (transl. of *Zhurnal Tekhnicheskoi Fiziki*), vol. 5, no. 3, Sept. 1960, pp. 313–319.

On the Interaction Between Stream and Body in a Free-molecule Flow. Part I: Energy Exchanges, by Silvo Nocilla, *Torino, Laboratorio di Meccanica Applicata del Politechnico, Tech. Note* 15, June 1960, 27 pp.

Blast Waves Produced by Exploding Wire, by Koichi Oshima, *Tokyo Univ., Aeron. Res. Inst. Rep.* no. 358, July 1960, vol. 26, no. 9, pp. 137–194.

Simultaneous Transfer of Momentum, Heat and Mass. Part I: Homogeneous Gases, by Gianni Jarre, *Torino, Laboratorio di Meccanica Applicata del Politechnico Tech. Note* 16, July 1960, 10 pp.

Effect on Gaseous Film Cooling of Coolant Injection Through Angled Slots and Normal Holes, by S. Stephen Papell, *NASA TN* D-299, Sept. 1960, 27 pp.

The Influence of Low Wall Temperature on Boundary-layer Transition and Local Heat Transfer on 2-inch-diameter Hemispheres at a Mach Number of 4.95 and a Reynolds Number Per Foot of 73.2 × 10^6, by Morton Cooper, Edward E. Mayo and Jerome D. Julius, *NASA TN* D-391, July 1960, 37 pp.

Calculation of Electron Drift Velocity and Mean Energy Based on "Collision Time" Approximation, by Ching-Sheng Wu, *Calif. Inst. Tech., Jet Prop. Lab., Tech. Rep.* no. 32–20, July 5, 1960, 8 pp.

Annual Review of Physical Chemistry, vol. 11, 1960, H. Eyring, C. J. Christensen and H. S. Johnston, eds., Annual Reviews, Inc., Palo Alto, Calif., 1960, 588 pp.

Some Aspects of the Statistical Theory of Transport, by Stuart A. Rice and Harry L. Frisch, pp. 187–272.

On the Effects Due to Dissociation and Ionisation at Hypersonic Velocities, by G. Jarre, *L'Aerotecnica,* vol. 40, no. 2, April 1960, pp. 99–111. (In Italian.)

Inviscid Hypersonic Flow near the Forward Stagnation Point of a Blunt Axisymmetric Body, by A. Muggia, *L'Aerotecnica,* vol. 40, no. 2, April 1960, pp. 112–118. (In Italian.)

Note on Evaporation, by S. A. Zwick, *J. Appl. Phys.,* vol. 31, Oct. 1960, pp. 1735–1741.

The Propagation of Sound in Relaxing Gases in Tubes at Low Frequencies, by D. H. Smith and H. J. Wintle, *J. Fluid Mech.,* vol. 9, Sept. 1960, pp. 29–38.

Observations on Bubble Growths in Various Superheated Liquids, by Paul Dergarabedian, *J. Fluid Mech.,* vol. 9, Sept. 1960, pp. 39–48.

A Study of the Structure o' the Magnetohydrodynamic Switch-on Shock in Steady Plane Motion, by Z. O. Bleviss, *J. Fluid Mech.,* vol. 9, Sept. 1960, pp. 49–67.

A Transformation for Non-homentropic Flows, with an Application to Large-amplitude Motion in the Atmosphere, by Chia-Shun Yih, *J. Fluid Mech.,* vol. 9, Sept. 1960, pp. 68–80.

The Propagation of Waves Along and Through a Conducting Layer of Gas, by G. S. S. Ludford, *J. Fluid Mech.,* vol. 9, Sept. 1960, pp. 119–132.

Transport Coefficients of Plasmas in Magnetic Field, by Shobu Kaneko, *Physical Soc. of Japan J.,* vol. 15, Sept. 1960, pp. 1685–1696.

The Compressible Viscous Layer in Rarefied Hypersonic Flow, by Hung-ta Ho and Ronald F. Probstein, *Brown Univ., Div. Engng.,* Aug. 1960, 37 pp.

An Approximate Treatment of Lamina Heat Transfer Coefficient and Its Application to the Calculation of Temperature of Supersonic Vehicles, by Koryo Miura, *Tokyo Univ. Aeron. Res. Inst. Rep.* no. 355, May 1960, 13 pp.

The Free Stream Properties of Argon Free Air in Chemical Equilibrium for a One Dimensional Isentropic Expansion Process, by E. M. Kaegi and W. R. Warren, *General Electric Co., Missile and Space Aerodyn. Lab., Tech. Memo.* no. 104, June 1960, 6 pp.

On an Approximate Solution of the Energy Equation and Its Application to McClimans' Data, by Eugene E. Covert, *MIT, Naval Supersonic Lab., Tech. Rep.* 403, Nov. 1959, 27 pp.

Arc Heating Techniques for a Shock Tube Driver, by Lawrence Y. Lamb, *Space Tech. Labs. Inc.,* STL/TN-60-0000-09145, June 1960, 32 pp.

Continuum Infrared Spectrum of High Temperature Air, by Raymond L. Taylor, *Avco-Everett Res. Lab. Res. Rep.* 88, June 1960, 17 pp.

Natural Convection of an Electrically Conducting Fluid in the Presence of a Magnetic Field, by Paul S. Lykoudis, *Purdue Univ. School of Aero. Engng. Rep.* A-60-1 Aug. 1960, 27 pp.

Low-density Shock Tube for Chemical Kinetic Studies, by Shao-Chi Lin and Walter L. Fyfe, *Avco-Everett Res. Lab., Everett, Mass., Res. Rep.* 91, July 1960, 36 pp. (*AF Ballistic Missile Div. TR* 60-183.)

Recent Advances in Non-equilibrium Flow in Gas Dynamics, by Ting Yi Li, *Rensselaer Polytech. Inst., Res. Div., Tech. Rep.* AE6001, May 1960, 59 pp.

Normal Shock Waves in Air with Chemical and Vibrational Relaxation Effects by R. A. Batchelder, *Douglas Aircraft Co., Rep.* SM-37627, July 1960, 84 pp.

Design, Fabrication and Evaluation of Axisymmetric Nozzles, by Larry L. Lynes, *Univ. California, Berkeley, Inst. of Engng. Res., Tech. Rep.* HE-150-174, Sept. 1959, 34 pp. 8 figs.

On Three-dimensional Free-mixing, by Martin H. Bloom, *Brooklyn Polytech. Inst., Dept. of Aerospace Engng. and Appl. Mech., PIBAL Rep.* no. 474, Aug. 1960, 11 pp.

A Study of Some Fluid Mixing Problems, by K. Toba and M. Breslau, *Rensselaer Polytech. Inst., Res. Div. Tech. Rep.* AE6003, Aug. 1960, 32 pp. (*AFOSR TN* 60-1023.)

A Contribution to the Energy Decay of Law of Isotropic Turbulence in the Initial Period, by Hiroshi Tsuji, *Tokyo Univ., Aeron. Res. Inst., Rep.* no. 345, May 1959, 22 pp.

Distribution of Time-averaged Pressure Fluctuations along the Boundary of a Round Subsonic Jet, by Walton L. Howes, *NASA TN* D-468, Oct. 1960, 20 pp.

Charged Particle Orbits in Varying Magnetic Fields, by E. I. Gordon, *Bell Telephone Labs., Inc.,* 1960, 15 pp.

Charged Particle Radiation in Space, by T. R. Riethof, *General Electric Co., Missile and Space Vehicle Dept., TIS Rep.* R60-SD391, Aug. 1960, 30 pp.

Particle Motion in an Axially Symetric Magnetic Field, by Alan S. Penford, *Litton Systems, Inc., Space Res. Lab. Res. Study* 29.15, May 1960, 54 pp. (*AFOSR Tech. Note* 60-841.)

A Magnetically Insulated Shock Tube, by Richard G. Fowler and Eugene B. Turner, *Space Tech. Lab., Inc., Phys. Res. Lab.* STL/TR-60-0000-09180, Nov. 1960, 44 pp.

Present-day Ideas Concerning the Mechanism of Electrical Breakdown in High Vacuum, by L. V. Tarasova, *NASA Tech. Translation* F-42, Oct. 1960, 35 pp.

A Solution of the Collisionless Boltzmann Equation Using a Diagram Technique, by Oldwig von Roos, *Calif. Inst. of Tech., Jet Prop. Lab., Tech. Rep.* no. 32–19, May 1960, 23 pp.

Quantum Corrections to the Dispersion Relation of Longitudinal Oscillations in an Electron Plasma, by Oldwig von Roos, *Calif. Inst. of Tech., Jet Prop. Lab., Tech. Rep.* no. 32–16, April 1960, 19 pp.

International Astronautical Congress, 10th,/London, 1959, Proceedings, F. Hecht, ed., Springer-Verlag, Vienna, 1960, 2 vols.

Magnetohydrodynamics and Its Application to Propulsion and Re-entry, by Rudolf X. Meyer, vol. 1, pp. 33–42.

Measurement of Jupiter Re-entry Radiation, by David D. Woodbridge and Warren N. Arnquist, vol. 1, pp. 245–253.

The Image Furnace as a Research Tool, by Nevin K. Hiester and R. E. De LaRue, ARS JOURNAL, vol. 20, Oct. 1960, pp. 928–937.

Heat Diffusion in Gases Including Effects of Chemical Reaction, by C. Frederick Hansen, ARS JOURNAL, vol. 20, Oct. 1960, pp. 942–946.

Shock Tube Design for Producing High Gas Temperatures, by Hugh N. Powell, ARS JOURNAL, vol. 20, Oct. 1960, pp. 980–982.

Inviscid Flow with Nonequilibrium Molecular Dissociation for Pressure Distributions Encountered in Hypersonic Flight, by Martin H. Bloom and Martin H. Steiger, *J. Aero/Space Sci.*, vol. 27, Nov. 1960, pp. 821–835.

Radiation Versus Mass-transfer Effects for Ablating Re-entry Shields of a Non-lifting Satellite, by Ernst Wilhelm Adams, *J. Aero/Space Sci.*, vol. 27, Nov. 1960, p. 868.

On Minimum-weight Rectangular Radiating Fins, by Chen-Ya Liu, *J. Aero/Space Sci.*, vol. 27, Nov. 1960, p. 871.

An Equivalence Principle for Water-exit and -entry Problems, by John P. Moran, *J. Aero/Space Sci.*, vol. 27, Nov. 1960, p. 876.

Growth of Vapor Bubbles in a Rapidly Heated Liquid, by S. A. Zwick, *Phys. Fluids*, vol. 9, Sept.-Oct. 1960, pp. 685–692.

Transport Properties for Gases Assuming Inverse Power Intermolecular Potentials, by Taro Kihara, Marion H. Taylor and Joseph O. Hirshfelder, *Phys. Fluids*, vol. 9, Sept.–Oct. 1960, pp. 715–720.

Propagation of Small Amplitude Magnetodrodynamic Waves, by W. E. Williams, *Quarterly J. Mech. and Appl. Math.*, vol. 13, Part 3, Aug. 1960, pp. 272–277.

Motion of an Axially Symmetric Gas Jet with Small Conductivity in an Axially Symmetric Magnetic Field, by G. M. Bam-Zelikovich, *Soviet Physics: Doklady*, vol. 5, Sept.–Oct. 1960, pp. 231–234.

The Calculation of Oblique Shock Waves in Magnetogasdynamic, by M. I. Kiselev and N. I. Kolosnitsyn, *Soviet Physics: Doklady*, vol. 5, Sept.–Oct. 1960, pp. 246–248.

Hypersonic Flow About a Thin Body at Large Angles of Attack, by V. V. Sychev, *Soviet Physics: Doklady*, vol. 5, Sept.–Oct. 1960, pp. 249–252.

The Motion of a Conducting Plasma Under the Action of a Piston, by G. A. Skuidin and K. P. Stanyukovich, *Soviet Physics: Doklady*, vol. 5, Sept.–Oct. 1960, pp. 283–286.

Flight Mechanics

International Astronautical Congress, 10th, London, 1959, Proceedings, F. Hecht, ed., Springer-Verlag, Vienna, 1959, 2 vols., 946 pp.

Re-entry Paths for Manned Satellites, by W. F. Hilton, vol. 2, pp. 526–536, 8 figs.

Launching Conditions and the Geometry of Orbits in a Central Gravity Field, by F. T. Sun, vol. 2, pp. 537–559.

On the Apparent Motion of an Earth's Artificial Satellite, by J. J. de Orus, vol. 2, pp. 723–727.

Relativity Advances of the Perigee of Artificial Earth Satellites, by J. Tharrats, vol. 2, pp. 772–777, 4 figs.

Theorie der Relativistischen n-Stufenrakete, by Von M. Subotowicz, vol. 2, pp. 852–864.

The Fluctuation of the Accelerations of Satellites and the Changing of the Upper Atmospheric Conditions, by H. K. Paetzold and H. Zschermer, vol. 2, pp. 865–870.

Damping of the Satellite Wake in the Ionosphere, by S. Rand, *Phys. Fluids*, vol. 3, July-Aug. 1960, pp. 588–599.

The Theory of Satellite Orbits, Based on a New Co-ordinate System, by J. L. Brenner and G. E. Latta, *Royal Society, London, Proceedings*, vol. 258A, Nov. 8, 1960, pp. 470–485.

The Effect of Atmospheric Rotation on the Orbital Plane of a Near-Earth Satellite, by G. E. Cook and R. N. A. Plimmer, *Royal Society, London, Proceedings*, vol. 258A, Nov. 8, 1960, pp. 516–528.

Relativistic Rocket Mechanics, by H. G. L. Krause, *NASA Tech. Translation* F-36, Oct. 1960, 22 pp.

The Differences Between Satellite and Ballistic Missile Re-entry Problems, by F. R. Riddell and J. D. Teare, *Avco-Everett Research Lab., Research Rep.* 31, Sept. 1958, 30 pp. (Avco-Everett Research Laboratory Research Reports, vol. 2.)

A Theoretical Study of the Angular Motions of Spinning Bodies in Space, by Jerrold H. Suddath, *NASA Tech. Rep.* R-83, 1960, 29 pp.

A Modified Hansen's Theory as Applied to the Motion of Artificial Satellites, by Peter Musen, *NASA Tech. Note* D-492, Nov. 1960, 39 pp.

Dependence of Secular Variations of Orbit Elements on the Air Resistance, by P. E. El'yasberg, *NASA Tech. Translation* F-47, Nov. 1960, 10 pp.

First-order Perturbations in the Motion of Earth Satellites Due to Oblateness of the Earth, by V. F. Proskurin and Yu. V. Batrakov, *NASA Tech. Translation* F-45, Nov. 1960, 12 pp.

NASA-Industry Program Plans Conferences, 1st Proceedings, July 28–29, 1960, 23 pp.

Research Problems in Aerodynamics and Flight Mechanics, by Milton B. Ames, pp. 16–22.

The Contraction of Satellite Orbits Under the Influence of Air Drag. I. With Spherically Symmetrical Atmosphere, by G. E. Cook, D. G. King-Hele and D. M. C. Walker, *Royal Society of London, Proceedings of the Series A, Mathematical and Physical Sciences*, vol. 257, no. 1289, Sept. 6, 1960, pp. 224–249.

On the Trajectories of Near Satellites, by J. Levy, *Bulletin Geodesique* (N.S.), no. 53, 1959, pp. 7–20. (In French.)

Determination of Satellite Orbits from Radar Data, by I. Harris and W. F. Cahill, *IRE Proceedings*, vol. 48, no. 9, Sept. 1960, pp. 1657–1658.

On the Computation of Nearly Parabolic Two-Body Orbits, by C. E. Herrick, *Astron. J.*, vol. 65, no. 6, Aug. 1960, pp. 386–388.

Periodic Drag Perturbations of Artificial Satellites, by I. G. Izsak, *Astron. J.*, vol. 65, no. 6, Aug. 1960, pp. 355–357.

Effect of Upper Atmosphere Wind on

the Rotation of Satellite 1958δ 1, by C. R. Faulkner, *Nature*, vol. 187, no. 4741, Sept. 10, 1960, pp. 926–927.

Decennial Symposium, Proceedings, *Toronto University, Institute of Aerophysics*, Oct. 14–16, 1959, 3 parts, 512 pp.

Longitudinal Dynamics of a Lifting Vehicle in a Circular Orbit, by B. Etkin, pp. 393–428.

A Complete Solution to a Simple Rendezvous Problem, by Frank D. F. Faulkner, *Naval Postgraduate School, Research Paper* No. 22, July 1960, 6 pp.

Astrodynamics, by Robert M. L. Baker, Jr., ASTRONAUTICS, vol 5, Nov. 1960, p. 30.

Vehicle Design, Testing and Performance

Research Summary No. 36-4, vol. 1, for the period, June 1, 1960 to Aug. 1960, *Calif. Inst. Tech., Jet Prop. Lab.*, 9 pp.

Research Summary No. 6-4, vol. II, for the period June 1, 1960 to Aug. 1, 1960, *Calif. Inst. of Tech., Jet Prop. Lab.*, 88 pp.

Decennial Symposium, *Toronto University, Institute of Aerophysics*, Oct. 14–16, 1959, 3 parts, 512 pp.

Considerations in the Design and Operation of High Altitude Research Rockets, by E. Bendor, pp. 365–392.

The Urge Toward Space Conquest, by J. C. Evvard, pp. 445–477.

International Astronautical Congress, 10th London, 1959, Proceedings, F. Hecht, ed., Springer-Verlag, Vienna, 1959, 2 vols., 946 pp.

The Drage Brake Manned Satellite System, by R. W. D. Detra, A. R. Kantrowitz, F. R. Riddell and P. H. Rose, vol. 2, pp. 728–747, 14 figs.

Fuel Requirements for Inter-orbital Transfer of a Rocket, by R. N. A. Plimmer, vol. 2, pp. 911–932.

Design of a Pressurized Missile Body, by D. S. Houghton and A. S. I. Chan, *Aircraft Engng.*, vol. 32, Nov. 1960, pp. 320–327.

Trailer Streamlines Atlas Pneumatic Checkout, by I. Stambler, *Space/Aeron.*, vol. 34, no. 4, Oct. 1960, pp. 63–65.

Eye-Witness Report on Pacific's First Nose Cone Recovery-Operation NERV, by W. Keeshen Jr., *Western Aviation*, vol. 40, no. 10, Oct 1960, pp. 8–10, 60.

The Echo Communications Satellite, *National Academy of Sciences, IGY Bulletin*, no. 39, Sept. 1960, pp. 13–17.

Guidance and Control

Analysis of Radio-command Mid-course Guidance, by A. R. M. Noton, E. Cutting and F. L. Barnes, *Calif. Inst. Tech., Jet Prop. Lab., Tech. Rep.* no. 32–28, Sept. 1960, 23 pp.

A Two-Impulse Plan for Performing Rendezvous on a Once-a-day Basis, by John D. Bird and David F. Thomas Jr., *NASA TN* D-437, Nov. 1960, 36 pp.

Guidance and Navigation, by James S. Farrior, ASTRONAUTICS, vol. 5, Nov. 1960, p. 34.

Experience with a Three-axis Side-located Controller During a Static and Centrifuge Simulation of the Piloted Launch of a Manned Multistage Vehicle, by William H. Andrews and Euclid C. Holleman, *NASA TN* D-546, Nov. 1960, 26 pp.

Satellite Attitude Control Using a Combination of Inertia Wheels and a Bar Magnet, by James J. Adams and Roy F. Brissenden *NASA TN* D-626, Nov. 1960, 42 pp.

Decennial Symposium, Proceedings, *Toronto University, Institute of Aerophysics*, Oct. 14–16, 1959, 3 parts, 512 pp.

A Method for Navigating Satellite Ferry Vehicles, by P. A. Lapp, pp. 429–444.

International Astronautical Congress, 10th, London, 1959, Proceedings, F. Hecht, ed., Springer-Verlag, Vienna, 1959, 2 vols., 946 pp.

Interplanetary Navigation, by I. Sinra, vol. 2, pp. 705–714, 5 figs.

Adaptive Servomechanisms and the X-15 Inertial Reference System, by S. Cap, *Sperry Engng. Review*, vol. 13, no. 3, Oct. 1960, pp. 12–19.

Terminal Guidance System for Satellite Rendezvous, by W. H. Clohessy and R. S. Wiltshire, *J. Aero/Space Sci.*, vol. 27, no. 9, Sept. 1960, pp. 653–658, 674.

Which Accelerometers for Space Guidance, by J. M. Slater, *Space/Aeron.*, vol. 34, no. 4, Oct. 1960, pp. 227–234, 238–240.

Instrumentation and Communications

Instrumentation for Magnetoaerodynamic Heat Transfer, by Richard W. Ziemer, *Space Tech. Lab., Inc., Physical Res. Lab.*, STL/TR 60-0000-09290, Sept. 1960, 35 pp.

The Strainistor, a Semiconductor Strain Sensor, by C. O. Vogt, *Century Electronics & Instruments, Inc., Tulsa, Okla.*, 22 pp. (Presented at Sixth National Flight Test Instrumentation Symposium, San Diego, Calif., May 2–5, 1960.)

Atmospheric and Space Physics

Evolution of a Dark Filament at the Time of the Solar Eruption of July 16, 1959, by A. Koeckelenbergh, *Ciel et Terre*, France, vol. 76, no. 7–8, July-Aug. 1960, pp. 216–220. (In French.)

Equatorial Coronal Streamers of the Sun, by K. Saito, *Astronomical Society of Japan, Publications*, vol. 11, no. 4, 1959, pp. 234–252.

Relation Between Solar Radio Noise Storms and Chromospheric Eruptions, by A. M. Malinge, *Annales d'Astrophysique*, France, vol. 23, no. 4, 1960, pp. 574–584, (In French.)

Depth of Formation in the Solar Spectrum—1. Application to the Inversion of the Laplace Relation, by S. Dumont and J. C. Pecker, *Annales d'Astrophysique*, France, vol. 23, no. 4, 1960, pp. 655–657. (In French.)

Polarized Bursts and Noise Storms of Solar Radio Emission. II. Storm Bursts and Background Continuum, by T. Takakura, *Astronomical Society of Japan, Publications*, vol. 11, no. 2, 1959, pp. 50–70.

Polarized Bursts and Noise Storms of Solar Radio Emission. III. The Post-detection Low Frequency Spectra of Noise Storms, by T. Takakura, *Astronomical Society of Japan, Publications*, vol. 11, no. 2, 1959, pp. 71–78.

The Exploration of the Solar System, by F. Godwin, *Rivista Aeronautica*, Italy, vol. 36, no. 9, Sept. 1960, pp. 1482–1484. (In Italian.)

The Sun, by M. A. Ellison, *Discovery*, vol. 21, no. 1, Jan. 1960, pp. 6–11.

Venus Will Be in Semi-rapid Rotation and Too Cold for Human Beings, by P. Guerin, *La Nature*, France, no. 3297, Jan. 1960, pp. 16–17. (In French.)

Variations of the Balance and Abundance Within the Solar and Stellar Photospheres—II. The Case of Neutral Atoms, of Titanium, Vanadium and Chromium in the Solar Atmosphere, by J. C. Pecker and L. Vogel, *Annales d'Astrophysique*, France, vol. 23, no. 4, 1960, pp. 594–621. (In French.)

Astronauts Don't Grow Older: The Einstein Theory Proved by Russian Scientists, *Rivista Aeronautics*, Italy, vol. 36, no. 8, Aug. 1960, pp. 1299–1302. (In Italian.)

Unique Sun Simulator Proposed, by H. Gettings, *Missiles and Rockets*, vol. 7, no. 13, Sept. 26, 1960, pp. 34–38.

Phenomena of the Solar Atmosphere by R. G. Athay, *Science*, vol. 131, no. 3429, Sept. 16, 1960, pp. 707–711.

On the Behavior of the Monochromatic Corona in the 11-Year Cycle, by M. Waldmeier, *Zeitschrift fur Astrophysik*, vol. 50, no. 3, July 26, 1960, pp. 145–154. (In German.)

Observation of a Persistent Coronal Stream, by J. L. Leroy, *Annales d'Astrophysique*, vol. 23, no. 4, 1960, pp. 567–573. (In French.)

Flash Spectrum by a Grazing Incidence Method at the Total Solar Eclipse of Oct. 12, 1958, by Z. Suemoto and E. Hiei, *Astronomical Society of Japan, Publications*, vol. 11, no. 2, 1959, pp. 122–125.

Solar Eclipse of 1959 October 7, by F. Addey and O. D. Macnamara, *British Astronomical Association J.*, vol. 70, no. 6, Aug. 1960, pp. 264–269.

Human Factors and Bioastronautics

International Astronautical Congress, 10th, London, 1959, Proceedings, F. Hecht, ed., Springer-Verlag, Vienna, 1959, 2 vols., 946 pp.

Multi-directional G-protection During Experimental Sled Runs, by H. J. von Beckh, vol. 2, pp. 671–682.

The Human Eye in Space (Physiologic Aspect), by H. Strughold, vol. 2, pp. 715–722.

The Reactions of Terrestrial Microorganisms to Simulated Martian Conditions, by I. Davis and J. B. Fulton, vol. 2, pp. 778–785.

Centrifuge Study of Pilot Tolerance to Acceleration and the Effects of Acceleration on Pilot Performance, by Brent Y. Creer, Harold A. Smedal and Rodney C. Wingrove, *NASA TN* D-337, Nov. 1960, 35 pp.

NASA-Industry Program Plans Conferences, 1st, Proceedings, July 28–29, 1960, 23 pp.

Manned Space Flight, by George M. Low, pp. 79–85.

Life Sciences Programs, by Clark T. Randt, pp. 96–100.

Human Factors and Bioastronautics, by Stanley C. White, ASTRONAUTICS, vol. 5, Nov. 1960, p. 35.

Education, Sociology and Law

Education, by Irving Michelson, ASTRONAUTICS, vol. 5, Nov. 1960, p. 32.

Space Law and Sociology, by Andrew G. Haley, ASTRONAUTICS, vol. 5, Nov. 1960, p. 46.

About Space Law, by L. Mowbray, *La Nature*, France, no. 3303, July 1960, pp. 289–294. (In French.)

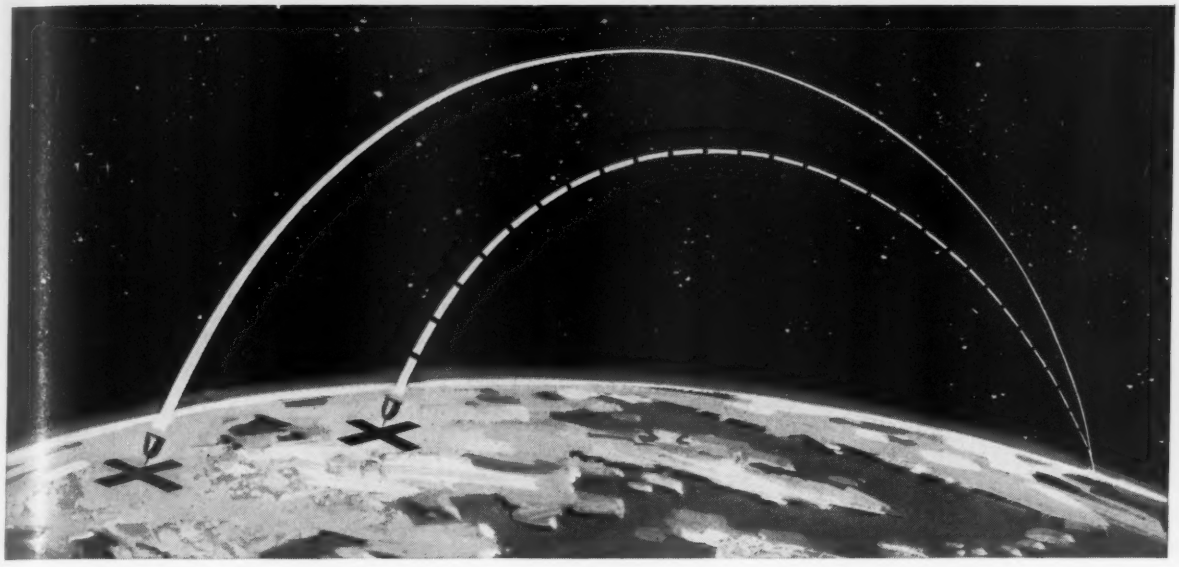

20% to 50% increase in rocket range promised by CTF... *advanced storable oxidizer*

Chlorine trifluoride is a "lamb" to store and handle...a "tiger" in power and performance—provides instant readiness, proved dependability

Many experts believe CTF, in combination with rocket fuels such as hydrazine, can give increases in range on the order of 20% to 50%! Yet CTF handles, ships and stores easily!

General Chemical knows Chlorine Trifluoride well. We have been making it commercially for over 10 years. We have summarized pertinent data on this advanced storable oxidizer in a technical bulletin, "Chlorine Trifluoride," which is available free to those interested in rocket and missile research. Simply write on company or official letterhead.

First in fluorine chemistry

Allied Chemical

GENERAL CHEMICAL DIVISION
40 Rector Street, New York 6, N. Y.

CTF is packaged commercially by General Chemical in 150-lb. and one-ton steel cylinders. Storage is simple and convenient . . . no special safety precautions are needed.

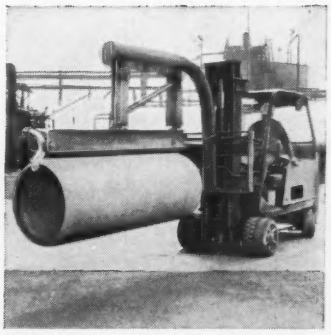

CTF is completely insensitive to shock and can be shipped cross country by common carriers . . . has low freezing and moderate boiling point . . . needs no refrigeration.

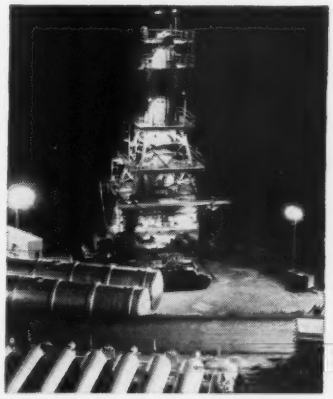

CTF is one of the most powerful rocket fuel oxidizers known. Its high density leads to outstanding density impulse values with a variety of rocket fuels such as hydrazine.

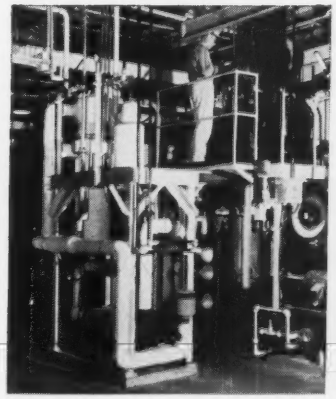

CTF has been produced commercially by General Chemical for 10 years. Reactors like this at General's Baton Rouge, La., Works produce more than 100 tons per year.